COMPUTATIONAL SIMULATION OF THE INTERVERTEBRAL DISC

Bethany Jane Luxmoore

Submitted in accordance with the requirements for the degree of Doctorate of Philosophy.

The University of Leeds
School of Mechanical Engineering

February 2013

The candidate confirms that the work submitted is her own and that appropriate credit has been given where reference has been made to the work of others.

ACKNOWLEDGEMENTS

My greatest appreciations go to my supervisors, Dr. Sarrawat Rehman, Dr. Nagitha Wijyaythunga and especially to Professor Ruth Wilcox, whose expertise and guidance helped me to shape and develop this thesis. Above all, I thank them for their tireless encouragement and belief in my work over the past three and a half years.

Thanks go to the team at Leeds Musculoskeletal Research Unit, especially to Dr. Richard Hodgson and Robert Evans for their significant contributions and assistance in the imaging work completed.

I am very grateful to Professor Neil Broom for hosting me during a visit to his laboratory at the University of Auckland and to Kelly Wade and Samantha Rodrigues for their advice and companionship during my stay and for all their help during my microscopy studies.

Thank you to all of the technical staff at the Institute of Medical and Biological Engineering for their assistance during my experimental work and to Dr. Sami Tarsuslugil for his photography skills and equipment.

I am very appreciative to Dr. Joseph Luxmoore and Robin Luxmoore who bravely volunteered to proof-read this thesis.

The completion of this PhD has been made much easier by all those to whom I am grateful, including a loving group of friends and family. Thank you to my partner, Nick, for his wonderful support, patience and understanding over the past three years and to my Parents, whose support and unfaltering belief in me has buoyed me through my entire education and for which I will always be grateful.

Finally, thank you to Corinne who understands what this challenge has been more than anyone; I would not have wanted to do it without you by my side.

ABSTRACT

The intervertebral disc is a complex structure unlike any other in the human body. The capability to withstand high loads and deformations in six degrees of freedom is facilitated by the unique soft tissue structures. However, the mechanical behaviour of these tissues is not well understood.

The aim of this project was to investigate methods of deriving structural information about the tissues of the intervertebral disc for application in computational simulation, with particular focus on the mechanical function of the annulus fibrosis and how the behaviour of this tissue is governed by its substructures.

Magnetic resonance imaging techniques were assessed for potential to inform specimen specific models of the disc. Imaging sequences were developed and validated to image *in vitro* disc samples in unloaded and compressed states. These images captured the lamellar structure of the annulus in three dimensions to a level of detail not previously published.

The image data facilitated the development of a novel method of specimen specific model construction, as well as providing experimental deformation data, against which the models were directly validated.

Sensitivity analyses on both generalised and specimen specific models illustrated the influence of interlamellar interaction representation on the gross mechanics of the disc models. The models were adapted to illustrate the effects of tissue degeneration and intervention on disc mechanics.

Interlamellar interactions and tissue level mechanics were further investigated by developing specimen specific models of disc tissue samples based on microscopy data. Novel methods were developed to implement qualitative histological data into finite element analyses of annulus tissue samples. Interlamellar interactions were shown to provide a strong bond between lamellae.

The parameters and variables involved in the mechanical system of the disc pose major challenges for experimental investigation. This study has successfully laid the ground work to negotiate these challenges using a computational approach.

CONTENTS

NOMENCLATURE

AF	annulus fibrosus
B	Bulk modulus
CT, µCT	computed topography, micro computed topography
E	Young's modulus
EP	end plate
FE, FEA	finite element (analysis)
FSU	functional spinal unit
G	shear modulus
IVD	intervertebral disc
MR, MRI	magnetic resonance (imaging)
NP	nucleus pulposus
NPR	nucleus pulposus replacement
TDR	total disc replacement
TZ	transition zone
VB	vertebral body
v	Poisson's ratio

TERMINOLOGY

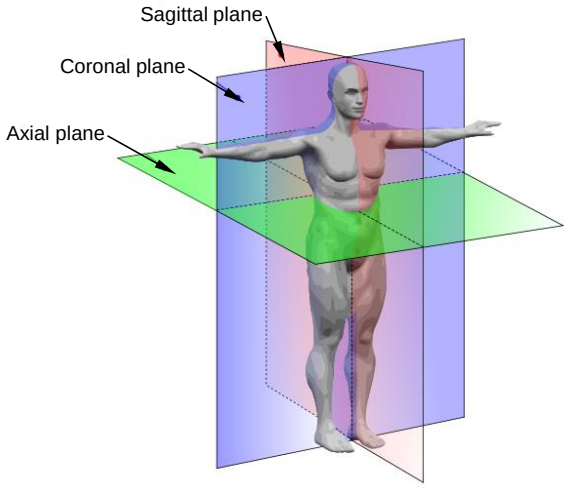

Figure a – The planes of dissection through the body. Adapted from Adams et al. (2002).

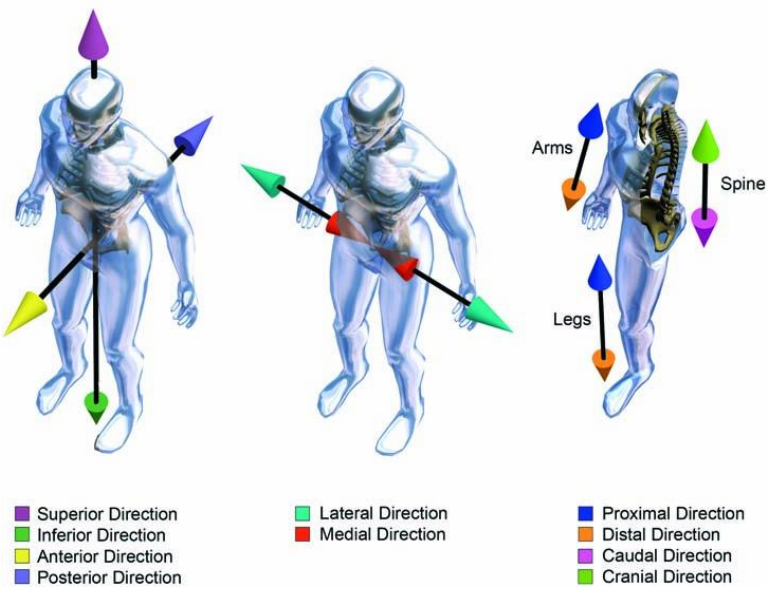

Figure b – Anatomic reference directions. Adapted from Kurtz and Edidin (2006).

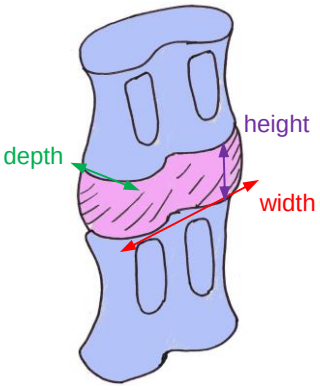

Figure c – Terms used to describe the dimensions of the disc.

1 INTRODUCTION

Back pain is a major public health problem, affecting up to 80% of the population of industrialised countries at some point in their lifetime (Maniadakis and Gray 2000; Palmer *et al.* 2000). Only the common cold exceeds back pain in terms of the frequency of complaints that are received by primary care physicians (Katz 2006). In the U.K., healthcare costs for back pain were estimated at £1.6 billion per year (Maniadakis and Gray 2000). In the year from April 2008 to April 2009, 3.5 million working days were lost as a result of back pain, the equivalent of 0.7% of the working population on sick leave at any one time due to the condition (HSE 2009).

The intervertebral disc is the fibrous-cartilaginous joint that connects the vertebrae of the spine and facilitates the movement of the spinal joints. The disc is similar in material composition to connective tissues found elsewhere in the body; however, its unique structure gives the joint freedom of movement in six degrees and a large load bearing capacity that distinguishes it from other tissues and joints.

From a relatively early age, the material properties of the tissues in the disc begin to change, and years of accumulated damage can have significant effects on disc function. This can cause pain and mobility problems directly, or indirectly, by altering the loading patterns of the spine and affecting other components and tissues (Harris and MacNab 1954). Luoma *et al.* (2000) reported a significant association between disc degeneration and nonspecific and chronic low back pain.

The most established surgical treatment for disc degeneration is fusion of the motion segment (Kurtz and Edidin 2006). As a result of this irreversible procedure, all motion is lost from the joint. Recent developments in the disc treatment research show a trend away from fusion, towards methods that better mimic the natural biomechanics of the spine, providing better mobility and reducing knock-on effects in adjacent segments.

Total disc replacements (TDR) offer the solution of entirely removing a problematic disc and replacing it with a prosthesis intended to restore movement to the joint. However, the success of such procedures has been limited, and the range of motion recovered by the patient has been shown to be only marginally greater than that recovered following fusion (Freeman and Davenport 2006).

Focus has moved away from TDR and towards techniques that minimise the disruption of natural tissue such as nucleus pulposus replacement (NPR). The field

of tissue engineering also offers exciting new prospects for treating disc degeneration with tissue replacement solutions that are closer to the natural, healthy functioning state of the disc. For these theoretical techniques to develop into real solutions for the treatment of discogenic back pain, it is necessary to gain a thorough understanding of how disc tissues function in their natural, healthy state and how they may be affected by degeneration and by subsequent interventions.

Computational methods of representing the mechanical function of the spine have been developed to aid biomechanical and medical engineering research, without the difficulties of recreating mechanical conditions necessary for *in vitro* studies and without the limitations of *in vivo* approaches. Computational simulations facilitate the application of wide ranges of conditions and parameters quickly and efficiently, whilst also providing data that may not be measurable using experimental techniques alone.

Finite element analysis (FEA) is a numerical approach to solving complex problems by dividing a system into small elements that can be solved in relation to each other. It is a method that has been widely adopted in many engineering applications. The main purposes of FEA in orthopaedics are outlined by Prendergast (1997) and summarised as:

(i) design and pre-clinical analysis of prostheses;
(ii) to obtain fundamental biomechanical knowledge about musculoskeletal structures;
(iii) to investigate time-dependent adaptation processes in tissues.

In their review of lumbar spinal mechanics (1995), Adams and Dolan suggest that analytical models of the spine have limited predictive power because the complexity of the mechanical environment necessitates a large number of assumptions, resulting in simulations that are designed merely to “appear reasonable” rather than fully represent the *in vivo* conditions. The decisions and assumptions made when developing simulations determine the success of the entire study.

Recent advances in techniques, software and hardware have greatly improved the reliability of models. As modelling techniques advance and data for the development of input parameters improve, model complexity and reliability should both increase; as such the worth of simulations to orthopaedic developments will also improve.

Finite element analysis of the vertebrae has been more comprehensive than that of the disc. The relatively simple structure and the methods with which bone image data can be captured and manipulated have facilitated extensive development of this field. From this, essential foundations have been developed for model verification, validation and sensitivity analysis that can now be applied to other areas of biomechanical study, including analysis focussing on the disc (Jones and Wilcox 2008).

Models of disc mechanics at a macro level have been successfully developed (Yin and Elliott 2005; Schmidt *et al.* 2007) but these studies are not extensive and are lacking in direct validation between computational and experimental models. There still remains a lack of knowledge about how the constituent tissues of the disc behave and contribute to the overall function of the joint. The process of developing FE models of the disc at a more intricate level could help to improve understanding in this area (Nerurkar *et al.* 2010).

Developments in computational techniques have provided the technology to include an increased level of structural detail to simulations of the disc. Modelling structures at a sub-disc level has, however, been limited by a lack of experimental and image data for internal soft tissue behaviour in the intact mechanical environment.

From a clinical perspective, there is a demand for non-invasive analysis tools that can be used to better understand the anatomy, function and pathology of the spine. FE modelling has the potential to provide a valuable tool for the analysis and development of new treatment methods. Subject specific models for individual patients may eventually be capable of analysing patient specific treatment options.

1.1 AIMS

The aim of this project was to investigate methods of deriving structural information about the tissues of the intervertebral disc for application in computational simulation, with particular focus on the mechanical function of the annulus fibrosis and how the behaviour of this tissue is governed by its substructures.

1.2 OBJECTIVES

To achieve the aim described above, the following objectives were pursued:

1. The structural parameters of the disc system that have greatest significant during model development were evaluated by developing a generalised model of the disc and undertaking a series of sensitivity studies.
2. Non-destructive methods of imaging the disc in an intact and loaded state were investigated with the intention of providing data for model generation and validation.
3. Image data was used to develop specimen specific models of the disc to illustrate the variation between specimens and to facilitate direct validation of models with experimental data.
4. The disc models were adapted to represent surgical interventions to analyse the changes in the mechanical behaviour of the system and to illustrate potential clinical applications of the models.
5. The tissue level mechanics of the annulus were investigated using a combination of microscopy imaging techniques and FE models to establish an appropriate representation of the tissue structure in a whole disc model.

2 LITERATURE REVIEW

This chapter presents an introduction to the mechanical environment of the intervertebral disc with particular focus on the tissue level structure of the annulus fibrosis. Experimental methods of studying the disc tissues, such as histology and imaging techniques were reviewed with their relevance to computational simulation analysed. Published models of the disc were reviewed, and a comparison of techniques presented, with emphasis on analysis techniques used to model the annulus.

2.1 INTRODUCTION

The intervertebral disc is a fibrous-cartilaginous structure that connects adjacent vertebral bodies of the spine to form a spinal joint. The disc facilitates movement of the spine in six degrees of freedom whilst the range of motion is restricted by the facet joints and surrounding muscles and ligaments. The mechanical environment of the disc is influenced by surrounding tissue structures such as ligaments and muscles which, combined with the acting weight of the body and limbs apply considerable loads to the disc even when the body is at rest.

The major functional components and ligaments of the lumbar spine are illustrated in Figure 2.1.

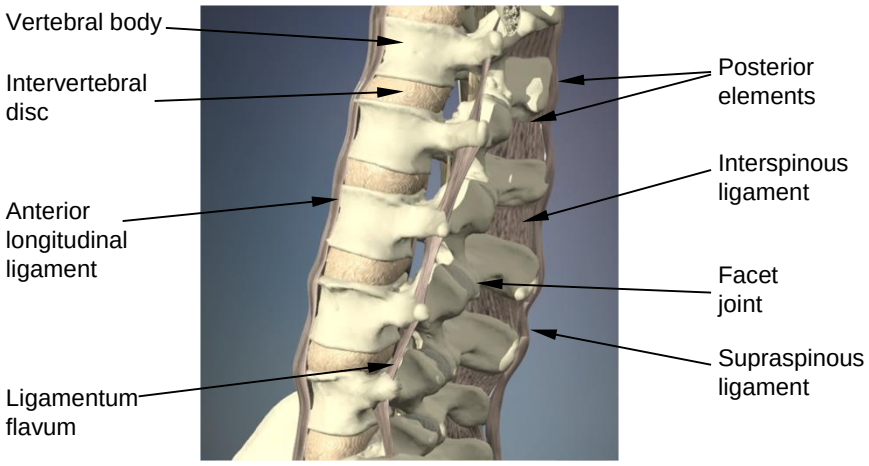

Figure 2.1 – The bones, ligaments and joints of the lumbar spine. Image adapted from anatomy.tv.

The discs vary in size and shape through the spine, depending on the spinal level, the size of adjacent vertebrae and the curves of the spine; thoracic discs are smaller with an oval cross-section whereas the lumbar level discs are the larger, kidney

shaped with a wedge profile. A typical human lumbar disc is 30-40 mm wide and 10-14 mm in height (Urban and Roberts, 2003).

To analyse the mechanical function of the disc system, it is necessary to understand the structural anatomy of the disc tissues and their relationship and behaviour within the disc.

2.2 STRUCTURE OF THE INTERVERTEBRAL DISC

The disc consists of collagen fibres embedded in a highly hydrated gel-like substance. The tissue structure can be interpreted as fibre reinforced composite with fibre and matrix[1] constituents. The proportion of fibre to matrix varies between the components of the disc.

The three main components of the disc are the nucleus pulpous (nucleus), the annulus fibrosis (annulus) and the cartilaginous, vertebral end plates (EP), as shown in Figure 2.2.

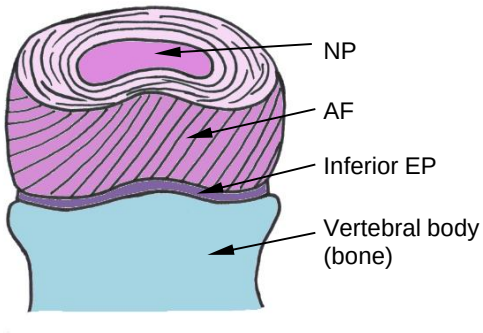

Figure 2.2 – Schematic diagram of the components of the disc, isolated from the surrounding structures of the spine.

The different scales and model levels discussed throughout this project are outlined in Figure 2.4.

[1] For the purpose of this study, the term “matrix” will refer to the proteoglycan rich ground substance of the annulus. This should not be confused with the biological term “extra cellular matrix” which refers to all components of connective tissue, both ground substance and fibrous components of connective tissue.

2.2.1 END PLATES

The end plates (EPs) are located between the vertebrae and the disc. They comprise a calcified layer covered by a layer of hyaline cartilage and play a crucial role in the biological and mechanical functions of the disc.

The end plates are thickest at the periphery of the disc and become thinner moving inwards radially, with an average thickness of approximately 0.6mm. The central region has a higher water and proteoglycan content, whereas the collagen content increases towards the periphery (Kurtz and Edidin, 2006).

Histological examination by Pezowicz *et al.* (2005) and Rodrigues *et al.* (2012) have revealed a high degree of integration of annulus fibres within the end plates which is thought to contribute significantly to the overall strength of the disc.

2.2.2 NUCLEUS PULPOSUS

The nucleus lies at the centre of the disc. It is a translucent, gelatinous, semi-solid structure which consists of randomly distributed collagen fibres within a hydrated matrix. Until recently, the nucleus had generally been thought of as a gel that was unconnected and somewhat free to move within the disc. However a recent histological study by Wade *et al*. (2010) showed how it contains continuous fibres that are imbedded into the end plates and curled up in the centre of the nucleus.

The nucleus is 70-80% water. The water within the nucleus is retained by long chains of molecules called proteoglycans. These molecules carry fixed negative charges that attract positively charged water molecules into the nucleus. The amount of proteoglycans in the nucleus is much greater than in the annulus, resulting in increased hydrophilic properties (Middleditch and Oliver 2005). The high water content is responsible for the fluid-like behaviour and near-incompressible properties of the nucleus (Kurtz and Edidin, 2006).

It is difficult to distinguish where the nucleus ends and the annulus begins. There is no distinct boundary between the tissues; instead there is a region in which the nucleus becomes more fibrous and the annulus more gel like (Wade *et al.* 2012).

2.2.3 ANNULUS FIBROSIS

The annulus is made up of concentric layers of collagen fibres embedded in a proteoglycan matrix (Kurtz and Edidin 2006). Each layer of fibre is referred to as a

lamella. Within a lamella, the fibres are highly organised in one direction at an angle of 30˚ to 60˚ to the longitudinal axis of the spine[2]. This angle alternates between adjacent lamellae, as shown in Figure 2.3.

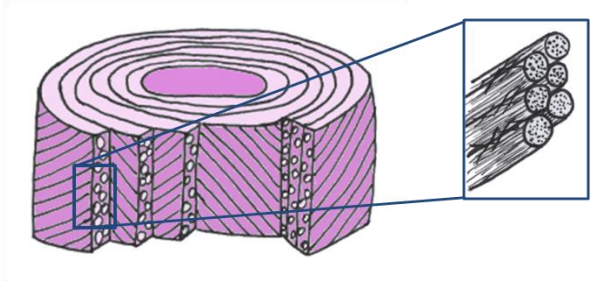

Figure 2.3 – Diagram of the annulus structure showing alternating fibre angle of adjacent lamellae and fibre bundles within a lamella.

The fibres of the annulus are largely a combination of type I and type II collagens. At the outer edge of the annulus, more than 95% of the collagen is type I. The type I collagen contributes to the tensile load bearing capabilities of the tissue in this region. This percentage decreases to less than 5% in the nucleus. An opposing gradient exists for collagen type II, which is more suited to compressive loading. More than 95% of the collagen of the nucleus is type II, decreasing to less than 5% of the collagen in the outer annulus (Cassidy *et al.,* 1989).

The thickness of the annulus varies with location circumferentially around the disc; the anterior region is significantly thicker than the posterior.

[2] Throughout this study fibre angles are given with respect to the longitudinal axis of the spine.

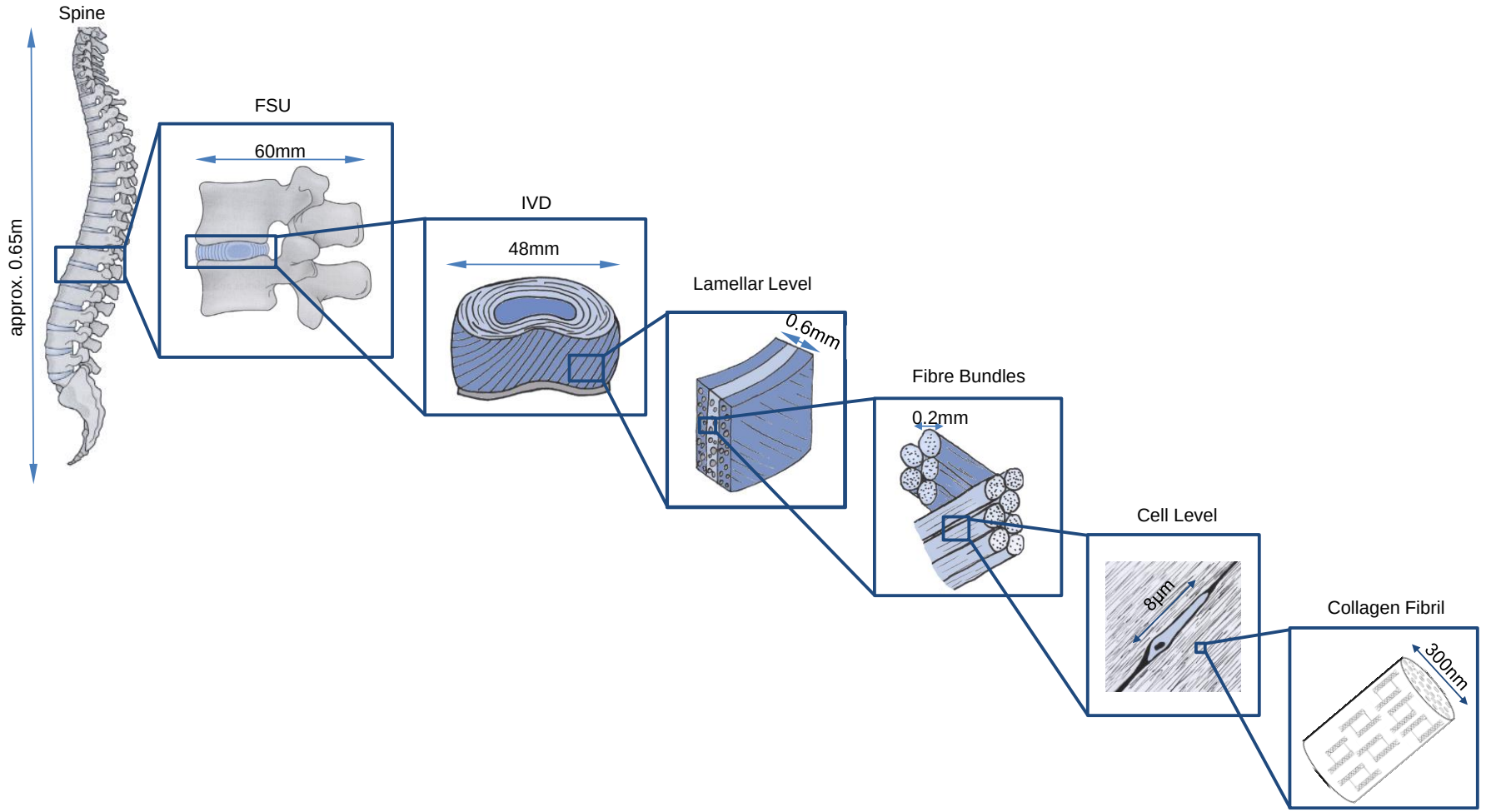

Figure 2.4 – Scale of the hierarchical structure of the disc as referred to in this thesis. The dimensions given are typical for the lumbar region of an average human adult.

LAMELLAR ORGANISATION

Cassidy *et al.* (1989) suggested that there are a constant number of lamellae circumferentially around the disc that vary in thickness. Lamellae were reportedly thinner and more tightly packed in the posterior region of the annulus than those in the anterior region. Marchand and Ahmed (1990) studied the lamellar structure in more detail by sectioning human disc tissue in various planes and found that the lamellae are not regular or uniformly concentric. Approximately 15-25 distinct lamellae were reported across the annulus, varying between specimens depending on age, degeneration and spine level. Within any 20° section nearly half of all the layers were found to terminate or originate. This causes local lamellar irregularities that affect the mechanical behaviour of the annulus.

The mechanical properties of the lamellae vary across the disc. Lamellae are stiffer at the periphery of the disc than those in the inner layers of the annulus and the crimp of the unloaded fibres is much smaller (Cassidy *et al.*, 1989). The attachment of lamellae to other components of the disc also depends on the lamella location. The outermost layers contribute most to the resistance of torsion, shear and separation of the vertebral bodies. To facilitate this they are attached directly into the vertebral bone around the ring apophysis. This is known as the ligamentous portion of the annulus. The inner lamellae attach into the cartilaginous end plates. Because they can be traced through the end plate these lamellae are referred to as the capsular portion of the annulus (Adams *et al.*, 2002).

The distinctive material properties of the annulus tissue are, in large, attributable to the arrangement of fibres into lamellae and the arrangement of lamellae within the disc. The fibrillar architecture of the annulus and the incompressibility of the nucleus ensure that fibres bear tension when the spine is under load (Elliott and Setton, 2001). As the typical load varies across the tissue, so does the angle of fibre orientation. Within a single disc specimen, the angle varies, from ±62° at the disc periphery to ±45°[3] at the inner annulus (Cassidy *et al.* 1989). Within a single lamella, the fibre angle has also been shown to vary across the height of the disc (Marchand and Ahmed, 1990).

Within a lamella, fibres are arranged in bundles. In one study, the number of fibre bundles over the height of the disc was found to vary between 20 and 62 (Marchand

[3] In this case ± refers to the opposite fibre angle between adjacent lamellae relative to the longitudinal axis.

and Ahmed, 1990). The material anisotropy and stress-strain nonlinearity characteristic of the annulus tissue is mirrored at a smaller scale within a single lamella (Nerurkar *et al.* 2010).

INTERLAMELLAR INTERACTIONS

In 1967, Galante published a series of experimental results that analysed the mechanical properties of annulus tissue samples isolated from the surrounding disc structures. Based on these results, the connections between adjacent lamellae and the mechanical contributions of such interactions have often been considered negligible in the mechanics of disc deformation (Broberg 1983), with the assumption that disc deformations are facilitated by the slip of adjacent lamellae over one another.

Adams and Green (1993) postulated that the weaknesses reported by Galante were caused by the small specimens used for testing that would have had a severely disrupted collagen network, and when *in situ*, the resistance of the annulus to damage comes from many factors aside from solely the strength of the collagen fibre bundles.

Histological investigations into the microstructure of the annulus (Pezowicz *et al.* 2006; Schollum *et al.* 2008), have found that a high level of connectivity between lamellae exists and may provide a significant contribution to annulus mechanical behaviour. This can be in the form of tissue connections such as collagen fibres, bridging structures and elastic fibres, or frictional adhesion between the surfaces of two lamellae. A schematic diagram of the annulus micro-scale architecture is shown in Figure 2.5.

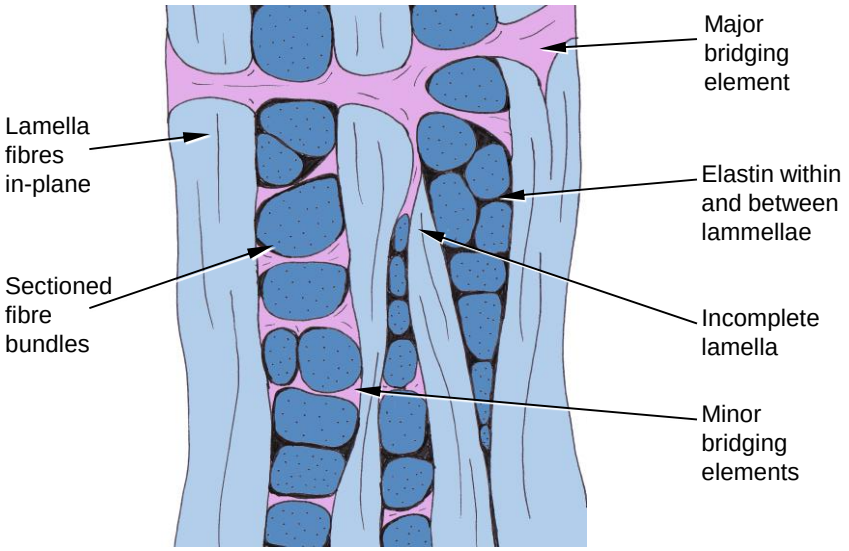

Figure 2.5 - Schematic diagram showing a radial slice through the annulus tissue based on the histological data presented by Pezowicz et al. (2006) and Schollum et al. (2008, 2009). The components of the annulus micro-scale architecture are shown, including: interlamellar connections and bridging elements, elastin network and incomplete lamellae. Cross sectioned lamellar fibre bundles are represented in dark blue and in-plane lamellae in pale blue. The elastin network is shown between bundles in black and minor and major bridging structures are shown in pink.

Pezowicz *et al.* (2005) conducted a histological examination of annulus tissue, in which lamellae were pulled apart from each other in the radial direction, revealing a complex set of interconnecting structures, with bridging structures anchored within lamellae. It was hypothesised that the high connectivity both between lamellae and between fibre bundles within lamellae may act as a captive network retaining the proteoglycan aggregates whilst still allowing the outflow of water during mechanical activity of the disc.

COLLAGEN BRIDGING ELEMENTS

The collagen bundles of the lamellae are connected by collagen bridging structures. Frequent minor bridges pass between collagen bundles and connect lamellae with the same fibre orientation direction, as illustrated in Figure 2.6.

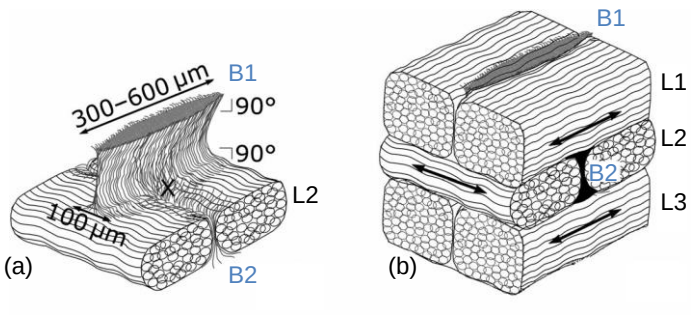

Figure 2.6 – Schematic diagram to show the three dimensional geometric relationship between collagen bundles within lamellae and minor bridging structures between lamellae, adapted from Schollum et al. (2009): (a) collagen bundles from a single lamella (L2) with minor bridges B1 and B2; (b) three adjacent lamellae with bridging structures integrated between collagen bundles.

In addition to minor collagen connections between fibres, occasional substantial collagen bridges span between lamellae, often crossing through multiple lamellae, as illustrated in Figure 2.5. Two independent studies (Schollum *et al.* 2008; Smith and Elliott, 2011) have found approximately one multi-lamellar bridge per 20° section of anterior annulus tissue. Whereas smaller links penetrate fibre bundles, anchoring within a lamella, the larger bridging elements pass between bundles crossing though several lamellae (Pezowicz *et al.,* 2006a). Bridging elements often branch and continue through the tissue as minor bridges and connections, contributing to a complex web of interconnectivity that anchors and adheres the annulus tissue (Pezowicz *et al.,* 2006a).

How and why the major bridging structures develop is unknown. Smith and Elliott (2011) proposed that the bridges were the remnants of disc vascularisation. Ovine discs of a range of ages from foetal to skeletally mature were reviewed with no reported change in the number of major bridges. The tissue stained positive for blood related cells along the major bridging elements in the younger specimens but not in the more developed discs. From this it was postulated that during development, blood vessels are present along the routes of the bridges. As the loads on the disc increase with age, blood vessels regress, leaving behind the bridge structure. As a residue of vascularisation, it was proposed that the bridges do not serve a mechanical purpose.

Melrose *et al.* (2008) also reported evidence of blood related components along the bridging elements, however significantly more bridging structures were observed in skeletally mature, adult specimens than in those from younger sheep, contradictory to the vascularisation hypothesis presented by Smith and Elliott (2011).

A change in the constituents of the major bridges with age was also reported by Melrose *et al.* (2008). These changes were suggested to represent an adaptation to the complex biomechanical forces experienced by the annulus, as loading patterns change with age related degeneration of the nucleus.

Additionally, Schollum *et al.* (2010) observed the development of bridging structures as a response to a change in stress distribution through the disc tissues.

The minor and major bridging elements comprise different tissue constituents (Yu *et al.* 2005; Melrose *et al.* 2008). The elastin present in the minor bridges suggests that these are part of the elastic network between fibre bundles whereas the major bridges are not. The elastin encapsulates the lamellar collagen bundles bonding them together within and between lamellae.

The studies presented here were all early stage histological investigations, which are not conclusive about disc mechanics *in vivo.* The histological method of reviewing the tissue structure in only one slice direction limited the understanding of the three dimensional structure. With conflicting hypotheses on the origin of these structures, it is difficult to postulate their role in the mechanical function of the disc from histological evidence alone. If the bridging structures are related to the vascular system, an extensive and connected network would be required, which has not yet been confirmed. These studies need extending for greater sample sizes and assessment of the robustness of the stain tests, to ensure that features are correctly identified.

ELASTIC FIBRES

Studies by Yu *et al.* (2002, 2005, 2007) identified a complex network of elastic fibres extending throughout the disc. Elastic fibres are present in both the annulus and nucleus, with a concentration at the boundary between the two tissues (Middleditch and Oliver, 2005). They consist of an elastin core, surrounded by a scaffold of micro-fibrilar glycoproteins, facilitating unique, linear and extensible material properties (Smith and Fazzalari, 2009). This intimate association between collagen and elastic fibres can make unambiguous distinction between the two difficult to achieve (Pezowicz *et al.* 2006b). In the healthy disc, elastin by dry weight has been found to be 2.0% (±0.3%) (Cloyd and Elliott 2007).

Elastic fibres exist both within lamellae and as connections between lamellae, penetrating through and anchoring within the fibre bundles of the lamellae (Smith

and Fazzalari 2006). In their 2007 study, Yu *et al.* reported a higher density of elastic microfibrils in the interlamellar bridging elements and the interlamellar spaces.

OTHER EXTRA-CELLULAR CONSTITUENTS

There are significant spatial variations of water, collagen and proteoglycan in the annulus tissue that also contribute to its anisotropic and inhomogeneous mechanical properties. Proteoglycan molecules in the annulus matrix form aggregate molecules that can be large enough to cause physical entrapment between the collagen fibrils, contributing to fibre-matrix interactions (Adams and Green 1993).

2.2.4 CELLS OF THE DISC

Relative to other soft tissues in the body, the disc is sparsely populated with cells. The cells of the nucleus are similar to chondrocytes found in tissues subjected to compressive loading such as articular cartilage. The main function of these cells is to synthesise the extra-cellular constituents of the tissues. The cells in the nucleus predominantly produce type II collagen and aggrecan. Similar cells are found in the inner layers of the annulus, but are more fibrocyte-like similar to those found in ligaments. The cells are elongated and align along the direction of the collagen fibres (Kurtz and Edidin 2006). The size of cells within the disc tissue, relative to other structures is outlined in Figure 2.4.

2.3 FUNCTION OF THE DISC

The main function of the disc is to assist with articulation of the spine and distribution of forces acting on it. As a result, the components of the disc undergo complex loading regimes.

2.3.1 MECHANICAL ENVIRONMENT OF THE DISC

The disc is under a constant compressive load from the weight of the body and muscle forces. This results in shear forces and bending moments in the spine due to the kyphotic and lordotic curves of the spine (Kurtz and Edidin 2006).

Under compression, the nucleus pressure increases. As a nearly incompressible material, the nucleus expands radially, which is constrained by the annulus. This results in tensile loading of the annulus as illustrated in Figure 2.7.

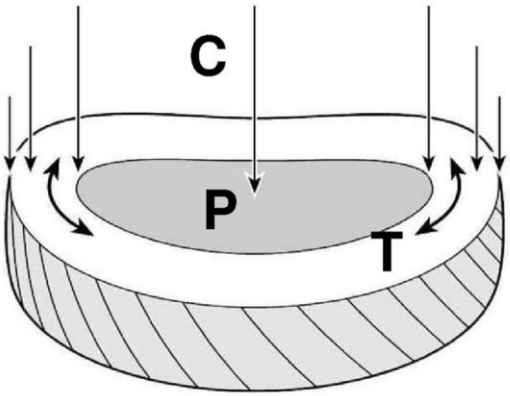

Figure 2.7 - The transmission of loads through the disc. Compressive load (C) is transferred through the EPs to the disc, causing an increase in hydrostatic pressure (P) in the nucleus. The nucleus bulges and loads the annulus in circumferential tension (T). Adapted from Adams and Roughley (2006).

The magnitude of the forces experienced by the disc varies widely depending on posture and activity. A typical load acting on the lumbar spine in a standing posture has been derived as approximately 0.7kN (Broberg 1983), varying depending on body weight, size, age and spine location. This will increase significantly during some activities, for example, it could increase to over 6kN to when lifting a 90kg weight (Giles and Singer 1997).

The basic mechanisms of disc deformation are outlined in Figure 2.8.

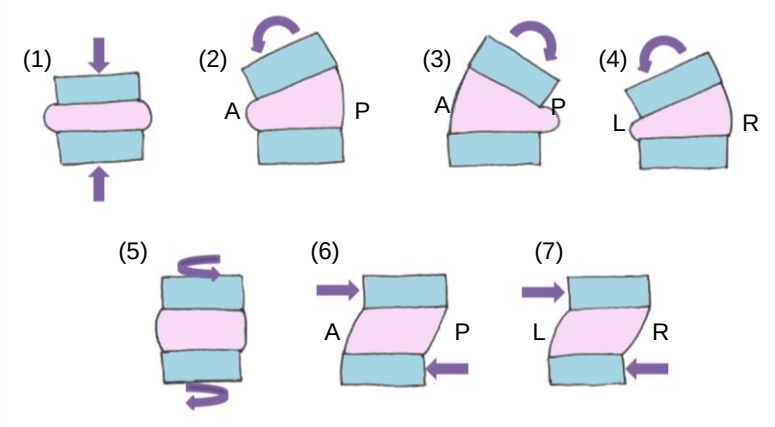

Figure 2.8 – Basic deformations of the disc. A=anterior side, P=posterior side, L=left side, R=right side.

1. *Compression* – The distance between the upper and lower endplates is reduced. All components of the disc are compressed.
2. *Flexion* – Bending forward. Anterior section of the disc experiences compression and the posterior experiences tension.
3. *Extension* – Bending backwards. Anterior section of the disc experiences tension and the posterior experiences compression.
4. *Lateral bending* – Bending to the side. One side of the disc experiences tension whilst the other is under compression.

5. *Axial rotation* – Twisting. Endplates are rotated about the vertical axis in opposing directions.
6. *Anterior-posterior shear* – the endplates are displaced in opposing directions in the coronal plane.
7. *Lateral shear* – the endplates are displaced in opposing directions in the transverse plane

In vivo the disc simultaneously experiences multiple deformation modes, as demonstrated in Broberg's experiments (1983). For example, muscles forces and body weight load the disc in compression; additional loads are applied during body movements such as flexion of the whole spine.

It was previously believed that the nucleus migrated within the disc during loading, moving anteriorly during extension and posteriorly during flexion. However, Nazari *et al.* (2011) used MRI techniques to capture how the shape of the nucleus is affected by different postures, suggesting that the nucleus deforms rather than migrates within the disc. This theory is supported by evidence from the histological study by Wade *et al.* (2010) that suggests the fibres of the nucleus are embedded in the end plates.

The change in shape of the nucleus causes the annulus to be loaded in tension during compression of the disc. Experimental observations presented by Cassidy *et al.* (1990) outlined three potential responses of the lamellar structure during disc compression:

i. Lamellae all bulge outwards.
ii. Lamellae bulge inwards at the inner annulus.
iii. Lamellae buckle at the inner annulus

The mechanism of deformation in the annulus was seen to vary with circumferential position in the disc. A relationship was drawn between the varying height of the disc and the deformation of the lamellae.

Cassidy hypothesised that as water flows out of the nucleus and inner annulus, the outward bulge of the inner annulus is relieved; they then buckle to conform to the decreased disc height. Although this does not explain the mixture of deformation modalities recorded, it is likely that the response of the annulus bulge is dependent upon the water content and compressibility of the nucleus.

A typical force-deformation curve for annulus tissue, showing the characteristic nonlinearity of the tissue is illustrated in Figure 2.9. There is an initial toe region followed by an approximately linear region of deformation.

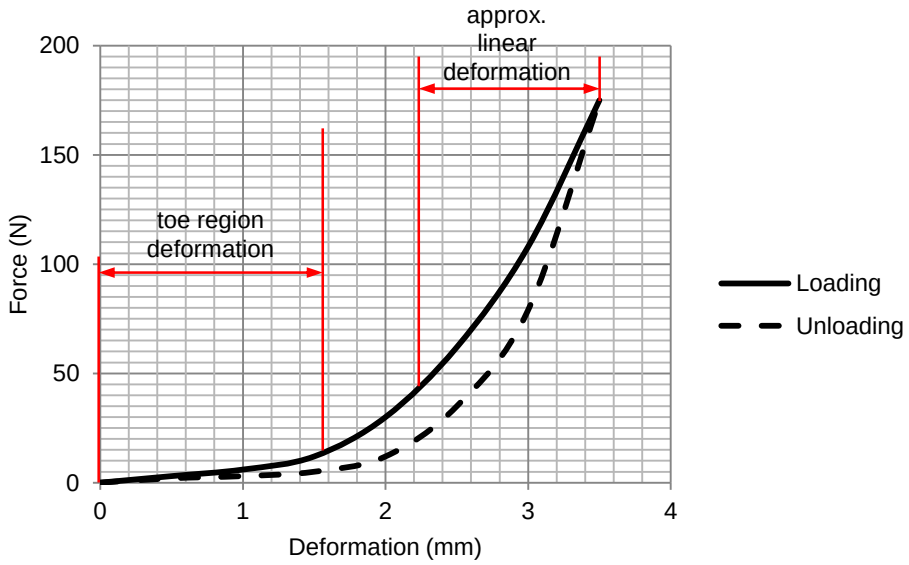

Figure 2.9 – Deformation curve for the tensile loading and unloading of annulus tissue, showing the approximated toe and linear deformation regions. Data taken from Adams and Green, 1993.

When not loaded, the collagen fibres of the annulus are crimped. As load is applied, the fibres straighten and the tisse shows a large deformation for a small applied load (Cassidy *et al.* 1990), this is known as the toe region of deformation, as illustrated in Figure 2.9. As the fibres become straightened, the material behaviour becomes more linear.

The behaviour of the tissue is not governed by the collagen fibres alone. Interactions between fibres, interlamellar interactions and other tissue constituents such as elastin and collagen bridges all contribute to the tissue mechanics. As such the mechanical behaviour of the tissue is never perfectly linear.

When loaded as an intact system, the disc illustrates similar patterns of force-deformation. Within the toe region, the Young's modulus of the total disc is approximately 2-5MPa. In the linear region this increases to approximately 20MPa (Elliott and Setton 2001; Guerin and Elliott 2006).

2.3.2 MECHANICS OF THE END PLATES

Under load, the end plates have been shown to bulge axially against the vertebral bodies. This assists in the even distribution of load through the disc and helps

reduce the strain in the annulus. The significance of this behaviour increases for short loading times when there is insufficient time for fluid flow out of the disc (i.e. the disc behaves as if incompressible) and the annulus is at greater risk of damage. Natarajan *et al.* (1994) identified the end plates as weak components in the functional spinal unit. The study found that failure of the unit under compression was always initiated in the end plate, often at the junction between annulus and end plate.

The end plates also play a role in the transient behaviour of the disc. MacLean *et al.* (2007) found that on reduction of the end plate porosity the creep and recovery time of the disc increased significantly. Fluid flow through the end plates also assists in delivery of nutrients to and removal of waste products from the disc tissues. The end plates play a fundamental role in the health of the disc and their physiological dysfunction can contribute significantly to the degeneration of the entire disc (Adams *et al.* 2002)

2.3.3 MECHANICS OF THE NUCLEUS PULPOSUS

When the spine is loaded in compression, the hydrostatic pressure of the nucleus increases and fluid is forced to flow out of the disc. The proteoglycans in the nucleus give the tissue hydrophilic properties. Thus, when load is releases from the disc, fluid flows back into the nucleus. This fluid flow occurs on a diurnal cycle; throughout the day, the disc is under compression and fluid continuously flows out of the discs. During periods of rest, the spine is under low loads and fluid can flow back into the disc. These cycles of loading and restoration can also happen over a shorter time period during cyclic loading regimes experiences during repetitive activity, such as walking.

The high water content of the nucleus results in near-incompressible properties. The low compressibility of the nucleus is important for maintaining tensile loading in the annulus.

2.3.4 TISSUE LEVEL MECHANICS OF THE ANNULUS FIBROSIS

Despite extensive research into the histology and microstructure of the annulus (Pezowicz *et al.* 2005, 2006; Schollum *et al.* 2008; Smith and Elliott 2011; Yu *et al.* 2002, 2005), there has been limited study of the mechanical function of the tissue at these intricate levels of structural detail. It is still unknown how the mechanical

function of the tissue components at the micro or nano scale relates to the function at a whole disc level (Nerurkar *et al.* 2010).

In the 1993 study by Adams and Green, the tensile stiffness and strength of annulus tissue was shown to depend on the mean length of collagen fibre bundles within the tissue, and that the mechanical behaviour of the tissue could be described using Spencer's theory of fibre reinforced composites (1984): the collagen fibres act as reinforcement to the matrix substance in which they are imbedded. In the annulus, the collagen fibres are often shorter than their critical length. This means that the fibres alone are not long enough to carry the maximum load. As tensile loads increase, the fibres separate and may eventually pull out. This separation is the governing failure mechanism of the tissue rather than failure of the fibres and gives the material its toughness and ability to absorb impact.

THE ROLE OF THE MATRIX IN DISC MECHANICS

The proteoglycan matrix of the annulus is permeable to fluids. This, combined with frictional interaction between collagen fibres and the matrix, results in time dependent material behaviour such as creep and stress relaxation (Yin and Elliott 2005). The matrix plays an important contribution to bearing loads placed on the disc; however the sharing of load between the annulus constituents is not well understood.

THE ROLE OF INTERLAMELLAR INTERACTIONS IN DISC MECHANICS

Very little is understood about the mechanisms of interlamellar interactions. The evidence presented in the literature suggests that interlamellar interactions may play more than one mechanical role in the function of annulus tissue.

Michalek *et al.* (2009) presented two potential mechanisms for interlamellar deformation, described as "sliding" in which adjacent lamellae move over one another with minimal deformation of the lamellae and "skewing", in which the interlamellar bond is strong and the lamellae deform during applied shear. These mechanisms are illustrated in Figure 2.10.

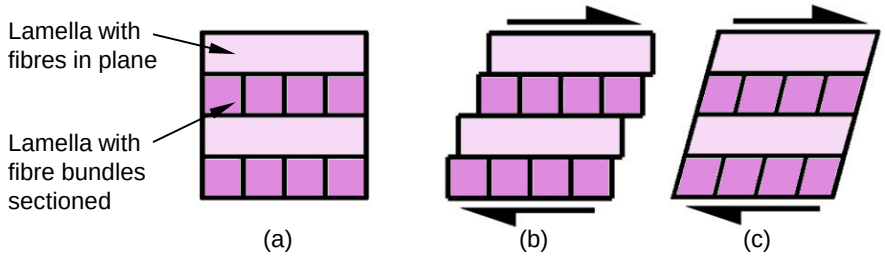

Figure 2.10 – Mechanisms of annulus shear deformation, as described by Michalek et al. (2009): (a) neutral position, (B) sliding mechanism: lamellae have moved over each other and have not deformed, (C) Skewing mechanism: lamellae have deformed and point of attachment to adjacent lamella is maintained.

Several experimental studies have attempted to examine lamellar deformation in detail. Michalek *et al.* (2009) and Gregory *et al.* (2010) used isolated specimens of annulus tissue to conduct tensile tests whereas Bruehlman *et al.* (2004) examined lamellar deformation of specimens for which the height of the disc including the anchorage of fibres in the end plates was maintained.

Michalek *et al.* (2009) observed a lack of interlamellar sliding and concluded that the skewing mechanism dominated annulus deformation. This was attributed to strong interlamellar bonds and connectivity.

Gregory *et al.* (2010) presented a tensile “lap test” in which specimens that comprised two adjacent lamellar were loaded in tensile shear with the intention of quantifying the mechanical strength of the interlamellar bond.

The specimens showed two distinct phases of deformation: firstly a bonded phase in which the lamellae deformed in tension, followed by a sliding phase when, after a certain level of tension had been applied it appeared that the interlamellar interactions failed and the two lamellae slid over one another. The interlamellar bond peak strength was found as 0.3±0.05N per mm of specimen width. It was also shown that the interlamellar bond could carry substantial load even when there had been large relative displacement between the two lamellae, supporting the skewing method presented by Michalek *et al.* (2009).

Two studies by Bruehlman *et al.* (2004a, 2004b) presented conflicting results. Confocal microscopy techniques were used to monitor the strains experienced by the cells of the annulus during loading. Intralamellar cells were relatively shielded from applied tissue strains whereas interlamellar cells were subjected to large shear strains as adjacent lamellae rotated relative to each other, suggesting that the sliding mechanism was dominant over the skewing mechanism.

By maintaining the structural integrity of the annulus tissue samples tested, the results presented by Bruehlman *et al.* could be considered more relevant to the *in vivo* mechanics of annulus deformation. The tensile deformations applied in the tests by Michalek *et al.* (2009) and Gregory *et al.* (2010) were not representative of deformations regularly experienced by the tissue *in situ*. However these tests are still a useful examination of the mechanical properties of the tissue. The investigations presented here have conducted a limited number of tests and there is still insufficient data available to draw conclusions on the mechanics of interlamellar interactions.

The mechanical roles of the major and minor collagen bridges are not understood. They may aid in maintaining cohesiveness between lamellae in the radial direction, however their disruption to the otherwise regular annulus structure could cause stress concentrations in the annulus that could be detrimental to the tissue health. This has not yet been investigated in detail.

THE ROLE OF ELASTIC FIBRES IN DISC MECHANICS

The role of elastin components of the annulus in the mechanical function of the tissue is under debate. Hypotheses have been presented based on experimental studies and the known role of elastic fibres in other dynamic biological tissues.

In 2009 Michalek *et al.* reviewed the role of elastin during shear loading of annulus tissue and found that the elastin primarily stiffened the tissue in the radial direction. It was also shown to play a role in the orthotropic damping properties of the annulus.

Elastic fibre density has been shown vary across different regions of the annulus. Smith and Fazzalari (2006) suggested that the elastin density per region was commensurate with the magnitude of the tensile deformation experienced therein.

During typical annulus tissue deformation, collagen fibres straighten and lose their crimp in the toe region. In the second stage of deformation, they re-orientate and slide over one another, during which the bulk of tissue extension occurs. Schollum *et al.* (2008) proposed that elastic fibres play a subservient role to collagen links, aiding in the restoration of collagen fibre crimp at very low stress.

However Smith and Fazzalari (2006, 2009) claim that the presence of parallel crimp in elastic fibres shows that they are not responsible for maintaining collagen crimp. Instead they suggest that elastic fibres are necessary to provide connectivity between collagen fibres and to help restore collagen alignment on removal of load.

On a larger scale, they may contribute to a similar mechanical function in restoring lamellar alignment.

The histological studies of Smith and Fazzalari (2006) observed elastic fibres that connected between adjacent lamellae, some of which were kinked at the point of insertion to the collagen bundles of the lamellae. It was postulated that relative shear movement had occurred between the lamellae, suggesting that the elastic fibres could be functioning as mechanical links between them.

Simillarly, work by Yu *et al.* in 2007, suggested that microfibrils and elastic fibres in the interlamellar space and within interlamellar bridging elements reinforce the lamellae and assist the recoil of lamellae after deformation.

2.3.5 SUMMARY

The load bearing and flexibility capabilities of the intervertebral disc are facilitated by the unique combination of tissues that comprise the structure. The incompressible, fluid-like behaviour of the nucleus is responsible for loading the annulus in tension.

Many of the characteristic qualities of the annulus tissue are determined by the lamellar structure. However, little is known about the function of this structure, particularly the interlamellar interactions. This tissue level behaviour is a vital influencing factor of the cellular environment of the tissue, which in turn affects the activity of the cell and the biology of the disc. Improved understanding of this tissue structure and mechanical behaviour could influence understanding of disc degeneration and aid the development of clinical interventions.

A network of tissue constituents is integrated with the collagen fibre bundles of the lamellae. This network encapsulates the bundles bonding them together within and between lamellae. This provides the tissue structure with elasticity, facilitating deformation through inter-bundle shear and assisting in returning tissue to its original state on the removal of load. Intralamellar interactions may play as significant a role facilitating annulus deformation as interlamellar interactions.

2.4 AGEING AND DEGENERATION OF THE DISC

Luomo *et al.* (2000) found that chronic back pain is often associated with degenerated discs. The effects of natural ageing and degeneration of the disc due

to some external injury or force are very similar. A degenerated disc will often have all of the features of an aged disc plus additional gross structural changes, especially in the annulus and cartilaginous end plates (Adams *et al.* 2002).

The level of degeneration in a disc can be classified based on its degenerative features by using scales such as the Thompson grading scheme (Thompson *et al.* 1990) or Pfirrmann scale used clinically in conjunction with magnetic resonance imaging (Pfirrmann *et al.* 2001). These scales are presented in detail in Chapter 4.

Degenerative changes in the disc result from mechanical loading combined with biochemical changes in the tissues. During daily activities, the disc experiences constant repetitive loading. Short load cycles do not allow sufficient time for the disc to fully recover and reabsorb all fluid expelled during load application, leading to cumulative damage in the disc. The nucleus loses fluid and becomes fibrous and overall the disc becomes stiffer (Iatridis *et al.* 1997; Natarajan *et al.* 2004).

The annulus changes in several ways. Degeneration of elastic fibres results in a loss of resilience and elasticity to the tissue (Smith and Fazzalari 2006). Where several individual lamellae would exist in a young disc, there may be a single, thicker lamella in an older disc (Marchand and Ahmed 1990).

Inter-bundle space increases and the distribution of fibre bundles through the annulus becomes uneven, affecting the strength of the annulus tissue. Where concentric clefts develop between adjacent lamellae, there is a loss of interlamellar cohesion and localised delamination may occur (Pezowicz *et al.* 2006).

The failure mechanism of the annulus composite structure is not well understood. Damage to the annulus is unlikely to be caused by pure compressive loading of the disc (Natarajan *et al.* 1994). Rather, it is during bending, when the disc is experiencing multiple loading regimes such as shear and torsion that the annulus becomes stretched and is most vulnerable.

2.4.1 HEALING AND REGENERATION OF THE DISC

The avascularity of the disc means that regenerative ability is limited; once degeneration has occurred it is rare for the disc to fully recover through natural rehabilitation (Di Martino *et al.* 2005). However some studies have observed regenerative changes in the disc tissue structures. Such observations could be useful in understanding the mechanical roles of tissue structures and constituents.

Long term clinical studies by Videmann *et al.* (2003) and Sharma *et al.* (2009) presented little evidence of annulus tears healing, rather further degeneration was reported. However the *in vivo* magnetic resonance imaging (MRI) methods used were not capable of capturing changes to the tissue structure at a sub-disc scale. Equally, biochemical changes associated with regeneration were not considered.

Long term studies using animal models by Lappalainen *et al.* (2003) and Schollum *et al.* (2010b) have provided opportunity for more thorough investigation of the regenerative changes in the disc. Both studies initiated lesions in the discs of sheep. The animals were kept alive for a number of months following to allow time for the discs to heal. The discs were dissected post-mortem and histological analyses revealed the changes to the disc structures.

Lappalainen *et al.* reported cell-rich granulation tissue with blood capillaries in the injured areas, indicating a regenerative response. Schollum *et al.* observed changes to the lamellar structure, including atypical major bridging structures, increased minor bridges and distorted lamellae in locations remote from the lesions. The authors suggested that some components of the annulus (specifically the bridging structures) are capable of adapting their structure as a response to changes in stress.

The regenerative responses reported by Lappalainen *et al.* and Schollum *et al.* would not have been visible on MR images and as such may have occurred in the studies by Videmann *et al.* and Sharma *et al.* without being recorded.

Although Schollum *et al.* (2010b) showed that the number of bridges increased following damage to the annulus, it was unclear from the study whether the changes in tissue structure were adaptive remodelling that was assisting the function of the disc or merely an automated response to the redistribution of stresses. In the latter case, the presence of the cross bridges may even be a stress raiser, predisposing the annulus to further damage.

2.4.2 TREATMENT METHODS FOR DISCOGENIC BACK PAIN

The most established surgical treatment for degeneration of the disc is fusion of the motion segment (Kurtz and Edidin 2006), during which two or more vertebrae are joined together using bone grafts to encourage bone tissue to grow over the space previously occupied by the disc. The procedure results in loss of motion of the joint.

The biomechanics of the spine are drastically altered at the treated segment, resulting in changes to the forces and movement experienced by segments throughout the whole spine, often leading to further damage and degeneration of soft tissues in other locations (Adams *et al.* 2002).

Recent research relating to treatment techniques are showing a trend away from fusion, towards developing motion preserving methods that better mimic the natural mechanics of the spine, facilitating mobility in the treated segment and reducing the impact in adjacent segments. At the research stage, focus has been away from total disc replacements and towards tissue preserving, early intervention nucleus replacements.

Total disc replacement (TDR) prosthetics aim to restore physical movement to the functional spinal unit where severely degenerate discs need to be removed. However the devices dramatically alter the loading of the underlying bone, causing knock-on effects in the rest of the spine. Hence, the long term benefits of TDR in preventing adjacent level disc degeneration remain unproven and post-surgical results have been disappointing (Freeman and Davenport 2006).

Nucleus replacement procedures aim to restore biomechanical function to the disc in a less surgically intrusive method than TDR while maintaining the original, functioning annulus and end plate tissue and closely imitating the material properties of the natural nucleus. The principal aim of a nucleus device or material is to restore the biomechanical function of the annulus by placing its fibres in tension (Di Martino *et al.* 2005). For the procedure to be successful, the annulus tissue must still be intact and of reasonable health.

Nucleus replacements are inserted into the disc through the annulus tissue resulting in a tissue defect which raises the risk of device migration which has been a problem in some trials (Di Martino *et al.* 2005). Curable fluids, such as hydrogels offer an attractive alternative to solid implants. They can be injected into the disc, therefore the surgical procedure is minimally invasive, aiding recovery and improving preservation of the annulus tissue, decreasing the chances of annulus defect induced degeneration and complications, provided the needle is of a small gauge (Carragee *et al.* 2009).

Although not yet in use clinically, several hydrogel nucleus replacements are in development, with research on-going as to the appropriate chemical composition to mimic natural disc tissue material properties (Vernego *et al.* 2008).

Another important design consideration is the choice between cavity filling and non-filling techniques: whether the device volume should be equal to or larger than the original nucleus (cavity filling) or smaller than the original nucleus (non-filling). Cavity filling techniques have been shown to result in high stresses in the underlying bone when they are carrying the majority of the load, but are more successful at reproducing tensile forces in the annulus tissue than non-filling devices (Di Martino *et al.* 2005).

2.4.3 DISCUSSION

Degeneration of the intervertebral disc can cause debilitating back pain. A lack of understanding of healthy tissue behaviour has limited the advancement of prostheses and treatments.

The success of all intervention techniques is dependent upon a thorough understanding of disc tissue mechanics in a healthy condition, so that devices can aspire to emulate such behaviour. For tissue preserving interventions, it is also necessary to understand the implications of techniques on the existing tissues.

2.5 IMAGING THE DISC

Image data is useful when modelling biological systems as a means of accurately capturing complex geometries in a form that can be converted into finite element models. Techniques for developing computational models from image data have been extensively developed for bone but modelling soft tissue structures to the same level of detail presents a greater challenge.

Heuer *et al.* (2008) used a laser scanner technique to spatially digitise the surface of a lumbar functional spinal unit before, during and after loading. This facilitated the calculation of the disc bulge and surface strains experienced by the outermost layer of the annulus during the different stages during the loading cycle. Although these techniques provide data for the deformation of the disc, only the external soft tissues can be monitored, no data is available for the deformation of internal tissues.

2.5.1 MICROSCOPY

A range of microscopy techniques have been used during structural analysis of the annulus tissue (Section 2.2.3). Differential interference contrast (DIC) microscopy uses polarised light and interference effects to reveal tissue fibres and structures that would not otherwise be visible without further processing of the tissue. Schollum *et al.* (2008) took serial sections of annulus tissue in different planes, illustrating the success of this technique for imaging the fibrous structure of the annulus (Figure 2.11). From these images, a three dimensional model for the tissue structures was compiled, illustrating the interaction between constituents.

Figure 2.11 – An example DIC microscopy image of the annulus structure taken from Schollum et al. (2008). The technique captures the fibrous structure of the annulus. The in-plane and sectioned lamellae are clearly visible as are the inter-lamellar connections.

Confocal microscopy was used by Bruehlman *et al.* (2004) to investigate cell strain within and between lamellae. The tissue was first stained so that the cells were highlighted in the images. The technique was successful but had a limited penetration depth of only one lamella.

The techniques used by Bruehlman *et al.* (2004) and Schollum *et al.* (2008) required the chemical fixation or staining of the tissue, altering its mechanical properties. To investigate the mechanical properties of the disc without fixing the tissue, Pezowicz *et al.* (2006a; 2006b) used DIC microscopy techniques. However, this technique still required the tissue to be cut into slices, thus the loading tests were conducted on the tissue outside of its *in vivo* mechanical environment.

Scanning acoustic microscopy has been shown to have potential for imaging the internal structures of the disc without fixation or dissection and was used to capture the fibre orientations and structures of the annulus in an unloaded and loaded state

(Rehman, 2007). However the technique could not be used to capture the whole disc.

2.5.2 COMPUTED TOPOGRAPHY

Micro computed tomography (µCT) has been used extensively in specimen specific computational modelling as a method of capturing the geometry of complex musculoskeletal systems, including spinal applications (Crawford *et al.* 2003; Liebschner *et al.* 2003, Wilcox 2007). Three dimensional greyscale images are captured using x-rays and are based on the density of the material scanned. The image greyscale, related to the material density, can be used to calculate material properties (e.g. elastic modulus) and the spatial data can be used to define the specimen specific geometry.

CT techniques have limited ability to distinguish between structures with similar densities. The low mineral content and lack of density variation in the soft tissues of the disc results makes the disc unsuitable for imaging using CT techniques.

2.5.3 MAGNETIC RESONANCE IMAGING

Magnetic resonance imaging (MRI) has been used extensively for the clinical diagnosis of disc degeneration. Pfirrmann *et al.* (2001) devised a scale for grading the degeneration of discs based on the intensity of the T2 signal, which has been related to the level of hydration of the tissue (Liess *et al.* 2002). With degeneration this became less homogenous and faded to grey, as illustrated in Figure 2.12.

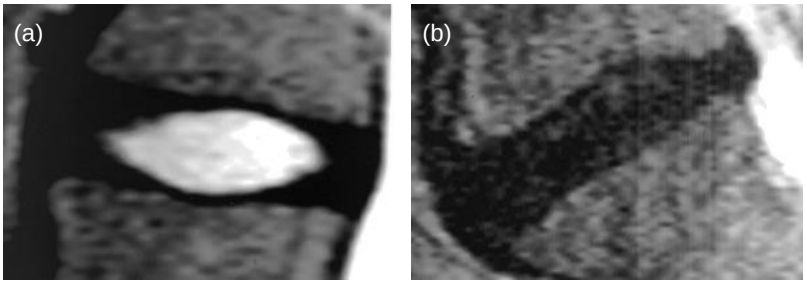

Figure 2.12 – MR images from Pfirrmann et al. (2001) of discs in vivo, showing a healthy disc (a) and a grade IV degenerated disc (b). The signal intensity from the nucleus of the healthy disc is hyperintense. For the degenerated disc, the signal is much darker and the nucleus cannot be distinguished from the annulus.

MRI was used by Sharma *et al.* (2009) to distinguish features of disc degeneration such as annulus tears. These are shown as small areas of intense signal in the annulus, as illustrated in Figure 2.13.

Figure 2.13 – MR image of a human spine, taken from Sharma et al. (2009). The arrow indicates an intense region in the annulus, assumed to be an annular tear.

Videman *et al.* (2003; 2006) also used MRI to detect signs of degeneration such as annulus tears, disc height, nucleus signal and herniations in the discs of identical twins. Both the studies by Videman and Sharma were long term *in vivo* investigations that monitored changes in degenerative discs. Both studies reported some level of recovery of degenerative discs and MRI was useful in monitoring the (partial) healing of annular tears. It was not possible to validate the findings of these studies.

Lappalainen *et al.* (2002) compared MR images of ovine discs with identifiable annular lesions taken *in vivo* with histological images from the same discs. Contrary to the studies by Videman and Sharma, the authors concluded that MRI techniques were not sensitive enough detect acute annulus injuries. It was found that the intensity of the signal did not always relate to the size of the injury casting doubt on the usefulness of MRI as a reliable method of detecting the details of annulus structure.

The level of detail captured in MR images may depend on, among other factors, the state of the specimen and whether it is *in vivo* or *in vitro*. Studies by O'Connell *et al.* (2007; 2009) used two dimensional MRI to construct a detailed map of the strain experienced across the annulus. Cadaveric discs were scanned in both an unloaded and a compressed state. Texture correlation techniques were used to determine the displacements of the tissue between scans by matching unique pixel intensity patterns, from which a strain map for the annulus was constructed.

Meakin *et al.* (2001) were successful in capturing soft tissue structures of *in vitro* discs using MRI. As their published images illustrate (Figure 2.14), the layered structure of the annulus can be identified and seen to bulge on loading of the disc. However out of 11 disc specimens, it was only possible to identify the lamellar structure on three discs, indicating that these MRI techniques are not repeatable.

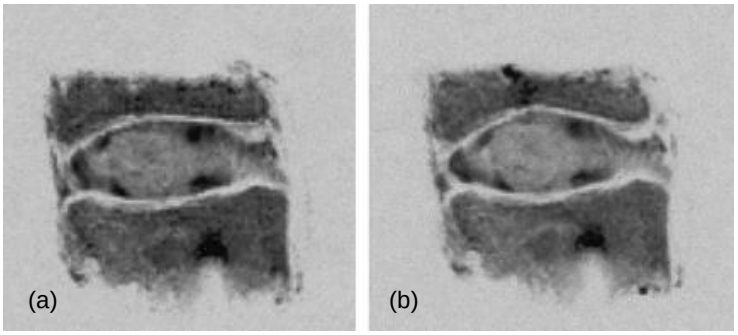

Figure 2.14 – MRI images from Meakin et al.'s study (2001) showing an in vivo disc in its unloaded (a) and compressed (b) states. With compression, the nucleus and layers of the annulus are seen to bulge radially.

The studies presented here illustrate the wide range of image quality and detail that can be captured using MR techniques, depending on the specimen set up and the scan sequence used.

MRI has been used to capture the internal structures of the disc, without disrupting the tissues. This has allowed images to be captured of the disc loaded in a way that is similar to the *in vivo* conditions and directly comparable to unloaded image data. However, the wide variation in results and the lack of verified correlation between image data (e.g. greyscale, texture) and tissue properties means that MR data must be validated for a given MR protocol before further use in biomechanical analyses.

2.6 COMPUTATIONAL ANALYSIS OF THE DISC

The first published finite element model of the intervertebral disc was by Belytschko *et al.* in 1974. This analysis modelled the annulus as a linear orthotropic material and assumed that the disc was axi-symmetric. Since then, models have developed extensively to include a wide range of the disc's unique and complex characteristics, although simplistic models of the disc, if robustly developed, reviewed and designed relative to the purposes of study, are still useful tools for analysis.

A number of approaches and techniques exist that may be used to model the disc. The complexity of these approaches varies and will depend on the intended use of

the model. The disc may be represented as a complete unit; with or without separate representation of the tissue components (nucleus, annulus, end plate, ligaments, etc.) or these components may be considered in isolation from surrounding components.

Model complexity is increasing, as researchers strive towards an ever closer representation of the physiological function of the disc. As the complexity of models increases, so does the time and computer power required to create and solve them, reducing their practicality for all applications. Simplifications can be beneficial and may be made without losing necessary detail of the features that are most significant to the aims of the study.

FE models of the disc can be developed to represent an individual specimen or a generalised model, intended to represent an "average" case. It is often convenient to take data from a specific specimen, so that models may be created using imaging data and validated directly with experimental data. Due to inter-specimen variability, the performance of such models will not be applicable to other specimens.

Specimen specific FE analysis of the spinal components is often based upon digitised images generated using computed tomography (CT) techniques that can capture the highly irregular geometries. Voxel information obtained from scans can be converted directly into finite elements. This is a technique that has been extensively used to study the bony elements of the spine (Crawford *et al.* 2003; Liebschner *et al.* 2003; Wilcox 2007).

To include specimen specific geometry of the soft tissues, CT image data can be combined with MR image data and reconstructed into one data set, as demonstrated by Schmidt *et al.* (2006) and Li and Wang (2006), although these techniques are in their infancy and as such to date have only been used to capture gross, external geometries used for model construction. Such techniques have the potential to capture increased levels of detail that could aid with the construction of more complex models as well as be used for direct model validation.

Creating a generalised model requires assumptions to make a useful representation of a population. Espino *et al.* (2003) suggested the use of statistical techniques to incorporate variability into FEA. This approach allows a confidence interval to be placed on predictions, which may help make the model more useful in the application to specific patient diagnosis.

2.6.1 MODEL DEVELOPMENT PROCESS

A complete understanding of the behaviour of the disc requires a combination of computational models, *in vivo* and *in vitro* studies. It is essential that models developed are accurately and critically related to the natural function of the disc. This should be conducted in parallel with, and at every stage of model development. This process was outlined in the study by Anderson *et al.* (2007) in which the stages of model verification, sensitivity analysis and validation were discussed. The review paper by Jones and Wilcox (2008) related these aspects of model development to studies of the spine.

CALIBRATION

For many biological materials, tissue properties are often unknown and may behave differently if tested in isolation to surrounding tissues and structures. One approach to developing appropriate material models to represent tissue mechanics is to 'tune' the properties in the model to match to experimental data (*in vivo* or *in vitro*). This process is often referred to as calibration.

The process of calibration should be conducted in isolation to that of model validation. The goal of calibration is to find the ideal material parameter combination so that the model is designed to behave in a manner that is reasonably close to that measured *in vitro*. This process was outlined in relation to the disc by Schmidt *et al.* (2006). In this study, an optimisation algorithm was formulated in order to determine the relationship between behaviour of the matrix and the fibres of the annulus.

VERIFICATION

The process of verification is conducted to ensure the computational model accurately predicts the results of the theoretical model on which it is based (Viceconti *et al.* 2005). For most commercial software, the code used has already been verified and this process documented. In this case, the most important verification step is an assessment of the mesh resolution, completed by conducting a mesh convergence test. Automated methods can be used for meshing; however the effect of mesh refinement on results of particular interest should be assessed specifically.

SENSITIVITY

A thorough assessment of the sensitivity of model results with respect to changes to input parameters should be undertaken for all finite element analyses. This provides

information on the significance of the inputs and thus also their potential contribution to the system. The complex loading patterns and the relative lack of knowledge of tissue properties in the disc means that a detailed sensitivity analysis is essential to achieve an accurate model (Jones and Wilcox 2008).

VALIDATION

Following calibration, verification and sensitivity analysis of the model, experimental results should be used to ensure that the results outputted from the model are in agreement with the physiological behaviour of the disc under conditions of relevance to the study.

The method of validation should be relevant to the aims of the study. For example, a model that has been validated at the whole disc level may not accurately represent the tissue level mechanics (Klisch and Lotz 1999). Ideally data from a variety of experimental deformations should be used for validation (Klisch and Lotz 1999; Peng *et al.* 2006). For example, compressive behaviour of the disc is affected by a range of factors such as geometric shape, loading conditions and fibre angle. To consider only the effects of the stress-strain relationship would be incomplete (Peng *et al.* 2006).

CALIBRATION AND VALIDATION OF DISC MODELS

Some methods of calibrating and validating models of the disc with respect to experimental data are presented in Table 2.1.

Study	Calibration	Validation
Belytschko (1974)	Annulus model calibrated to agree with experimental data by Rolander (1966)	FE performance compared to *in vitro* data by Markolf (1971; 1972), showing FE axial stiffness to be within the experimental range.
Lin *et al.* (1978)	Optimisation method to establish annulus material properties based on *in vitro* study of 12 specimens.	Same experimental data set used for validation, agreement range of 0.1 – 9% for the 12 specimens.
Ueno *et al.* (1987)	Material properties all based on data from the literature.	Brief comparison with experimental studies in the literature. Differences between FE and experimental data are attributed to degeneration and removal of facets.
Shirazi-Adl *et al.* (1984; 1989)	Material properties based on previous studies by the same author.	Records "general agreement" with *in vitro* measurements from studies in the literature – no further discussion presented.
Schmidt *et al.* (2005; 2007)	Calibration method developed to hone annulus material properties based on individual specimen performance *in vitro*.	Compares the performance of the calibrated and non-calibrated models to *in vitro* data collected by the same authors.
Strange *et al.* (2010)	Uses material models based on Schmidt *et al.* (2007).	Reports consistency of FE results with experimental data in the literature citing model performance as "within the range of experimental values"

Table 2.1 – Summary of calibration and validation methods used by a selection of studies.

Due to the highly variable nature of soft tissue, there is often a large range in experimental data. Thus, there is not one agreed threshold at which stage a model can be confirmed as validated. The validation process encompasses some degree of discretion. The aim of validation should be to realistically represent the important characteristics of the natural tissues. The level of agreement between the tissue and the model will depend on the aims of the study.

Many studies, as outlined in Table 2.1, have not included thorough validation procedures and instead quote general agreement with *in vitro* measurements without giving full details (Shirazi-Adl 1984, 1989; Ueno *et al.* 1987; Strange 2010). General statements regarding validation are of little practical use due to the wide range of disc mechanics recorded *in vitro* (Figure 2.16 and Figure 2.17).

The validation of simulations can often appear secondary to the particular interests or focus of the study. In studies by Schmidt *et al.* (2005; 2007) however, the calibration and validation of the FE models is the main focus of the model. Validation is conducted against *in vitro* data (based on six specimens, Heur *et al.* 2008) with the same boundary conditions and loading as the computational models. The resulting models had high levels of reliability and when the optimisation method was used for the calibration of annulus material properties, the models had excellent (>90%) agreement.

USE OF DATA FROM THE LITERATURE

A wide range of experimental studies into the biomechanical function of the disc have been published. If used with consideration, this can contribute towards the development of models, particularly in the initial honing of material performance. Computational studies should always be validated against experimental data and not against existing models in which case there is no direct link to the physiological performance of the system being modelled.

Two typical deformation curves for disc under uni-axial compression taken from the literature are shown in Figure 2.15.

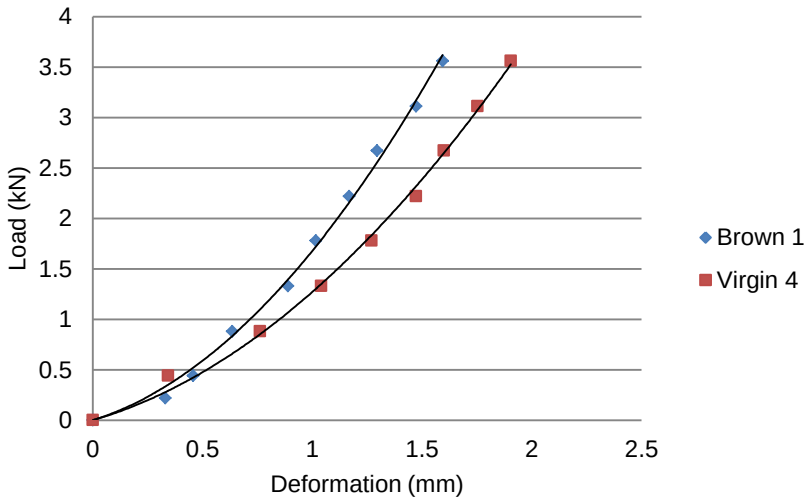

Figure 2.15 – Example specimen deformation curves taken from two experimental studies (Virgin 1951; Brown, Hansen et al. 1957). Each data set is from an individual specimen test.

When a larger number of studies are considered, the significance of result variability is illustrated. Data from four experimental studies with a total of 11 specimens is presented in Figure 2.16 and Figure 2.17; a linear approximation to the toe region deformations is shown in Figure 2.16 and an approximation of the linear region is shown in Figure 2.17. The studies reviewed were those by: Virgin (1951); Brown *et al.* (1957); Markolf (1972) and Markolf and Morris (1974). These studies were extensively cited in the literature for validation of previous FEA studies (Shirazi-Adl *et al.* 1984; Lu *et al.* 1996; Meakin and Hukins 2001). All data presented here was for experimental FSU specimens with the posterior elements removed and loaded under axial compression.

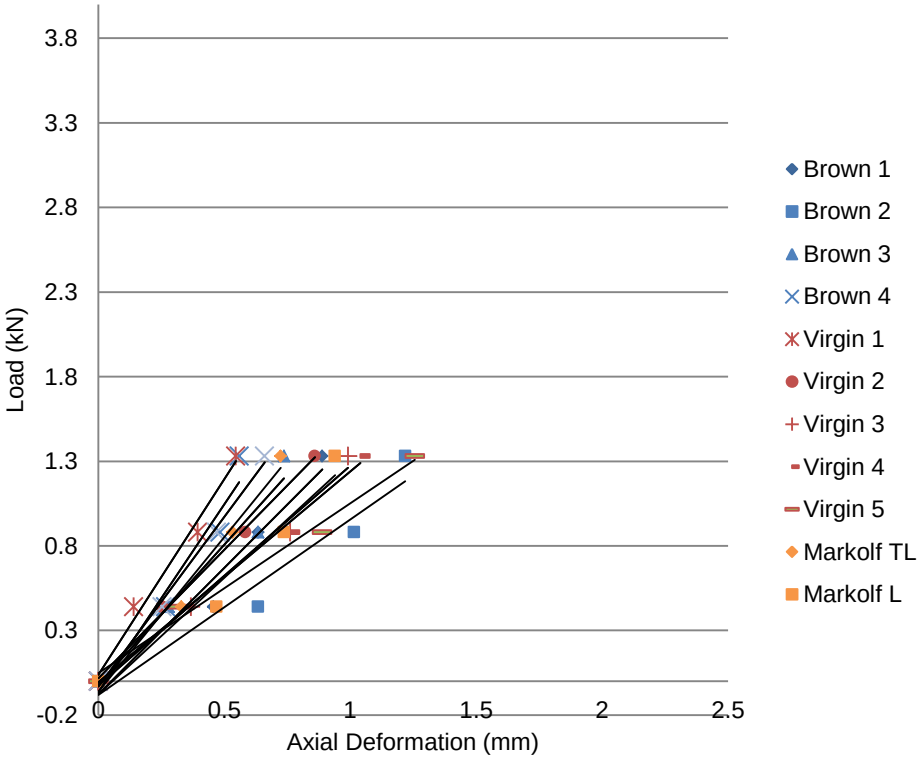

Figure 2.16 - stiffness of specimens tested in experimental studies - toe region of deformation curve. each curve represents a single specimen. multiple specimens were taken from some studies.

In this study, the toe region is defined as the initial, non-linear stage of deformation. This includes deformation due to fibre uncrimping and includes the initial stages of fibre stretch to establish a bilinear material model of disc deformation.

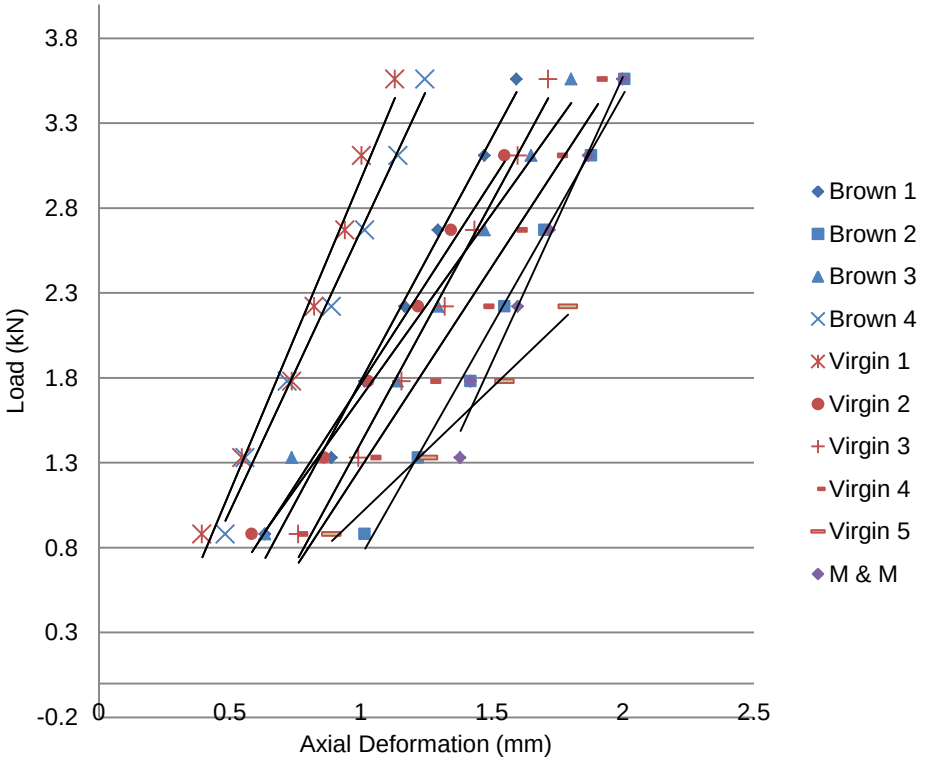

Figure 2.17 - stiffness of specimens tested in experimental studies - linear region of deformation curve. each curve represents a single specimen. multiple specimens were taken from some studies.

The spread of data in Figure 2.16 and Figure 2.17 is caused by inter-specimen variation due to, among other factors, age, sex, species, hydration, storage and loading history. A similar level of spread is observed for other physiological parameters, such as radial bulge, as reported by O'Connell *et al.* (2007), illustrated in Figure 2.18.

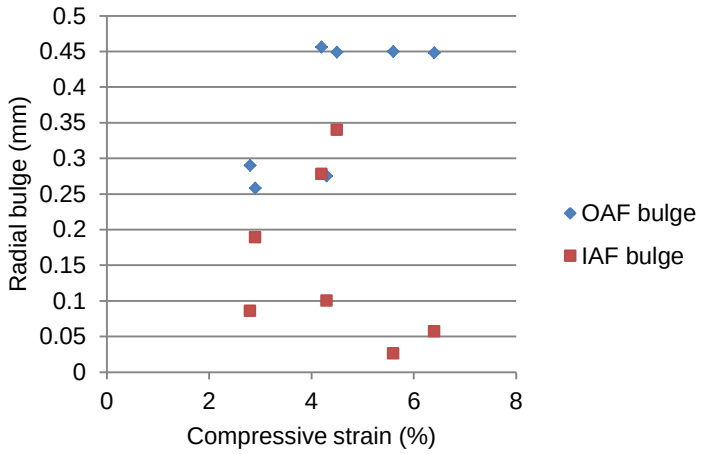

Figure 2.18 – Radial bulge at the inner and outer annulus varying with respect to applied compressive load for seven human disc specimens, as reported by O'Connell et al. al. (2007).

2.6.2 MATERIAL PROPERTY ASSIGNMENT

The accurate assignment of material parameters to model elements is one of the most critical stages in developing models of the disc. Adams *et al.* (2002) and Natarajan *et al.* (2004) both reported that material property has more effect on mechanical behaviour than the geometry of the disc. The development of accurate parameters has been the focus of many studies. To understand and replicate the complex mechanical characteristics of the disc, the level of structural detail and the assumptions about material properties are important. A more detailed model could be more accurate, however the greater the level of detail in the model, the more computationally expensive it becomes. With this increase in detail there may also be an increase in the number of unknown parameters in the model, requiring development of calibration and validation methods. Although this has been investigated in models of annulus tissue samples (Elliott and Setton 2000, 2001; Gregory *et al.* 2009) this level of tissue detail has not been implemented into a full disc model.

As with all biological tissues, every component of the disc exhibits non-linear behaviour; materials exhibit stiffening with increasing strain. However, in some situations and simulations, linear assumptions can be reasonably made to simplify the model or to answer simple questions (Adams *et al.* 2002). Additionally, *in vivo*, many biological tissues are under pre-strain before loaded during activity so may be operating within a linear range. Thorough assessment must be conducted to ensure that if linear assumptions are to be made during model simplification, they will not adversely affect the reliability of the results. This is dependent upon the specifics of the study, for example Fagan *et al.* (2002) conducted a sensitivity analysis that found material nonlinearity was more important during flexion and torsion than compression.

Biphasic material models have been developed with the aim of representing the fluid flow and volumetric changes that occur during the loading of the disc *in vivo*. Such aspects of disc mechanical behaviour are difficult to control experimentally; achieving the correct conditions in the disc surroundings and measuring fluid flow are extremely challenging. Thus using computational simulations provide a convenient alternative to *in vitro* or *in vivo* methods for studying these phenomena (Natarajan *et al.* 2004).

A poroelastic material model has two distinct phases: a fluid phase and a permeable solid phase. In the disc, the fluid phase is the interstitial fluid and the solid phase

the collagen, proteoglycan and protein constituents. Using a poroelastic material model facilitates the modelling of the volumetric response of the disc to mechanical loading and unloading and the fluid flow into and out of the disc (Goel *et al.* 1995). It also facilitates the characterisation of the viscoelastic properties of the tissue, which is dependent on the permeability of the solid phase.

It has been argued that when modelling short load times only, incompressibility assumptions may be justified, provided the load time is short enough to ensure that there would not be fluid to flow out of the structure (Brinckmann *et al.* 1983). The decision to include biphasic properties in a model should be based on the aims of the study and the loading conditions that will be investigated.

Boundary conditions that best represent disc mechanics *in vivo* can be difficult to define. The following criteria should be considered: physiologic boundary conditions (attachments to muscles, ligaments, ribs, etc.), muscle forces, pre-stressed conditions, kinematic constraints, load history and load rate (Adams *et al.* 2002). Boundary conditions must be considered relative to the situation of interest, it is not necessary to recreate every possible boundary condition for every analysis. Many FEA studies of the FSU, such as that presented by Meakin and Hukins (2001) impose a clamped condition on the inferior vertebra and apply all loads and displacements to the top vertebrae, assuming symmetrical loading through the longitudinal axis of the spine in the transverse plane.

MODELLING THE NUCLEUS PULPOSUS

Fagan *et al.* (2002) outlined three possible ways of modelling the nucleus:

i) incompressible solid,
ii) poroelastic solid,
iii) fluid.

Assuming incompressibility is straightforward; however, does not take into account the effect of volumetric change on bulk properties and restricts the inclusion of poroelastic effects. Table 2.2 summarises some of the approaches used in the literature.

Study	Nucleus modelling approach
Kurowski and Kubo (1986)	Hydrostatic pressure applied to walls of annulus
Shirazi-Adl (1989)	Inviscid incompressible fluid
Natarajan *et al.* (1994)	Fluid, B=2210MPa
Argoubi and ShiraziAdl (1996)	Poroelastic material. E=1.5MPa, v=0.1
Meakin and Hukins (2001)	Fluid, B=1720MPa
Schmidt *et al.* (2006)	Incompressible solid, E=2MPa, v=0.4999
Strange *et al.* (2010)	Hyperelastic Mooney-Rivlin model

Table 2.2 – Examples method for modelling the nucleus

When modelling the nucleus it is necessary to accurately consider the defining boundaries of the nucleus and its size relative to the disc (Adams *et al.* 2002). However, this boundary can be difficult to distinguish as discussed previously in Section 2.2.

MODELLING THE END PLATES

Material properties for the end plates often vary widely between studies, however, there has been little discussion regarding the most appropriate approach. Some studies model only one of either the cartilage or bony portion of the end plates whereas others incorporate both material models. Table 2.3 summarises some of the approaches used in the literature.

Study	End plate modelling approach
Shirazi-Adl (1989)	Bony EP covers annulus (E=12,000MPa, v=0.3), cartilaginous EP covers nucleus (E=24MPa, v=0.4)
Lu *et al.* (1996)	Linear elastic model, E=23.8MPa, v=0.4
Schmidt *et al.* (2010)	Bony layer (E=10,000MPa, v=0.3) and cartilaginous layer (E=5, v=0.1). Poroelastic material models for both.
Swider *et al.* (2010)	Linear isotropic model of the cartilaginous layer only with E=3MPa, v=0.1

Table 2.3 - Summary of modelling approaches used to represent the end plates

When modelling only the disc as opposed to the entire FSU, it is often the case that the end plates are not included in the model, and the load is instead applied directly to the nucleus and annulus (Meakin and Hukins 2001).

2.6.3 DISCUSSION

Both generalised and specimen specific models can be useful tools in understanding the function of the intervertebral disc. For all methods, it is essential that computational simulations are consistently related to physiological systems for accurate calibration and validation.

Specimen specific models of the disc lag in development behind those of the bony components of the spine due to difficulties in accurately imaging the soft tissues. MR imaging techniques have shown potential for capturing details of the tissue structure *in vivo* (Videmann *et al.* 2006; Sharma *et al.* 2009), suggesting that techniques could be developed for *in vitro* studies that may achieve clearer detail. Such image data could then be used to construct specimen specific models with that could be validated directly with experimental results. Promising results were presented by O'Connell *et al.* (2006, 2009); that illustrated the potential for MRI to capture increased levels of soft tissue structure data for the disc. However the image data was not translated into FE analysis. MR image quality is dependent on many factors. If MR imaging is to be used to understand the soft tissue structure, sequences must be developed and validated thoroughly.

Many computational studies of the disc have focussed on developing sophisticated material models to represent characteristic features of the tissue mechanics such as fluid flow, biphasic properties and hyperelasticity. However, the implications of structural parameters are still not well understood and a necessary minimum level of structural detail required has not been established. These considerations will have implications in the development of specimen specific models and the assumptions made during this process.

2.7 MODELLING THE ANNULUS FIBROSIS

Techniques for modelling the annulus can be broadly grouped into two categories, based on the method of model construction. The tissue can be represented as a

homogeneous continuum or as discrete fibres embedded in a matrix. For the purpose of this thesis, these methods are referred to as the "homogenised" and "structural" modelling methods respectively. Some element construction approaches for these methods are illustrated schematically in Figure 2.19.

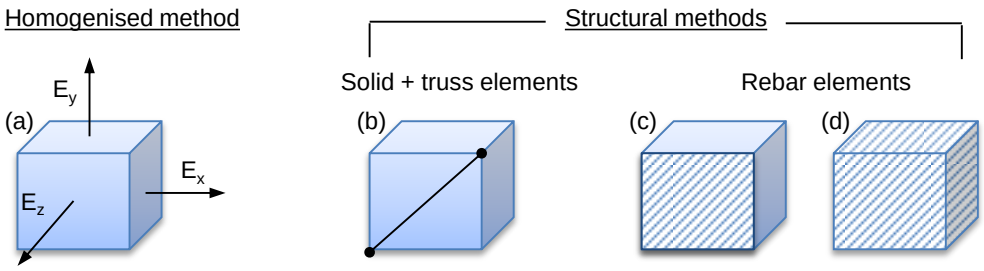

Figure 2.19 – Schematic diagram to illustrate different approaches for annulus element construction: (a) homogenised element for which orthotropic material properties are defined; (b) 3D solid elements and 1D truss or cable elements are combined to represent the matrix and fibres respectively; (c) rebar model in which a membrane of 2D rebar elements is combined with 3D matrix elements; (d) 3D rebar element.

2.7.1 HOMOGENISED MODELLING METHODS

Homogenisation is the method of representing a heterogeneous material as a homogeneous continuum. Anisotropic properties can be assigned based on axes defined relevant to fibre orientation. Within the element, there is no distinction between the matrix and the fibres, as presented in models by Shirazi-Adl (1989) and Nerurkar *et al.* (2008). It is assumed that the microstructure is repetitive, and a length scale is determined. The behaviour of the material at a scale below this cannot be directly predicted from the model (Prendergast 1997).

A range of material models have been developed to represent the characteristic material properties of the annulus, such as hyperelasticity, nonlinearity and anisotropy. Many studies have focused on refining material models in order to produce a model that performs with accurate representation of the natural function of the disc at a macro level (Guo *et al.* 2006; Peng *et al.* 2006; Guerin and Elliott 2007). The complexity of the material model implemented should be suited to the aims and interests of the model and consideration should be taken to accurately represent the characteristic annulus material behaviour.

An alternative approach is to assign a fibre reinforced composite material model to the elements of the annulus, in which parameters are defined to represent the properties of the annulus fibres and matrix and the percentage volume of these constituents (see Section 2.3.4) (Guo *et al.* 2006; Wu and Yao 1976).

Some examples of homogenised modelling methods used for the annulus in previous studies are presented in Table 2.4

Study	**annulus modelling approach**
Lin *et al.* (1978)	Optimisation scheme to establish linear orthotropic material properties for the annulus.
Shirazi-Adl (1989)	Linear elastic orthotropic material model.
Guo *et al.* (2006)	Fibre reinforced composites-based hyperelastic constitutive model.
Guerin and Elliott (2007)	Nonlinear, anisotropic, hyperelastic material model.
Nerurkar *et al.* (2008)	Hyperelastic, nonlinear material model represented by a scalar strain energy density function.

Table 2.4 - Summary of homogenised modelling approaches used to represent the annulus.

2.7.2 STRUCTURALLY REPRESENTATIVE MODELS

When modelling the annulus using structural techniques, the constituents of the tissue are modelled individually; with separate elements to represent the fibres and the matrix of the annulus, as illustrated schematically in Figure 2.19.

When using one dimensional elements to represent the fibres of the annulus, they are distributed among three dimensional elements representing the matrix and nodes are shared between the two element types, such as the model presented by Shirazi-Adl *et al.* (1984) and Schmidt *et al.* (2006). The orientation of the fibres is defined by the angle of the 1D elements. The distribution, orientation and properties of the 1D elements can be varied to represent the variation in collagen fibres across the natural tissue.

An alternative approach to implementing a structural model is to use pre-defined “rebar” elements available in many commercially available FEA software packages. These elements allow the properties and distribution of fibres embedded in a matrix to be defined. This presents an efficient method of creating a heterogeneous, anisotropic, fibre reinforced material model and has been successfully implemented as a material model for the annulus in studies by Goel *et al.* (1995) and Strange *et al.* (2010).

However these elements are not suitable for all applications. The orientation, size, spacing and properties of the fibres can be easily defined within an element, but further information about the architecture cannot be included such as, connections and interactions between lamellae and interactions between the material constituents cannot be extracted from results.

Study	**annulus modelling approach**
Shirazi-Adl *et al.* (1984)	1D cable elements distributed through eight layers of 3D matrix elements.
Goel *et al.* (1995)	3D rebar elements. Used to model sequential degeneration through the annulus tissue.
McNally and Arridge (1995)	Single membrane to represent fibres encasing the solid matrix.
Schmidt *et al.* (2006)	3D spring elements embedded in 3D elements assigned Mooney-Rivlin strain energy formulation.
Strange *et al.* (2010)	Four membrane layers of rebar elements to represent annulus fibres embedded within homogeneous 3D matrix elements.

Table 2.5 - Summary of structural modelling approaches used to represent the annulus.

2.7.3 COMPARISON OF TECHNIQUES

Shirazi-Adl *et al.* (1989) conducted a study to compare the homogeneous and structural modelling techniques. Two models were developed for the same specimen data using the different approaches. The results from the models were compared against each other and against physical validation data, with significant differences recorded for the stress distributions between the two models. For the structural model, in the fibre direction, the fibres and matrix experienced different stresses, even though the strains were identical, representative of the annulus behaviour *in vivo*. The homogenous model could not replicate this behaviour and so it was suggested that the structural model yielded a more realistic simulation of the behaviour of the annulus tissue.

However, the superior modelling approach is dependent upon the aims of the study in question as both techniques present advantages and complications.

Implementation of a homogenised material model is simple and efficient and the parameters can be varied with ease. Conversely, the construction and variation of a structural model is complex and time consuming.

Eberlein *et al.* (2000) illustrated the use of a homogeneous annulus with a fibre-reinforced material model, allowed the arbitrary adjustment of fibre angle and properties, as opposed to the time consuming process of altering individual truss or spring elements previously used to model fibres in structural models.

The development of homogeneous material models can be related directly to experimental data for the gross behaviour of the annulus tissue. In a structural model, the material properties for the fibres and matrix must be individually defined. These properties and others such as fibre volume fraction and fibre-matrix interactions, are difficult to measure experimentally. Instead, these parameters must be approximated through extrapolation of material laws to apply them at a micro-structural level. Thus, calibration with *in vitro* data is not possible and these assumptions could lead to significant errors, particularly in the application of theoretical predictions to scales smaller than those explicitly included in the development of the material law (Klisch and Lotz 1999).

For a homogeneous model to represent the anisotropic characteristics of the annulus, it is necessary to define the material model relative to a set of defined axes. This works well for cylindrical models, however when more complex annulus geometries are considered, a single cylindrical coordinate system may not be applicable to the whole model. By defining the orientation of fibres individually, the structural method can be used to model more complex annulus geometries and allows the fibre orientation, abundance and properties to be varied through the annulus.

Both the homogenised and structural method can be used to represent the regional variations of the annulus. For homogenised models, the annulus can be split into sections with varying parameters applied to each. Adding regional variation to structural models may require the variation of individual elements.

The individual representation of tissue constituents in the structural method implies that increased detail can be included regarding the architecture of the tissue. In the homogenised approach, a repetitive structure must be assumed with a defined length scale, below which tissue behaviour cannot be analysed.

2.7.4 MODELLING THE ANNULUS FIBROSIS MICROSTRUCTURE

Annulus mechanics are now well understood on a macro-scale and the knowledge of annulus histology is improving. However, the literature is lacking a multi-scale

understanding of the tissue mechanics and an accurate model of the annulus behaviour at a lamellar scale. How the loading of annulus tissue effects interlamellar and fibrillar mechanics is not well understood and studies have suggested that simplified, gross models of the disc do not represent the actual tissue behaviour of the annulus (Michalek *et al.* 2009; Lewis *et al.* 2008).

Material models for the annulus components may be validated on either a micro or a macroscopic scale but very rarely for both regimes (Adams *et al.* 2002). Assumptions may not be simultaneously valid on both scales.

In 2006, Caner and Carol developed a “microplane” model to represent the fibre reinforced soft tissue of blood vessels. Microplane models apply homogenised models at a smaller scale than conventional macro-scale models. The aim was to reproduce the physics of the material more accurately by representing the behaviour of tissue constituents in vectoral form on planes of various orientations. Microplane models can account for more complex material behaviour, beyond the scope of macro-scale homogenised models, facilitating variation of fibre distributions, constituent interactions and shear within the material.

In 2007, Caner *et al.* used this technique to model an isolated sample of human annulus tissue. When shear interactions were included in the model, the agreement with experimental data from the literature was improved.

INTERLAMELLAR INTERACTIONS

The mechanical contribution of interlamellar interactions to the deformation of the annulus has not been considered in detail in FE analysis of the disc. In many cases, the contributions of interlamellar interactions have been considered negligible to the gross deformations of the tissue.

Following scrutiny of Galante’s work (1967), Broberg (1983) indicated that the fibre layer anisotropy can be reasonably represented without consideration of interlamellar interactions.

Wagner and Lotz (2004) hypothesised that the interactions between collagen fibres within a lamellae would be much stronger and more numerous due to the proximity of the fibres to one another. Thus the interlamellar interactions were assumed to be negligible by comparison, without further investigation into their mechanical roles.

Following advances in computational capabilities and developments in histological knowledge (Adams and Green 1993; Tsuji *et al.* 1993; Schollum *et al.* 2008), it would be reasonable and appropriate to now consider these interactions in FEA.

McNally and Arridge (1995) used two variations of a model to represent extreme cases of the interactions between adjacent fibre layers: (i) the layers were fully independent of each other (ii) pin-joints were implemented between adjacent layers. Thus adjacent lamellae were either totally independent or totally dependent of one another. The authors discussed that the most realistic solution would be somewhere between these two extremes, the microstructure of the tissue was not investigated further.

2.7.5 DISCUSSION

Given the complexity of the annulus tissue, many assumptions and simplifications are required in the development of computational simulations. Model development should focus on how assumptions made effect the accuracy of the model. This should consistently be related back to experimental performance of the tissue.

Both the homogenisation and structural methods of modelling the annulus can be useful, yet both have inherent disadvantages. The modelling approaches adopted must be appropriate for the end purpose of the model.

Homogenised models have been shown to effectively and efficiently facilitate mechanics of the joint on a macro-scale. If a model is required to assess the mechanical environment of the disc at a smaller scale, increased detail is required in the model and the technique adopted must be appropriate for this. Structural methods may be suitable as different element types can be employed to represent the contrasting behaviour of tissue constituents. However the technique should be analysed for potential model development at a smaller scale when considering sub-disc level tissue mechanics. For example, when rebar elements are used; there is little or no control available over fibre connections. Using a model constructed from a combination of 1D and 3D elements may make model variation difficult and time consuming and may not be a computationally efficient approach to modelling an intricate level of tissue detail.

FE analysis of the annulus is developing to address microstructure mechanics, but existing models of the annulus do not represent the recent developments made regarding the histology and microstructure of the annulus (as discussed in Section

2.2.3). Much of the structural architecture of the annulus has been neglected in past analyses in favour of capturing the characteristic anisotropic and inhomogeneous behaviour of the disc on a macro scale through contributions from the fibres and matrix alone.

Models that do seek to include tissue level mechanical behaviour are often incomplete, and tend to focus on a single feature of the microstructure rather that encapsulating the characteristic behaviour of all of the features. For example, Guerin and Elliott (2007) review and quantify the intralamellar interactions, but the model does not account for interactions between adjacent lamellae or other contributing factors such as elastic fibres.

A promising approach for developing the level of detail of annulus models is to analyse isolated samples of tissue. This method allows the finer details of the tissue to be analysed and provides opportunity for direct validation against experimental data for methods such as micro-tensile and shear loading tests observed under microscopy.

The use of such methods requires additional considerations. Analyses of tissue samples cannot be used to investigate the intrinsic strength of the annulus as a whole. Sectioning of annulus tissue results in substantial destruction of crucial structural continuity of the tissue in its intact, *in vivo* form and it is impossible to accurately address the question of absolute strength without preserving in situ embedding of lamellar fibres in vertebral end plates (Pezowicz *et al.* 2006). This principle transposes to FEA of the tissue. If a detailed section of the tissue is to be modelled independent of the disc system, care must be taken in assigning boundary conditions and loads and in the interpretation of results relative to *in vivo* conditions.

However such methods have the potential to improve understanding of annulus tissue level mechanics, and could aid the development of a sophisticated annulus material model. If implemented into macro-scale disc models understanding of healthy tissue function may be improved.

2.8 CHAPTER SUMMARY

The disc is a complex and unique structure which has been described in detail through histological studies however these alone cannot decipher tissue mechanics. Computational analysis could be useful in testing proposed mechanisms of tissue

deformations and may assist in developing understanding of how the tissue behaves mechanically.

A greater understanding of the sensitivity of the disc system to how the tissue structures are represented would be useful as this area of model development has not been considered in detail in previous analyses.

The findings and imaging techniques presented by histological investigations could be useful in generating computational analyses of the annulus tissue that consider the lamellar structure in finer detail than previously studied.

MR imaging techniques have shown potential for use in the development of specimen specific models with increased levels of soft tissue structural detail. If developed, such techniques could also facilitate improved one-to-one validation of simulations with experimental data. The further development of specimen specific models would also be useful in understanding variation between specimens and how this affects the mechanical function of the disc system.

Improved simulations of the disc system could help investigate the implications of disc interventions and may aid in the development of discogenic degeneration and pain.

3 GENERALISED MODELS OF THE DISC

A generalised model of the disc was developed based on biomechanical performance targets from the literature review to represent the average case for a wide range of human lumbar discs in terms of size, age and gender. The model was used as a tool to analyse the sensitivity of the disc system to a number of parameters related to the soft tissue structures, such as the size of the nucleus and the representation of the annulus lamellar structure. The results showed that, of the parameters tested, the radial properties of the disc were more sensitive to the changes than the axial stiffness. The study gave weight to the hypothesis that the representation of soft tissue structures, such as the interlamellar interactions, has a considerable effect on the performance of disc models at a micro and macro scale. This will have implications on specimen specific models. Improved representation of these features could result in more accurate characterisation of disc mechanics.

3.1 INTRODUCTION

Generalised models of the disc assume simplified geometries and components to represent an "average" case. This approach may compromise the levels of accuracy of the model, but has a major benefit over specimen specific models in that one model can be relevant to a range of discs and spines as opposed to a single case.

The development of a generalised model of the disc necessitates many decisions on how to simplify the many parameters of the disc when selecting properties and geometries from the wide range seen within natural variation. Calibration and validation of generalised models present additional challenges: even with population limitations in place (e.g. age or sex), there is still a wide variability in disc mechanics, as discussed in Chapter 2.

This study focused on the parameters associated with the soft tissue structural organisation and geometry of the disc. These are aspects of the disc that have not been sufficiently addressed in published generalised models of the disc. Soft tissue structural variables such as the size, shape and position of the nucleus and the representation of the lamellar structure of the annulus could play significant roles in the macro-scale performance of disc models.

The aim of this Chapter was to develop a simplistic model of the disc to be used as a method of guidance for developing more complex generalised and specimen specific models of the disc. The sensitivity of the model to changes in soft tissue

structural parameters was evaluated with the intention of understanding the implications for specimen specific modelling.

3.2 CONTROL MODEL DEVELOPMENT

A simplified model of the disc and half of each adjacent vertebral bodies was developed as a control case, against which parametric variations could be compared to assess the sensitivity. The control model is described in detail below.

3.2.1 GEOMETRY

The posterior and transverse processes, ligaments and muscles were not considered in the model (Figure 3.1), in order to focus on the soft tissue components of the disc. The model comprised of four basic components: the nucleus pulposus (NP) and annulus fibrosis (AF) of the disc and half the thickness of the superior and inferior vertebral bodies, (Figure 3.2). All comparisons with *in vitro* data were made with studies of specimens that also had these components removed.

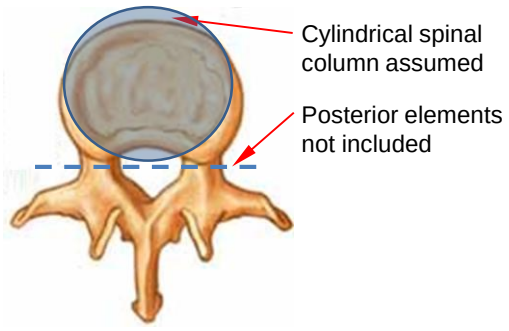

Figure 3.1 – Plan view of a lumbar vertebra showing assumptions made regarding the cylindrical shape of the vertebral column and the exclusion of posterior elements from the analyses.

Material properties for the model were developed based on data available in the literature. The end plates (EPs) were not considered as separate components within the model. This was because understanding of end plate mechanics and behaviour is lagging behind that of the other disc components and so suitable data for the end plate behaviour under compression was not available.

Model dimensions were chosen to represent the upper lumbar spine of an average sized, skeletally mature human. The height of the vertebral bodies was taken as half that given in the literature for the height of a human lumbar vertebra (Shirazi-Adl, 1984; Meakin and Hukins, 2001). The geometry of each model component is summarised in Table 3.1.

AXISYMMETRIC TWO DIMENSIONAL MODEL

The disc and vertebral bodies were assumed as cylindrical for efficient modelling, an approach that has been used previously for simplified models of the disc (Meakin and Hukins 2001). This allowed rotational symmetry to be assumed about the central axis, thus 2D axisymmetric elements could be used for computational efficiency. The axisymmetric model is illustrated in Figure 3.2.

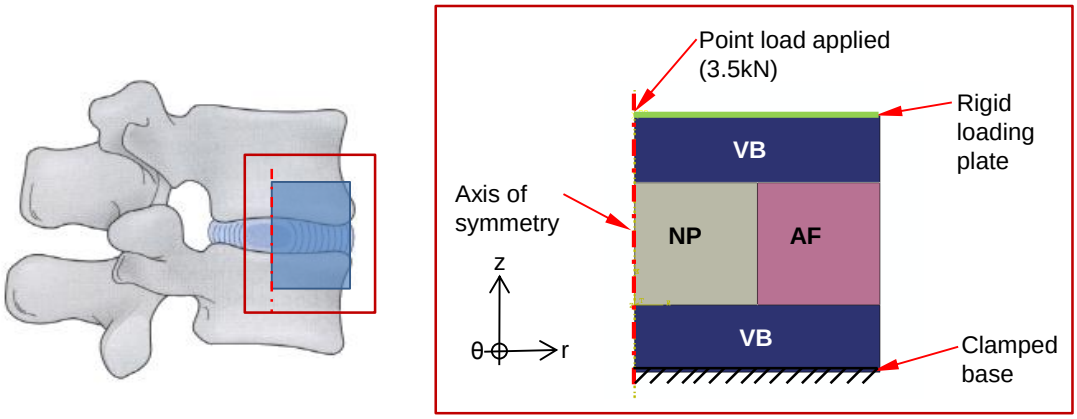

Figure 3.2 - The 2D axisymmetric model in relation to the natural disc, showing model components, orientation, boundary conditions and applied compressive load. VB = vertebral body, NP = nucleus pulposus, AF = annulus fibrosis. The axisymmetric assumption facilitates the representation of a cylindrical model using 2D elements. The nodes along the inferior base of the model are constrained in all directions. A point load is applied to a rigid plate attached to the superior surface of the model, so that all nodes along the superior surface experience the same displacement.

The axisymmetric model was used throughout this study apart from in two cases of the sensitivity analysis in which the assumption of axisymmetry was not valid.

THREE DIMENSIONAL MODEL

In two of the sensitivity tests conducted (see Sections 3.3.7 and 3.3.8), the nucleus was not centred in the disc, hence rotational symmetry could not be assumed. In these cases a comparable 3D model was used as the control model and basis for parametric analysis. All conditions were consistent between the axisymmetric and 3D models and verification checks were conducted to confirm agreement for the performance of the models (see Section 3.2.3).

3.2.2 BOUNDARY CONDITIONS AND LOADING

The nodes on the base surface of the inferior vertebral body were constrained in all degrees of freedom. In the axisymmetric model, rotation was prevented in the circumferential direction and the nodes along the central axis were restrained in the radial direction to satisfy the conditions for axisymmetry. Thus the model shown in

Figure 3.2 behaved as a cylindrical assembly, with symmetry about the centre line and in agreement with the equivalent 3D model that was used when the axisymmetric assumption was not valid.

The model was loaded in uni-axial compression. This loading regime enabled comparison to published data and replicated the compression experienced by the disc *in vivo*. A point load was applied to the centre of a rigid plate that was tied to the upper surface of the superior vertebral body, ensuring that the whole of the upper surface was compressed evenly and was restrained from movement in the radial direction.

The value of the point load, 3.5kN represented the average upper limit of the linear region of deformation as derived from the literature data (see Section 2.6.1).

The load-deformation behaviour of the disc under compression has a distinct toe and elastic region. Taking the average of load-deformation data available from literature, these regions can be represented by two linear curves (Figure 3.3). The application of the load was instantaneous.

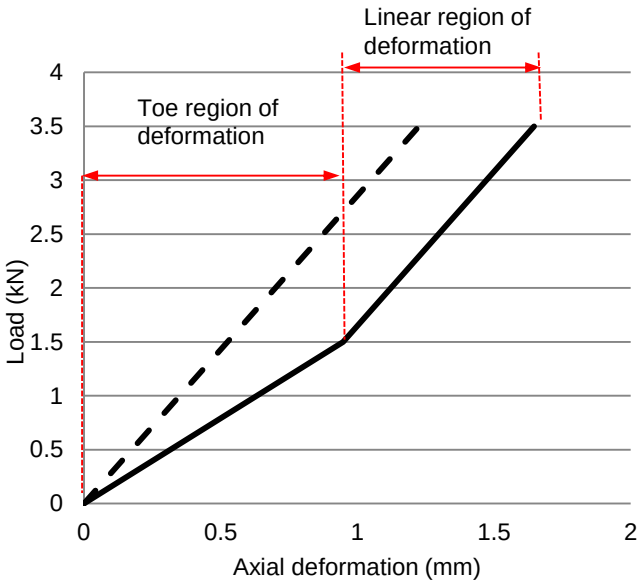

Figure 3.3 – Load/deformation curves for the disc in axial compression based on the average of the data from the literature (solid line, based on the data presented in Figure 2.16 and Figure 2.17) and the target curve for the control model (dashed line). The stiffness (slope) of the control model is equal to that of the linear region (in the load range 1.5 – 3.5kN) of the validation data. All data is for a single disc constrained between two vertebral bodies with posterior elements and ligaments removed.

3.2.3 MATERIAL PROPERTIES

Linear elastic material models were applied to each of the model components. These were based on previous *in vitro* and computational studies from the literature and are summarised in Table 3.1.

Component	Parameter	Magnitude	Unit	References
Annulus Fibrosus (annulus)	E	8.24	MPa	Determined from literature
	v	0.4		Meakin and Hukins (2001)
	D_o	48	mm	
	D_i	24	mm	
	H	12	mm	
Nucleus Pulposus (nucleus)	E	1.5	MPa	Argoubi and Shirazi-Adl (1996), Swider et al. (2010)
	v	0.5		
	D_o	24	mm	
	H	12	mm	
Vertebral bodies (VB) - cancellous bone	E	100	MPa	Shirazi-Adl et al. (1984)
	v	0.2		
	G	4615	MPa	
	D_o	48	mm	
	H	6	mm	

Table 3.1 – Summary of model components, geometry and material properties for the generalised model of the disc. E = Young's modulus, v = Poisson's ratio, D_o = outer diameter, D_i = inner diameter, H = height.

The nucleus was assumed to be incompressible and fluid flow and poroelastic material properties were not included because of the instantaneous loading condition applied.

The annulus is of particular interest to this study. The material models applied to the annulus component of the model were calibrated to ensure performance of the model was in agreement with axial disc compression in the literature. *In vitro* studies were analysed to determine an idealised stiffness and radial bulge for the disc when loaded in axial compression for the linear region of deformation, as summarised in Figure 3.4. The Young's modulus of the annulus was tuned to achieve agreement with the mean stiffness for the linear region of deformation for the data reviewed (2.86kN/mm).

Two material models were adopted:

i. Isotropic Model – to facilitate comparison with other components of the model and between model variations. Used in the "control model".
ii. Orthotropic Model – to capture the directionally dependent material properties of the annulus.

DEVELOPMENT OF ISOTROPIC ANNULUS FIBROSIS MATERIAL MODEL

The elastic modulus of the annulus ($E_{annulus}$) was varied and the effect of this on the overall stiffness of the disc system was observed.

With $E_{annulus}$=12.85MPa, the axisymmetric disc model had an overall axial stiffness of 2.72kN/mm, -4.8% error with the target stiffness of 2.86kN/mm. With the same value of $E_{annulus}$, the 3D model had a disc stiffness of 2.85, 0.1% error with the target. For both models, the disc stiffness varied linearly with change in $E_{annulus}$. The variation of model stiffness relative to annulus elastic modulus is shown in Figure 3.4.

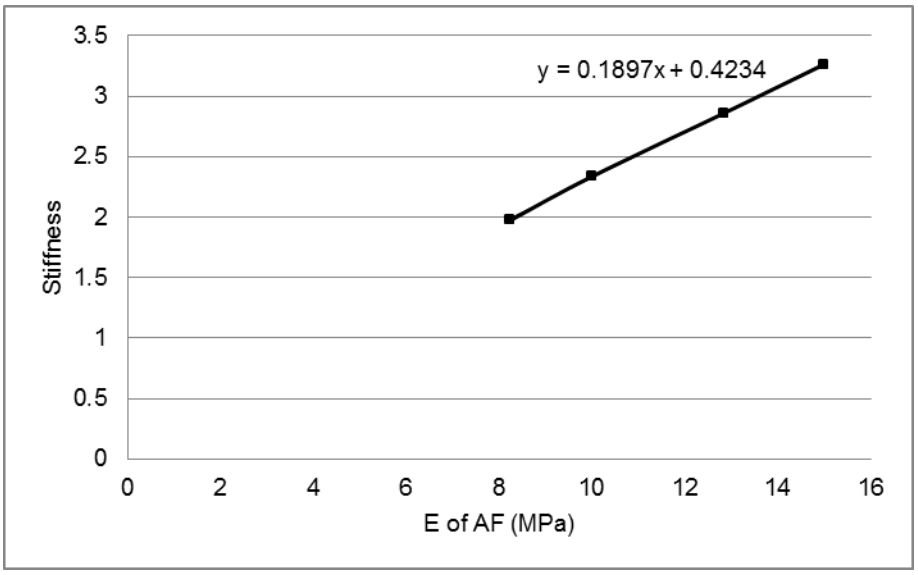

Figure 3.4 – Change of disc stiffness with variation to Young's modulus of annulus within the linear region of deformation (1.5 - 3.5kN) for the 3D isotropic model.

The key biomechanical performance benchmarks were derived based on a literature review of *in vitro* compression studies of human lumbar discs, as presented in Section 2.6.1. The data used to derive the targets is summarised in Table 3.2.

	Number of specimens	Standard deviation	Mean (used as target value)
Stiffness	10	0.66kN/mm	2.86 kN/mm
Radial bulge	7	0.09mm	1.6 mm

Table 3.2 – Summary of literature data used to derive the target values for the biomechanical performance of the control models.

The performance of the axisymmetric and 3D models relative to the benchmarks are presented in Table 3.3, in which the discrepancy between the agreement of the stiffness and the agreement of the radial bulge is also highlighted, where:

$$Deformation\,ratio = \frac{change\,in\,disc\,height}{OAF\,radial\,bulge}$$

	Stiffness (kN/mm)	Annulus radial bulge (mm)	Deformation ratio
Target values (literature review)	2.86	1.60	0.76
Control model (axisymmetric)	2.72 (-4.8%)	0.96 (-40.0%)	1.34 (+34%)
Control model (3D)	2.862 (+0.1%)	0.74 (-54%)	1.65 (+117%)

Table 3.3 – Summary of target performance values (from published data) and results for the axisymmetric and 3D control models, including percentage difference with respect to target values. Target values were taken as the mean values for stiffness and radial bulge based on the literature review of in vitro compression studies.

DEVELOPMENT OF ORTHOTROPIC ANNULUS FIBROSIS MATERIAL MODEL

Orthotropic material properties developed by Sutton and Elliott (2001) were applied to the annulus of the control model. These properties are summarised in Table 3.4 and were used as the base values since parameters were tuned.

The magnitude of the elastic modulus in the 3-axes system were first varied, followed by the magnitude of the Poisson's ratios. The ratios of Young's moduli, Poisson's ratios and shear moduli in the principle directions were maintained throughout.

The resulting axial stiffness and radial bulge at the inner and outer annulus (IAF and OAF, respectively) were recorded for all permutations of E and v values so that the optimal combination of parameters could be chosen based on disc stiffness and radial bulge, as presented in Table 3.3.

The properties derived for the orthotropic model of the annulus are presented and compared to those derived by Elliott and Setton (2001) in Table 3.4.

	E_r (MPa)	E_z (MPa)	E_θ (MPa)	ν_{rz}	$\nu_{r\theta}$	$\nu_{z\theta}$	G_{rz} (MPa)	$G_{r\theta}$ (MPa)	$G_{z\theta}$ (MPa)
Elliott & Sutton (2001)	0.2	35	8	0.020	0.065	1.20	0.1	0.1	0.1
Derived	0.4	70	16	0.023	0.075	1.38	0.1	0.1	0.1

Table 3.4 – Material properties derived for the orthotropic model of the annulus and those derived by Elliott and Setton (2001).

When compared to the target values from the literature, the orthotropic model performed closer to the target values than the isotropic model, as summarised in Table 3.5.

	Stiffness (kN/mm)	annulus radial bulge (mm)	Deformation ratio
Target values	2.86	1.60	0.76
Elliott and Setton (2001) annulus model	5.2 (+82%)	0.38 (-76%)	1.76 (+132%)
Orthotropic model (derived)	2.79 (-2.4%)	1.41 (-11.9%)	0.89 (-11%)

Table 3.5 – Summary of target performance values (from published data), model performance using Elliott and Setton (2001) orthotropic material properties and results for the derived orthotropic annulus material properties. Percentage error with respect to target values is shown in brackets.

3.2.4 MESH DEVELOPMENT

The model was meshed with an approximate element size of 0.5mm. The number of elements per model varied throughout the study, depending on the changes made to the model during the sensitivity tests. Approximately 3,000 linear, 2D axisymmetric stress elements were used in the axisymmetric models. Approximately 150,000 3D solid, tetrahedral, hexahedral, pyramidal and wedge elements were used in the 3D models.

Hybrid element formulation was applied to the elements of the nucleus elements to better represent the fully incompressible behaviour of the tissue. This formulation is recommended for the case when a very small change in displacement produces a large change in pressure, making a purely displacement-based solution too sensitive for the computational process (ABAQUS Users' Guide).

MESH SENSITIVITY RESULTS

Mesh sensitivity analyses were conducted with each model development to assess the potential error encountered from mesh deficiencies. The results for the axisymmetric model are summarised in Figure 3.5.

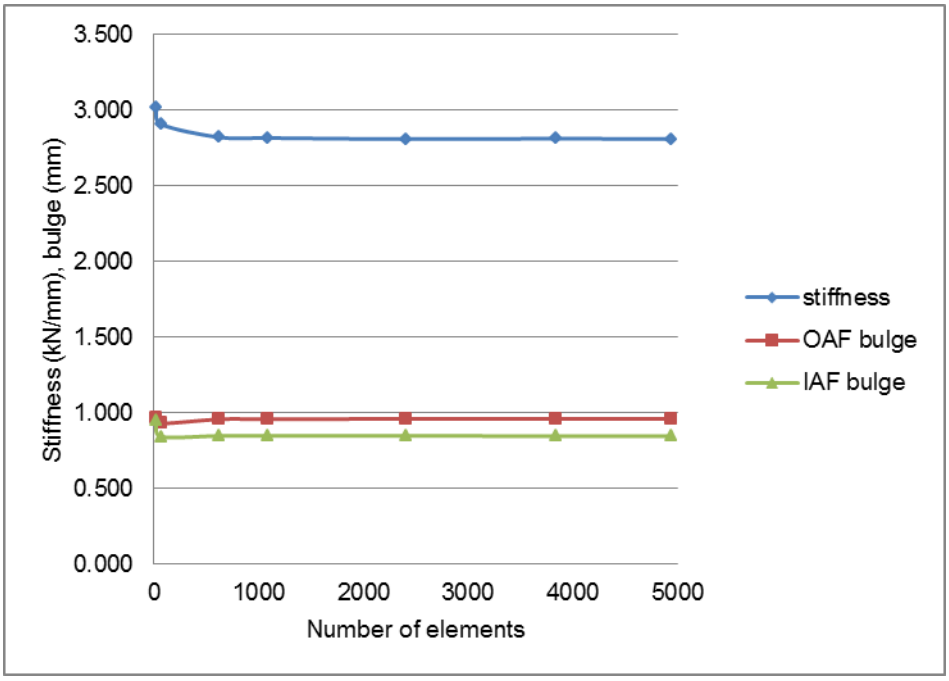

Figure 3.5 – Mesh sensitivity analysis for the axisymmetric control model.

With greater than 1,000 elements, the performance of the axisymmetric model converged for radial bulge and axial stiffness. Around 3,000 elements were used in the axisymmetric models, thus the error incurred from mesh inaccuracies was negligible.

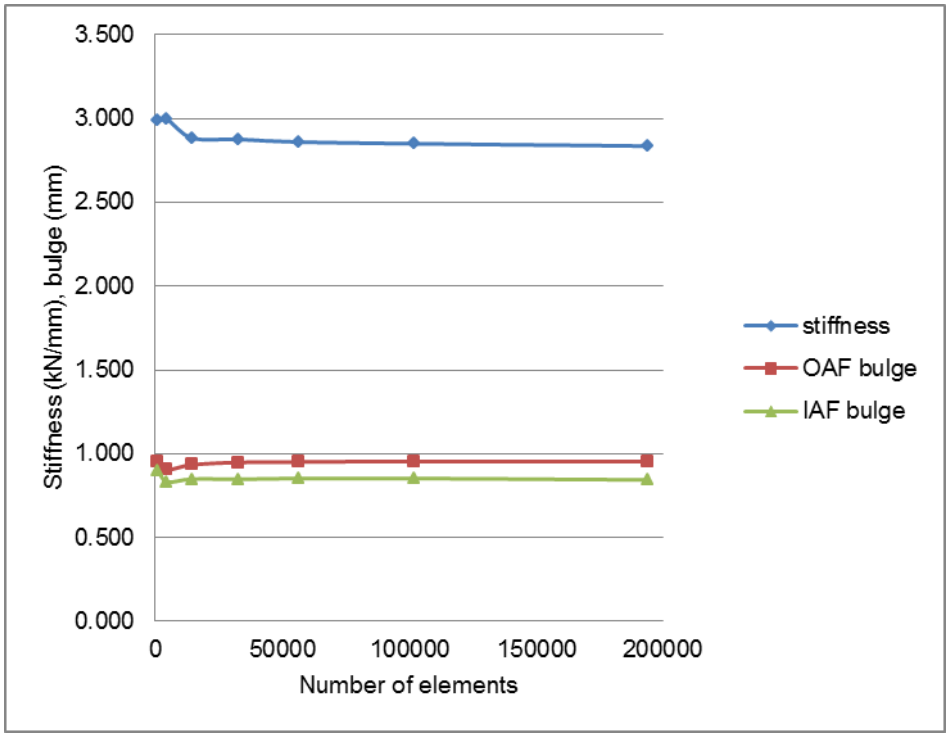

Figure 3.6 – Mesh sensitivity analysis for the 3D control model.

The results for the 3D model are presented in Figure 3.6. Similarly for the 3D model, the performance converges well below the 150,000 used per model in this study, again resulting in negligible error.

3.3 SENSITIVITY TESTS

This Section describes the variations that were made to assess the model's sensitivity to changes to several model parameters. The parameters varied were relevant to assumptions that may have to be made during specimen specific modeling techniques.

3.3.1 HOMOGENOUS DISC

A variation of the control model was developed in which there was no distinction between the annulus and nucleus. The disc was modelled as one homogenous part with a Young's modulus of 7.2MPa, the average of the $E_{annulus}$ and $E_{nucleus}$ applied in the control model, and a Poisson's ratio of 0.4.

3.3.2 TRANSITION ZONE MODEL

To imitate the blurred distinction between the annulus and nucleus recorded during physiological and histological examination, a model variation was developed in which an additional component, called here the “transition zone” (TZ) was included between the nucleus and annulus. The transition zone was 2mm wide with a modulus of 7.2MPa, (the average of $E_{annulus}$ and $E_{nucleus}$, as discussed in Section 3.3.1) and a Poisson’s ratio of 0.4.

3.3.3 RADIAL VARIATION OF ANNULUS MODULUS

In this test the annulus was split into concentric rings. The Young’s modulus varied from lower at the inner annulus fibrosis (IAF) to higher at the outer annulus fibrosis (OAF) to represent the gradient of properties observed *in vivo* (Chapter 2). This approach has been adopted in previous FEA studies of the disc such as those by Lu *et al.* (1996), Shirazi-Adl *et al.* (2010) and Strange *et al.* (2010).

The number of rings to the annulus was varied between two and eight. Isotropic material properties were applied throughout the annulus. The average modulus of the annulus was maintained at 12.85MPa (±0.5%), and the Poisson’s ratio was 0.4 throughout as described in Section 3.2.3. The material properties applied are summarised in Table 3.6. Tied connections were applied between adjacent rings, thus there was no relative movement between them.

Model	AF1	AF2	AF3	AF4	AF5	AF6	AF7	AF8	Average
2 ring	6.43	19.28	-	-	-	-	-	-	12.9
4 ring	2	7.4	18.3	23.7	-	-	-	-	12.9
8 ring	2	3.5	6	9	13	18	23	28	12.8

Table 3.6 – Young’s moduli applied to concentric rings for radial variation of annulus model. All values in MPa. Values were chosen to represent the extremes of moduli applied in previous computational simulations of the disc and to ensure an average moduli of 12.9MPa for comparison to control model.

3.3.4 INTERLAMELLAR INTERACTIONS

The concentric ring model was modified to assess the sensitivity to representation of interlamellar interactions. The contacts between the concentric rings were varied to represent different levels of interlamellar cohesion. The interactions considered were:

a. Frictionless contact – adjacent lamellae slide over one another without resistance
b. Intermediate level of cohesion – "interface model"

The interlamellar cohesion was simulated using a fine layer of deformable "interface" elements. The overall geometric parameters of the model were not changed; the interface elements were accommodated by reducing the thickness of the annulus rings. The material properties for the interface elements were developed based on published *in vitro* testing data, as discussed below.

INTERLAMELLAR INTERFACE MATERIAL

A model was created to replicate the *in vitro* tensile tests conducted by Gregory *et al.* (2010). The specimen represented by the model consisted of two adjacent lamellae, isolated from the surrounding tissue of the annulus and separated by a layer of "interface" elements to represent the interlamellar space and cohesion. The geometry was simplified greatly, as shown in Figure 3.7.

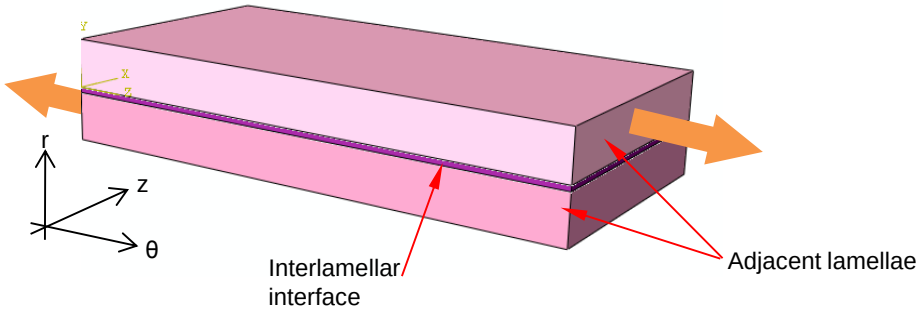

Figure 3.7 – Interface specimen model, consisting of two adjacent lamellae with an interlamellar interface layer. Dimensions (mm): single lamella thickness = 0.18, interlamellar space = 0.02, width = 1, length = 2. Specimen was loaded in tension in the axial direction, as shown by the orange arrows.

The base of the model was restrained in the radial (r) direction for stability. The specimen was loaded in tension in the axial direction by applying opposing displacement to the opposite ends of each of the lamellae (Figure 3.7).

Initially, isotropic material properties based on those developed for the control model (Section 3.2.3) were applied to the lamellae.

Point loads of 0.5kN were applied to two rigid plates attached to the different lamellae and at opposite ends of the specimen, so that the specimen was loaded in shear. The rigid plates were restrained to allow movement only in the direction of the load.

Using data from Gregory *et al.'s* study (2010); the stiffness of the test specimen in the linear region of deformation when loaded in axial tension was derived as 1.97N/mm (0.00197kN/mm). The Young's modulus of the interface elements was tuned to give an overall specimen stiffness to replicate this. The interface elements were assumed to have the same Poisson's ratio as the lamellae (v=0.4).

The tests were then repeated using the orthotropic material model which was developed and presented in Section 3.2.3 for the lamellae. Isotropic properties were assigned to the interface and the Young's modulus of the interface was again tuned to replicate the specimen stiffness in the same way.

INTERFACE DISC MODEL

The interface elements derived in the specimen model above were implemented between the concentric rings of the disc model. The aim of this test was to assess the effect of representing interlamellar interactions in this way on the gross mechanics of the disc.

The thickness of the interfaces between the concentric rings of the annulus was varied based on the number of rings, maintaining a constant volume of interface material relative to the lamellar material, as shown in Table 3.7. This ratio was based on the findings of Marchand and Ahmed (1990). All other model dimensions remained constant.

Number of rings	Single ring thickness (mm)	Number of interfaces	Single interface thickness (mm)	Equivalent number of lamellae (interlamellar space=0.02mm)
2	5.800	1	0.4	21
4	2.925	3	0.1	16
8	1.45625	7	0.05	18.5

Table 3.7 – Geometries of interface model variations. The Equivalent number of lamellae is calculated by dividing the total interface thickness across the whole annulus by 0.02mm to understand approximately how many lamellae as recorded histologically by Marchand and Ahmed (1990) are represented in the model.

The performance of these model variations were compared to the control model with a homogenous annulus.

The mesh density across the annulus was increased to maintain acceptable element aspect ratios with the change in geometry. The approximate element size applied to

the annulus rings was reduced to 0.2mm. The interface elements had an approximate size of 0.1mm.

3.3.5 SIZE OF NUCLEUS

In this test the size of the nucleus was varied from 20% to 80% of the total disc volume, so that the nucleus outer diameter (and thus the annulus inner diameter) varied between 9.6 and 38.4mm. All other model parameters were kept constant, as described for the control model in Section 3.2.

3.3.6 SHAPE OF NUCLEUS

This test was used to assess the effect of changing the shape of the nucleus/annulus boundary. In the control model this boundary was assumed as straight and perpendicular to the end plates. Three variations of this were tested with different shapes to this profile: circular arc, elliptical arc and hyperbolic curve. These model variations are illustrated in Figure 3.8.

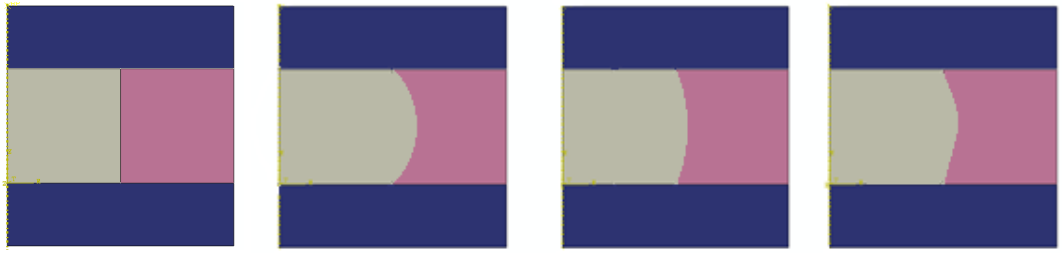

Figure 3.8 – The model variations tested, showing the different shape profiles applied to the nucleus/annulus boundary, from left to right: control model, circular, elliptical and hyperbolic (right).

The changes made to the nucleus outer profile were all within a radial distance band of 2mm (i.e. the height of the arc was 2mm for each variation). The ratio of nucleus volume to annulus volume was maintained in each test.

3.3.7 ECCENTRICITY OF NUCLEUS

A test was completed to assess the model's sensitivity to the eccentricity of the nucleus within the disc. The nucleus was moved towards the posterior within the disc by an offset of 3-9mm, in steps of 3mm, from the central axis, as shown in Figure 3.9.

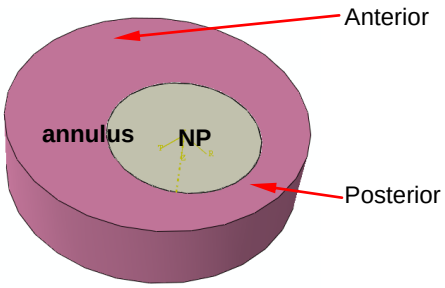

Figure 3.9 – 3D model of the disc with the nucleus eccentric by 6mm.

This change in geometry made the previous axisymmetric assumptions invalid, thus a 3D version of the model was used for these tests. Verification tests were taken to quantify agreement between the 2D and 3D models, as presented in Section 3.2.3.

3.3.8 ANNULUS SPLIT TYPE

With an eccentric nucleus, the annulus cannot be split into concentric rings. Two different approaches for splitting the annulus into "lamellae" when the nucleus is located eccentrically were investigated:

COMPLETE LAMELLAE MODEL

In this model, the annulus was split into three rings and the number of lamellae remained constant circumferentially. To compensate for the eccentricity of the nucleus, the thickness of the rings varied, as illustrated in Figure 3.10.

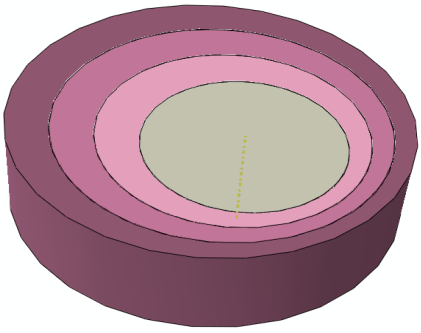

Figure 3.10 – 3D model of the disc with the nucleus eccentric and the annulus split into three rings using the "complete lamellae" method. All three rings are thicker at the anterior than the posterior. Each lamella has the same thickness along a selected radial line.

INCOMPLETE LAMELLAE MODEL

In this model the annulus was split into three rings, two of which had constant thickness circumferentially. To account for the change in overall thickness of the

annulus that results from the eccentric nucleus, the middle lamella had a variable thickness and was not complete circumferentially, as illustrated in Figure 3.11.

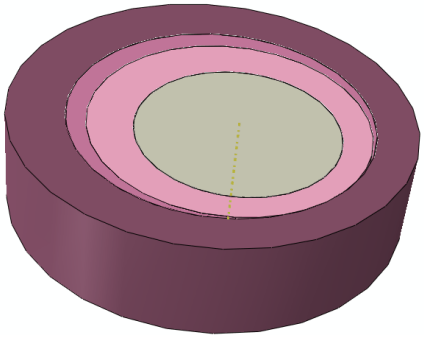

Figure 3.11 – 3D model of the disc with the nucleus eccentric and the annulus split into three rings using the "incomplete lamellae" model. The inner and outer rings have constant thickness. The central ring has variable thickness and is incomplete posteriorly.

3.4 SENSITIVITY RESULTS

The results of the sensitivity tests are summarised in Figure 3.12.

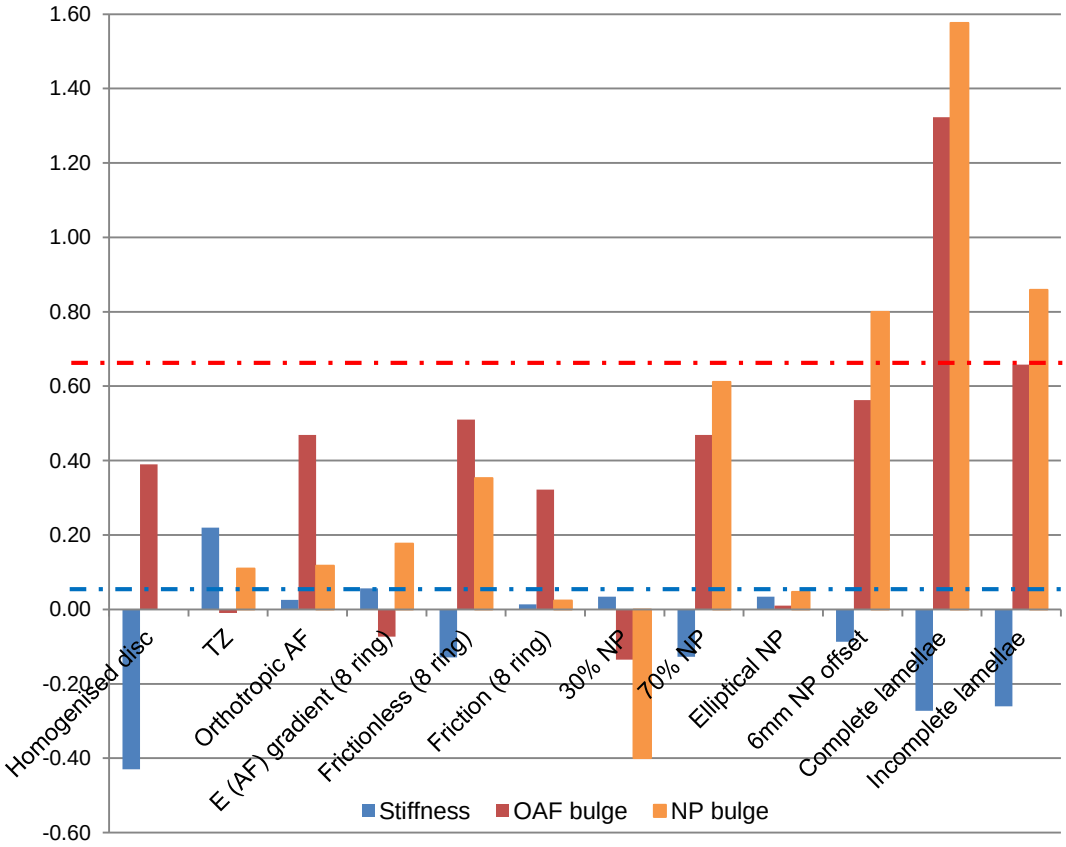

Figure 3.12 – Summary of model sensitivity to the parametric changes tested. All data is given relative to the performance of the control (isotropic) model. The horizontal axis represents the control model performance; deviation from this shows the difference between the control model and the variations. Values on the y-axis are normalised to show relative sensitivity. The dashed lines show the targets for disc stiffness (blue, at 0.05) and radial bulge (red, at 0.67) as taken from the literature review of in vitro data.

3.4.1 HOMOGENOUS DISC

When the disc was represented as a continual, homogenous material, the stiffness of the model was reduced by 43% with respect to the control model. This resulted in a loss of agreement of the deformation ratio with the target value, despite the improvement seen for outer annulus bulge compared to the control model, as illustrated in Figure 3.13[4].

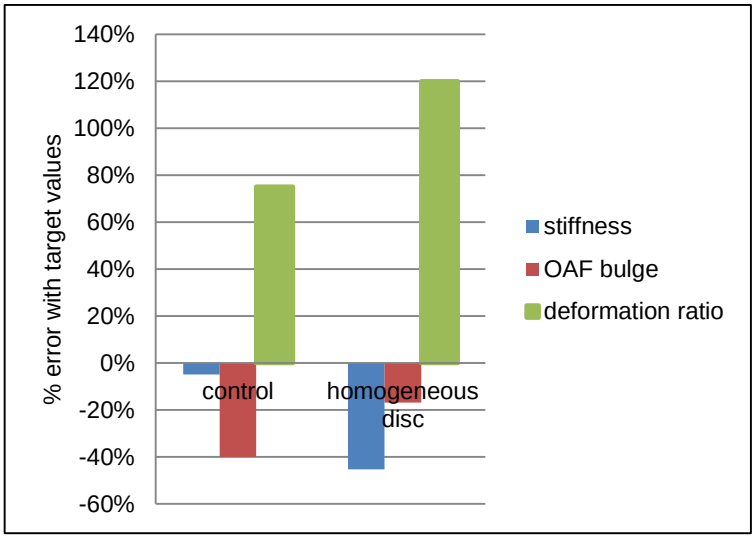

Figure 3.13 – Percentage error of homogeneous disc model with respect to the target values and in comparison to the control model.

3.4.2 TRANSITION ZONE MODEL

The introduction of the transition zone to the disc model had a negligible influence on the bulge of the annulus, however the nucleus bulge increased by 10% with respect to the control model. The stiffness of the model also increased, as illustrated in Figure 3.14.

[4] Throughout this thesis, the term "percentage error" is used to describe the difference between the performance of the computational models and the target values derived from the literature.

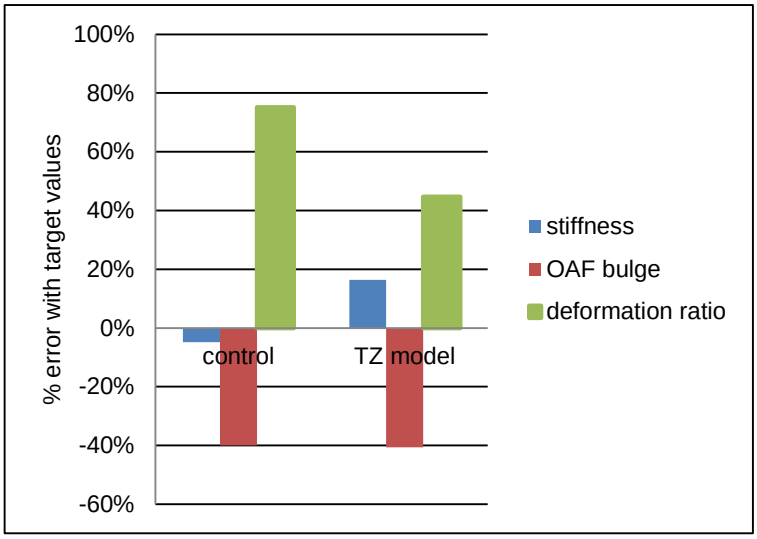

Figure 3.14 – Percentage error of the transition zone model with respect to the target values from the literature and in comparison to the control model.

3.4.3 RADIAL VARIATION OF ANNULUS MODULUS

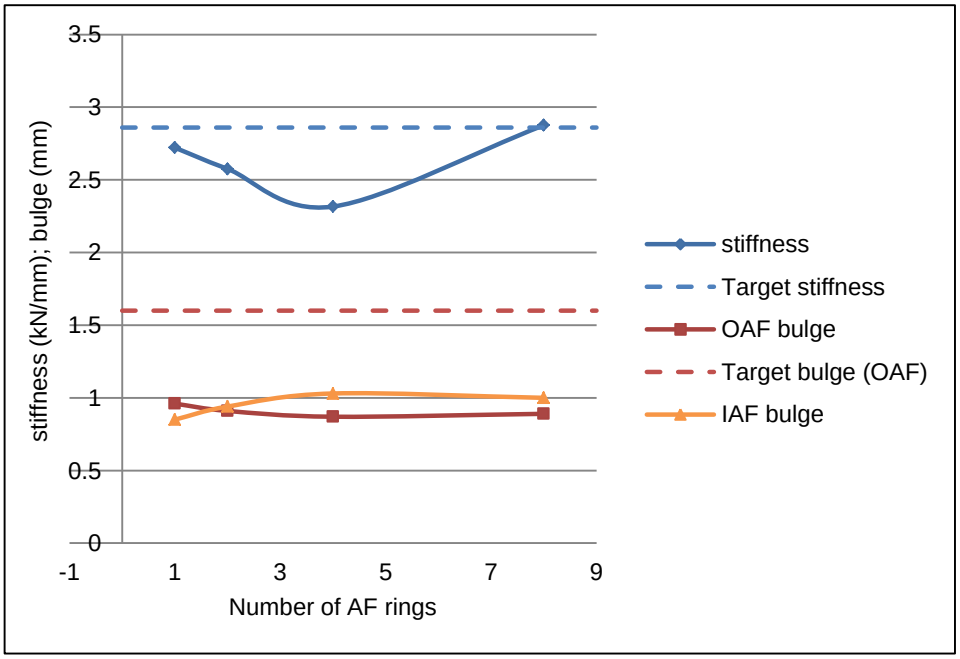

Figure 3.15 – Results for the effect of a variable annulus modulus on the gross mechanics of the disc model.

The change in stiffness between the model variations is shown in Figure 3.15. The radial bulge at the outer annulus decreased as the gradient of the Young's modulus in the outer layers of the annulus increased. Conversely, the bulge of the nucleus at the inner annulus increased. This also had an effect on the angle of the deformed boundary, as highlighted in Figure 3.16.

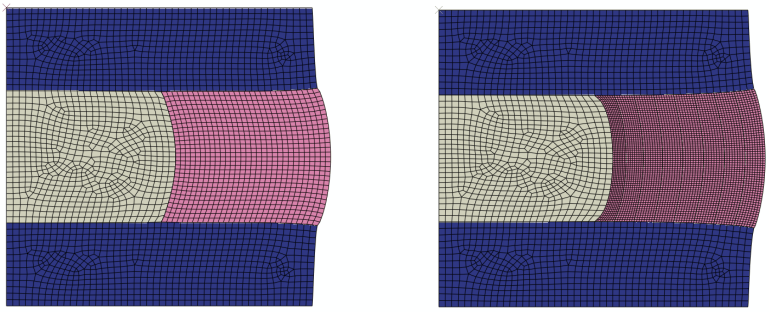

Figure 3.16 – Control model (left) and 8 ring model (right) in the loaded state. For the same load, the 8 ring model has bulged more at the inner annulus and less at the outer annulus than the control model, due to the varied modulus across the annulus. The deformed shape of the nucleus/annulus has also changed between the two, again due to a decreased modulus of the inner annulus in the 8 ring model.

3.4.4 INTERLAMELLAR INTERACTIONS

INTERLAMELLAR INTERFACE MATERIAL

With a Young's modulus of 5.38MPa for the interlamellar interface elements, the stiffness of the specimen model was within 0.33% of that derived from the work of Gregory *et al.* (2010) for the isotropic variant. The overall deformation of the model was partially within the interface and partially within the lamellae.

With the use of the orthotropic material model for the lamellae, there was increased deformation of the lamellar tissue. Thus the model was much less sensitive to changes in the properties of the interface material. The orthotropic model was found to converge to the target bulk axial stiffness with an elastic modulus value of E=65.7MPa for the interface material. The bulk stiffness of the model was within 0.15% of the stiffness derived from the work of Gregory *et al.*

The relationship between interface stiffness and specimen stiffness is shown in Figure 3.17 which highlights the disparity between the two model variations.

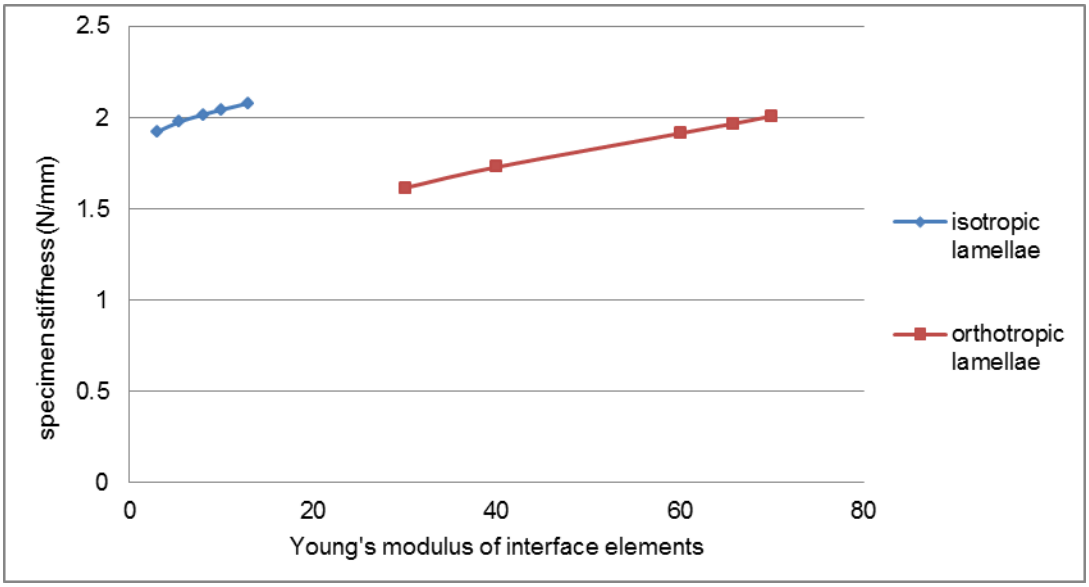

Figure 3.17 – Change in specimen stiffness with variation in interface stiffness for both isotropic and orthotropic lamellae.

INTERLAMELLAR INTERACTIONS IN DISC MODEL

The introduction of frictionless interlamellar interactions to the model had a minor effect on the stiffness of the disc. However there was a large influence on the bulge of both the nucleus and at the outer annulus, as illustrated in Figure 3.18.

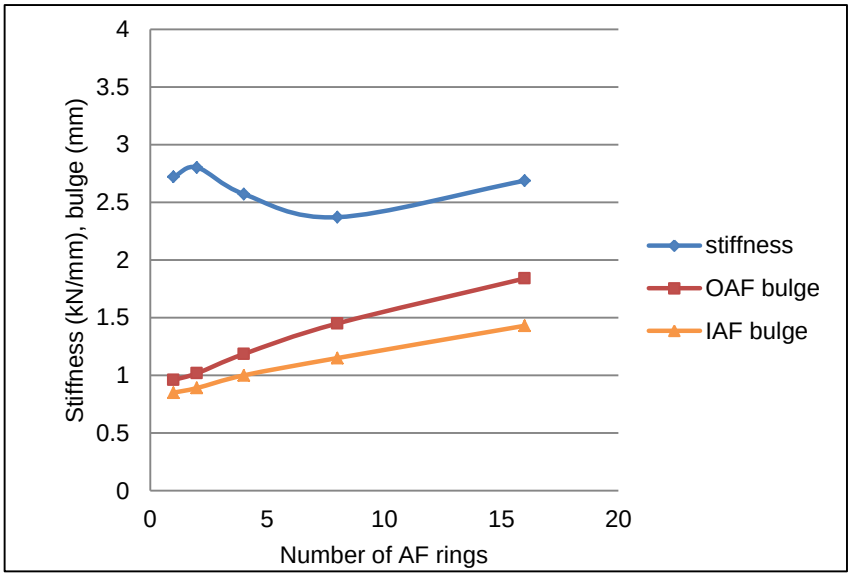

Figure 3.18 – The change in disc mechanics with respect to the number of annulus rings for the sliding model, in which interlamellar interactions were frictionless.

The relationship between interlamellar surface area and radial bulge is shown in Figure 3.19.

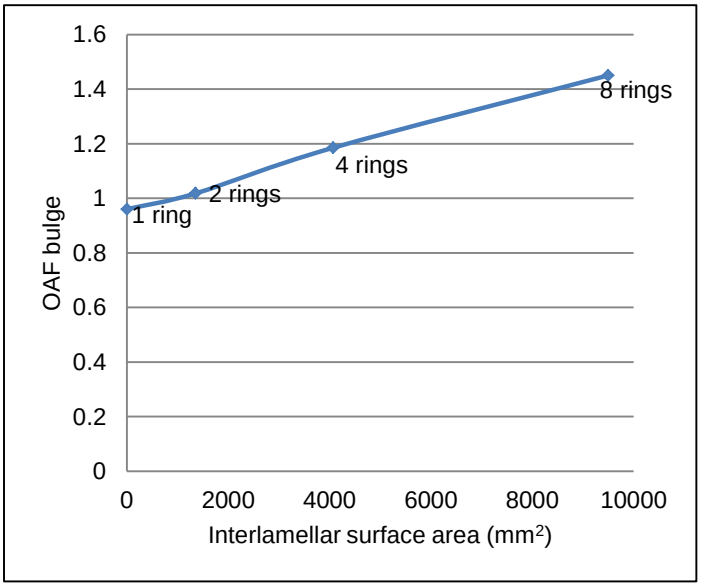

Figure 3.19 – Change in bulge at the outer annulus with increasing interlamellar surface area for frictionless ring model.

With the use of interface elements there was an initial change in mechanics between the control model and the two ring model, as illustrated Figure 3.20 due to the introduction of the interface elements. Beyond this, however, the average stiffness of the disc volume remained constant and thus the mechanics of the disc did not vary greatly.

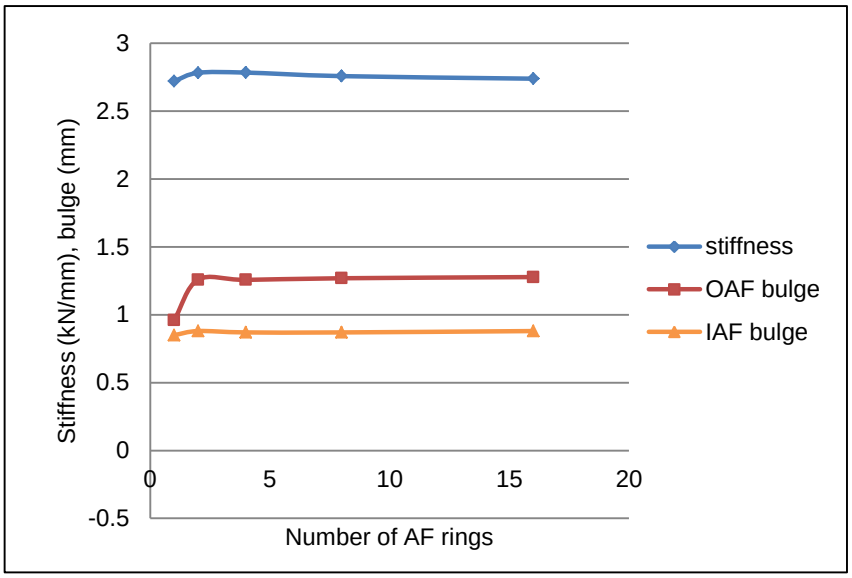

Figure 3.20 – The change in disc mechanics with respect to the number of annulus rings for the interlamellar interface model, in which the interlamellar interactions were represented by a layer of deformable elements.

A comparison between the two variations of interlamellar interactions is shown in Figure 3.21. The introduction of the frictionless interactions resulted in an overall more compliant disc.

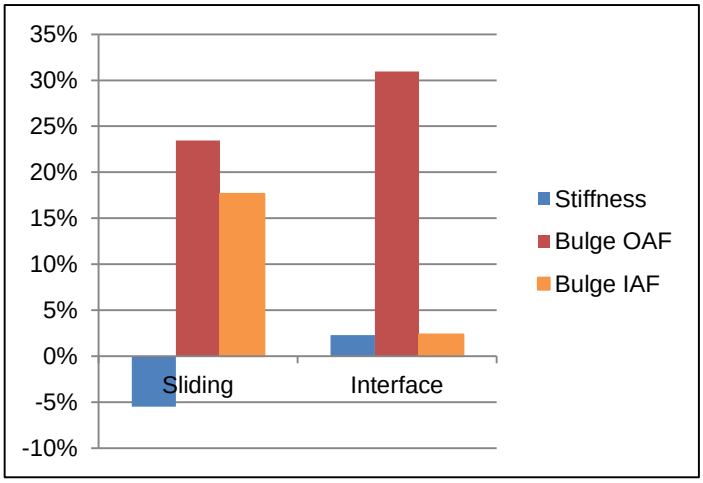

Figure 3.21 – The percentage change in disc mechanics of the four ring models with respect to the control model.

These model variants were also useful for investigating the effects of interlamellar interaction representation on the relative movement between lamellae. The vector plots presented in Figure 3.22 illustrate how this movement changes between the model variations. In the frictionless model, the nodes along the interlamellar boundary displace along paths that are divergent, indicating that there is relative shear occurring as the surfaces of the adjacent lamellae slide over one another. However in the interface plot, the paths of the nodes are parallel, suggesting that the interlamellar cohesion is limiting the relative shear.

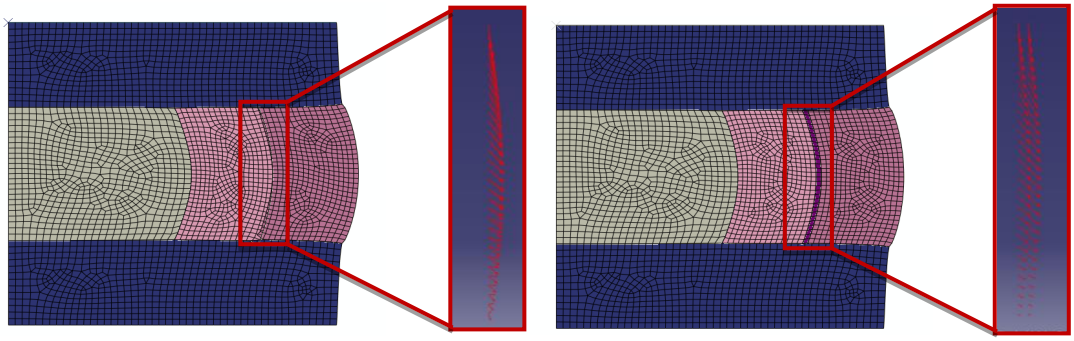

Figure 3.22 – Deformed models for the frictionless (left) and interface (right) two ring models. The accompanying vector plots illustrate the displacement of the nodes along the interlamellar boundary.

3.4.5 Size of nucleus

As expected, with the nucleus occupying a larger proportion of the disc volume, the stiffness of the disc reduces. Simultaneously, the bulge of both the nucleus and outer annulus increases, with increased sensitivity, as illustrated in Figure 3.23.

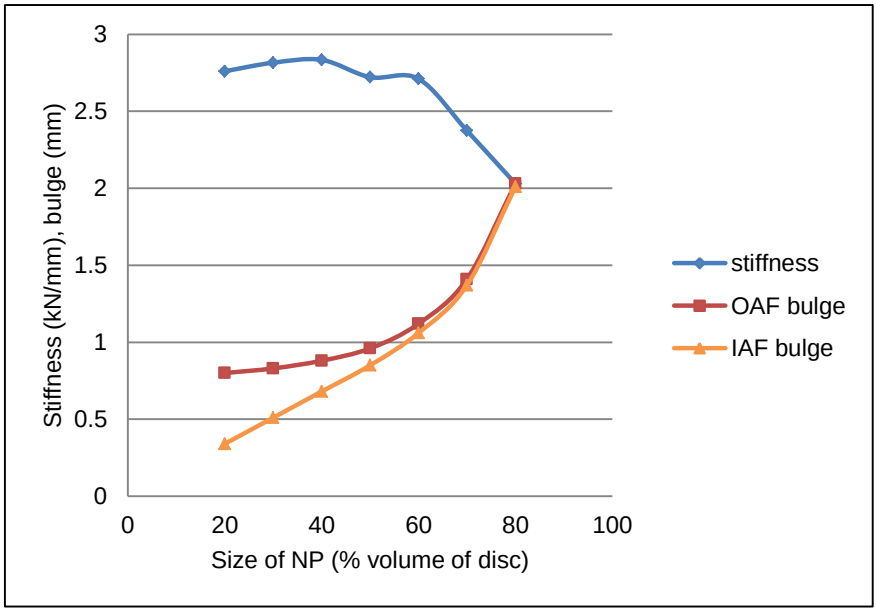

Figure 3.23 – The change in disc mechanics with the change in nucleus size as a percentage of total disc volume.

A clear change in the shape of the nucleus/annulus boundary in the disc's loaded state was observed, and is highlighted in Figure 3.24. In the 20% nucleus model, there is only a slight curve to the boundary, as the nucleus is bulging only very slightly into the annulus. As the volume of the nucleus increases, so does this bulge and the curvature of the boundary becomes more pronounced. In the 80% version, the boundary has formed the shape of a hyperbolic curve.

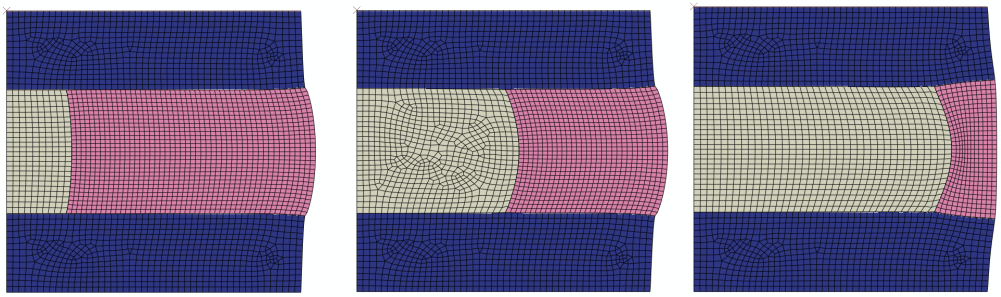

Figure 3.24 – Images of models in loaded state showing model components. From left to right: 20% nucleus, 50% nucleus (control model), and 80% nucleus variants. The change in deformation is highlighted between the three models.

As the nucleus/annulus proportions of the disc were changed, the error of the model with respect to the targets developed from the literature view varied, as shown in Figure 3.25. The optimal nucleus size would be 60 - 70% of disc volume.

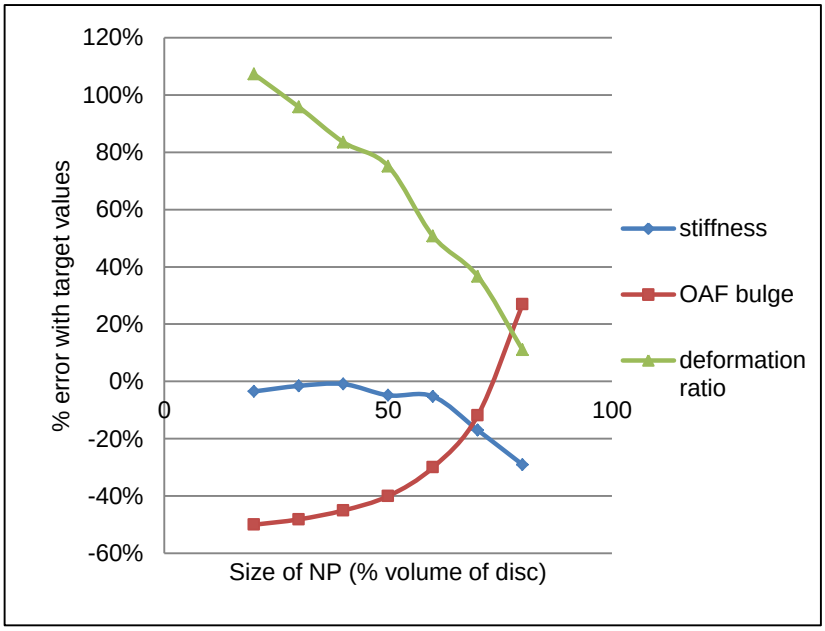

Figure 3.25 – Error of the model with respect to the target values (based on literature review) for varying nucleus/annulus proportions.

3.4.6 SHAPE OF NUCLEUS

The results showed only minor changes in the disc mechanics when the external profile of the nucleus was altered (see Figure 3.26).

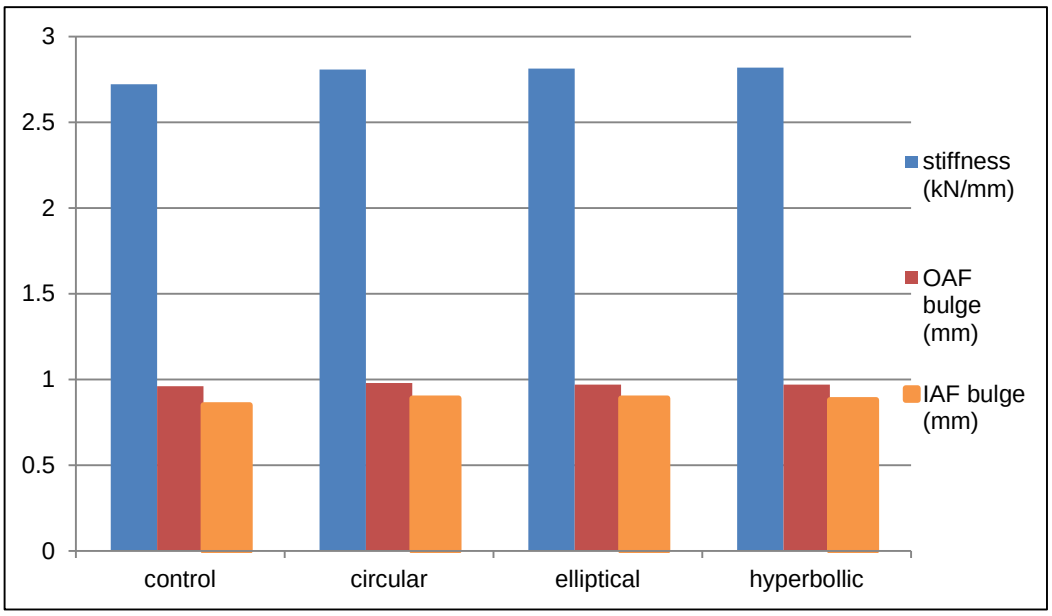

Figure 3.26 – Change in disc mechanics with change in initial nucleus/annulus boundary shape.

Although only small adjustments were made to the profile, the changes were of similar magnitude to the displacements recorded for these areas hence these alterations to the geometry were considered a sufficient test of model sensitivity.

3.4.7 ECCENTRICITY OF NUCLEUS

The most noteworthy effect of having an eccentric nucleus in this study is that the biomechanical indicators analysed become dependent upon location around the disc. The results presented here are taken from the posterior. In all cases, the maximum nucleus and annulus bulge was at the posterior of the disc, where the annulus was narrower and the nucleus had a greater effect on the disc deformation, as shown in Figure 3.27.

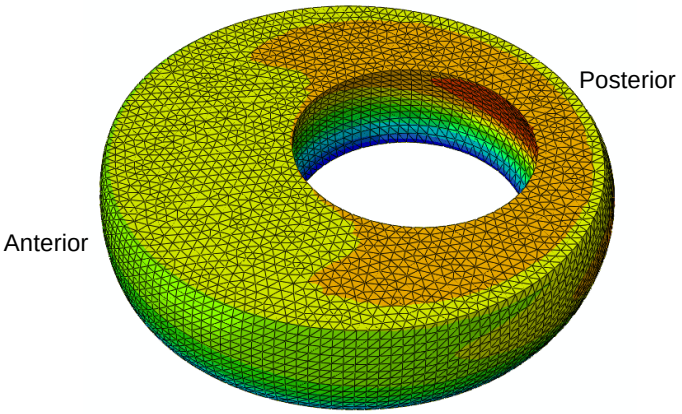

Figure 3.27 – annulus isolated from the 3D model in the loaded state with contours plotted for resultant displacement magnitude. The maximum displacement (red) is located in the posterior (inner annulus) of the disc where the annulus is narrowest.

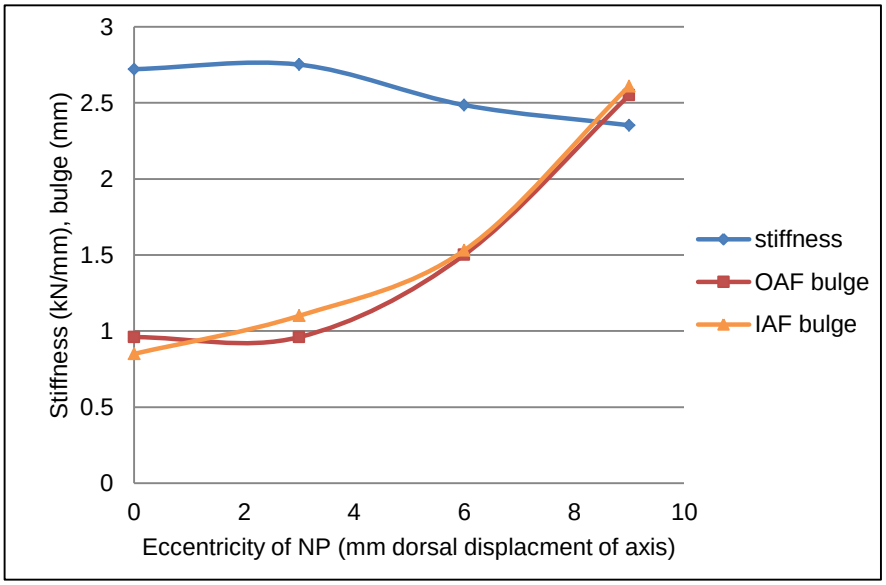

Figure 3.28 - The change in disc mechanics with the change in nucleus eccentricity.

As shown in Figure 3.28 the radial bulge at the inner and outer annulus were both highly sensitive to the eccentricity of the nucleus. For the 9mm eccentric model, the radial bulge at the outer annulus increased by 166% with respect to the control model. Conversely, the disc stiffness decreased by only 14%, this was due to the

consistency of the nucleus volume; hence the average Young's modulus across the disc remained constant.

Stress concentrations in the posterior of the annulus are shown in the contour plot in Figure 3.29.

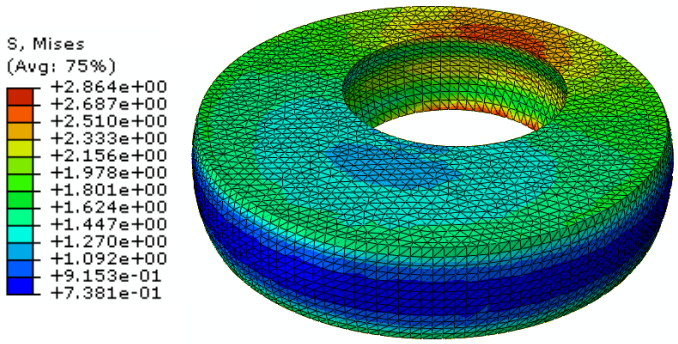

Figure 3.29 – Mises stress plot for eccentric nucleus model (6mm). Stress concentrations arise in the posterior region of the annulus, as shown here by the red areas. Units are in MPa.

3.4.8 ANNULUS SPLIT TYPE

In agreement with the results presented in Section 3.4.4, with the introduction of frictionless interlamellar interactions, the disc becomes more compliant and the radial bulge increases at both the inner and outer annulus, as illustrated in Figure 3.30. The results are compared here to the 6mm offset eccentric nucleus model as opposed to the control model to observe the effect of the annulus split methods.

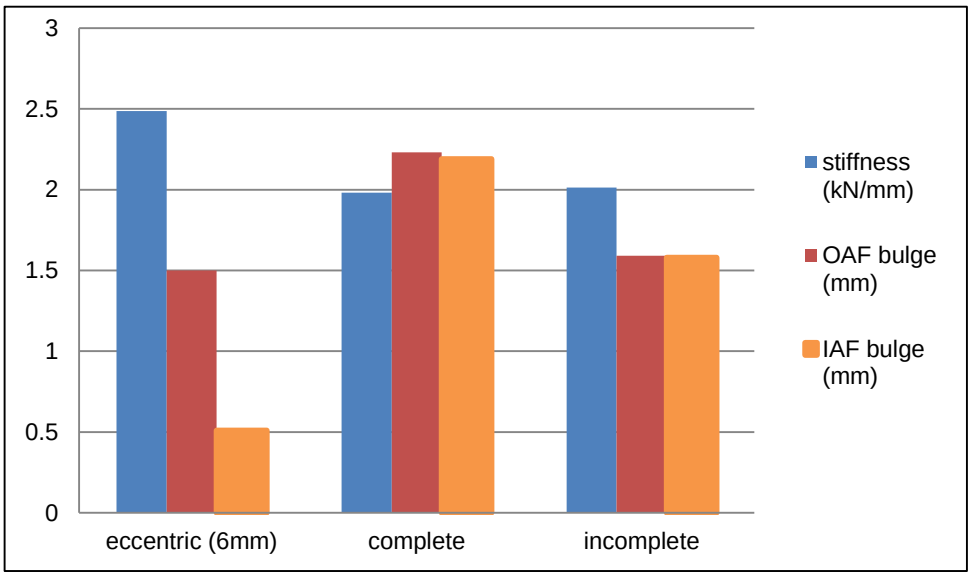

Figure 3.30 – The change in disc mechanics for different methods of splitting the annulus when the nucleus is eccentric. All results were taken at the posterior section of the annulus, where maximum deformation occurred due to the nucleus offset.

The discrepancies between the “complete” and “incomplete” models are caused by the difference in frictionless interlamellar surface area between the two models. The incomplete model has 10% less frictionless contact area than the complete model, as illustrated in Figure 3.31.

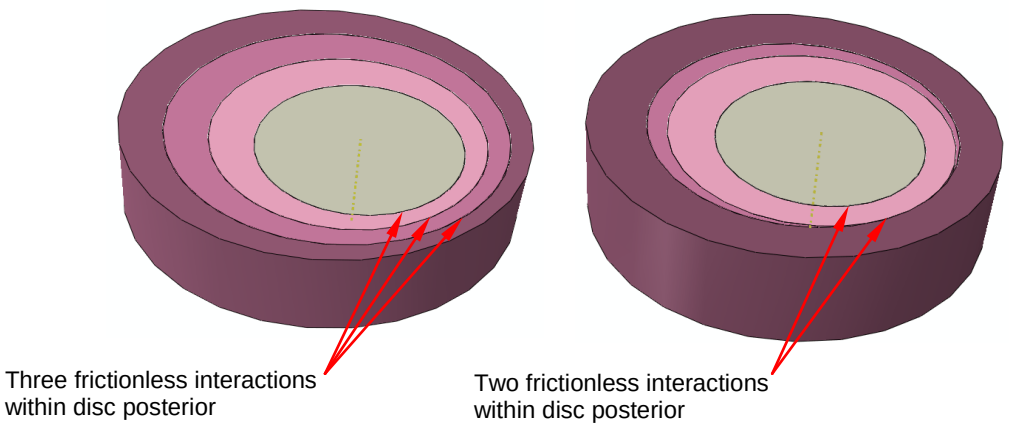

Figure 3.31 – Images of the model constructions, showing the discrepancy between the internal contact areas between the complete lamellae model (left) and the incomplete lamellae model (right).

In the complete lamellae model, there are three effective interlamellar layers that are contributing to the posterior radial bulge, in the incomplete lamellae model there are only two, resulting in the posterior annulus of the complete model having increased radial compliance than the incomplete model.

3.5 DISCUSSION

A simplified model designed to represent the biomechanical behaviour of the human intervertebral disc was presented. The geometry of the spinal column was represented as cylindrical; this made the model applicable to a wider range of variables and increased computational efficiency. The posterior elements, ligaments and muscles were not accounted for in this study for ease of comparison with *in vitro* data and to eliminate some parameters deemed superfluous to the key focus of the study, the structural soft tissue parameters.

The development of the generalised model allowed it to be used as a decision making tool and was used to assess the sensitivity of the disc biomechanics to parametric changes to the soft tissue structures.

The disc was loaded in uni-axial compression only. *In vivo* the disc experiences many complex loading regimes. Using this simple loading regime allowed comparison with many *in vitro* and computational studies in the literature. Linear

elastic deformation was assumed. Biological tissues are non-linear, however linear deformation occurs after the toe-regions of deformation (see Section 2.6.1). *In vivo*, the toe region deformation does not occur during to day-to-day activities; constant preloads applied to the disc as a result of body weight and muscular loads prevent deformation in this region (Kurtz and Edidin, 2006), hence the linear material deformation assumption was considered reasonable for this study.

The isotropic material model for the annulus was developed to achieve the optimal agreement for overall disc stiffness in the axial direction, for both the axisymmetric and 3D models. This was achieved with -4.8% error with the target value for the axisymmetric model and -0.1% for the 3D model. These levels are deemed negligible when compared to the wide range of values recorded for disc biomechanics in *in vitro* studies (Section 2.6.1). However, tuning to match only the stiffness to the target value came at the cost of the radial bulge agreement.

The development of the orthotropic material properties for the annulus was initially based on a material model presented by Elliott and Setton (2000). The original model was developed based on experimental data for annulus tissue samples tested in isolation, independent of the disc system. These properties were implemented into the full disc model and were tuned to optimise the gross mechanics of the disc model relative to the target indicators obtained from the literature review. The elastic moduli of the resultant annulus material model were double those presented by Elliott and Setton in all three directions (Table 3.4). This illustrates the discrepancies that can occur between apparent annulus tissue properties based on the mechanical environment of the tissue.

Once implemented in the disc model, the orthotropic annulus facilitated different material behaviour in the axial and radial directions and a more representative behaviour for axial stiffness and radial bulge was achieved, with improved agreement with the target values.

The orthotropic material model for the annulus was not used in the sensitivity analysis as it was deemed unsuitable for several of the tests to be conducted. For example, when the annulus properties were varied across the tissue, the orthotropic model would have introduced additional parameters for variation across the annulus thickness. For the models with a non-eccentric nucleus, the annulus was not cylindrical and so unsuited to material properties oriented with a cylindrical coordinate system. Using the isotropic model throughout the study simplified comparison between the parametric sensitivity tests.

The parametric tests were designed to analyse the sensitivity of the model performance to changes in the soft tissue structures that were relevant to the future development of specimen specific models. The level of detail included in the annulus was sequentially increased to analyse the effect of including lamellar level detail.

Radial properties were consistently more sensitive to the changes tested than the axial stiffness, as illustrated in Figure 3.12. This suggests that some of the features introduced during the parametric analysis could be useful tools for capturing the characteristic behaviour of the disc even with an isotropic material model for the annulus.

The transition zone model was designed to replicate the lack of distinction between the nucleus and annulus that has been recorded histologically (Wade *et al.* 2012). The introduction of the transition zone had a negligible effect on the radial bulge at the outer annulus but increased the nucleus bulge by 10%, as a result of a more compliant material constraining the nucleus compared to in the control model.

Material properties were varied across the whole annulus to represent the variation in tissue properties and fibre angle recorded in the literature (Marchand and Ahmed 1990). The average modulus of the annulus was maintained throughout the tests, thus the overall stiffness of the disc did not vary significantly.

Varying the number of rings within the annulus facilitated bulk representation of interlamellar interactions. When frictionless interactions were implemented, the radial properties were improved; however the axial stiffness was compromised and decreased as additional contact surfaces were introduced.

The annulus interface specimen models allowed the interface element properties to be tuned to histological data before they were used in a disc model. The specimen model results suggested that a greater stiffness was required for the interface between isotropic lamellae model than between orthotropic lamellae.

Both the stiffness and radial properties were improved in the interface model. These findings are in keeping with Michalek *et al.*'s hypothesis (2009), that during deformation of the disc, lamellae do not slide over one another, they are more likely to adopt a skewing mechanism, in which there is interlamellar cohesion, and much of the deformation occurs within the lamellae (discussed in Section 2.3.4).

When the interface elements were implemented into the disc model, the mechanical role of the interface elements depended on the properties of the lamellae. In the isotropic model the interface assisted in making the annulus more compliant in the radial direction, whereas for the same model but with the orthotropic properties assigned to the lamellae, the interface elements would act to stabilise and stiffen in the radial direction.

The concept of a stiff interlamellar interface agrees with histological studies of annulus tissue mechanics. Gregory *et al.* (2010) observed that large deformations occurred within individual lamellae, rather than as a result of interlamellar sliding, and suggests that this is due to the high stiffness of the interface compared to the lamellae. This concurs with observations by Veres *et al.* (2010) who found that during nucleus herniation, the nucleus material is more likely to migrate through the lamellae rather than the interlamellar space.

Care should be taken when using the same material model for the annulus sample model and the complete disc model. The differences in scale, boundary conditions and loading between the two scenarios may result in perceived differences in the annulus tissue properties. The implantation of the interface elements into the lamellar disc model adjusted the overall properties of the annulus component and changed the biaxial behaviour of the model to improve the agreement with the experimental data. However, this does not necessarily mean that the material properties of the annulus are an accurate representation annulus tissue properties at lamellar scale.

The results presented (Section 3.4.4) showed how the model mechanics were affected by the number of rings in the model for the frictionless model but not for the interface model. This was because the ratio of interface volume to lamellar volume remained constant throughout. This implies that when gross disc mechanics are of interest, it may be suitable to represent interlamellar interactions in bulk rather than modelling individual lamellae. The number of lamellae modelled should be dependent on the focus of the study; they may not be significant in studies of gross disc mechanics but a method has been presented that could be used to investigate interlamellar mechanics in more detail within the mechanical environment of the disc system.

The size and position of the nucleus had a considerable effect on the disc mechanics. The challenge of deciphering the internal structures of the disc's soft tissues has resulted in many previous FE studies of the disc making assumptions as

to the geometry of the nucleus (Schmidt *et al.* 2010; Strange *et al.* 2010). This study has shown such assumptions, if not accurate, could have a significant and possibly detrimental effect on the performance and reliability of a model.

In the natural spine the nucleus is located towards the posterior of the disc (see Chapter 2), thus the annulus is narrower in the posterior than the anterior. This affects many aspects of disc biomechanics. The position of the nucleus within the disc affected the stiffness and bulge of the disc and it also caused variation in deformation across the structure. In more complex loading scenarios likely to be experienced by the disc *in vivo*, this variation may become even more pronounced. This becomes significant to the clinical and pathological aspects of disc performance as stress and strain concentrations have been associated with the initiation and propagation of disc degeneration.

For the eccentric nucleus configuration, the method of splitting the annulus was shown to be important. A comparison between the performance of the frictionless, 8 ring model (centric nucleus) and that of the split annulus models (eccentric nucleus) is shown in Figure 3.12 which highlights the effect these alterations had on radial bulge.

These methods represent two different features of the lamellar structure reported by Marchand and Ahmed (1990). This detailed histological investigation reported that the number of lamellae was found to be constant circumferentially and also recorded many incomplete lamellae with few lamellae forming complete rings. This study cannot conclude that either of these two methods is more representative of the natural disc. A more useful conclusion to be drawn is that how the lamellar structure is modelled is significant and should be considered relative to the aims and interest of the model in question.

These approaches for modelling the lamellar structure in a non-concentric system could also be useful for modelling different non-concentric variations of the disc, for example, an elliptical nucleus within a kidney-shaped annulus.

This study has investigated novel approaches to increasing the level of soft tissue structural detail included in generalised models of the disc. The results of the sensitivity analyses presented are relevant to the development of specimen specific models of the disc.

The importance of how interlamellar interactions are represented has been highlighted. The lamellar structure of the annulus can affect the gross mechanics of the disc. Characteristic features such as incomplete lamellae and lamellae of varying thickness should be considered to improve the annulus simulations.

The size and position of the nucleus within the disc has been shown to have a considerable effect on the disc mechanics. More information about soft tissue structures and geometries could be useful in improving model representation of the natural disc, particularly in specimen specific models, as the nucleus size and position may vary between individuals.

4 IMAGING THE DISC

The aim of this study was to procure comprehensive image data of the intact soft tissues of the disc in an unloaded and a loaded state. Micro-computed topography and magnetic resonance (MR) imaging techniques were investigated. MRI methods were developed with the aim of capturing the geometry of the nucleus and the lamellar structure of the annulus. The resultant image data was validated using a range of techniques, including post-scan dissection analysis. The deformation of the tissue between the unloaded and loaded images was analysed. The MRI techniques were successful in capturing specimen specific details of the annulus soft tissue structure. Definition of the nucleus/annulus boundary was not possible due to a lack of distinction in the soft tissues.

4.1 INTRODUCTION

Computed topography (CT) imaging has been used extensively to capture image data for specimen specific models of the spine (Crawford *et al.* 2003; Liebschner *et al.* 2003). Using these techniques, the bone structures are imaged in clear and refined detail, enabling the development of models with specimen specific geometry and material properties based on greyscale values.

Imaging the soft tissues of the disc, in their natural, intact state to a similar level of detail is a greater challenge. Histological studies (Schollum *et al.* 2008; Yu *et al.* 2005) have provided image data useful in characterising these soft tissues; however such studies necessitate the dissection of the disc and the removal of tissue from the complete disc system, preventing study of the tissues in their natural mechanical environment.

Comprehensive image data for the disc in its intact state and whilst under load would be valuable in the development and validation of computational simulations of the tissues. The results from the generalised model presented in Chapter 3 illustrated the significance of lamellae structural representation and the geometry of the nucleus to the gross mechanics of the disc. Thus these features were of particular interest to this study.

Magnetic resonance imaging techniques have been used to image the tissues of the disc (Haughton 2004; Videmann *et al.* 2006; Sharma *et al.* 2009). MR imaging techniques have developed with a focus on pathological concerns of discs *in vivo,* and have aimed to monitor changes in chemical composition (Urban and Winlove 2007). As such, these techniques have previously provided limited information on the structure of the soft tissues.

The aim of this study was to image the internal soft tissues structures of the disc in their intact and loaded states. MR and μCT imaging techniques were investigated, with the intention of developing methods of characterising the geometries of the disc tissue structures and the relationships between the tissue constituents.

4.2 METHODS

4.2.1 SPECIMEN PREPARATION

Five specimens, each comprising four adjacent thoraco-lumbar vertebrae were dissected from five skeletally mature (4 - 6 years old) ovine spines. The details of the specimens are provided in Table 4.1. Due to the limited availability of sheep in this age range, it was not possible to procure all the specimens from the same breed.

	Sheep age (approx. years)	Sheep breed	Spine level	Disc of interest	Approx. disc dimensions	
					width (mm)	depth (mm)
S1	4.5	Texel	T10 – T13	T11T12	28	21
S2	6	Charrolais	T13 – L3	L1L2	24	19
S3	4.5	Suffolk	T13 – L3	L1L2	26	20
S4	5.5	Texel	T13 – L3	L1L2	22	21
S5	5	Texel	T13 – L3	L1L2	20	14

Table 4.1 – Specimens imaged during the study.

The central disc of the specimens was studied throughout; this was the L1L2 disc in all specimens except S1 for which it was T11T12. All muscle tissue and most ligament tissue was removed from the specimens whilst avoiding damage to the discs. The transverse processes were removed, as were the posterior elements and facet joints, by sawing through the spinal canal. Both ends of the specimens were potted in PMMA cement so they could be mounted in a bespoke loading rig suitable for use in the MRI scanner, as described in Section 4.2.3.

A fluid filled marker was attached to the anterior face of the vertebra superior to the central disc of each specimen (Ortho-Spots, Beekley Medical, Bristol, CT, USA). Glass shards were attached to the marker using adhesive. This marker system was developed to aid image registration during post-processing, with the fluid portion showing on MRI data and the glass in computed tomography (CT).

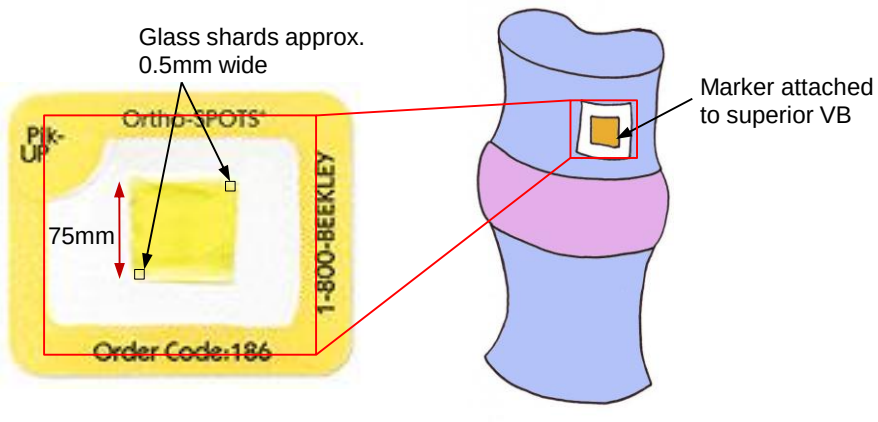

Figure 4.1 – "Ortho-spot" MRI marker (Beekley Medical, Bristol, CT, USA, 2012) labeled for position of glass shards attached using adhesive. The Schematic diagram shows the position of the marker attachment to the specimen.

Throughout the dissection and potting process, the hydration of the discs was maintained by wrapping the specimens in damp tissue paper. When complete, the specimens were each sealed in two air-tight layers of polythene and stored in the freezer at -20°C for less than three weeks. The specimens were removed from the freezer 24 hours before scanning. During this time they were stored at 2°C.

4.2.2 MICRO COMPUTED TOMOGRAPHY

As discussed in Chapter 2, µCT has been used extensively to image bony structures for use in computational simulation of biological systems. In this study, specimens were subjected to µCT scans as a method of capturing the geometry of the vertebral bodies and bony end plates adjacent to the discs.

Scans were taken of each specimen in its prior-to-loading state (XtremeCT scanner, Scanco Medical, Brüttisellen, Switzerland). The sample was loaded in the scanner a supine position. Each specimen was scanned once. The scan settings are presented in Table 4.2. The µCT technique used captured the geometry of the bones and calcified end plates to a high degree of accuracy.

voxel size	123µm
integration time	300ms
pulse voltage	70kV
current	114µA

Table 4.2 – Settings used for µCT scans.

4.2.3 MAGNETIC RESONANCE IMAGING

The use of MR imaging techniques was investigated to analyse the potential of techniques for imaging the soft tissue structures of the disc, in their intact condition, whilst under compressive load.

There are a wide range of MR sequences that can be used and manipulated to capture specific features and phenomena of interest. Thus for MR data to be reliable, a validation process must be completed for the sequences developed to verify that features are being identified from the image data correctly.

All MR scans were conducted using a 3T Siemens Verio scanner (Siemens Healthcare, Surrey, UK). Surface coils were placed either side of the central disc. During the scans, the specimens were held in a bespoke compression rig.

COMPRESSION RIG DEVELOPMENT

The compression rig used during the MRI scans is illustrated in Figure 4.2.

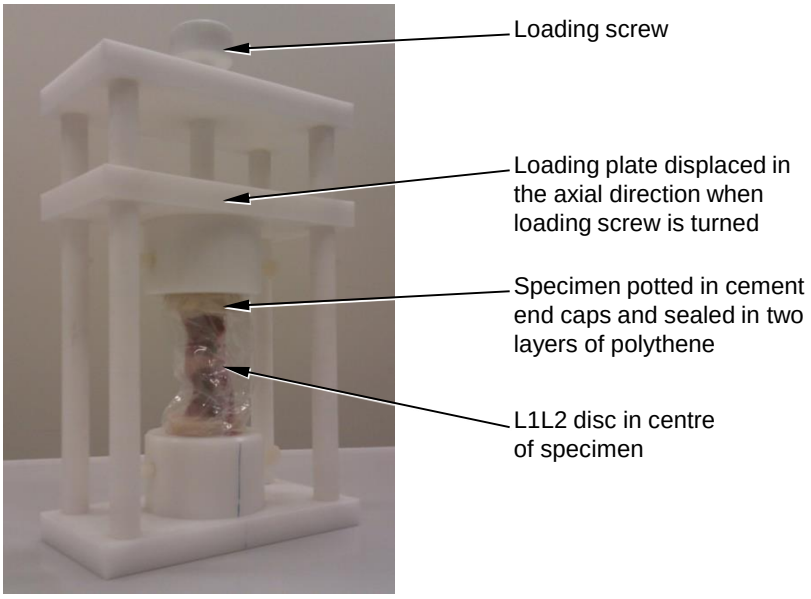

Figure 4.2 – MRI safe loading rig with specimen. The loading screw is turned by hand, displacing the loading plate and compressing the specimen in the axial direction.

The rig was designed to be MRI safe; all components were made from delrin plastic, no metallic components were used. As such it was not possible to include a load cell. The dimensions of the rig were chosen to accommodate the surface coils of the MR scanner – the distance between the PMMA end caps of the specimen was required to be a minimum of 650mm. The thread pitch of the loading screw was assigned so that one revolution displaced the loading plate by 1mm.

SEQUENCE DEVELOPMENT

A range of scan settings were tested during preliminary scans with the aim of developing sequences to clearly show:

a) The gross volume of the disc.
b) The geometry of the nucleus.
c) The geometry of the annulus structure, including individual lamellae.

The initial sequence settings were based on those used by O'Connell *et al.* (2007; 2008). Scan settings were varied to optimise the images for the features of interest. Some preliminary results from these tests are presented below.

i. Echo time

The effects of changing echo time are highlighted in Figure 4.3. The intense signal in the centre of the disc shows hydrated tissue. With a shorter echo time this volume increased.

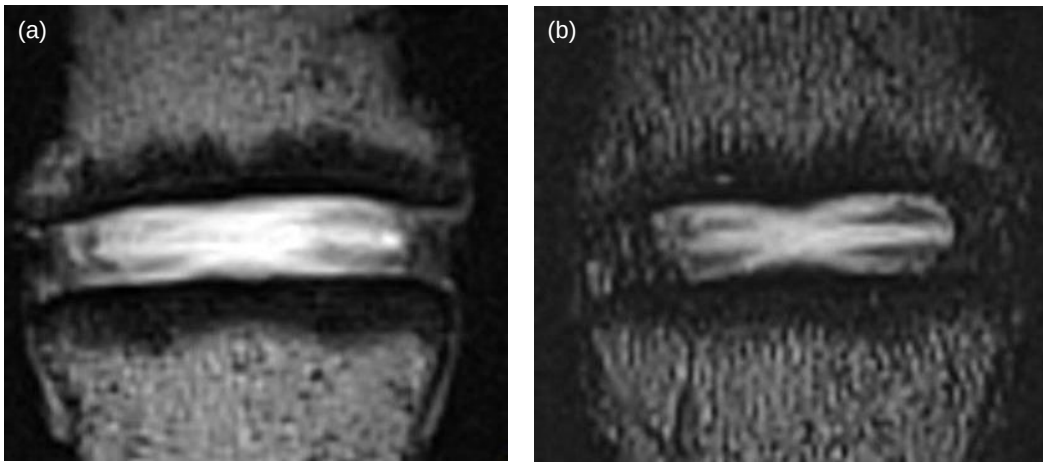

Figure 4.3 – Coronal slices from a turbo spin echo scan of S4 with (a) echo time = 36 ms and (b) echo time = 118 ms. The intensity of signal from the nucleus is reduced with a longer echo time, with only the most hydrated region of the nucleus shown bright.

A range of degeneration levels was observed in the specimens used. To capture a complete nucleus for all specimens, a shorter echo time was used in the turbo spin

echo (TSE) sequence developed to image the nucleus. Consistency in echo time allowed comparison of nucleus volume and hydration levels between specimens.

ii. Distortion correction

Distortion correction is a post-scan algorithm that corrects for warping of MR images caused by the non-linearity of the magnetic fields from the imaging gradient coils (Jovicich *et al.* 2005). Impact of this effect is greatest at the peripheries of the field of view. Distortion correction post-processing was applied to a selection of preliminary scan image data. The greatest change in the images was one pixel (approximately 0.2mm) at the periphery of the field of view. The disc of interest was located in the centre of the field of view. In this region, the distortion was negligible, thus distortion correction was not used on future scan data.

iii. Fat suppression

A 2D flash sequence was repeated with and without fat suppression to evaluate the effect on the images. With the application of fat suppression, the intensity of the signal from fat based tissue, (e.g. bone marrow) should reduce, whereas the signal intensity from water based tissue, (e.g. nucleus and annulus), should not be affected. This can aid with tissue classification based on the scan data.

With fat suppression implemented, the intensity of signal from the vertebral bodies was reduced; indicating that the tissue imaged in this area was fat based, and therefore probably bone marrow. The intensity of the signal from the disc tissues was maintained, indicating that this tissue was water based.

The clarity of the boundary between the disc and bone and the definition of the calcified end plates were improved by fat suppression, aiding observation of the end plate topography and disc deformation. The effect of using fat suppression is illustrated in Figure 4.4.

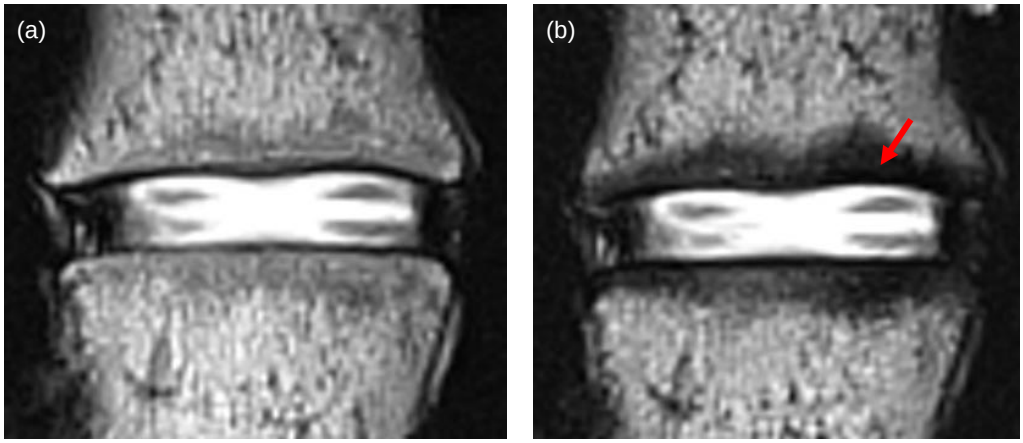

Figure 4.4 – Coronal slices from 2D flash sequences of S4 (a) without fat suppression and (b) with fat suppression. The signal intensity from the bone marrow is reduced, whereas the signal from the disc has the same intensity in both scans. The arrow highlights the improved distinction between bone and disc.

Fat suppression was used in the final sequences. This had greatest effect on the flash scan sequences.

iv. Specimen orientation

Tests were conducted to assess the effect of the orientation of the specimen within the magnetic field. A three-dimensional flash scan sequence was repeated for the same specimen, first with the y-axis of the specimen perpendicular to the primary direction of the magnetic field (B_0) and then with the y-axis of the specimen aligned with B_0, as illustrated in Figure 4.5.

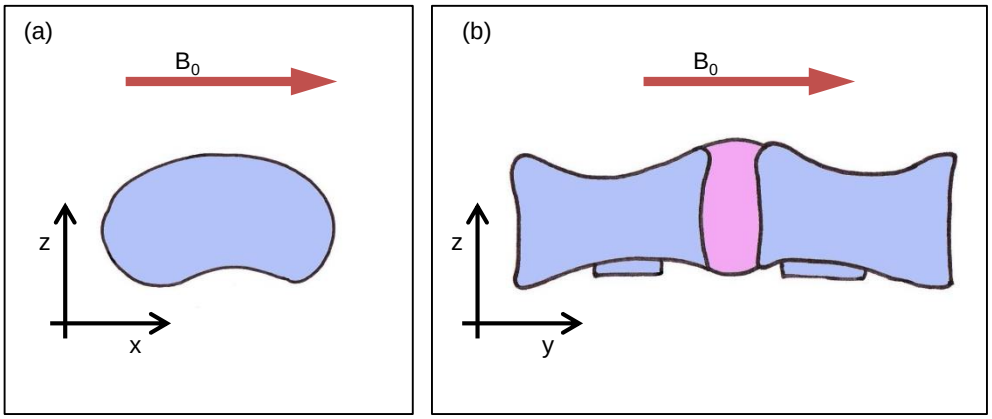

Figure 4.5 – Diagram to show the change in orientation of the specimen relative to the magnetic field. In the initial scan (left), the y-axis of the specimen is perpendicular to the primary direction of the magnetic field (B_0). In the second scan (right), the y-axis of the specimen is aligned with the magnetic field.

This test was conducted to assess the effect of the "magic angle" effect, as discussed by Dunn *et al.* (2004), in which the angle of the tissue fibres relative to the magnetic field affects the intensity of the signal. If the lamellae of the annulus are

detected, the signal from them should be less intense in the first of the two scans. The results of this test are illustrated in Figure 4.6.

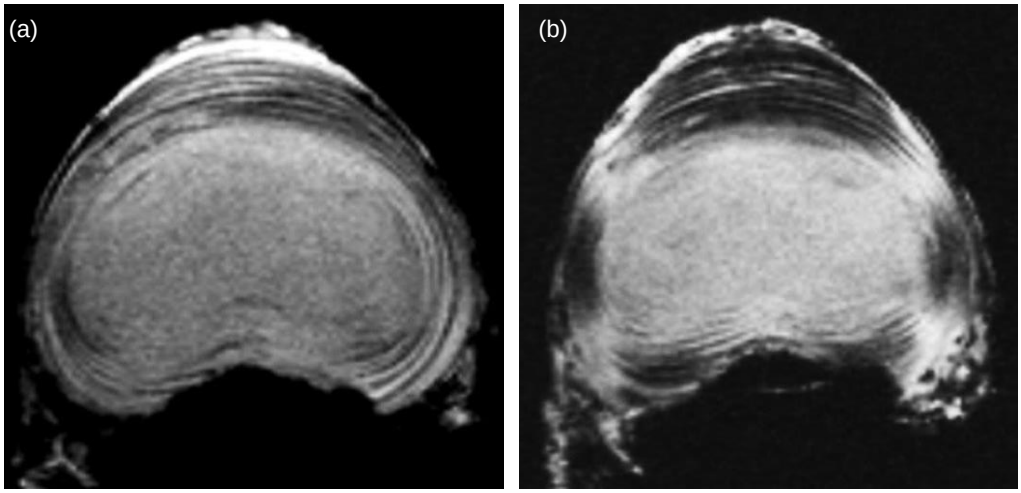

Figure 4.6 – Axial slice through the disc from the annulus, 3D flash scan of specimen S4 with variation in specimen alignment relative to magnetic field. Left: specimen y-axis aligned perpendicular to the primary direction of the magnetic field. Intense bands are recorded through the annulus at four points. Right: specimen y-axis is aligned with the primary direction of the magnetic field. The signal intensity from the annulus is more consistent.

When the y-axis was perpendicular to the direction of the magnetic field (Figure 4.6 – a), the annulus signal was darker, as a result of the magic angle effect. Dunn *et al.* (2004) reported similar findings from their tests. This supports the hypothesis that the striations in the annulus represent individual lamellae with alternating fibre orientations

FINAL SCAN SETTINGS

Two sequences were developed with the aim of individually capturing the nucleus and the annulus. The sequence settings are shown in Table 4.3; both scans were conducted for all specimens.

	nucleus scan	annulus scan
scan type	turbo spin echo	flash
in-plane resolution	0.31 mm	0.2mm
slice thickness	1.5mm	0.2mm
FoV	160 x 160	60 x 60
matrix size	512 x 512	256 x 256
TR	3200ms	50ms
TE	36ms	5ms
flip angle	n/a	30˚
number of averages	1	1
scan time	approx. 6 min	approx. 55 min
number of slices	21	256

Table 4.3 – Final settings used for nucleus and annulus MRI scans.

MR image results require validation before assumptions regarding the structure, geometry and physiology of the tissues can be drawn based on the data. A range of techniques were used for validation in this study such as comparisons with other imaging modalities, tissue dissection and observation of the effect of varying MR sequences. The results of the validation processes are discussed in Section 4.3.2.

SOFT TISSUE STRUCTURE

The specimens were initially scanned in their prior-to-loading (P) state to capture the soft tissue structures in their unloaded state.

Measurements were taken from the MRI data for the gross disc dimensions and the internal soft tissue structures. The number of lamellae visible was recorded for four different locations circumferentially.

SOFT TISSUE DEFORMATION

Following the P-scans, the rig discussed previously (Figure 4.2) was used to compress the specimens. The change in disc height was reviewed using a scout-view scan. When the change in height was greater than or equal to 20% of the original disc height, soft tissues were allowed to relax for 25 minutes before full scans were conducted.

As part of the method development, preliminary load tests were conducted on four ovine lumbar specimens that were not used for imaging. These specimens were compressed by 1.5mm in the C-C direction for 40 minutes using an electromechanical material testing machine (model number: 3366, Instron,

Norwood, MA, USA). The force exerted by the machine on the specimen was recorded throughout. As the fluid flowed out of the discs, the hydrostatic pressure reduced and the force required to maintain the compressed state reduced, as illustrated in Figure 4.7.

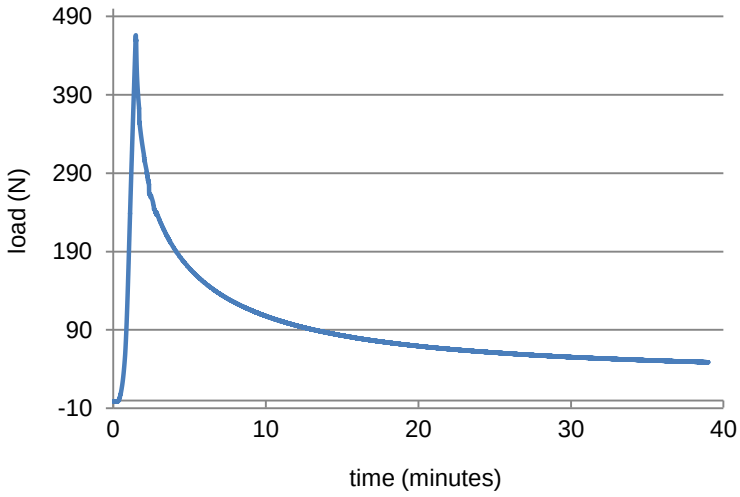

Figure 4.7 – An example load-time curve for an ovine, lumbar disc specimen compressed by 1.5mm in the C-C direction and held for 40 minutes.

After 25 minutes all four of the preliminary specimens were within 20% of their final state and so this was considered sufficient relaxation time for the MRI specimens.

Images from the P and L scans were analysed using image processing software (ImageJ, National Institute of Health, USA). Disc height was measured at nine locations on a 4mm grid that was centred on the intersection point of the mid coronal and mid sagittal slices of the annulus scan. These measurements were repeated for both the preloaded (MRI-P) and loaded (MRI-L) scans and the average change in disc height was calculated.

Changes to the soft tissue structures between the preloaded and loaded scans were observed, such as the radial bulge of the annulus and nucleus and the changes to the shape and position the annulus lamellar structure. Measurements were taken for disc width and depth at the mid-coronal and mid-sagittal slices respectively.

DEGENERATION ANALYSIS

A scale developed by Pfirrmann et al. (2001), based on the work of Pearce et al. (1991), was used to grade the degeneration of the tissue using the T2 weighted spin echo images (nucleus scan). The grading scale is outlined in Table 4.4.

Grade	Structure	Distinction of nucleus/annulus	Signal intensity	Disc height
I	homogenous, bright white	clear	hyper-intense	normal
II	inhomogeneous	clear	hyper-intense	normal
III	inhomogeneous, grey	unclear	intermediate	normal to slightly decreased
IV	inhomogeneous, grey to black	lost	intermediate to hypo-intense	normal to moderately decreased
V	inhomogeneous, black	lost	hypo-intense	collapsed disc space

Table 4.4 – Scale used for grading disc degeneration based on T2 weighted spin echo images captured during nucleus scan. Adapted from Pfirrmann et al (2001).

Each specimen was graded by four independent reviewers. The average degeneration grade assigned based on the MR images was calculated.

4.2.4 DISSECTION PHOTOGRAPHY AND ANALYSIS

Following scanning, the specimens were dissected and photographed for comparison with image data. The specimens were trimmed to remove the adjacent discs and PMMA end-caps. The specimens were then frozen before they were cut by hand using a hack saw through the bones and a scalpel through the soft tissue. A custom-built guide was used to keep the cut in plane (Figure 4.8) along either the mid-coronal or mid-axial plane, as presented in Table 4.5.

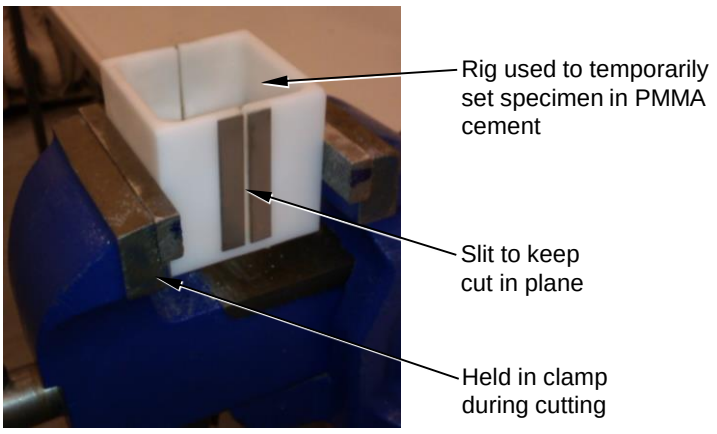

Figure 4.8 – Custom built cutting rig. The specimens were trimmed around the FSU of interest. The trimmed specimen was set in PMMA to fit the rig. A hack saw was used to cut through the specimen. The slit in the rig maintained the cutting plane through the specimen.

Specimen	Cutting plane
S1	axial
S2	axial
S3	axial
S4	coronal*
S5	coronal*

*Table 4.5 – Planes of dissection for each specimen. Those marked * were also cut in the axial plane following initial cutting in the coronal plane.*

Close-up photographs were taken (Canon 550d camera with a Canon EF, 100mm, F2.8 macro lens) of each specimen with the aim of capturing details of the internal soft tissue structures such as the lamellae and nucleus. A scale was included in each image for reference.

Each specimen was inspected in detail for signs of degeneration, and other unusual features. Measurements were taken for the external dimensions of the disc as well as the width and depth of the nucleus and the thickness of the annulus. The degeneration of each disc was graded based on a scale devised by Thompson *et al.* (1990), as outlined in Table 4.6.

Grade	nucleus	annulus	EP	VB
I	bulging gel	discrete, fibrous lamellae	uniform thickness	margins rounded
II	white fibrous tissue at periphery	mucinous material between lamellae	irregular thickness	margins pointed
III	consolidated fibrous tissue	extensive mucus, loss of annulus/nucleus distinction	focal defects in cartilage	early osteophytes at margins
IV	horizontal clefts, parallel to EPs	focal disruptions	fibrocartilage extending into VB, irregular, focal defects	osteophytes smaller than 2mm
V	clefts throughout	clefts throughout	diffuse sclerosis	osteophytes greater than 2mm

Table 4.6 – Scale used for grading disc degeneration adapted from Thompson et al. 1990.

Each specimen was graded by four independent reviewers, based on photographs of the specimens during dissection. The average degeneration grade assigned was calculated.

Following the dissection process, the images were analysed and the measurements were repeated. The number of lamellae was counted at four points across the

annulus, at the posterio-lateral and anterio-lateral corners. The width of a single lamella was measured using image processing software (ImageJ, National Institute of Health, USA) at four different locations and the average thickness was calculated.

4.2.5 COMPARISON BETWEEN IMAGING MODALITIES

MRI data was compared to corresponding µCT data to analyse how features of the disc were captured using the different modalities. This process aided with the identification of features in the MRI data, in particular the end plate topography, and contributed towards the validation of MRI data.

Measurements taken during dissection were compared to those taken from MRI data to improve understanding of how the structures are captured in the scans. Results were compared for disc width and depth, nucleus width and depth, annulus thickness, number of lamellae and lamella thickness.

4.3 RESULTS

The dimensions recorded from the MRI and dissection data are summarised in Figure 4.9.

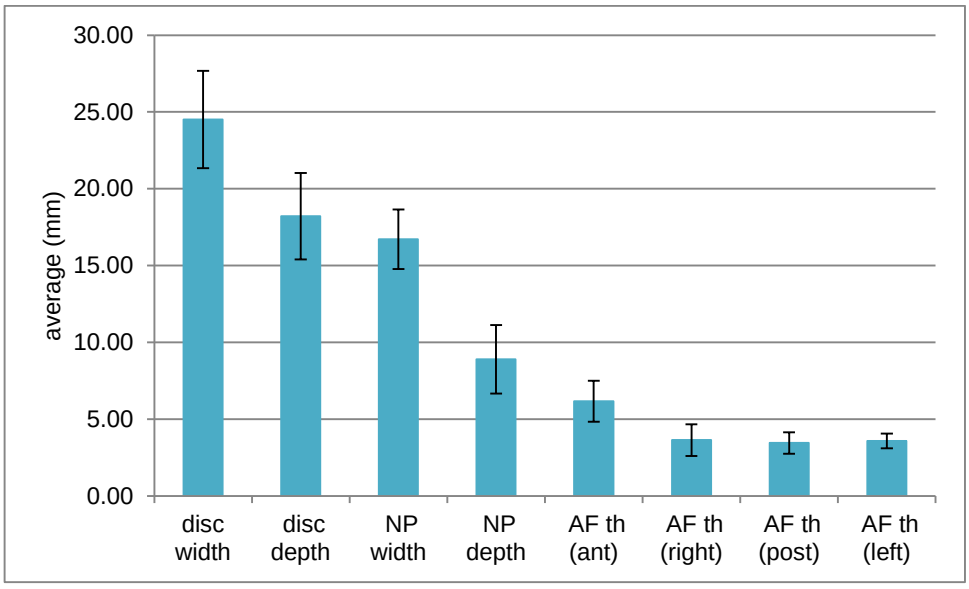

Figure 4.9 – Average dimensions for soft tissues of the disc, taken from annulus MRI-P and dissection data. Error bars show standard deviation across the five specimens from measurements using both techniques (MRI and dissection).

4.3.1 MICRO COMPUTED TOMOGRAPHY

A typical µCT image is presented in Figure 4.10. The trabecular structure of the vertebral bodies is shown in detail, as are the cortical shell and bony end plates. The disc is captured as a single, monotone shadow.

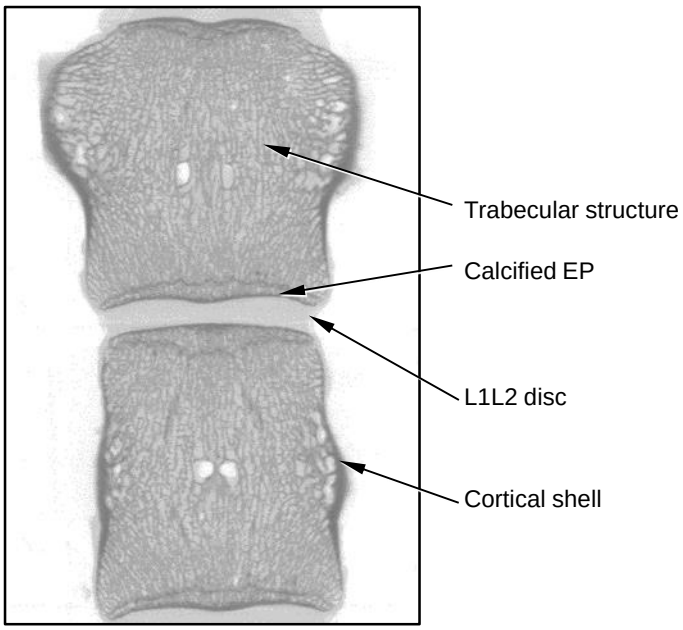

Figure 4.10 – Inverse image of a µCT slice through specimen S2 in the coronal plane, showing bony vertebral end plates, trabecular structure of the VBs and disc space.

Although the gross volume of the disc was captured in the µCT data, there was no detail of the internal soft tissue structures, such as a distinction between the nucleus and annulus, thus the applications of this technique to the development of computational models of the soft tissue was limited. However detailed geometric data was captured for the adjacent bone structures.

4.3.2 MAGNETIC RESONANCE IMAGING

SOFT TISSUE STRUCTURE

The quality of the images captured during the nucleus scans varied widely. For S1 and S3, a distinct region of intense signal was registered in the centre of the disc, suggesting this structure was the nucleus. Images for S1 and S3 are shown in Figure 4.11.

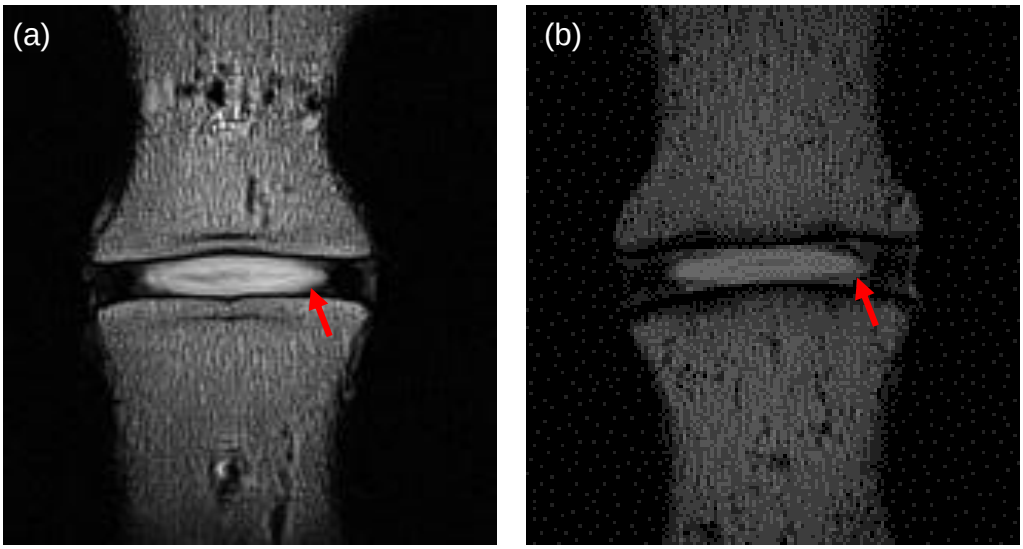

Figure 4.11 – Images from nucleus scans of (a) S1 and (b) S3 showing the mid-coronal slice in the prior to loading case. For both images the arrow indicates the suspected nucleus/annulus boarder.

However, this nucleus distinction was not observed in the remaining three scans. Irregular patterns of intensity were observed across the centre of the disc in the nucleus scan of S4, as show in Figure 4.12.

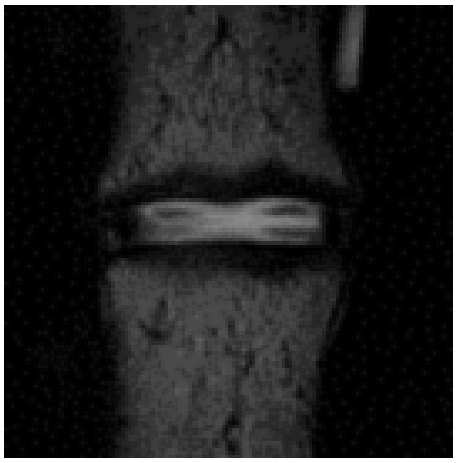

Figure 4.12 – Nucleus scan of S4 showing the mid-coronal slice of the specimen prior to loading. The centre of the disc has high intensity signal, however the patterns recorded do not identify the soft tissues of the disc.

In most cases, the annulus scans suggested a layered structure to the outer soft tissues of the discs. The 3D resolution of these scans allowed these structures to be captured in three planes, as illustrated in Figure 4.13 and Figure 4.14.

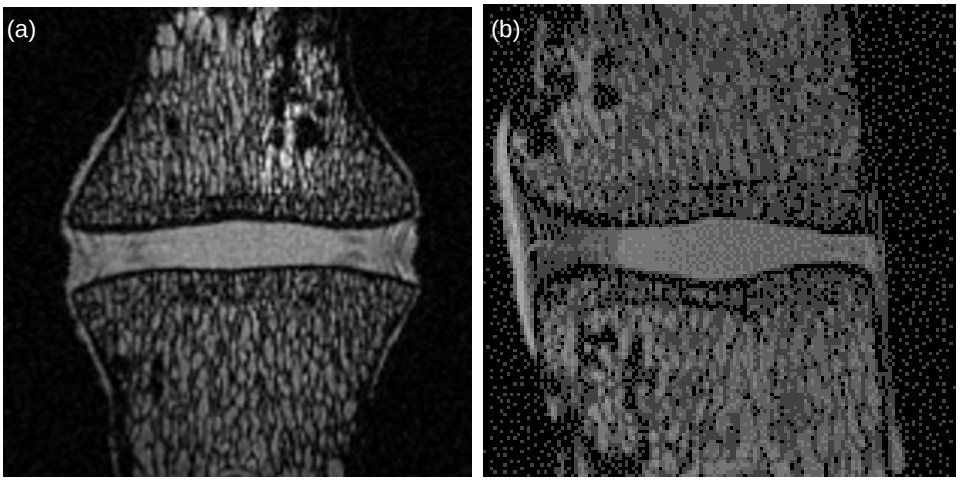

Figure 4.13 – Example (a) coronal and (b) sagittal slices taken from the annulus scan of S1, in which the layered structure can be seen in the outer soft tissues of the disc.

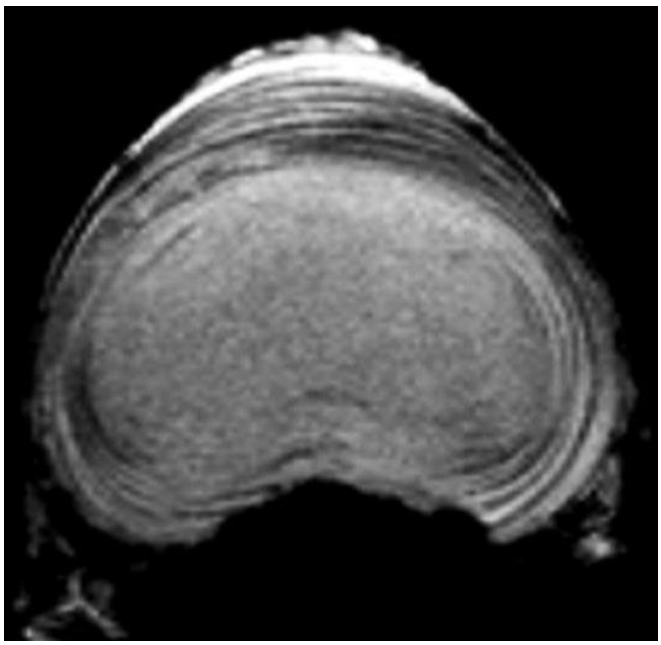

Figure 4.14 – Mid-axial slice from the annulus scan of S5 showing the layered structure of the soft tissues in the disc periphery.

As illustrated in Figure 4.13 and Figure 4.14, there was no clear boundary between the annulus and nucleus; however the texture of the tissues was very different in the centre of the disc to the outer tissues.

The quality and clarity of the images from the annulus scans varied between specimens. For example, much of the detail described for S1 and S3 above was not captured for S2, as shown in Figure 4.15, in which there are large portions of the outer soft tissues that are not imaged well.

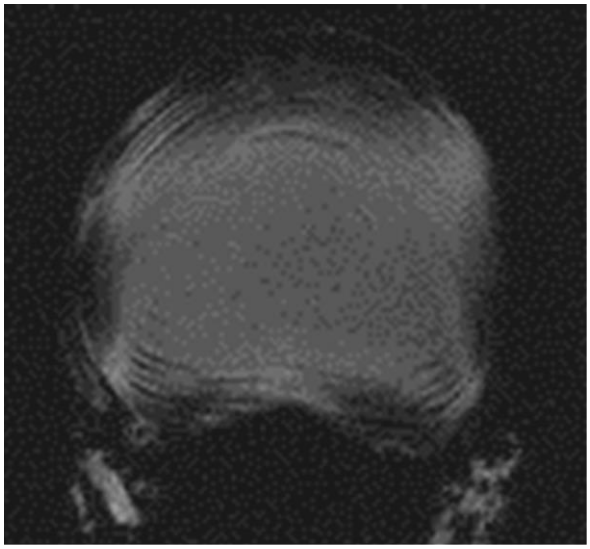

Figure 4.15 – Mid axial slice from the annulus scan of S2. The scan has not fully captured the soft tissues to as high level of detail as other specimens.

The data analysed during the MR sequence development process supports the assumption that each of the dark and bright bands within the annulus represents an individual lamella.

The number of lamellae was recorded in four locations circumferentially for each disc based on the annulus scan results. An example showing how the lamellae were counted based on greyscale value is shown in Figure 4.16. Results for the number of lamellae by location within the disc are summarised in Figure 4.32.

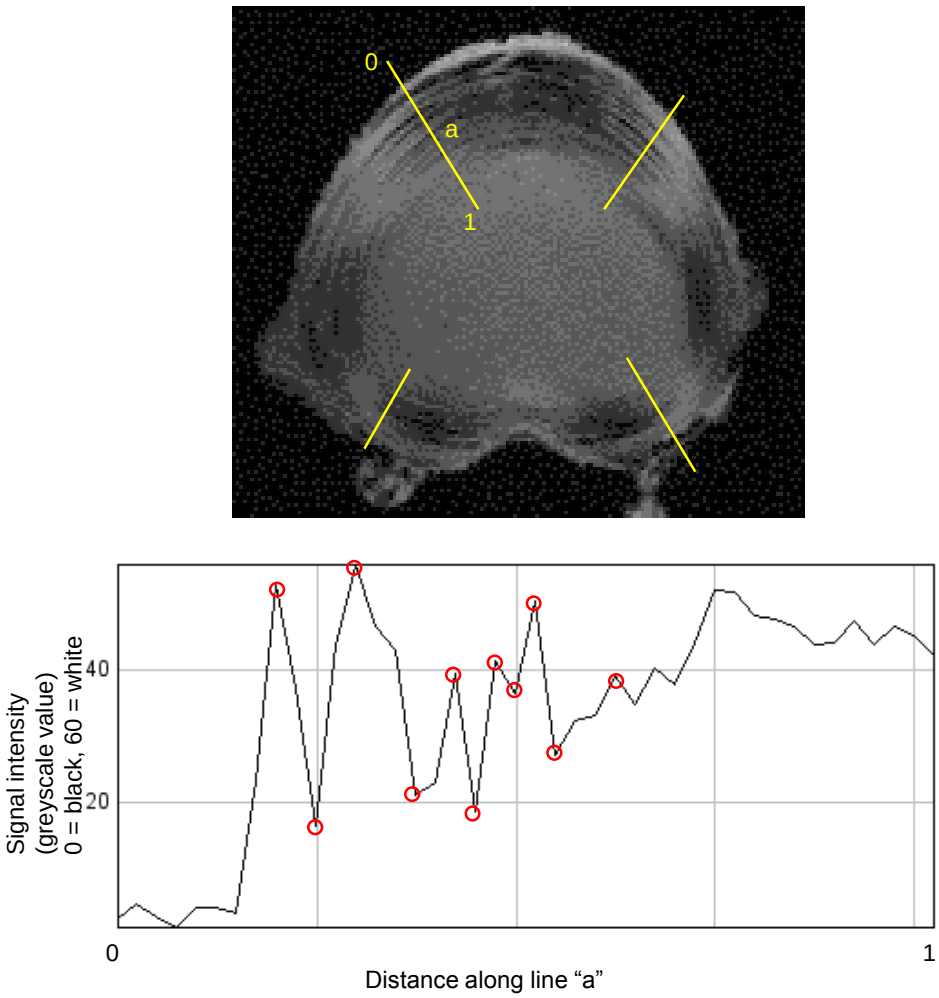

Figure 4.16 – Mid axial slice from the annulus scan of S1 (top) showing the four locations at which lamellae were counted based on greyscale value variation. The graph (bottom) shows the greyscale values along the line marked “a”. Each peak and trough along this graph was counted as a lamella (circled). 11 lamellae were counted for this example.

The coronal images from the annulus scan showing the extremities of the annulus gave an indication of the fibre angle of the tissue in this region, as illustrated in Figure 4.17.

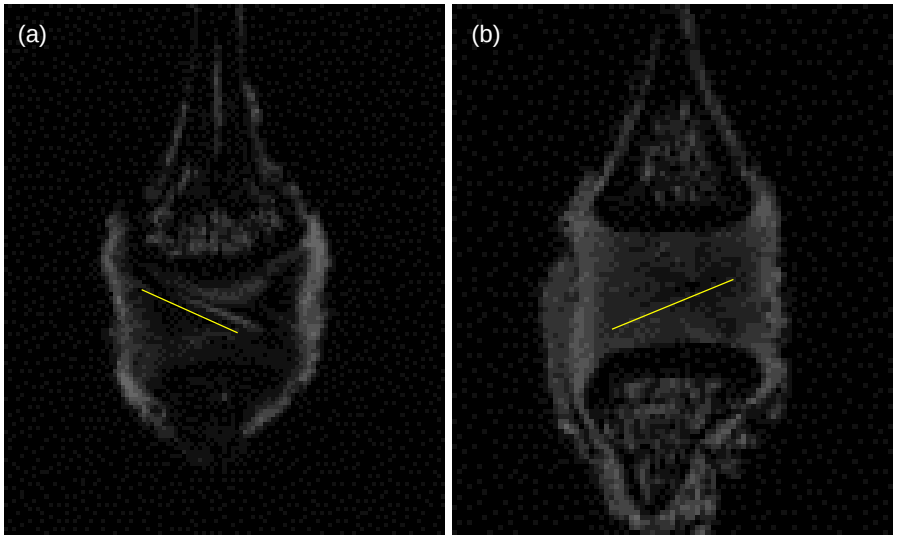

Figure 4.17 – Coronal slices from the annulus scans of S1 (left) and S3 (right) showing the outer extremity of the annulus. The signal pattern within the disc tissue gives an indication of the fibre angle for the tissue in this part of the disc.

SOFT TISSUE DEFORMATION

Images from the MRI-L (loaded) scans were compared to the equivalent images from the MRI-P (pre-loaded) scans to assess the deformation of the soft tissues that had been captured.

As for the MRI-P scans, the nucleus scan (L) was successful for S1 and S3, for which the intense region at the centre of the disc, assumed to be the nucleus elongated, suggesting the nucleus had bulged when compression was applied.

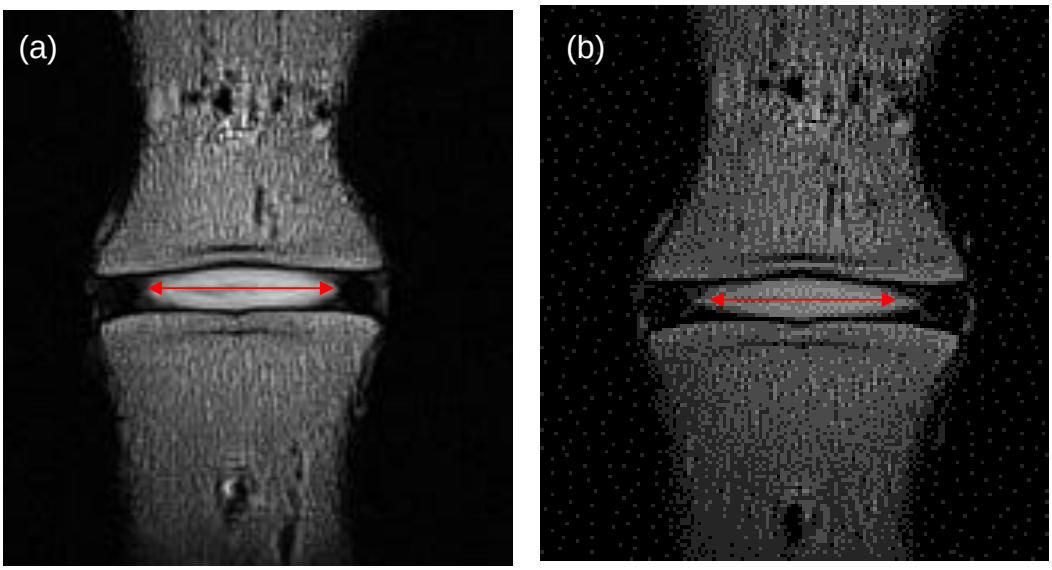

Figure 4.18 – Mid-coronal slice from the nucleus scan for S1 in (a) the prior to loading and (b) compressed state. The arrow shows the original width of the nucleus and is the same length in both images, illustrating how the nucleus appears to have bulged during compression.

These trends in deformation were not observed for all specimens. The unusual patterns captured in the P scan of S4 were again unidentifiable as tissue structures in the L scan, as shown in Figure 4.19.

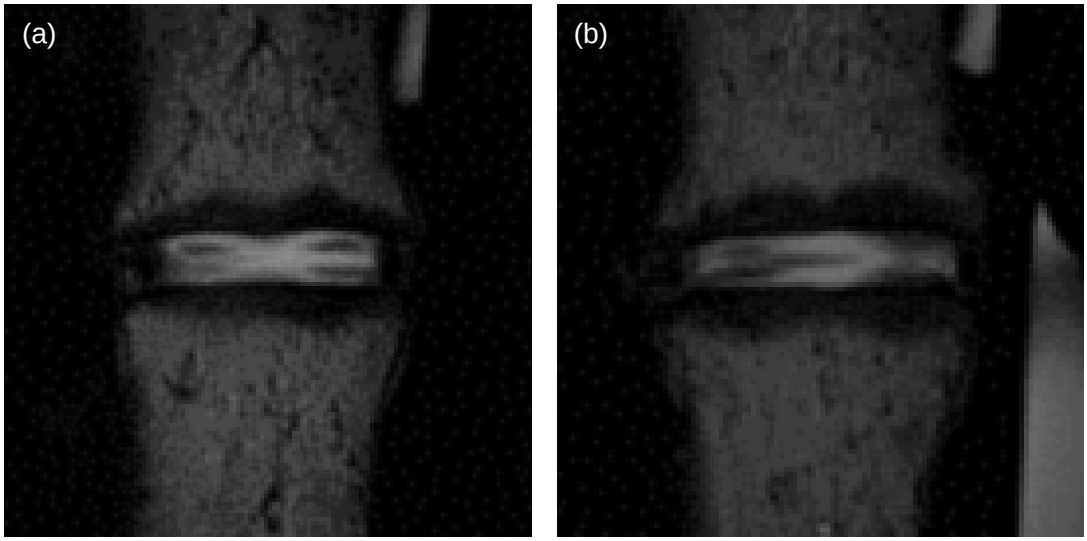

Figure 4.19 – Mid coronal slices from (a) the P and (b) the L nucleus scans of S4. Unusual patterns are captured in the centre of the disc. These change with applied compression but do not appear to relate directly to the soft tissue structure.

Equivalent images from the P and L versions of the annulus scans were compared to analyse the soft tissue deformation that had occurred during the applied compression. The magnitude of the deformation varied between sizes due to variation in specimen sizes, condition and applied displacement. For all specimens the reduction in disc height and the radial bulge at the outer annulus were recorded.

These deformations are illustrated in Figure 4.20 and Figure 4.21.

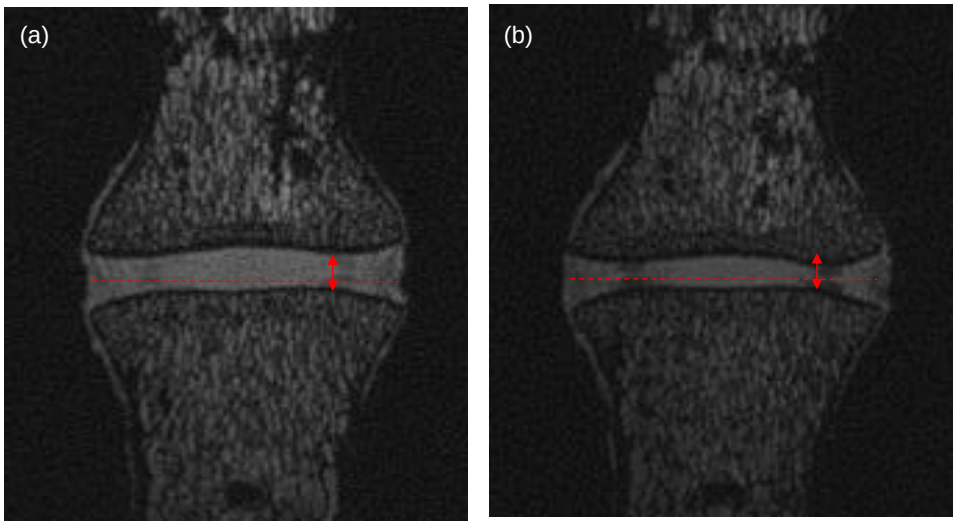

Figure 4.20 – Mid-coronal slices for the (a) P and (b) L versions of the annulus scan for S1. The dashed line indicates the original disc width and the arrow the disc height. Both are consistent lengths in the two images.

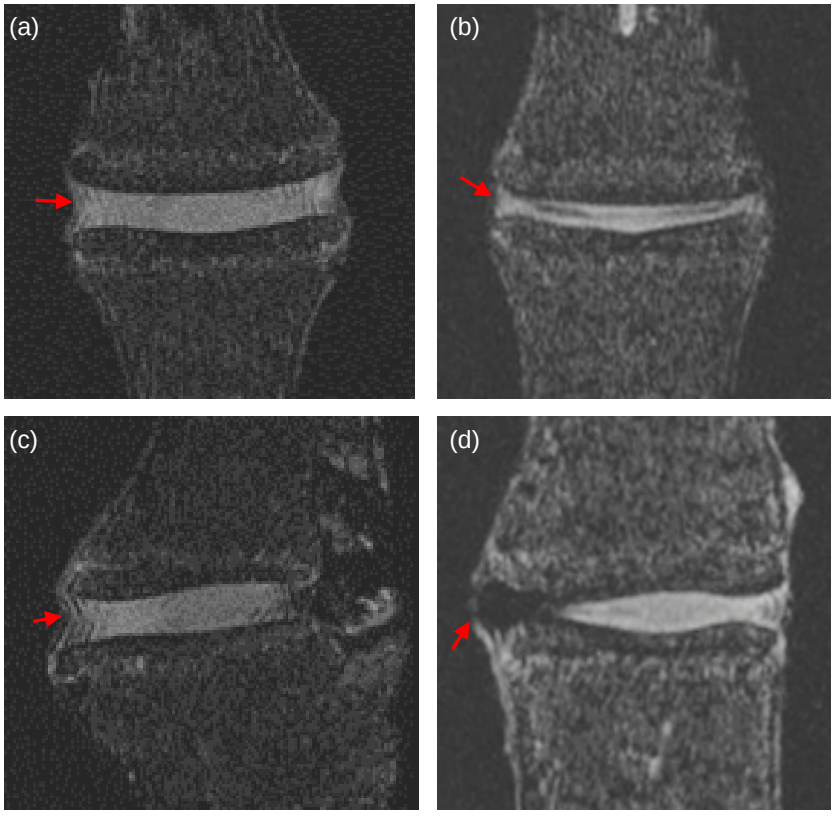

Figure 4.21 – Images taken from the P (a, c) and L (b, d) annulus scans of S2, showing the mid coronal (a, b) and mid sagittal (a, d) slices. The arrows indicate the outer annulus for which the curvature of the lamellae changed from convex prior to loading to concave during compression.

The change in the tissue structure between the P and L scans was most distinct in the anterior region of the disc, as illustrated in the images of S1 presented in Figure 4.22.

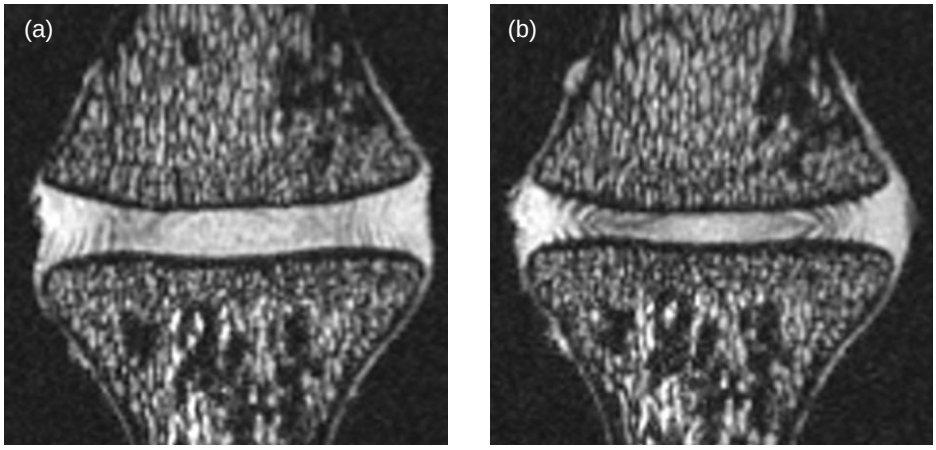

Figure 4.22 – Images from the anterior region of S1 for the MRI-P (a) and MRI-L (b) scans.

From the annulus MRI scans, the height, width and depth of the disc was measured using image processing software (ImageJ, NIH, USA). The changes in dimensions between the P and L scans are presented in Figure 4.23.

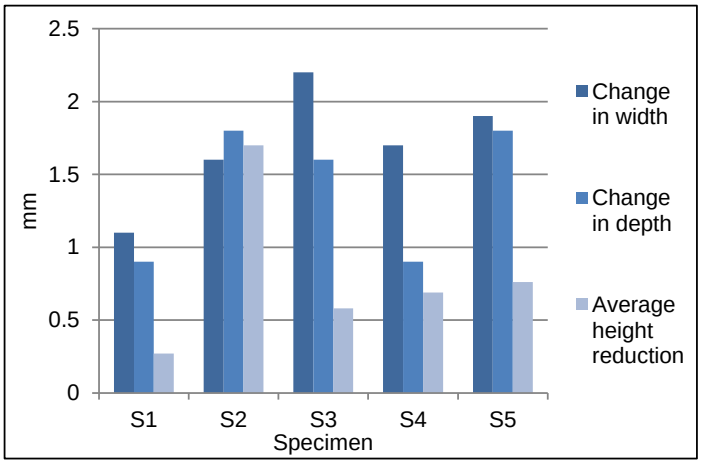

Figure 4.23 – Change in gross disc dimensions based on MRI scans. Width measurements were taken from the mid coronal slice, depth measurements were taken from the mid-sagittal slice and height measurements were an average of nine measurements taken across the disc.

For the MRI-L scans, the fibre angle was not clear in the outer annulus, as shown in Figure 4.24.

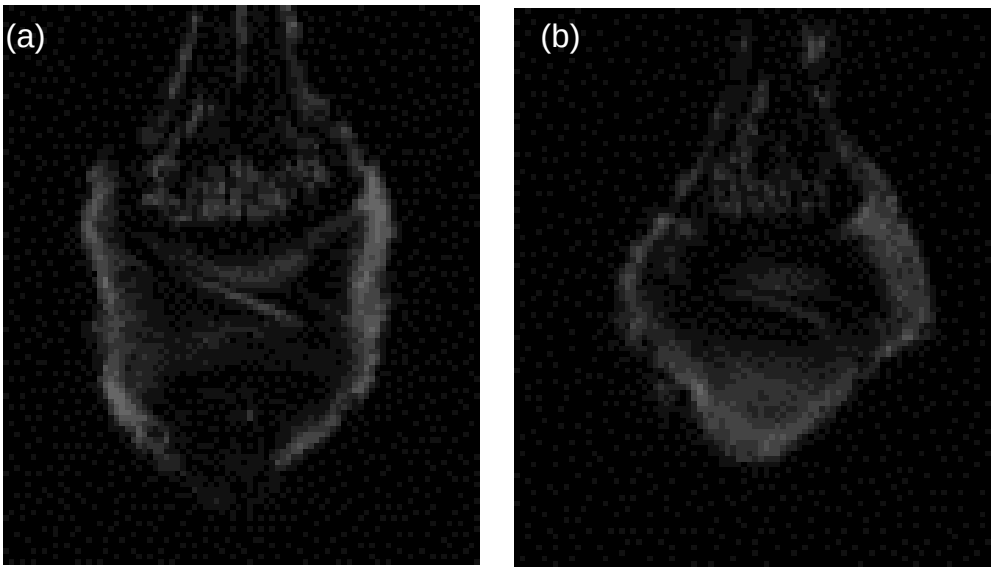

Figure 4.24 – The outer annulus taken from the P (a) and L (b) annulus scans of S1. The fibre angle is visible in the P scan but is unclear in the L scan.

4.3.3 DISSECTION PHOTOGRAPHY AND ANALYSIS

Individual lamellae could be identified on the photographs taken during dissection. For all specimens, the soft tissues were identified as nucleus and annulus. For some specimens, the transition zone was also identified, as illustrated for S2 in Figure 4.25.

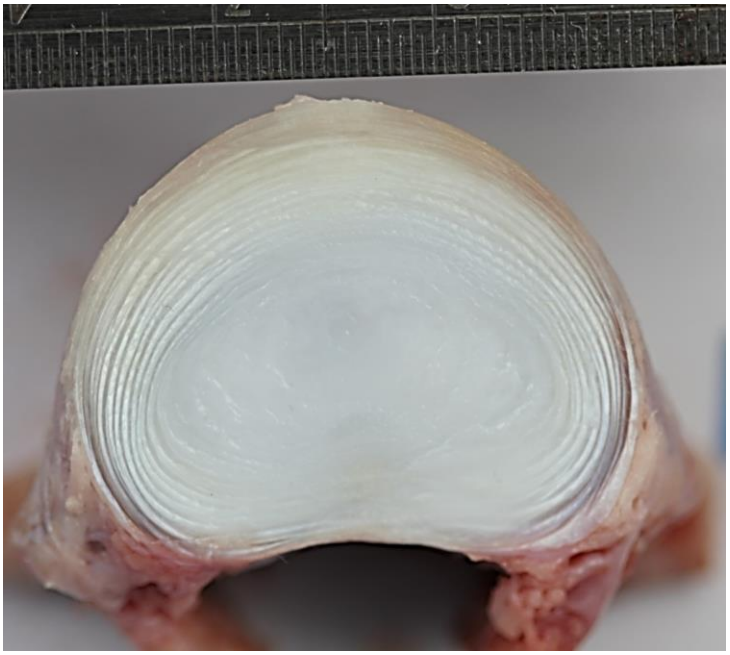

Figure 4.25 – Photograph of the axial section through S2. Individual lamellae are visible and the soft tissues are distinguishable as the annulus, nucleus and transition zone. Scale shows mm.

The distinction between tissues was not as clear for the coronal section photographs, as illustrated in Figure 4.26. In these sections, the nucleus and annulus had differing appearances but individual lamellae were not as distinguished and the boundary between tissues was not clear. Tissue measurements were taken from the axial sections for all specimens.

Figure 4.26 – Photograph of coronal section of S4. The nucleus and annulus have differing appearances but the boundary between them is not clear. Individual lamellae are not distinguishable. Scale shows mm.

The thickness of the annulus varied circumferentially for all specimens. The annulus was thickest in the anterior of the discs, with a similar thickness recorded for the posterior and lateral sides, as demonstrated in Figure 4.27 and Figure 4.9.

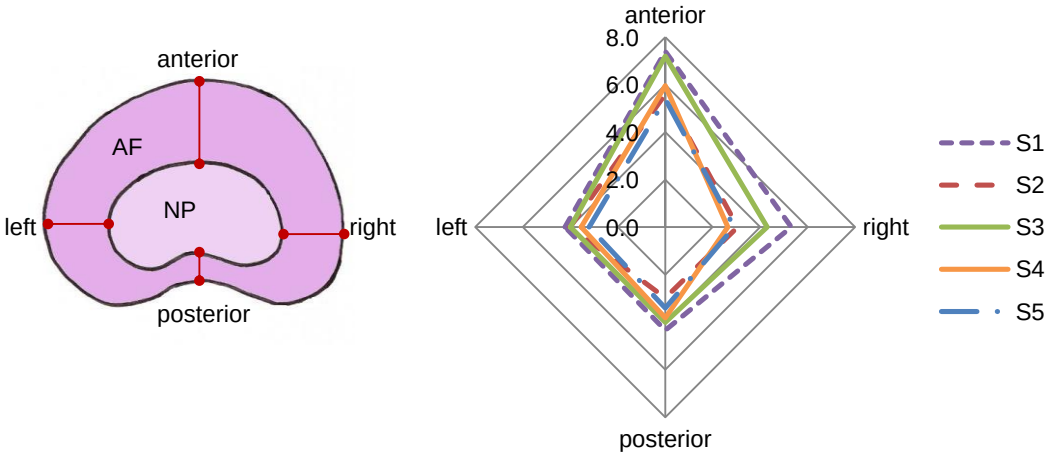

Figure 4.27 – Annulus thickness for all five specimens based on circumferential location with accompanying schematic diagram showing location of measurements. Scale is in mm. 0 = no thickness.

4.3.4 DEGENERATION ANALYSIS

Good agreement was recorded between the two methods used to grade the degeneration of the disc tissue, with approximately half a grade variation for each specimen with the exception of S2, as illustrated in Figure 4.28.

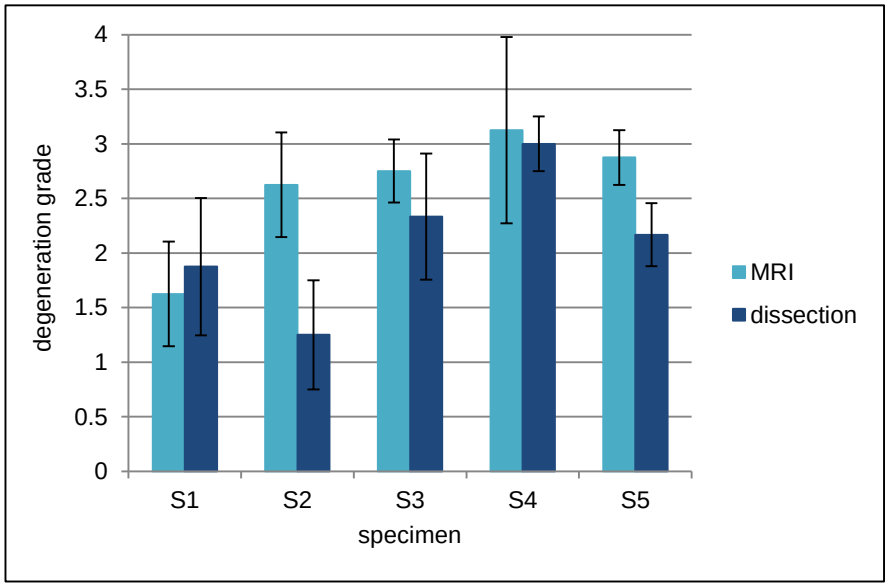

Figure 4.28 – Variation in degeneration grading for each specimen based on technique used. Error bars show standard deviation for the grades assigned by the four independent reviewers.

The final grades assigned to each specimen are summarised in Table 4.7.

Specimen	MRI grading	Dissection grading	Average
S1	I-II	I-II	I-II
S2	II-III	I	II
S3	II-III	II	II-III
S4	III	III	III
S5	II-III	II	II

Table 4.7 – Degeneration grades based on MRI data and observation during dissection for all specimens. Grades presented are the averages of results from four independent reviewers. The "average" column shows the average of all reviewers and both methods.

Examples of tissue grading based on the MR and dissection data are given in Figure 4.29.

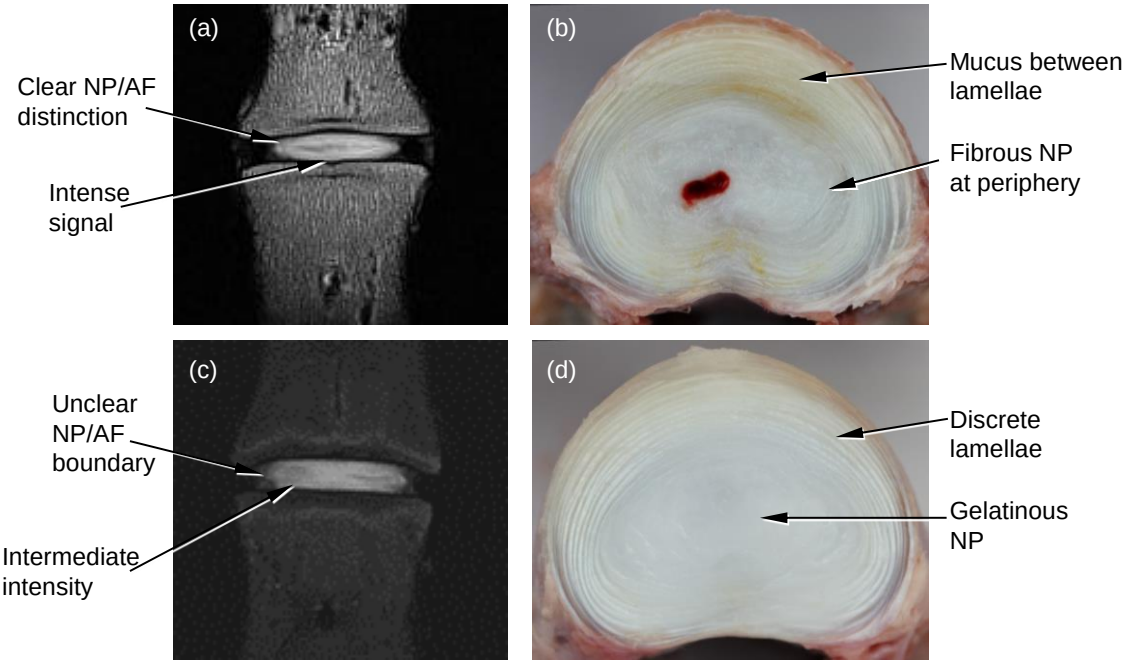

Figure 4.29 - T2 weighted spin echo MR images and dissection photographs for S1 (a, b) and S2 (c, d) used for degeneration grading. S1 was graded as level II for both MR and dissection analyses. The blood shown in the centre of the disc was believed to be a result of disruption or contamination during dissection. S2 was graded as level III from MR and level I from dissection.

4.3.5 COMPARISON BETWEEN IMAGING MODALITIES

The topography of the end plate was clear in both the annulus MRI scan data and the µCT data, as illustrated in Figure 4.30.

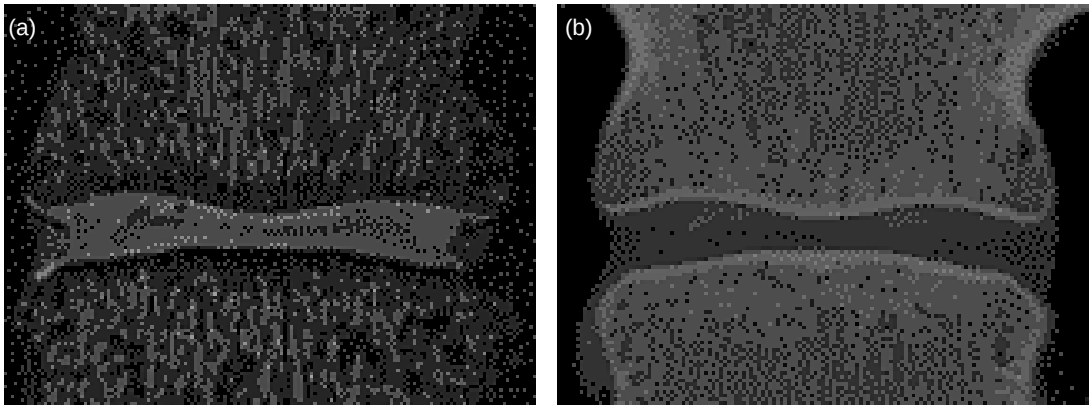

Figure 4.30 – Images developed from (a) annulus MR scan and (b) µCT scan of specimen S3 showing the EP topography. The subchondral bone immediately adjacent to the disc appears dark in the MR image and bright in the µCT image. Agreement between the two imaging modalities assists in validating the MR techniques and instils confidence in assumptions made about the EP topography based on the MR images.

The characteristic profiles of the end plates were captured using both imaging techniques. This improves confidence in the MR techniques used and suggests that the MR image data could be used to accurately characterise the geometry of the end plates.

There was a notable variation in signal intensity pattern between specimens for the nucleus scans that was not replicated in either the annulus scans or the dissection analysis. For the nucleus scans of S1 and S3 there appeared to be a clear nucleus/annulus boundary. For the remaining three specimens the boundary was very unclear and did not replicate the anticipated shape of the nucleus. Thus the data taken from the nucleus scans was not considered further in the analysis.

Disc dimensions recorded from the annulus scan and the dissection analysis for each of the specimens are compared in Figure 4.31.

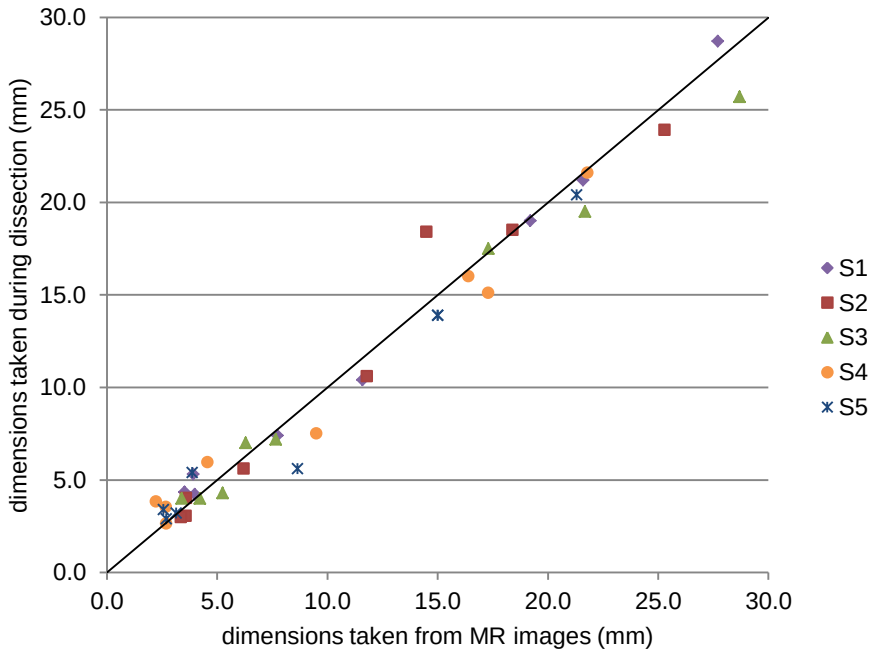

Figure 4.31 – Comparison of dimensions taken from MRI and dissection for each specimen. Dimensions are given (mm) for disc depth and width, nucleus depth and width (from annulus scans only) and annulus thickness at the anterior, posterior, left and right.

The percentage error of each soft tissue dimension taken from the MRI data was compared to the equivalent measurement taken from the dissection photographs. This error ranged from 0% to 23%. The best agreements were recorded for the overall disc dimensions which had on average 5% error. The worst errors were for the nucleus depth and annulus thickness at the posterior of the disc which were 23% and 21% (average error) respectively. S1 had the best agreement of the five specimens reviewed with an average of 9% error for the dimension data.

Poor agreement was recorded between the annulus scan and dissection analysis for the number of lamellae. The number of lamellae recorded from the annulus scan was typically 40-60% lower than that recorded during dissection. The data for S4 is shown as an example illustration of this in Figure 4.32.

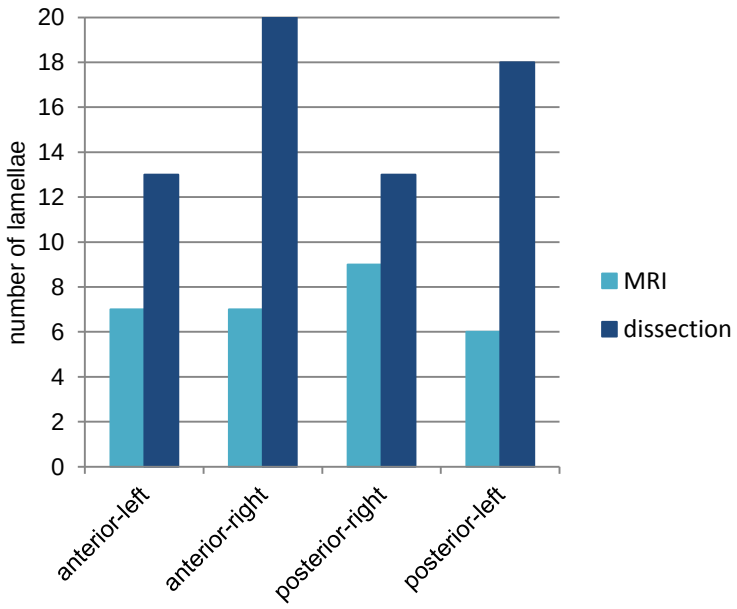

Figure 4.32 – Number of lamellae by circumferential location for S4 based on annulus scan and dissection analysis.

Better agreement was observed between the annulus scan and dissection data for the average thickness of lamellae per specimen, as shown in Figure 4.33; however these results had a large range. The approximate thickness of 0.2 – 0.3 mm agrees with the lamella thickness reported in histological studies (Marchand and Ahmed 1990).

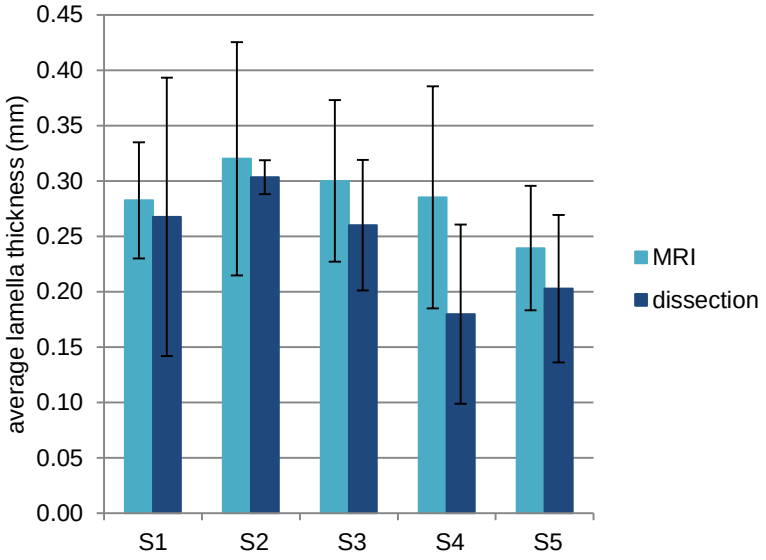

Figure 4.33 – Average lamella thicknesses for each specimen taken from MRI and dissection data. Error bars show standard deviation.

Comparing between image modalities facilitated an improved understanding of features of particular specimens. For example, for S3, some unusual marks were noticed in both the MRI and µCT data, as shown in Figure 4.34.

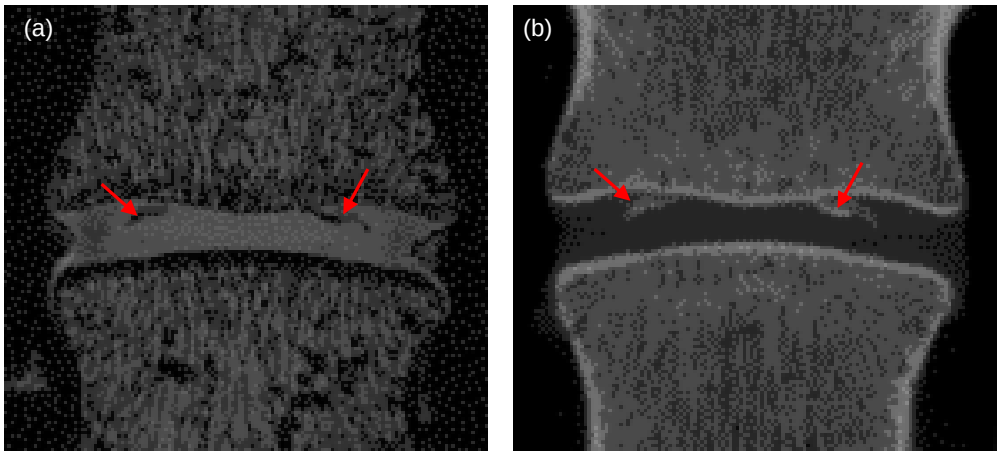

Figure 4.34 – Equivalent coronal slices from the annulus MR scan (a) and µCT scan (b) for S3. The arrows indicate some unusual features showed up in both modalities.

During dissection, these features were visible following the removal of some normal disc tissue. They were observed to be bright white in colour with a malleable, fibrous composition. The features are highlighted in Figure 4.35.

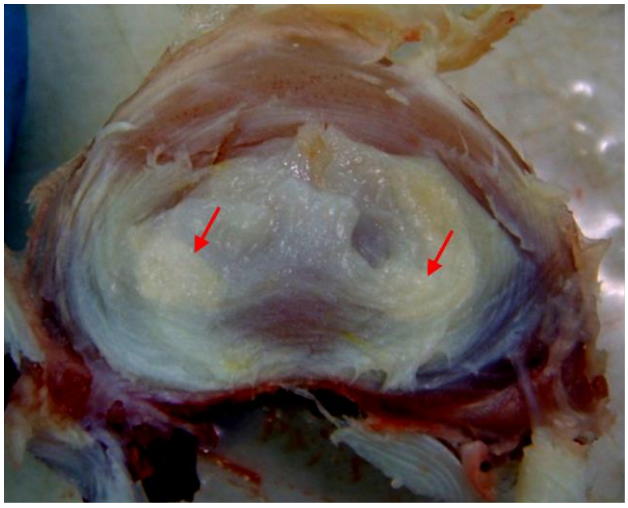

Figure 4.35 – Photograph taken during the dissection of S3. The arrows highlight the white anomalies within the disc tissue.

4.4 DISCUSSION

MR imaging of the disc has previously focussed on developing techniques to monitor the chemical composition of the tissue, relevant to clinical and pathological applications (Urban and Winlove 2007). This study took an alternative approach by developing MR techniques to image the internal structure and geometry of the soft

tissues of the disc in the intact and loaded state. This approach has facilitated an improved understanding of soft tissue deformations, particularly in the deformation of the lamellar structure of the annulus.

The challenges and limitations faced when working with MR techniques were highlighted, in particular, the need to validate MR image data before internal soft tissues can be identified with confidence.

Four approaches were taken towards validation of the MR data:

- The effect of fat suppression was used to identify the fat and water based tissues.
- The signal from the annulus was shown to be dependent upon the specimen orientation relative to the magnetic field, supporting the assumption that each dark and bright band within the annulus represented a lamella.
- Comparison between the MR and µCT data showed good agreement for the end plate topography.
- Comparison between the MR and dissection data allowed the accuracy of tissue geometric data to be analysed.

The capability to identify soft tissue structures based solely on MRI data was limited. The lack of reference points within the soft tissues diminished the possibilities for identifying the mechanics of specific structures. This was complicated further by the reorientation of fibres relative to the magnetic field during compression, which at times resulted in changes in signal intensity from the same tissues in the P and L scans. For example, it was not possible to identify individual lamellae between the P and L scan because the re-orientation of the fibre directions on application of compression may have changed the intensity of the signal from that lamella, so a lamella that appeared bright in the P scan may have appeared dark in the L scan.

The echo time used in the nucleus sequence developed was much shorter than those typically used during clinical imaging of the disc. An echo time of 112-149 ms is used in clinical studies (Sharma *et al.* 2009), much longer than the 36 ms used in this study. This shorter echo time was chosen to compensate for the range in degeneration levels of the specimens so that a complete nucleus volume was imaged for each. Despite this, the scan sequence was not appropriate for some of the specimens. It was not possible to accurately capture the geometry of the nucleus as a single, defined structure. This was partly a reflection of the natural

state of the disc soft tissues, in which there is not a distinct boundary between the annulus and nucleus.

For example, the nucleus scan of S4 did not produce images of the nucleus as anticipated. Instead of a single, coherent volume at the centre of the disc, the nucleus appeared as strata of intensity that deformed and appeared to move with compression. Upon dissection of this disc, the nucleus was observed to be fibrous, dehydrated and with several clefts. The fibrous nature of the nucleus could have caused the unexpected pattern of intensity in the MR images. During compression, the orientation of these fibres was altered, resulting in further unanticipated intensity patterns in the L scan.

As a result of these complications, the nucleus-scans were used only during the method development and were not used to obtain further data or in the FE study presented in Chapter 5.

For the annulus scans, it was concluded that each of the bright and dark bands in the annulus region was an individual lamella. Evidence supporting this conclusion was drawn from several sources.

When the orientation of the specimen relative to the magnetic field was adjusted, the pattern of signal intensity was affected, as described previously. These findings are in agreement with studies in the literature by Dunn *et al.* (2006), which presented similar results for MR images of discs.

Further MR studies in the literature have presented evidence for alternating fibre angle between these bands of bright and dark signal, such as the T_2 relaxation studies by Wright *et al.* (2004, 2009).

The lamellae appeared more distinct in the outer regions of the annulus. The thickness of individual lamellae in this region agreed with that recorded from the dissection photos. Towards the disc centre, the lamellae were not distinguishable in the MR images. This may be due to a lack in lamella distinction in the tissue and a decrease in the lamella thickness below the pixel size of the MR images (0.2 mm).

Changes in the soft tissue structure were evident between the P and L scans. In the P scans, the geometry of the outer annulus was concave in some specimens and convex in others. Under compression, the outer annulus bulged, resulting in a concave shape to the lamellae in the region for all specimens. However, due to the

lack of definition closer to the centre of the disc, such observations could not be made regarding the inner annulus.

All the deformation measurements recorded were of similar magnitudes. In general the disc height reduction was smaller than the radial bulge and the bulge was greater in the lateral direction than in the A-P direction. The exception to this was S2. This specimen was observed to bend more than the others during loading. Bulge measurements were taken from single slices and therefore may not be fully representative of the three dimensional deformation.

The change in fibre angle in the outer layers of the annulus was noted for some specimens. The techniques developed showed potential for further investigation of this feature of tissue deformation, however because this was not the main focus of this study, this was not taken further.

It is assumed that compression of the disc raised the internal hydrostatic pressure and caused fluid to flow within and out of the disc. The specimens were allowed to relax for 25 minutes between applying the deformation and conducting the L scan. This was to minimise the amount of fluid movement during the scan, as this could have been detrimental to the clarity of the images.

The fluid flow between the P and L scans will have affected the hydration levels of the tissue, and so the signal intensity from any given soft tissue in the P and L scans will have changed.

The image data acquired for the specimens using µCT provided geometric data for the hard tissues of the specimens to a high level of detail. Individual trabeculae as small as 0.15 mm wide were captured. In these images, the soft tissues of the specimen were captured with no detail of the internal structures, and only a shadowy outline of the external tissue boundary. This is due to the µCT imaging method for which the image greyscale values are dependent on the density of the tissue.

CT techniques are used in other fields to image soft tissues, thus with further development it may be possible to capture more information about the tissues of the disc using µCT. The scanner available for this study was designed primarily for the imaging of hard tissues and soft tissue scanning was outside of the scope of the manufacturer's guidelines.

During the post-imaging dissection of the specimens, the lack of clarity of the internal soft tissue structures was noted. The lamellae were clearly defined towards the outer annulus but towards the centre of the disc, they became indistinct. There was a gradual change in the composition of the tissue between the nucleus and the annulus. As such, the boundaries of the measurements taken were user defined which may have caused some variation in the results.

The lowest levels of agreement between the tissue dimensions taken from the MR image data and the dissection data was for the depth of the nucleus and the posterior thickness of the annulus. These were the regions with the least clear distinction between soft tissues in both the MR images and as observed during dissection.

Prior to dissection, the tissue had been compressed during the MR study. As such the tissue had experienced additional loading compared to when the MRI-P scan was conducted. Although the elastic and osmotic qualities of the soft tissues may have restored some of the soft tissue deformation, it is unlikely that the tissues would have entirely returned to their original state in terms of geometry and hydration. Damage may also have been caused during the dissection processes. This may have caused discrepancies between the MRI and dissection measurements.

Between the P scan and the dissection photographs, the specimens had also experienced a further freeze-thaw cycle. It is expected that this will have had a negligible effect on the tissue as previous studies have shown no evidence of significant changes in the biomechanics of ovine lumbar tissue as a result of freezing (Gleizes *et al.*, 1998).

Agreement was recorded for degeneration grading between the MR and dissection technique for all specimens except S2, which was classified as grade III degeneration from the MR images but upon dissection the tissue was found to be healthy and was classified as grade I. This may be a result of disc dehydration, post mortem. A decrease in hydration after the spine was harvested from the animal could have affected the quality of the MR images by decreasing the signal intensity.

The tissue grading was repeated by four independent reviewers to minimise the effect of the subjectivity of the technique. The results showed acceptable levels of variation between individuals. In general, there was greater variation for the dissection grading than the MRI grading. This may have been reduced had all

reviewers graded the tissues during dissection rather than based on photographic data.

Due to a lack of ovine specific degeneration studies in the literature, the scales used to grade the specimens were developed based on human tissue degeneration. These may not be suitable for use with ovine tissue as the degenerative changes observed in animal tissues are not the same as for human tissue (Urban and Winlove 2007).

The dissection of the specimens allowed abnormal features in the disc tissue to be inspected in further detail, such as those highlighted for S3 in Section 4.3.4. The appearance of these features as bright in the µCT images and dark in the MR images suggested that they were of high density and low hydration, and were initially suggested to be areas of disc calcification. However during dissection, they were found to be malleable and fibrous rather than brittle, calcified tissue.

Ovine tissue was used throughout this study because of its wide availability and the established similarities in biomechanics, geometry and composition with the human lumbar disc (Beckstein *et al.*, 2008; O'Connell *et al.*, 2007; Wilke *et al.*, 1997). Similarities have also been reported by Smith and Elliott (2011) between human and ovine disc tissue for the micro-structure of the annulus, such as the presence of interlamellar structures. Extension of this study into human specimens may be useful for investigating the effect of the larger disc size, especially the effects this may have on the clarity of the images obtained through MR techniques.

The MRI compression tests completed here did not include loading data for the compression of the specimen. The limitations on materials appropriate for use in the MR scanner prevented the inclusion of load cells in the experimental set up. Future work including loading data for similar tests would be useful, as was achieved by the similar studies by O'Connell *et al.* (2007; 2008). This study has improved upon the work by O'Connell *et al.* by developing scans that capture the structure of the disc soft tissues in three dimensions as opposed to their two dimensional scans.

Features of the annulus such as individual lamellae were distinguishable in the 3D scan, providing geometric information on the soft tissue structures in their intact state. Scans of the specimens under load showed the deformation of the soft tissues, including the change in shape of the lamellae to a level of comprehensive detail not previously published. The ability to capture such image data will be useful

in the construction and validation of specimen specific computational models. Imaging the nucleus was not as successful, but dissection of the specimens resulted in some geometric data for the nucleus which could be used in model development.

5 SPECIMEN SPECIFIC MODELS OF THE DISC

In this Chapter a method for constructing specimen specific models of the intervertebral disc, based on the MR and µCT image data acquired and presented in Chapter 4 is outlined. Three models were developed based on different experimental specimens. As in Chapter 3, a "control" version was developed for each model, within which linear elastic material models were used for the bone, nucleus and annulus components and parametric tests were applied to assess the sensitivity of the models to changes in how the soft tissue structures were represented. The models were loaded to replicate the compression applied during the imaging of the tissue (Chapter 4). The image data acquired for the soft tissues in their compressed state was used as a measure of the model performances. Results showed a wide spread in performance for the three models and their parametric variations, due to the range in experimental specimen size, condition and applied compression. The error incurred during model development also affected model performance. The inclusion of sub-annulus level detail did not dramatically affect the gross mechanics of the discs but did affect the annulus level deformations.

5.1 INTRODUCTION

Specimen specific models are useful in biological modelling for their capability to capture characteristics that may vary widely between individuals. For the FSU, there may be signification variations in size, shape and properties depending on species, gender, spinal level or degeneration of the specimens.

The aim of this study was to assess the possibility of creating specimen specific FE models based on the MR and µCT image data acquired in Chapter 4. MRI data has previously been used to construct models of the FSU (Schmidt *et al.* 2006; Li and Wang 2006); however, these studies have focused on the gross properties of the disc and have not probed the soft tissue structures and function. The detail of the data presented in the imaging study has the potential to provide increased levels of structural detail for model generation and could also provide information on how these structures deform, useful for model validation.

As a preliminary and novel investigation, methods for constructing models were developed with the intention of establishing protocols that could be used in larger scale future studies. The scope of the models presented here was dictated by the limitations of the imaging techniques used.

The resultant models were subjected to a range of parametric tests, similar to those presented in Chapter 3, to assess their sensitivity to changes in how the soft tissues

are modelled and to analyse if such changes would improve the performance relative to the disc deformations recorded experimentally.

5.2 MODEL DEVELOPMENT

Three sets of scan data presented in Chapter 4 were developed into FE models that replicated some aspects of the individual features of each specimen. The details of these specimens are summarised in Table 5.1.

	Sheep age (approx. years)	Sheep breed	Spine level	Disc of interest	Approx. disc dimensions	
					width (mm)	depth (mm)
S3	4.5	Suffolk	T13 – L3	L1L2	26	20
S4	5.5	Texel	T13 – L3	L1L2	22	21
S5	5	Texel	T13 – L3	L1L2	20	14

Table 5.1 – Specimens modelled during the study.

The three specimens were chosen for model development due to similarities in age and spine level and for the range in disc dimensions. As previously illustrated in Chapter 4, each of these specimens produced clear µCT images and MR images that captured the soft tissue structures in unloaded and compressed states.

The methods applied to develop each model are summarised in the flow chart shown in Figure 5.1 and discussed in further detail below. Throughout this study, the term “stack” is used to refer to a sequential set of two dimensional images that when combined create a three dimensional image.

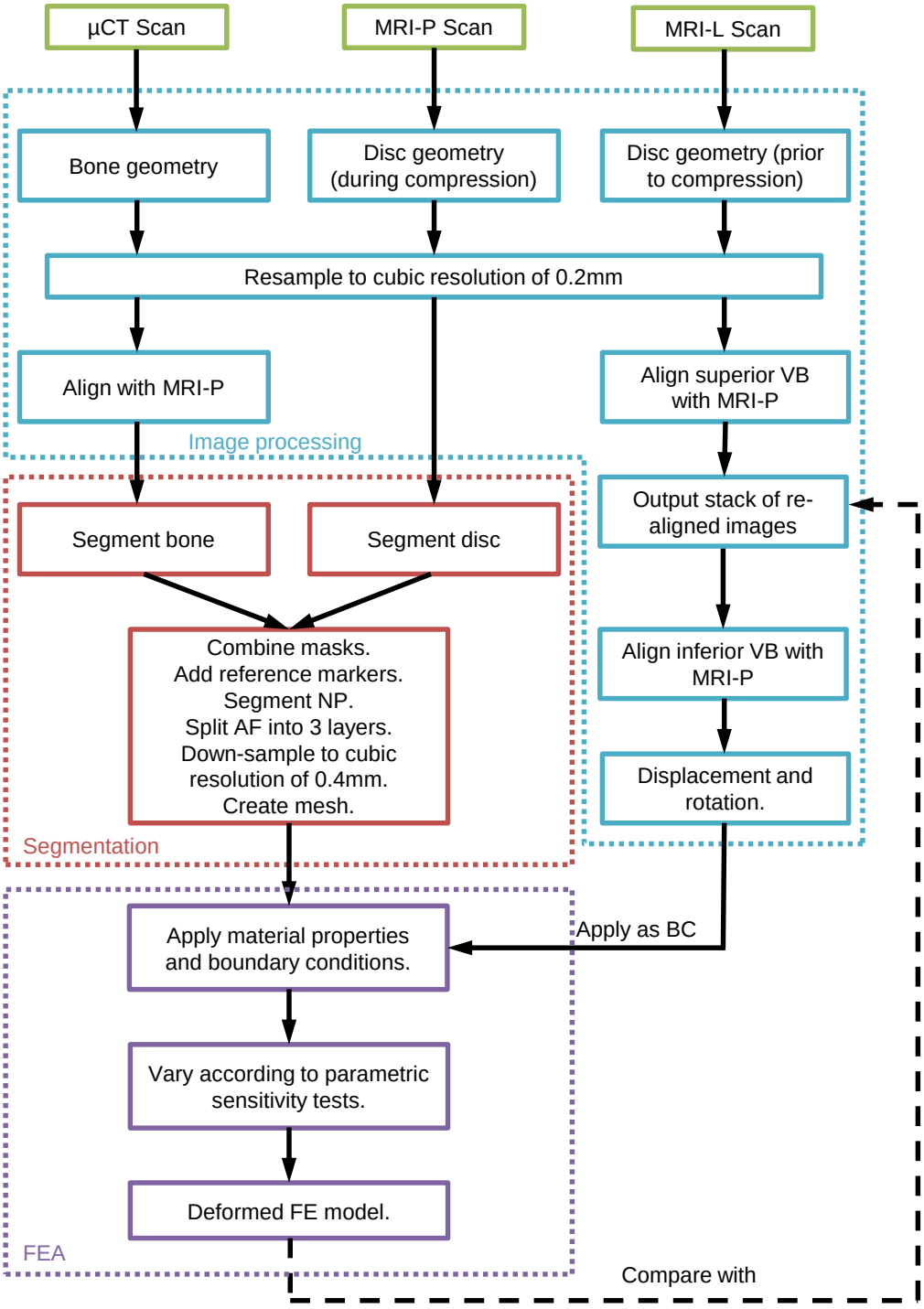

Figure 5.1 – Flow chart to summarise the methods used to create the three specimen specific models from the MR and µCT image data.

5.2.1 SOFTWARE AND HARDWARE

The software used in this study is outlined in Table 5.2.

Process	Software name and provider
Stack realignment and registration (bespoke algorithm)	Matlab, version 7.8.0 R2009a, MathWorks Inc., MA, USA
Image processing	ImageJ, National Institute of Health, USA
Segmentation and meshing	ScanIP, version 4, Simpleware Limited, Exeter, U.K.
Finite element analysis development and execution	ABAQUS CAE, version 6.9-1, Dassault Systèmes Simulia Corp, Providence, RI, USA

Table 5.2 – Software packages used in the study.

All image processing and model development was conducted on a desktop PC (Dell precision T5400, Dell UK, Bracknell, UK; Intel Xeon Processor, Intel, Santa Clara, CA, USA). The models were solved using the ARC1 high performance computing system at The University of Leeds.

5.2.2 IMAGE BASED GEOMETRY

The imaging techniques and data used in this study were presented in Chapter 4. For each specimen, three stacks of images were acquired:

i. μCT
ii. MRI prior to loading (MRI-P)
iii. MRI loaded in compression (MRI-L)

All three stacks were resampled to a cubic resolution of 0.2mm using the segmentation and meshing software to allow the comparison and combination of image data.

STACK REGISTRATION

Compression was applied to the specimens by displacing a single loading plate at the superior end, as shown in Figure 5.2 and discussed in Chapter 4.

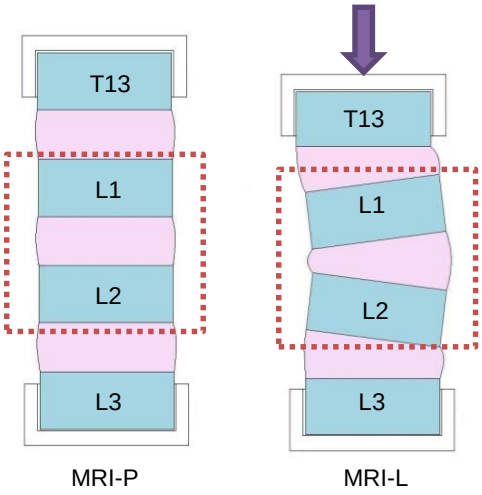

Figure 5.2 - Application of displacement during the MR scans results in an unknown displacement of the disc of interest and its adjacent VBs.

Due to the inclusion of the discs adjacent to the central FSU, it was necessary to realign image stacks to allow comparison between the prior-to-loading (P) and loaded (L) scans. Common points were manually picked between comparable slices in the P and L stacks. A minimum of 10 image pairs were aligned per stack. For each pair, the translation and rotation required to map the L image to the P image was calculated. The average translation from the 10 pairs was applied to the whole stack. This process was repeated in the coronal, sagittal and axial slice directions so the images were aligned in three dimensions.

The MRI-P stacks were used as a base to which the MRI-L stacks and the µCT stacks were aligned. The stacks were aligned according to the superior vertebral bodies, using common points on the markers and bony end plates which were clearly pictured in all stacks, as illustrated in Figure 5.3.

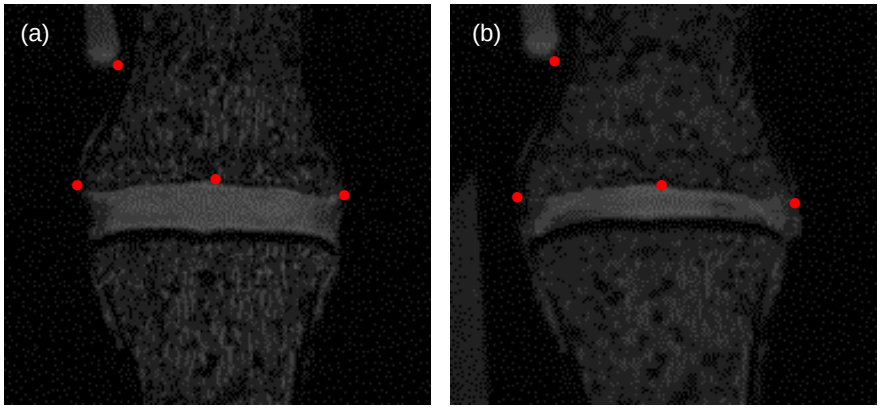

Figure 5.3 – Sample MR images in the (a) prior to loading and (b) loaded state. The red dots indicate common points on the marker and superior EP that were used during the image registration process.

The bony end plates were considered suitable for alignment reference because they and the underlying vertebral bodies were not anticipated to deform significantly compared to the disc.

As a result of this process, the MRI-P, MRI-L and µCT stacks were re-aligned in all three directions, with the same dimensions, slice numbers and voxel size. The superior (L1) vertebral bodies are aligned, as illustrated schematically in Figure 5.4.

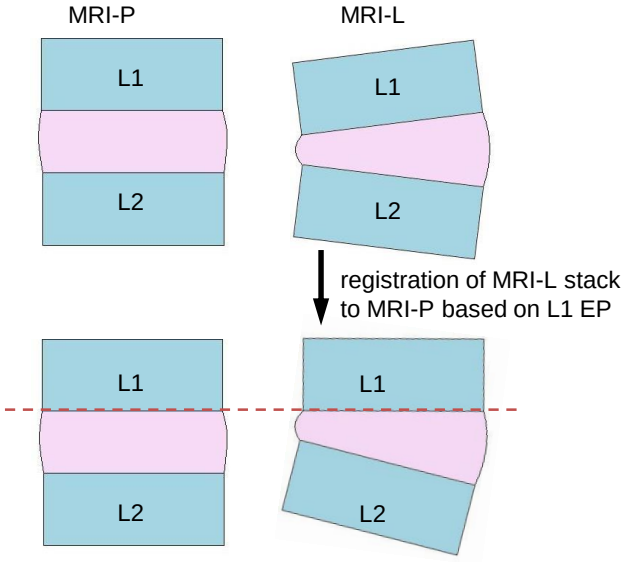

Figure 5.4 –The image registration process aligns the EPs of the superior (L1) VB, allowing comparison of slices between the stacks.

SEGMENTATION

The characteristic geometries of the specimens were captured and converted into three dimensional geometric models using the segmentation software. The bone was segmented based on the µCT stack using a fixed greyscale threshold. The disc was segmented separately based on the MRI-P stack. For the MR images, the greyscale was dependent on the quantity of water in the specimens, and so greyscale threshold values varied depending on disc hydration. The outer annulus boundary was not always clear, due to the effect of fibre angle of the tissue on the intensity of the MR signal, thus this boundary required adjusting manually in places, as illustrated in Figure 5.5.

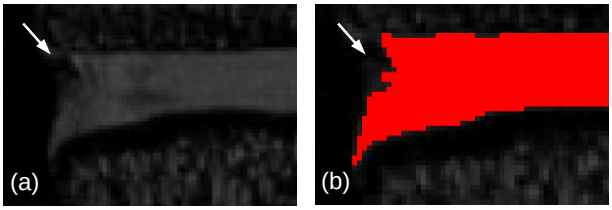

Figure 5.5 – Unclear outer edge of annulus from MRI data for S3. The annulus boundary is unclear in the MR image (a). Mid segmentation (b). The mask shown was applied using a greyscale threshold. The arrow indicates the area that was later completed manually.

The bone and disc masks were combined into one model by importing the bone masks into the MRI model. Any overlap between the two at the end plates was removed from the bone mask. Thus the end plate topography was based only on the MR data.

Reference points were added in the model at known distances from the MRI and CT markers. This facilitated easy identification of the central sagittal, coronal and axial slices. These slices were identifiable in all three (µCT, MRI-P and MRI-L) stacks so comparisons could be made between the model and the image data relative to these known points.

The vertebral body model components were trimmed in the caudal-cranial (C-C) direction to minimise the bone tissue included in the model.

It was necessary to segment the nucleus from the annulus to assign them as different parts within the FE model. However, it was not possible to identify the nucleus/annulus boundary in the MRI data (as discussed in Chapter 4); therefore dimensions for the width and depth of the nucleus were based on measurements recorded during dissection. A smoothing filter was applied to the nucleus mask to curve the edges of the nucleus with a radius of 0.6mm, resulting in a rounded shape nucleus in the centre of the disc. The nucleus size for each model is given as a percentage of the total disc volume in Table 5.3.

Model	S3	S4	S5
nucleus % volume	14%	11%	22%

Table 5.3 – Nucleus volume as a percentage of total disc size.

5.2.3 MESH

The models were meshed using the segmentation and meshing software. The target element size was 0.1mm. Elements were smoothed for improved geometry

with a maximum curvature of 0.2mm and were a mix of hexahedral, tetrahedral, pyramidal and wedge elements. The number of elements in each model varied depending on the size of the model and are summarised in Table 5.4.

Model	S3	S4	S5
Number of elements	450,000	400,000	250,000

Table 5.4 – Approximate total number of elements for each of the three models.

Mesh verification was not conducted for these models. The element size used was smaller than the voxel size of the MRI scans. Any further reduction in element size would not have improved the accuracy of the model relative to the experimental data as additional geometric data may have been "false". The element size was smaller than that used in the 3D generalised model presented in Chapter 3 which was shown to converge and detailed stress analysis was not conducted in this study so these assumptions were considered appropriate.

5.2.4 BOUNDARY CONDITIONS

Boundary conditions were applied using the FEA software. The upper surface of the superior vertebral body was clamped to prevent displacement and rotation in all degrees of freedom. A rigid plate was attached to the lower surface of the inferior vertebral body. An example model is illustrated in Figure 5.6.

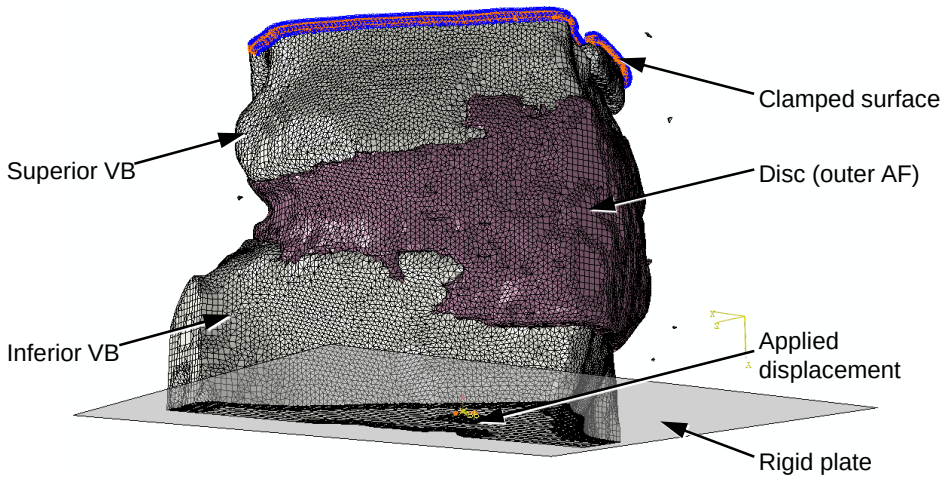

Figure 5.6 – Model assembly for S3 showing specimen components, rigid loading plate and applied boundary conditions.

A displacement and rotation boundary condition was applied to the reference point of the plate to replicate the deformation of the disc as recorded experimentally in the MRI data. The applied displacement was derived by repeating the image

registration process described previously in Section 5.2.1; this time with the inferior vertebral body of the MRI-P stack registered to that of the MRI-L stack. The translation and rotation required to displace the inferior vertebral body to its position in the loaded scan was recorded so that it could be applied in the model, replicating the displacement applied experimentally, as illustrated in Figure 5.7. This process calculated the displacement and rotation required to move the superior vertebral body to match the MRI-L scan when the inferior vertebral bodies were assumed as fixed.

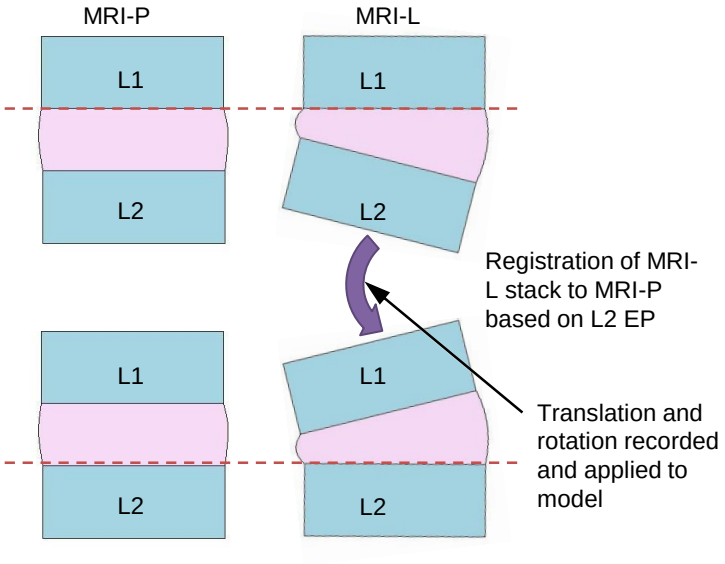

Figure 5.7 - The image registration process was repeated. The end plates of the inferior (L2) VB were aligned. The displacement and rotation required were recorded and applied to the FE models.

This image registration process was repeated for the stacks in the coronal, sagittal and axial planes, thus two values were recorded for the displacement in each of the three directions. For example, a value for the displacement in the x-direction was recorded from the coronal and axial registration, as illustrated in Figure 5.8.

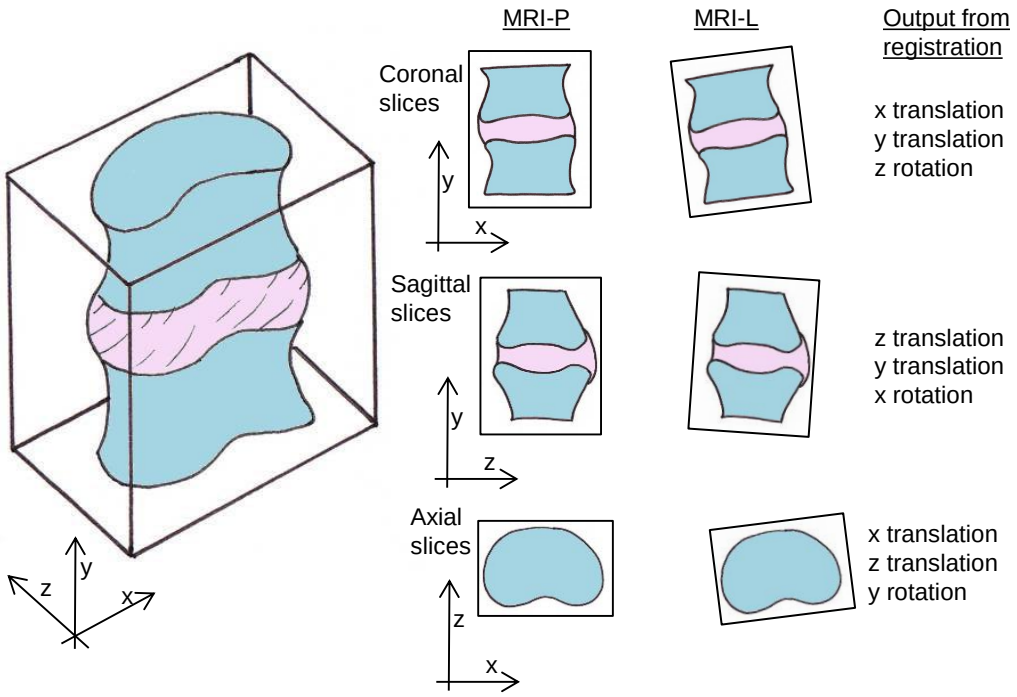

Figure 5.8 – Schematic illustration of translations and rotations in the x, y and z directions derived from registration between the P and L slices in the coronal, sagittal and axial direction.

Repeated values between slices should be the same; however some variation was recorded, as shown in Figure 5.9.

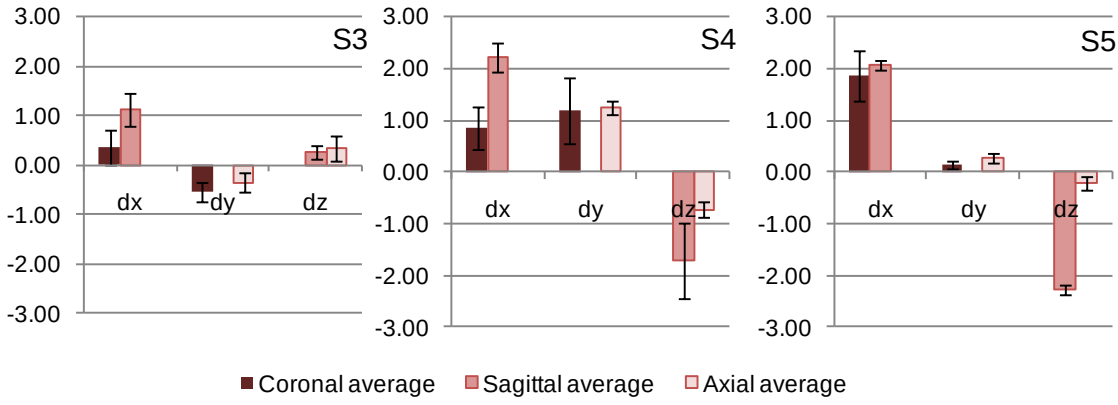

Figure 5.9 – Variation in the derived displacements for the three specimens. Vertical axis shows displacement in mm. Error bars show standard deviation of three repeated measurements (human error incurred during registration process).

Human error was a contributing cause of these variations, due to the manual nature of the registration process; the relatively poor resolution of the stacks (0.2mm) made it difficult to accurately select the same features in the two images.

In addition, the assumption that the vertebral bodies and end plates are rigid was not accurate. In reality there was deformation in the bones and the end plates

warped; causing variation in the displacement recorded for the different registration directions.

To minimise the effect of these errors, the registration process was repeated three times in each direction, for each model. The average displacements and rotations were applied to the models, these are summarised in Table 5.5.

	S3	S4	S5
displacement x	-0.45mm	1.22mm	0.21mm
displacement y	-0.74mm	-1.55mm	-1.97mm
displacement z	0.3mm	-1.21mm	-1.26mm
rotation x	0.32°	-2.11°	-3.35°
rotation y	0.84°	0.36°	0.29°
rotation z	-0.18°	2.58°	-1.1°

Table 5.5 – Displacements and rotations applied to the three models.

The reference point of the rigid plate in the model was located at the mid-point for both the sagittal and coronal stacks, as this was the point about which the rotations were calculated in the registration process.

5.2.5 MATERIAL PROPERTIES

Linear elastic, isotropic material properties were assigned to the model components as used in previous models (Chapter 3). Hybrid formulation was assigned to the elements of the nucleus to account for incompressibility.

5.2.6 ANALYSIS

The change in disc height was recorded at nine points across the experimental and computational models and compared as a measure of how well the compression of the specimen was replicated in the FE model.

The change in the width and depth of the disc was recorded at the mid slices and the reference slices for both the experimental data and the FE models, as illustrated in Figure 5.10.

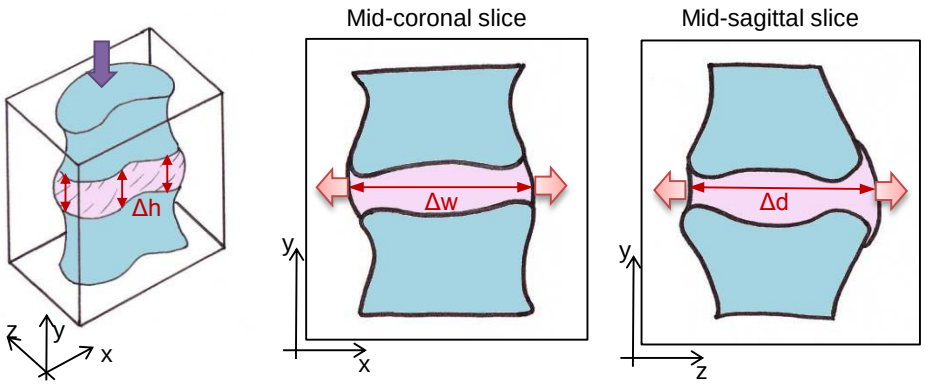

Figure 5.10 – Schematic diagrams to show the measurement of change in disc height (h), width (w) and depth (d).

The average radial bulge was derived for the two external edges of the annulus in the slice, however this did not account for non-symmetrical bulging.

From the FE results, the actual radial bulge could be taken for any point. This could not be directly compared to the MRI data, because it was not possible to precisely align the central axes of the disc, therefore the radial bulge could not be calculated relative to a known point. The radial bulge was instead expressed as the lateral bulge, taken from the change in disc width from the mid-coronal slice, and the anterial-posterial (A-P) bulge, taken from the change in disc depth in the mid-sagittal slice, as illustrated in Figure 5.10.

The reaction force across the clamped superior surface of the FE model was summed and used to calculate the stiffness of the FE model in the axial direction, based on the applied displacement in the y direction. Although loading data was not available for the experimental model, the stiffness calculated was compared to previous models and data in the literature.

For all the models, von Mises stress distribution plots were recorded to monitor the distribution of load through the specimen and potential areas of stress concentration.

5.3 SENSITIVITY TESTS

This section describes the variations that were made to the models to assess their sensitivity to several model parameters. The tests were conducted sequentially with increasing levels of detail included within the soft tissue structures of the disc. The final tests replicated the frictionless and interface methods of modelling the interlamellar interactions as previously investigated in Chapter 3.

All model variations investigated during the parametric analysis were compared to the "control model" for that specimen. As with the generalised models of the disc, the control model had a defined nucleus and annulus.

5.3.1 ORTHOTROPIC ANNULUS MODEL

Orthotropic material properties as developed in Section 3.2.3 were applied to the annulus, based on a cylindrical coordinate system with the origin located at the centre of the disc.

5.3.2 TRANSITION ZONE MODEL

Between the nucleus and annulus components, an intermediary "transition zone" (TZ) was included. The thickness of the transition zone varied between specimens, based on the data recorded during dissection, presented in Section 4.3 and is summarised in Table 5.6.

Model	S3	S4	S5
approx. TZ thickness (mm)	1.2	2.8	0.8
TZ % volume of disc	10%	28%	9%

Table 5.6 – Approximate thickness and percentage volume of the TZ for the three models.

5.3.3 GREYSCALE BASED BONE MODEL

The greyscale values obtained from the µCT scans were used to apply a variable modulus across the vertebral bodies to allow for the natural variation in material properties of the bone. A conversion factor was applied to calculate the Young's modulus of each element of bone in the model based on the local greyscale intensity of the µCT signal; the brightest pixels resulted in the highest modulus and the darkest, the lowest modulus.

A linear relationship between the greyscale and modulus was used as in previous studies (Tarsuslugil 2011) (i.e. $E = k \times GS$, where k is a determined conversion factor). The conversion factor was calculated so that the most frequently occurring greyscale for the bone corresponded to a Young's modulus of 200MPa. Hence the average modulus across the bone was approximately 200MPa (Table 5.7).

Model	S3	S4	S5
Average E_{VB} (MPa)	221	217	187
% change compared to control model	+11%	+9%	-7%

Table 5.7 – Average values for the modulus applied to the VBs of the three specimens.

With an average modulus of 200MPa for the bones, these models are comparable to the control model. This test was designed to understand the effect of using a variable stiffness to model the bones adjacent to the disc, specifically whether this changed the deformation of the end plates during compression.

5.3.4 FRICTIONLESS MODEL

For this model variation and the "interface model", the annulus was split into three layers using the "incomplete lamellae" method described in Chapter 3. The total contact area between layers of the annulus per specimen is given in Table 5.8.

Model	S3	S4	S5
Approx. contact area (mm^2)	348	328	212
Disc volume (mm^3)	1840	1510	960
Ratio contact area:disc volume	0.19	0.22	0.22

Table 5.8 – Contact surface area between layers of the annulus, disc volume and ratio of contact area:disc volume for each of the frictionless models.

A very low coefficient of static friction (μ=0.001 applied, μ=0.01 for super-lubricated interactions, Matthews 2009) was applied for the interlamellar interaction between all layers, resulting in negligible friction between the layers. All material properties remained consistent with previous model variations.

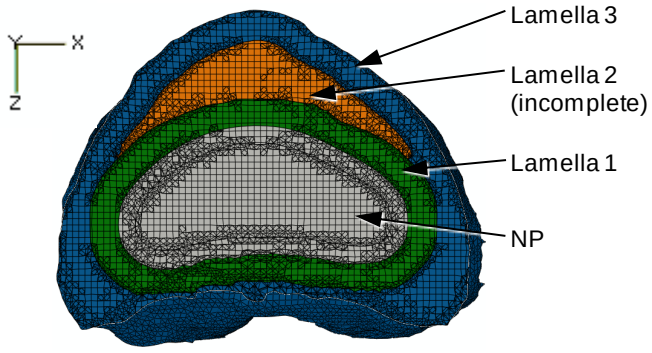

Figure 5.11 – Image of the split annulus model for S3, cut through the central axial plane, showing two complete layers and one incomplete.

5.3.5 INTERFACE MODEL

Continuing with the same split of the annulus into layers, interlamellar interactions were modelled by including interface elements, as included in the generic models described in Section 3.3.4 and illustrated in Figure 5.12.

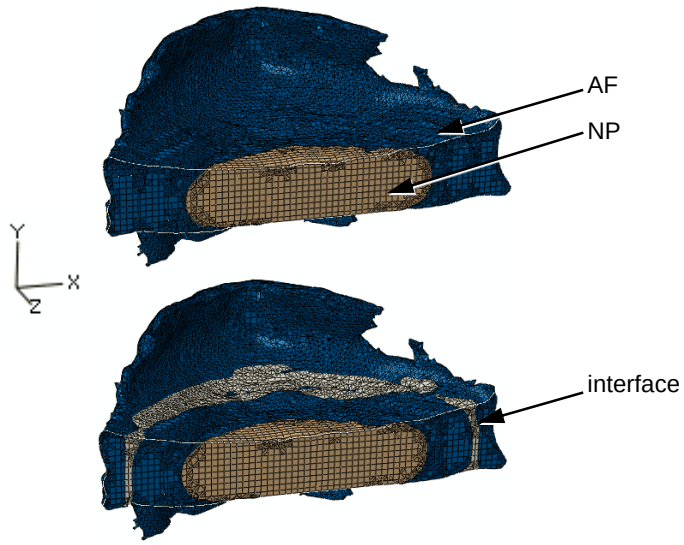

Figure 5.12 – Coronal slice through the disc of S5 for the control model (top) and interface model (bottom).

The thickness of the interface layer was determined based on the number of lamellae recorded during the specimen dissections (Chapter 4) and the estimated interlamellar space recorded from the literature (Marchand and Ahmed 1990). The thickness of the interface layer for each of the three models is presented in Table 5.9.

Model	S3	S4	S5
Interface % volume of disc	10%	8%	9%
Approx. interface thickness (mm)	1.0	0.7	0.8
Average number of lamellae (dissection)	24	16	17
Equivalent interface thickness per lamella (mm)	0.04	0.04	0.04

Table 5.9 – Approximate number of lamellae and equivalent interface layer thickness used in the FE models.

5.4 RESULTS

The variation between the model sizes and the applied deformation are illustrated in Figure 5.13 and Table 5.5. Specimen S5 was smaller than S3 and S4, with a width of 21mm compared to 26mm and 23mm for S3 and S4 respectively. Despite this, the deformations applied were greater than those for S3 and comparable to those for S4.

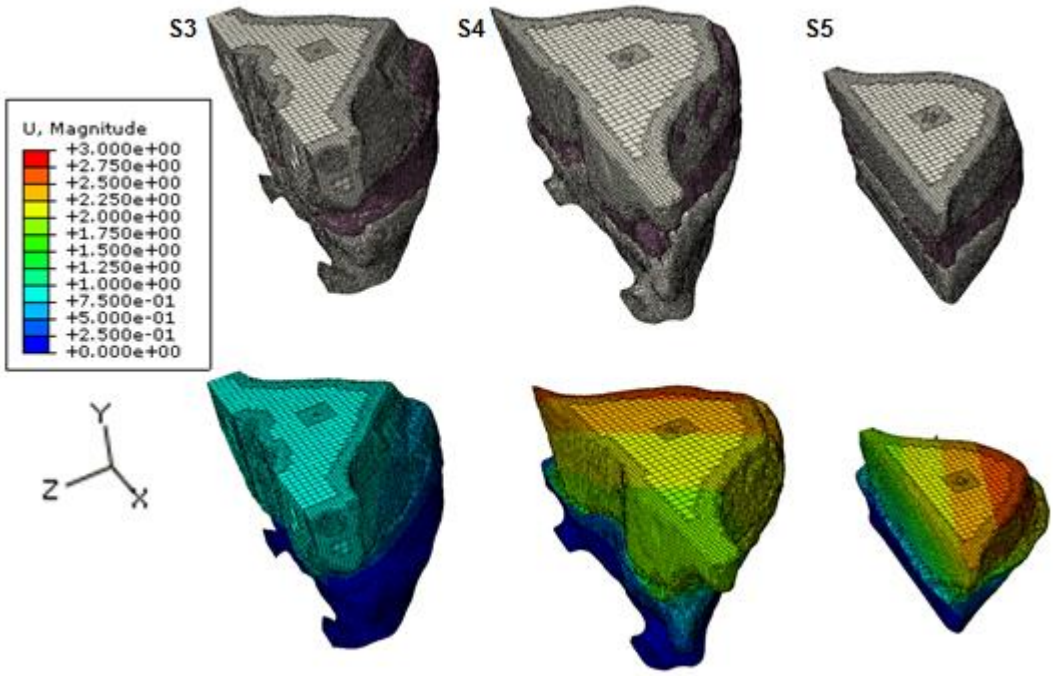

Figure 5.13 – All three models (from left to right: S3, S4, S5) in their uncompressed (top) and compressed (bottom) states. Displacement magnitude (mm) is plotted on the deformed models.

5.4.1 CONTROL MODELS – DEFORMATION RESULTS

The gross deformations of the discs in the FE models were compared to data from the experimental (MRI) data. A summary of the error of the control models for each specimen, relative to the experimental data is presented in Figure 5.14, in which it is illustrated that S5 performed with the lowest errors of the three specimens modelled.

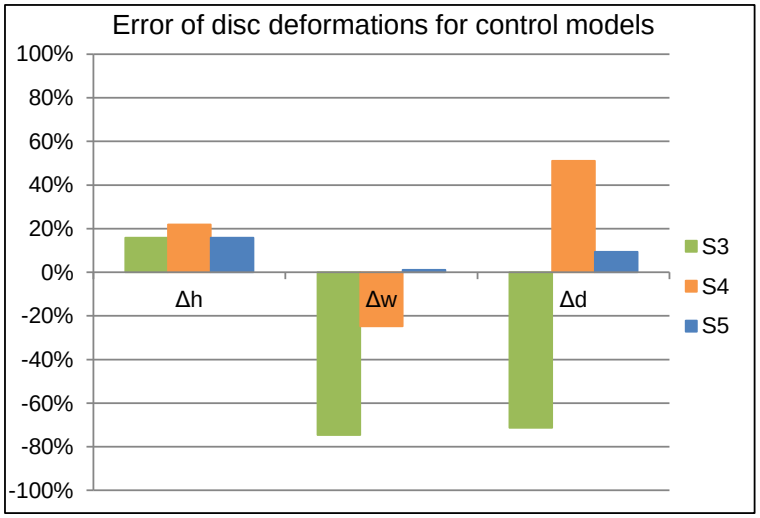

Figure 5.14 – Error of FE disc deformations with respect to experimental results for control model variants. Results are presented for change in disc height (Δh), change in disc width (Δw) and change in disc depth (Δd).

For S3, over-compression of the disc (positive Δh in Figure 5.14) resulted in large negative errors for radial bulge in all directions when compared to the experimental data, which was unexpected and counter-intuitive. Although this specimen had the best agreement with the experimental data for Δh, it had the worst agreement for change in width (Δw) and change in depth (Δd).

The over-compression of S4 however, resulted in an under-estimation of Δw and an over-performance of Δd.

S5 was the best performing model for change in height, width and depth. An over compression of the disc resulted in over-estimates of Δw and Δd, although these were minimal.

Similar patterns of deformation were observed between specimens S3 and S4, with the maximum radial bulge located in a posterior-lateral position. In contrast, S5 did not have a pronounced “kidney” shape, instead had a flatter posterior. This resulted in a more uniform maximum radial bulge along the posterior of S5.

5.4.2 Parametric study – deformation results

The variation in results for the change in width and depth were observed throughout of the parametric sensitivity tests and are summarised in Figure 5.15.

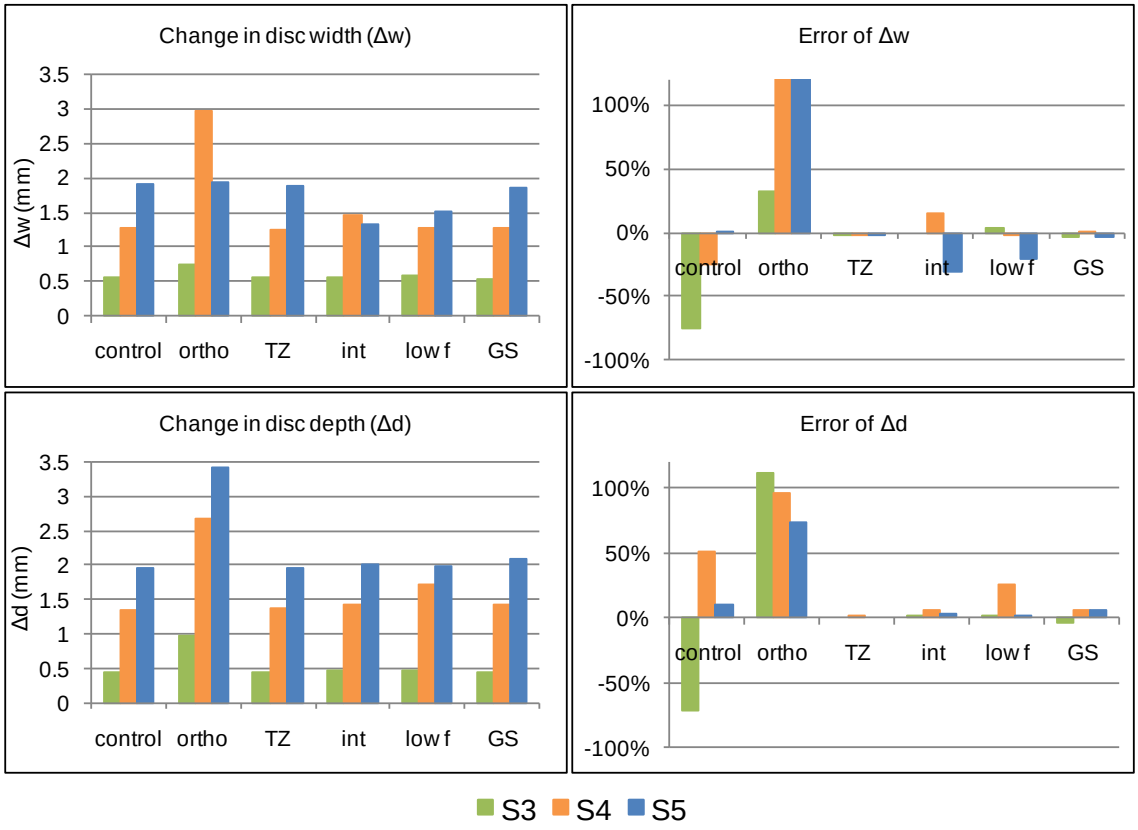

Figure 5.15 – Gross disc deformations for different model variants and errors with respect to experimental data. Ortho = orthotropic annulus model, TZ = transition zone model, int = interface model, low f = low-friction interaction model, GS = greyscale based bone model.

For all tests, the results presented in Figure 5.15 are consistent with those in Figure 5.14 for S3 and S4. The radial bulge of S3 was insufficient in both the lateral and A-P direction in all parametric tests and the radial bulge of S4 was too small in the lateral direction and too large in the A-P direction for all parametric tests.

The radial bulge in the A-P direction for S5 was consistently over estimated for all parametric tests, however in the lateral direction; the error results for this specimen were much more variable. Despite this, results for S5 outperformed those of S3 and S4 for agreement with experimental data in almost every test.

Result variability between parametric tests is examined in more detail in Figure 5.16.

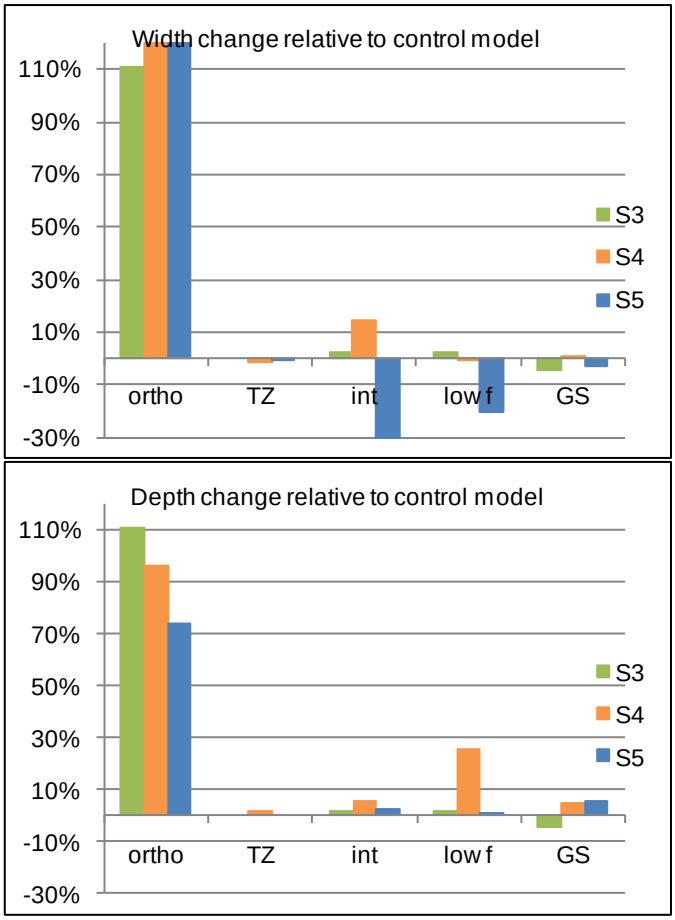

Figure 5.16 – Gross disc deformations for model variants relative to those of the control model. Ortho = orthotropic annulus model, TZ = transition zone model, int = interface model, low f = low-friction interaction model, GS = greyscale based bone model.

For all specimens, the bulge in the lateral direction had better agreement with the experimental data than the bulge in the A-P direction.

The bulge of specimen S3 was least sensitive to the parametric tests. For all specimens, the greatest change in bulge results was observed for the orthotropic annulus variation, for which Δw increased by over 100% in each case.

S5 was the most sensitive of the models to the parametric tests, with Δw decreasing by over 20% for the interface and frictionless tests.

S4 was also sensitive to these tests, with notable increases in Δw and Δd observed for the interface and frictionless tests respectively.

5.4.3 PARAMETRIC STUDY – STIFFNESS RESULTS

The axial stiffness of the specimen models was recorded throughout the parametric tests. These results are presented in Figure 5.18.

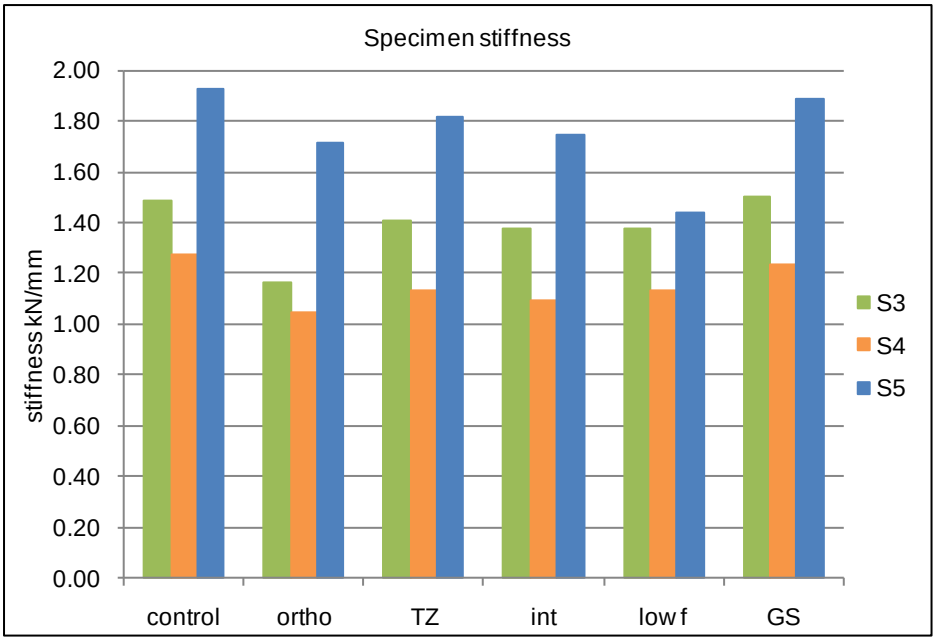

Figure 5.17 – Specimen stiffness in the axial direction for parametric tests. Ortho = orthotropic annulus model, TZ = transition zone model, int = interface model, low f = low-friction interaction model, GS = greyscale based bone model.

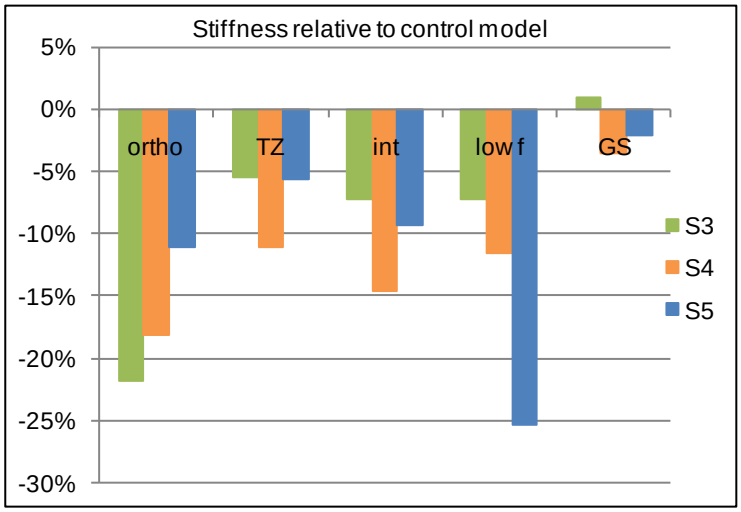

Figure 5.18 – Stiffness of parametric model variants for all three specimens, relative to that of the control model. Ortho = orthotropic annulus model, TZ = transition zone model, int = interface model, low f = low-friction interaction model, GS = greyscale based bone model.

The most substantial changes in stiffness relative to the control model were for the orthotropic annulus and low friction variants. The only increase in stiffness relative to the control model was recorded for the specimen specific vertebral body model for S3.

The results of each parametric test are outlined in more detail in Sections 5.4.4 to 5.4.8 below.

5.4.4 ORTHOTROPIC ANNULUS MODEL

The orthotropic annulus model was more compliant in the radial direction than the isotropic model. As a result, there was a dramatic increase in radial bulge for all three specimens, exceeding the experimental bulge data resulting in very high errors (greater than 110% error for change in width in all specimens)

The increased deformation of the annulus in the radial direction resulted in distorted elements along the posterior portion of the outer annulus for S5.

5.4.5 TRANSITION ZONE MODEL

The introduction of the transition zone had a minimal effect on the radial bulge of the disc. For all specimens, Δw and Δd were less than 2% different to those of the control model.

There was a decrease in stiffness relative to the control models for all specimens, the largest being a reduction of 11% for specimen S4.

Stress was more evenly distributed across the disc in the transition zone models than in the control model, as illustrated in Figure 5.19. The areas of high stress in the annulus were reduced.

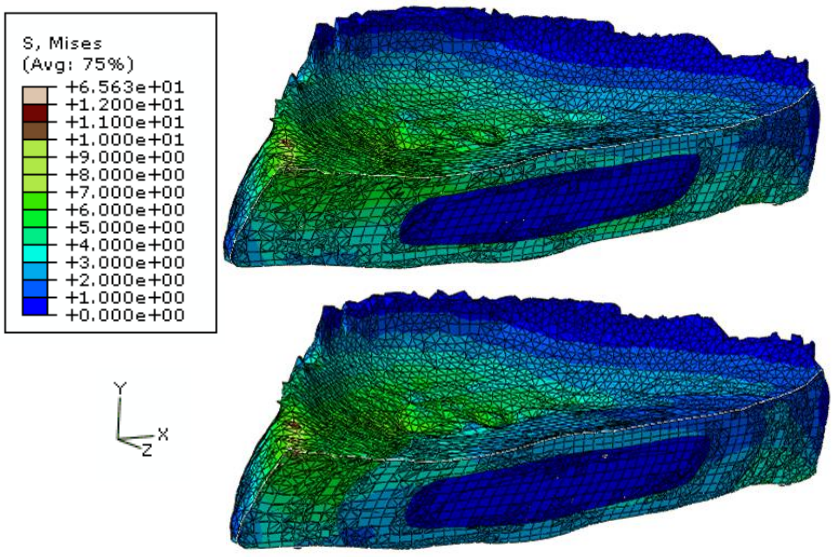

Figure 5.19 - Coronal section through the disc for model S4, showing Von Mises stress (MPa) plot for the control model (top) and transition zone model (bottom). Stress in the annulus is reduced following the introduction of the transition zone.

5.4.6 GREYSCALE BASED BONE MODEL

The application of greyscale based material properties to the vertebral bodies changed the characteristics of these components from effectively rigid bodies (relative to the disc materials) to deformable components. However, this did not result in increased deformation of the end plates. The agreement of change in disc height between the FE models and experimental data was improved by 0.2% for S3 but was reduced by 1.2% and 3.8% for S4 and S5 respectively. These results are illustrated in the plots presented in Figure 5.21 and the accompanying schematic illustration presented in Figure 5.20. For S3, the warp of the end plates increases slightly in the specimen specific vertebral bodies model, shown here by an increased curve across the plot. This is not the case for S4 and S5 in which the end plate warp does not increase, so the plots are "flatter" for these specimens compared to their experimental and control model plots.

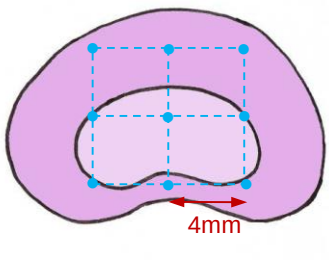

Figure 5.20 – Schematic illustration of the mid-axial section through the disc showing the grid of points at which the change in disc height was measured. The results for the change in disc height are illustrated in Figure 5.21.

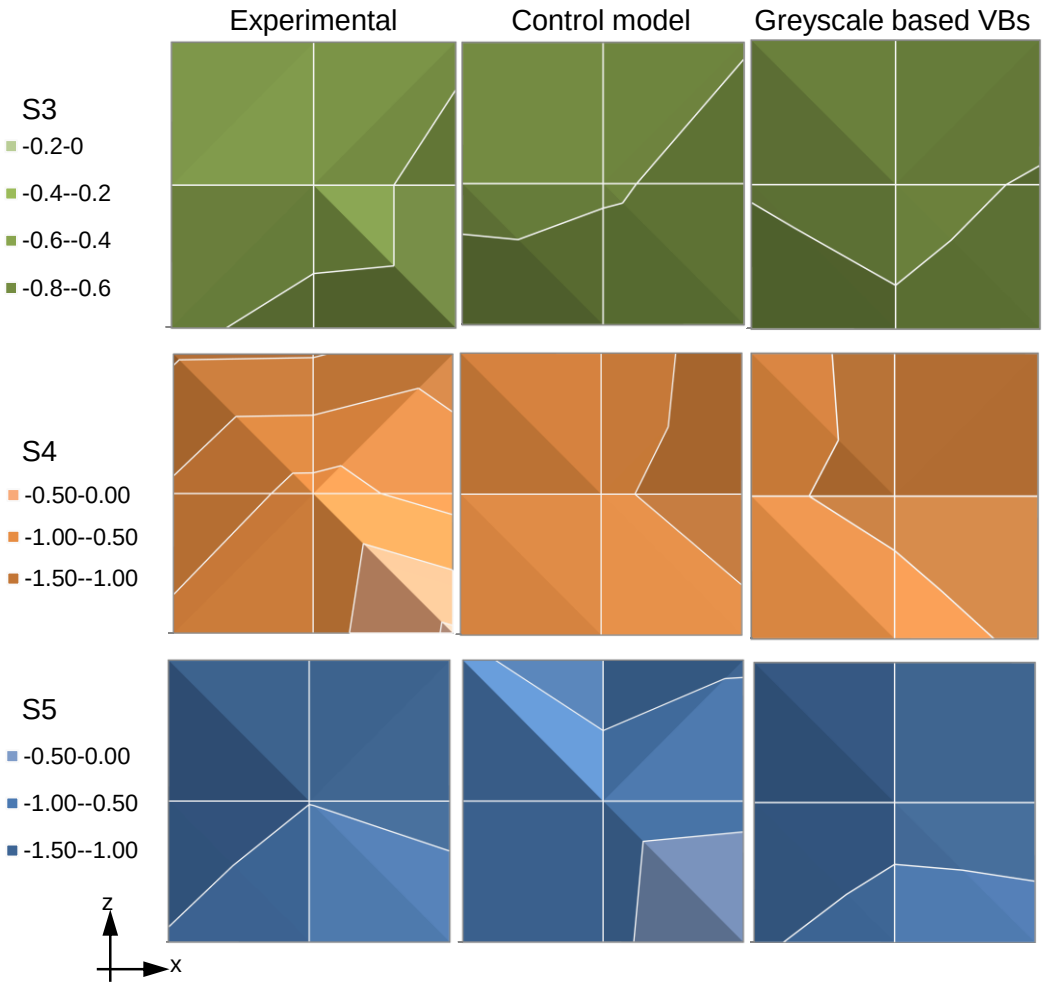

Figure 5.21 – Plots to show the change in height (mm) across the disc. Each plot is centred with the axis of the disc. Change in disc height measurements were taken on a 4mm grid (Figure 5.20) and are plotted for the experimental data, the control model and the specimen specific VBs model.

The stress distributions across the vertebral bodies are illustrated in Figure 5.22. With varied material properties across the bones, stress is less evenly distributed through the material. This results in areas of concentrated low stress within the bones and concentrated high stress on the end plates.

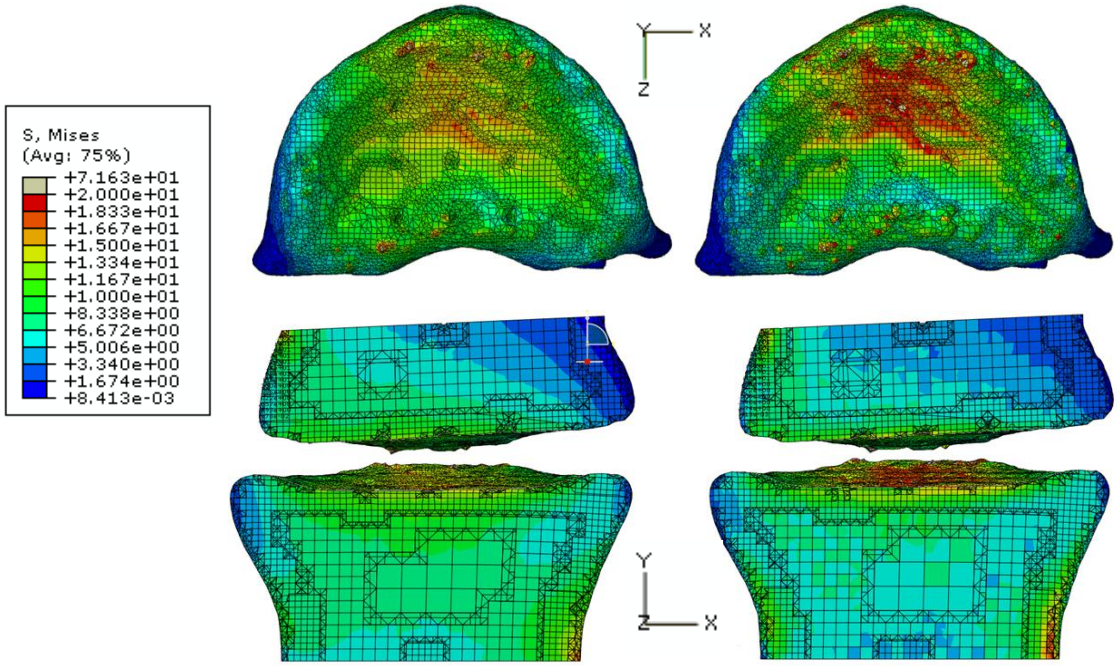

Figure 5.22 – Von Mises stress (MPa) plots for the VBs of S4 for the control model (left) and the specimen specific bone model (right) showing a view of the inferior end plate (top) and mid coronal section (bottom). The variation in Young's modulus across the bone in the specimen specific model results in a wider range of stresses within the bone and stress concentrations located on the EPs.

Generally, the changes between the control model and the greyscale based bone model were minor. The stiffness of S3 increased by 1% relative to the control, as expected due to the increase in modulus of the vertebral bodies. The decrease in stiffness of S5 by 2% is also in line with the decrease in the average modulus of the vertebral bodies. However for S4, there was an increase in vertebral body modulus of 9% yet the stiffness of the specimen decreased by 4%.

Minor changes to the radial bulges in both directions were observed for all specimens. For S3, the radial bulge decreased in both directions, for S4 there was an increase in both directions and for S5 the lateral bulge decreased and the A-P bulge increased.

5.4.7 FRICTIONLESS MODEL

The introduction of frictionless interactions between the layers of the annulus facilitated shear between these layers and resulted in a more compliant disc. This had a minimal effect on the bulge of specimen S3 with only a slight increase to Δw and Δd compared to the control model.

A major increase of 26% was recorded for the A-P bulge of S4 relative to the control model. This resulted in an error of 90% with respect to the experimental data.

However, the bulge in the lateral direction for S4 decreased by only 1% relative to the control model.

The bulge of S5 was also more sensitive in the lateral direction than the A-P direction. However, converse to the results for S3, the lateral bulge decreased by 20% and the A-P bulge increased by 1% relative to the control model.

The stiffness of all specimens was reduced with the introduction of the frictionless interactions, relative to the control models. The greatest reduction in stiffness was observed in S5 which was 25% more compliant in the axial direction than the control model.

There was a reduction in stress across the end plate-disc boundary in the frictionless models, as illustrated in Figure 5.23; however the stress distribution through the annulus was not significantly affected.

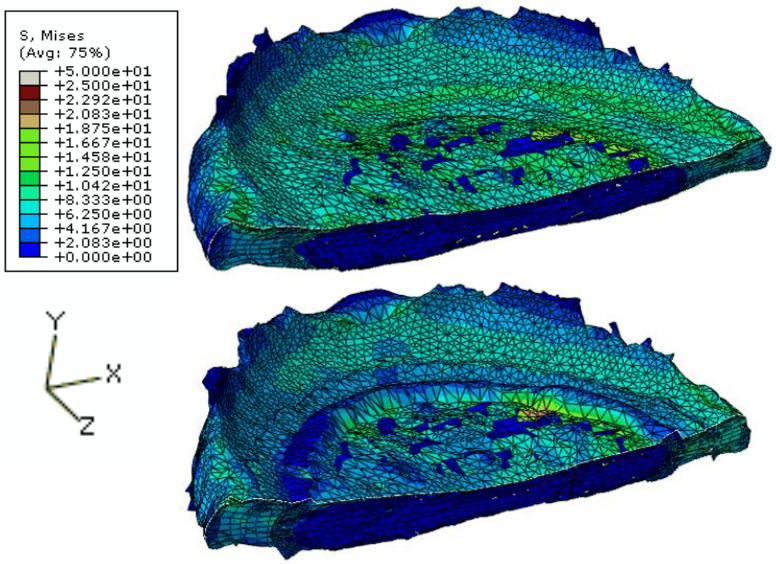

Figure 5.23 – Von mises stress (MPa) plots for control model (top) and frictionless interaction model (bottom) for S5. With the introduction of the frictionless interactions, there was a reduction in stress across the EP-disc boundary. The stress distribution through the annulus was not significantly affected.

5.4.8 INTERFACE MODEL

For S3 and S4 the bulge pattern changed significantly with the introduction of the interface elements between the layers of the annulus, as illustrated in Figure 5.24.

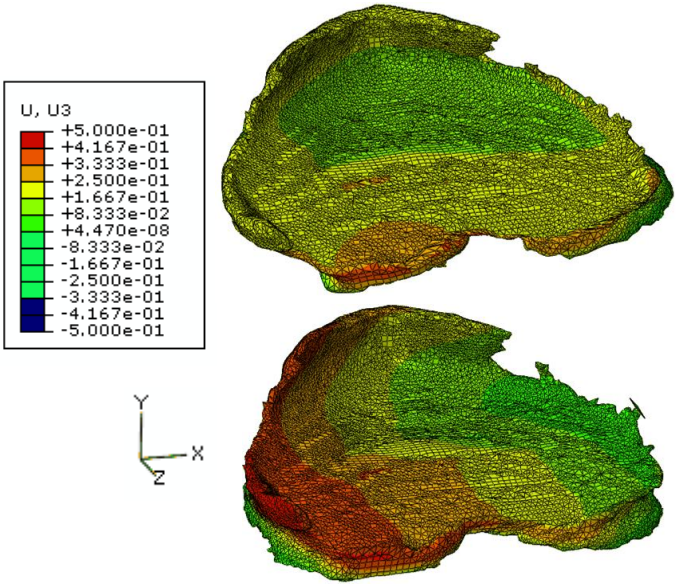

Figure 5.24 – The disc of S3 for the control model (top) and interface model (bottom) with displacement in the z direction plotted (mm). The introduction of the interface layers has changed the characteristics and magnitude of the radial bulge.

The introduction of interface elements between the layers of the annulus had very little effect on the radial bulge of S3, with only minimal increase in both directions. S4 experienced a more substantial increase in both directions, with the bulge in the lateral direction increasing by 15% relative to the control model. For S5 however, there was a decrease in bulge in the lateral direction of 30% and an increase in the A-P direction of 3%.

Stiffness was reduced in all three specimens. S4 had the largest reduction in stiffness of 15% relative to the control.

The interlamellar interface elements experienced lower stress than the surrounding annulus elements, resulting in a less even distribution of stress through the disc for the interface model compared to the control model, as illustrated in Figure 5.25 and Figure 5.26.

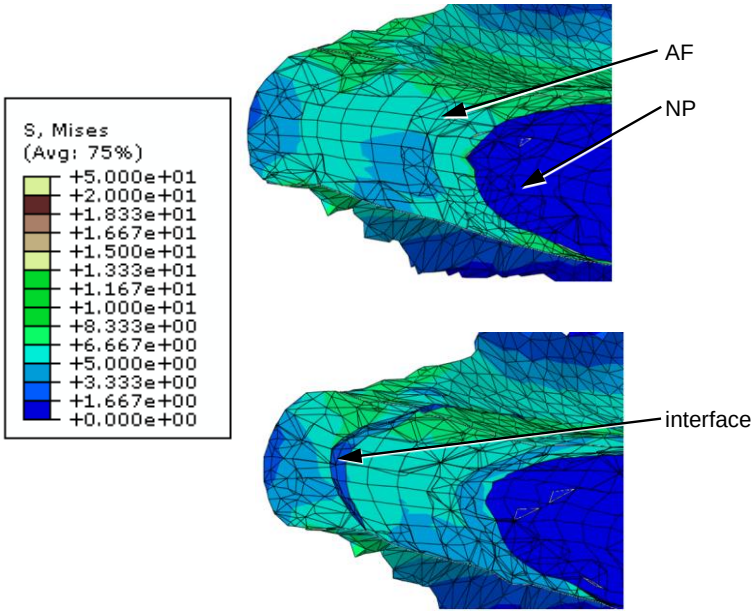

Figure 5.25 – Details from the control (top) and interface (bottom) variations of model S3, showing Von Mises stress distribution across a coronal section of the disc. The interface elements experience lower stresses than the annulus, resulting in a more varied stress distribution across the disc.

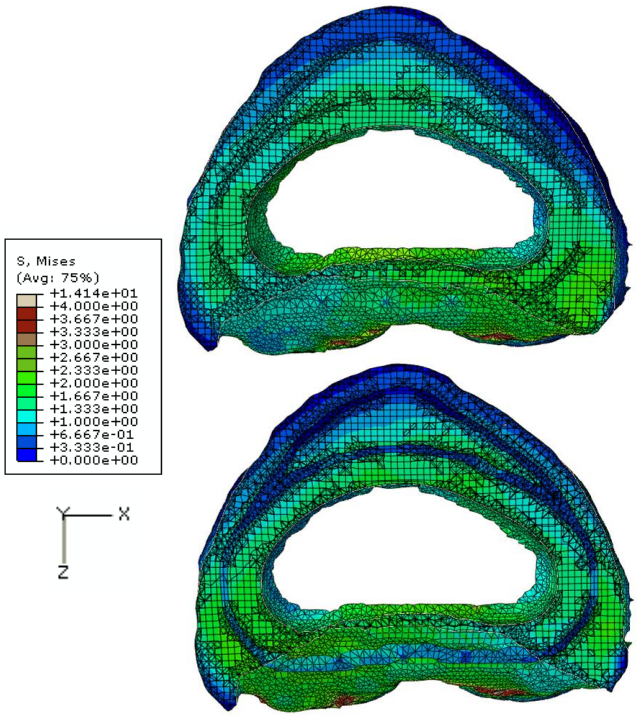

Figure 5.26 – Von Mises stress distribution across the inferior surface of the annulus for the control model (top) and the interface model (bottom) for S5. There is a variation between layers and the interface.

5.5 DISCUSSION

This study has presented a thorough investigation into the use of MRI data to create specimen specific models of the disc. It has been successful in developing a basic method for constructing such models using the data that was available following the imaging study presented in Chapter 4. This method has the potential for use in validation studies and the development into additional studies with focused interests. The use of this data facilitated direct comparison of the models with experimental data but also limited the study to some extent, particularly in the lack of loading data from the experimental study.

The initial intention of the study was to use MR image data to validate the soft tissue internal deformations of the disc model during applied compression. However, this was not possible due to the limitations of the experimental data acquired: methods could not be developed for tracking the deformation of internal soft tissues, nor could the image data be validated to confirm that the same soft tissue features were identified in the P and L scans. The models developed were instead validated using external tissue deformation data.

The models presented in this Chapter were created based on specimen specific geometries obtained from μCT, MRI and dissection data. The use of MRI data allowed characteristic soft tissue structures and geometry of each specimen to be individually represented. The models facilitated the investigation of the deformation of soft tissues whilst *in situ* in their specific geometric environment. The novel use of MRI data for discs in the deformed state allowed criteria to be established against which the performance of each model could be directly analysed. The methods developed during this study could be applied to discs from all levels of the spine and for *in vitro* spinal tissue of any species.

The bony end plates were used to derive the displacement applied in the models because they showed up clearly on the MRI data and because of their high stiffness relative to the disc. Because the end plates were used as part of the model development process they could not be used for reference during model validation. For this reason, the change in disc height is representative of how well the applied displacement and rotation is transferred through the vertebral body to the disc, but cannot be used as a measure of how well the models perform relative to the experimental data.

5.5.1 ERRORS IN METHOD

All the models presented have large errors relative to the experimental data acquired from MRI, ranging up to 80% in some permutations. These errors have accumulated from several sources during the experimental and computational methods.

During the experimental study, the displacement applied to the disc of interest was estimated but not directly recorded. For optimal contact between the MR surface coils and the disc, the specimens were required to be of a minimum length of 650mm and so the disc of interest was at the centre of a three-disc portion of the spinal column. Thus, the magnitude and directions of the actual deformation applied to the disc of interest during the experiments was established based on the image data. This could potentially be rectified by redesigning the compression rig system. If the PMMA pots could be extended it may be possible to scan a specimen comprising of only one disc. However this would be at the risk of increasing the distance between the disc tissues and the surface coils which could have a detrimental effect on the quality of the image data.

During the calculation of the experimentally applied displacements and rotations, there was a large spread in results from the image registration process employed (see Figure 5.9). During this calculation, the assumption was made that the vertebral bodies and end plates were rigid, relative to the tissues of the disc. In reality there was probably a small amount of warping experienced by the end plates, so the method was attempting to fit a flat plane to a curved surface. Thus the displacements obtained varied depending on the direction of the image stack that was used. The greater the end plate deformation, the greater the error encountered. It is likely that the differences in errors recorded between specimens were a result of variation in end plate warping between the specimens.

Due to the logistics of using the compression rig within the MR scanner, the specimens were moved between the P and L scans. Thus it was necessary to manually align the P and L image stacks. During this process, the resolution of the images made it difficult to select the same features to align from the different stacks. For example, a typical value for displacement was 0.7mm. The voxel size was 0.2mm. Therefore if a point chosen were one pixel out, an error of approximately 29% was incurred. An increase in the number of points aligned per image pair would have helped reduce this error, however this was not often possible due to the limited number of features and the restriction of using only points on one of the

vertebrae. The process was repeated three times and averages taken for the applied translations to minimise this error. The large values for standard deviation between the three measurements, as illustrated in Figure 5.9 are indication that this is likely to be a large source of error. This error could be rectified if the specimens could be compressed remotely, as illustrated in the experimental set up presented by O'Connell *et al.* (2007, 2010).

During the construction of the models, assumptions were made about the size and shape of the nucleus. Although these were based on dissection data, the data was only representative of a single slice and it was not possible to obtain the three dimensional geometry of the nucleus. Based on previous studies (Chapter 3) it is expected that the models would not be sensitive to the shape of the nucleus, however the volume and location of the nucleus is likely to have a significant effect on the model's performance.

Due to the nature of the imaging process, the MR image data for all specimens was incomplete in three dimensions. As a result, during the model construction process, some gaps in the soft tissue geometries were completed using manual segmentation. As evident in Figure 5.6 and Figure 5.19, this resulted in disc geometrical anomalies that were not entirely representative of the specimen *in vitro*. These inaccuracies in geometry may have affected the mechanical function of the models and caused errors in the performance of the simulations relative to the *in vitro* mechanics.

In some cases, the MRI data did not provide clear evidence for the full shape of the outer annulus boundary (Figure 5.5), requiring the external disc boundary to be defined manually. In the models, the outer annulus surface is a free edge and therefore its shape and deformation should not affect the function of the disc. Radial bulge calculations were based on this boundary so may have incurred errors from this method.

5.5.2 PARAMETRIC ANALYSIS

As a result of the sensitivity analysis, the parameters to which the models are most sensitive were identified.

The orthotropic annulus variant was investigated as a method of including directionality in the material properties of the annulus to replicate the characteristics of the tissue *in vivo*. The most significant effect of this model variant was the large

increase in radial bulge observed for all specimens. The same model was implemented in the generalised disc model, for which the increase in radial bulge reduced the error of the disc performance compared to the target values. However in this study, when the orthotropic model was implemented, the radial bulge of the discs far exceeded the experimental measurements. For S5, the large deformation in the radial direction caused distortion of the elements in the posterior region of the outer annulus

The orthotropic material model was defined relative to a cylindrical coordinate system, with the origin located in the centre of the disc. However, when using specimen specific geometry the annulus components were not cylindrical. In the natural disc, the properties of the annulus tissue are dependent on the orientation of the collagen fibres, which in turn depend on the shape of the lamellae. In the orthotropic models, some sections of the annulus do not have cylindrical geometries relative to the defined axes, making the material properties inappropriate for these sections. For this reason, the orthotropic material model was not used throughout this study. To rectify this, the use of an element based coordinate system could be investigated, however this was deemed beyond the scope of this project.

As the MRI and dissection data presented in Chapter 4 have shown, there are no clearly defined boundaries between the soft tissues in the natural disc; rather there is a gradual change between the tissues. The introduction of a transition zone between the nucleus and annulus was intended to replicate this gradient in the change of tissues and as such, changed the gradient in stress through the disc.

Severe stress variations were also observed in the annulus for the interface models. In these models, the interface elements had a lower Young's modulus than the surrounding annulus material and thus they experienced lower levels of stress. The bulk representation of the lamellar structure used in these models means that these stress variations were experienced in only limited sections of the annulus. There are up to 25 lamellae across the natural annulus, thus these variations would be more evenly spread across the tissue. There would also be additional variations in material properties within the lamellae. Thus the severe stress variations recorded in the interface models are an exaggerated representation of the *in vivo* mechanical environment.

The interlamellar tests for the specimen specific and generalised models had similar outcomes, with both studies recording a minimal effect on stiffness but an increase

in disc bulge for the interface model. In the frictionless model, an increase in radial bulge and a decrease in stiffness of around 15% were recorded in both studies.

For the parametric tests that analysed alterations to the gross structures of the disc (i.e. the distinction of the annulus, nucleus and transition zone) similar effects were observed for all models. However the tests that added detail at the sub-annulus level had varying effects on the different specimens.

In both the interface and frictionless tests, the annulus became more compliant (Figure 5.17). This was illustrated by the decrease in stiffness for all three specimens in both these tests. However, the variation in magnitude and distribution of radial bulge (Figure 5.15) indicates that the deformation of the annulus during compression depends on the method of representing the interactions.

Of the three specimens, S3 had the smallest inter-lamellar contact area, relative to the volume of the disc. As a result of this, the behaviour of this specimen changed the least during the frictionless and interface models.

S4 and S5 had the same ratio of contact area to disc volume, so the effect of the frictionless and interface models on their behaviour relative to the control models was expected to be similar. However, their deformations during these tests were very different. This is most likely due to the different displacements that were applied to the two specimens. The displacement applied in the x direction was almost six times greater for S4 than S5.

Overall, the best agreement with the experimental data for radial bulge was recorded for the transition zone model. However with such minor changes between model variations observed for some specimens, the small sample size presented and the lack of validation data, there is insufficient evidence to conclude that the transition zone variation is more accurate than the others.

The interface model variations performed with similar levels of agreement with the experimental data. In addition, they also provided an indication of the deformation occurring at a sub-annulus level.

5.5.3 STIFFNESS RESULTS

Loading data was not recorded when the specimens were compressed, as such the stiffness of the models can only be compared to data from the literature. The stiffness of the models ranged from 1 – 1.9kN/mm. Costi *et al.* (2002) conducted

experimental loading tests under similar conditions. Their results reported an average axial stiffness for ovine disc specimens of 1.2kN/mm from 11 specimens, with a range of 1.0 to 1.4 kN/mm. This adds confidence that the models developed are behaving within a reasonable range of axial stiffness for all parametric tests. Had the experimental applied load been recorded, this could have been applied to the models and thus the deformation and displacement data could have been used for model calibration and validation.

5.5.4 FUTURE WORK

O'Connell *et al.* (2007) used image correlation software to determine the strain across a two dimensional MR image between an unloaded and compressed state. The same software was investigated for potential use in this study, however it was deemed inappropriate for use with this image data. A trial study was conducted using the software, in which corresponding images from the MRI-P and L scans were compared to automatically generate strain maps. However the results from the software were incomplete, due to insufficient correlation data in the images. These were caused by the slice, or portions of the slice moving out of plane during compression. It is expected that these methods would be improved if remote loading of the specimen was possible and if the slice agreement between the P and L scan could be verified. MR sequences could be adapted to make the images more appropriate for this application, as presented by O'Connell *et al.* (2007), however this could be at the sacrifice of the image detail in three dimensions. The effects of fibre reorientation on MRI signal intensity should also be considered as this may cause errors in the correlation process. If this avenue of investigation was to be continued, further verification analysis into the use of the software would be recommended.

Adjustments to the methods used during scanning of the specimens could help to reduce the error in the modelling process. If the specimens had been loaded remotely, they could have remained stationary during the compression and the P and L scans would not have required registering to one another, reducing the error during model construction. Registration would still be required between the MR and µCT data. An increase in the number of markers used may have assisted this.

Higher resolution images would have assisted in improving the accuracy and detail of the models but were the optimal available from the imaging techniques applied.

To implement such changes, the limitations of using the MR scanner must be considered. This effects not only the images that can be developed but also the materials that can be used for apparatus, the time that scans take and the space available for specimens and equipment.

An increase in the mesh density of the models would have allowed more detail to be added to the annulus structure, for example increasing the number of lamellae represented to match the number of lamellae observed during MRI analysis and dissection. Use of a wider range of loading regimes and an increased sample size would be beneficial to improve the confidence in the material properties developed.

5.5.5 CONCLUSIONS

Novel methods were developed to produce specimen specific models of the disc based on MR and μCT image data with further geometric information contributed from dissection analysis. These methods facilitated direct comparison with the experimental performance of the tissues that illustrated the reasonable performance of the models and provide a foundation for future computational work The sensitivity studies showed that the model behaviour was governed most by the representation of the annulus, including its orthotropic properties, the transition to the nucleus and interlamellar representation, whereas the property distribution in the surrounding bone had little effect.

6 FINITE ELEMENT ANALYSIS OF DISCS FOLLOWING NUCLEUS REPLACEMENT

Previously presented models were used in a parametric analysis designed to evaluate how the mechanical performance of the annulus could be affected by changes to disc properties that may result from injectable nucleus replacement treatments. A generalised and a specimen specific model were analysed for changes to the modulus, compressibility and volume of the nucleus that could reasonably occur during nucleus replacement using injectable hydrogels. Similar trends were observed between the generalised and specimen specific models, with the exception of radial bulge at the inner annulus, which was attributed to the rounded shape of the nucleus cavity in the specimen specific model. This study illustrated a potential application of disc models for clinical challenges in the treatment of back pain.

6.1 INTRODUCTION

As discussed in Chapter 2, injectable hydrogels offer an attractive alternative to total disc replacement procedures. Although not yet in use clinically, several hydrogel nucleus replacements are in development, with research on-going as to the appropriate chemical composition to mimic natural disc tissue material properties (Vernengo *et al.* 2008).

A range of material properties have been recorded for the different gels developed (Vernego *et al.* 2008). The wide range of tissue properties occurring naturally and the many parameters governing nucleus mechanics means that optimal material properties for the hydrogel replacements may not be achieved. It is therefore important to understand the effect of altering the nucleus material properties on the annulus tissue that remains intact.

In this study, previously developed models of the disc were used to analyse the effect of changes to the nucleus material properties and size on the mechanics of the whole disc. Particular focus was paid to the effects on the annulus mechanics.

6.2 METHODS

A generalised and a specimen specific model were used in this study. All model parameters, including loading and boundary conditions were maintained as presented in previous chapters, whilst the parametric tests were conducted on the nucleus as outlined in Section 6.2.3.

6.2.1 GENERALISED MODEL

The eight-ring, axisymmetric, interlamellar interface model presented in Section 3.3.4 was used as the generalised model. This model previously performed well relative to the deformation targets in the literature and in comparison to the other model variants. This model also offers an increased level of detail to the annulus structure, useful for investigating annulus mechanics.

6.2.2 SPECIMEN SPECIFIC MODEL

Model S3 from Chapter 5 was used as the example specimen specific model due to its mid-range size and applied displacement. The most detailed variant, the "interface" model was used, as outlined in Section 5.3.5. The annulus/nucleus transition zone (TZ) was also included.

6.2.3 PARAMETRIC TESTS

Four parametric tests were applied to both the generalised and specimen specific model. For each test, one variable was altered and all other model conditions remained as previously described for the control variants. The tests were related to parameters that are considered during the development of injectable hydrogel nucleus replacements.

TOTAL NUCLEOTOMY

This test aimed to illustrate the role of the nucleus in normal function of the disc and the effect of removing the nucleus on the surrounding tissues, as would occur during a surgical total nucleotomy surgical procedure.

For both models, the material properties of the nucleus were altered to be deformable and compliant in comparison to the surrounding tissues. This method allowed the nucleus component to be effectively removed and avoided computational complications that could arise from the removal of elements from the models. *In vivo*, the space remaining following nucleotomy would fill with some fluid. These elements are henceforth referred to as "void" elements.

Preliminary tests using the generalised model were conducted and confirmed that using elements in place of the nucleus with $E = 0.1$ kPa and $v = 0.2$ produced annulus deformations that were within 0.1% agreement with a model without any nucleus elements (Figure 6.1).

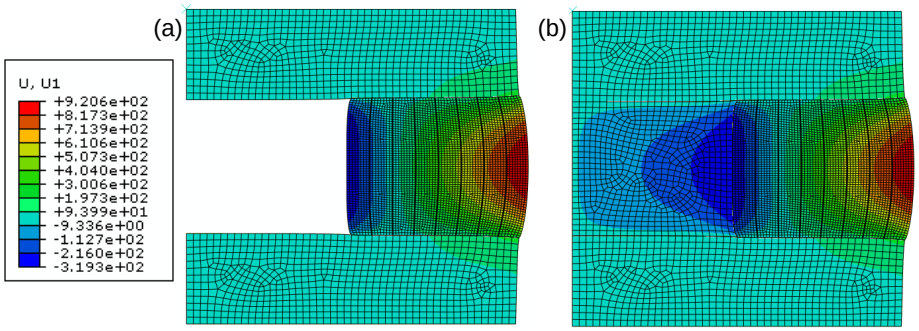

Figure 6.1 – Generalised model with (a) nucleus removed and (b) with "void" elements in place of the nucleus. Results for the two models were within 0.1% of each other.

NUCLEUS MODULUS REDUCTION

The modulus of the nucleus was reduced by 97% from 1.5 to 0.05MPa, the value stated by Vernengo *et al.* (2008) as the criteria for the minimum acceptable value for a hydrogel to be appropriate for use in nucleus replacement.

COMPRESSIBLE NUCLEUS

The Poisson's ratio of the nucleus was reduced to 0.3, causing the elements to become compressible. The value of 0.3 was chosen to make the nucleus more compressible than the annulus, for which v = 0.4.

NUCLEUS VOLUME REDUCTION

The volume of the nucleus was reduced by 5%. This was to simulate the effect of under filling the nucleus cavity with the replacement gel. The remaining internal elements were assigned "void" element properties. The void elements were located between the nucleus and annulus, as illustrated in Figure 6.2.

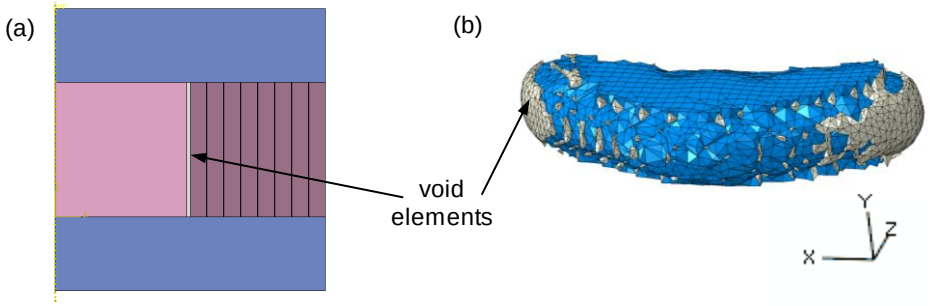

Figure 6.2 – nucleus volume reduction variations for (a) the generic model and (b) the specimen specific model, for which the nucleus elements are shown in blue and the void elements in white, located between the nucleus and annulus.

6.3 RESULTS

Throughout the parametric tests, similar trends were recorded for the generalised and specimen specific models, as illustrated in Figure 6.3 and Figure 6.4.

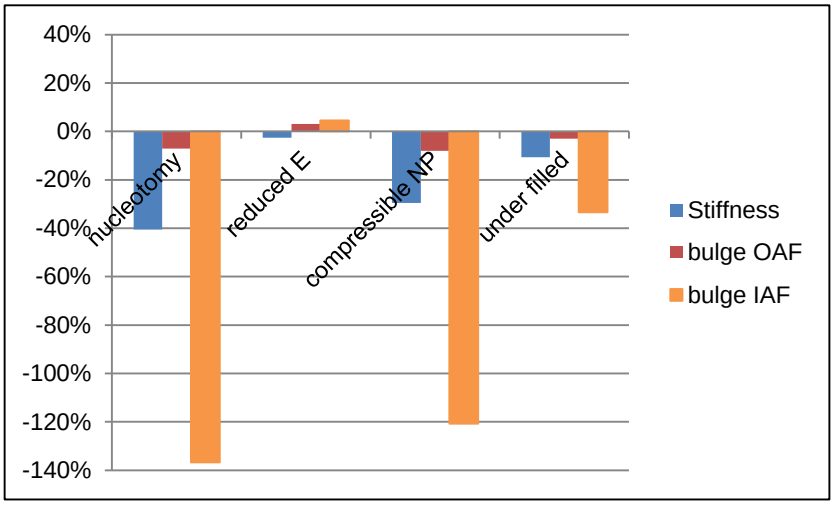

Figure 6.3 – Percentage changes in gross disc mechanics for the generalised model relative to the original generalised model. Positive results indicate an increase in magnitude and negative a decrease relative to the original model.

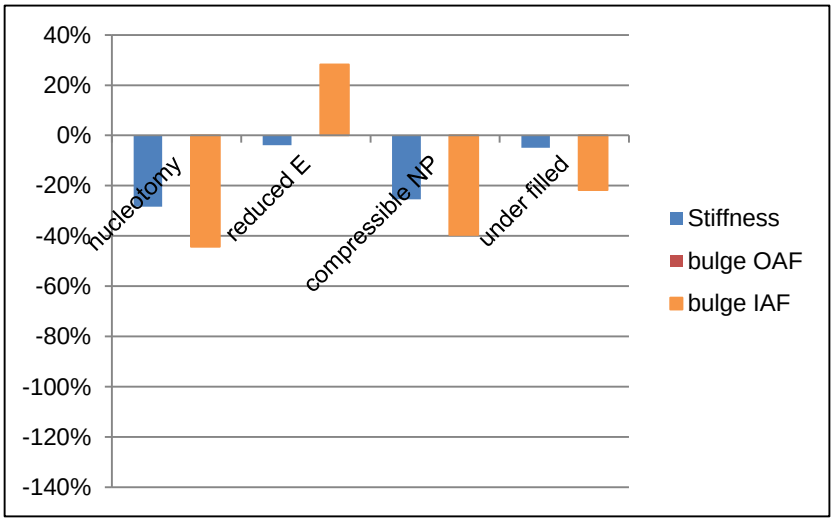

Figure 6.4 – Percentage changes in gross disc mechanics for the specimen specific model, relative to the original specimen specific model. Positive results indicate an increase in magnitude and negative a decrease relative to the original model.

The generalised model was more sensitive to the changes to the nucleus. The radial bulge at the inner annulus was the most sensitive variable in both the models whereas the bulge at the outer annulus was not notably changed in either mode.

6.3.1 GENERALISED MODEL

The results for the variations of the generalised model are summarised in Figure 6.5. Results for the original generalised model are also presented for comparison with the parametric test results.

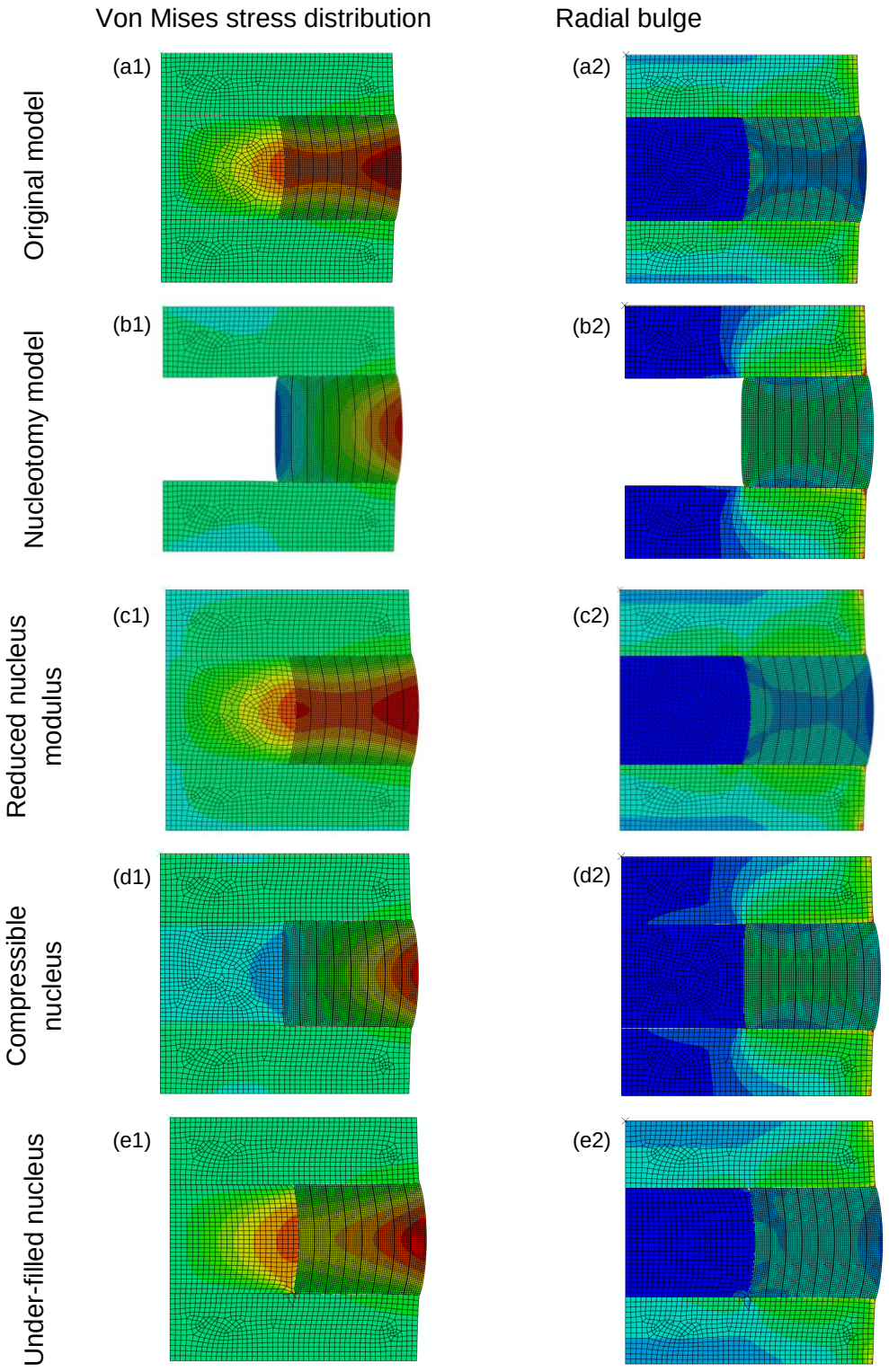

Figure 6.5 – Results plots showing (1) Von Mises stress distribution and (2) radial bulge for the variations of the generalised model. Legends for the distribution plots are presented in Figure 6.6.

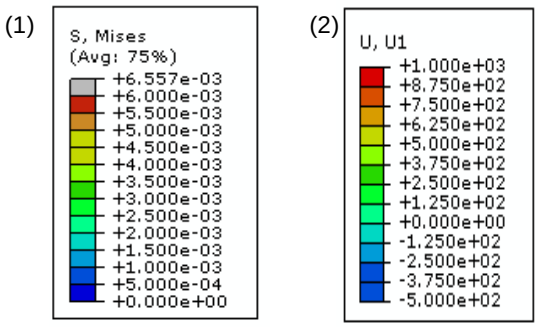

Figure 6.6 – Legends for the distribution plots presented in Figure 6.5 for (1) Von Mises stress and (2) radial bulge.

The gross mechanics of the model were not greatly changed during the reduced nucleus modulus tests, despite a 97% reduction in the Young's modulus. The model was much more sensitive to the compressibility of the nucleus.

The bulge of the annulus was significantly affected by the removal of the nucleus in the nucleotomy test. The direction of bulge at the inner annulus was reversed from outwards to inwards. The bulge at the outer annulus reduced by 7%.

With a compressible nucleus, the model behaved with similar characteristics to the nucleotomy test. The bulge of the inner annulus was again altered from outwards to inwards. The stress distribution in the adjacent vertebral bodies was also affected, with a much lower stress adjacent to the nucleus than recorded in the original model.

The change in disc mechanics when the nucleus becomes compressible is highlighted in Figure 6.7. When the nucleus is incompressible, it bulges against the annulus and loads it in tension in the circumferential direction (a2) and in compression in the radial direction (a1). When the nucleus is compressible, the inner annulus bulges inwards towards the centre of the disc, resulting in tensile strain in the radial direction (b1).

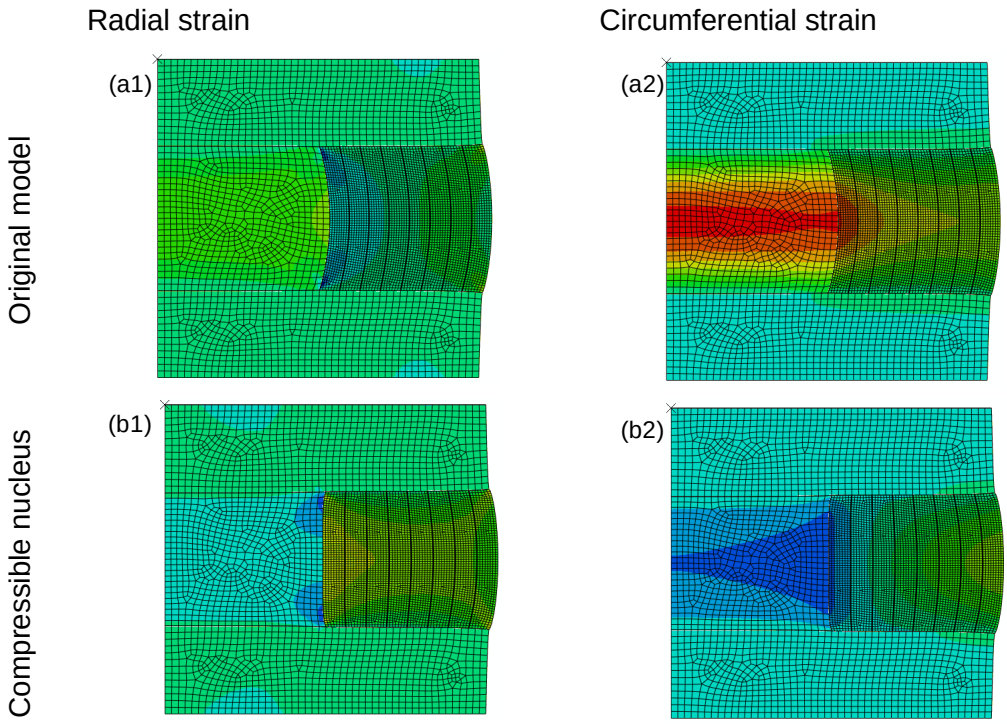

Figure 6.7 – The effect of nucleus compressibility on (1) radial and (2) circumferential strain. Plots shown for (a) original generalised model and (b) compressible nucleus generalised model. Strain legends are presented in Figure 6.8.

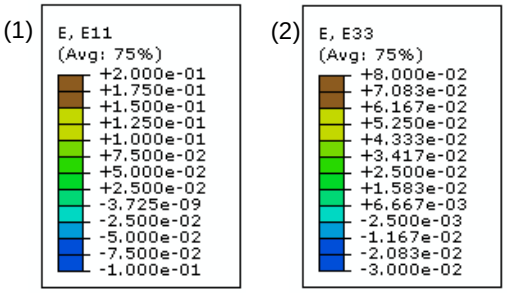

Figure 6.8 – Strain legends to accompany Figure 6.7: (1) strain in the radial direction, (2) strain in the circumferential direction. Tensile strain is positive and compressive strain is negative.

The distribution of load between the nucleus and the annulus and the effects of nucleus compressibility on this distribution are illustrated in Figure 6.9. For the original model, the load is shared relatively evenly between the nucleus and annulus, however for the compressible nucleus test, the load in the nucleus is much lower than that in the annulus.

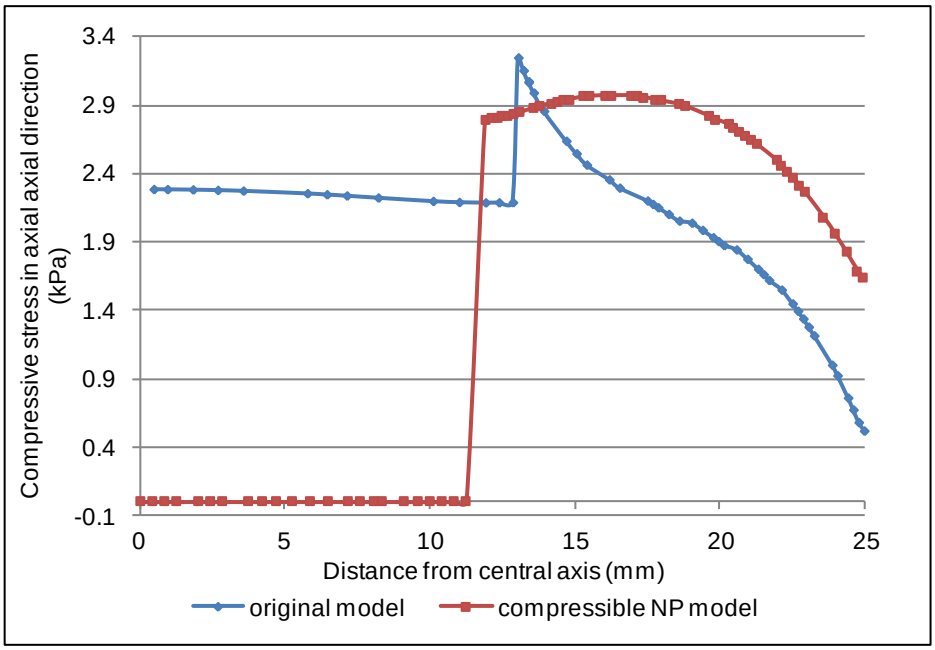

Figure 6.9 – The change in the load distribution between the nucleus and annulus for an incompressible and compressible nucleus. When the nucleus was incompressible, the axial load was shared with the annulus. When the nucleus was compressible, the annulus took much more of the load than the nucleus.

With a void introduced between the nucleus and annulus to represent an under-filled nucleus replacement, the bulge of the inner annulus was reduced. The pattern of the stress induced in the annulus by the nucleus was also affected, as illustrated in Figure 6.5.

6.3.2 SPECIMEN SPECIFIC MODEL

Although the same trends were observed for the mechanics of the specimen specific and generalised models, the magnitudes of the changes were much less for the specimen specific model (Figure 6.4).

Changes were observed to the stress distribution through the model with each of the tests, as presented in Figure 6.10. The Von Mises stress distribution for the original specimen specific model is also illustrated in Figure 6.10 for comparison, in which stress concentrations were observed in the vertebral bodies, adjacent to the nucleus.

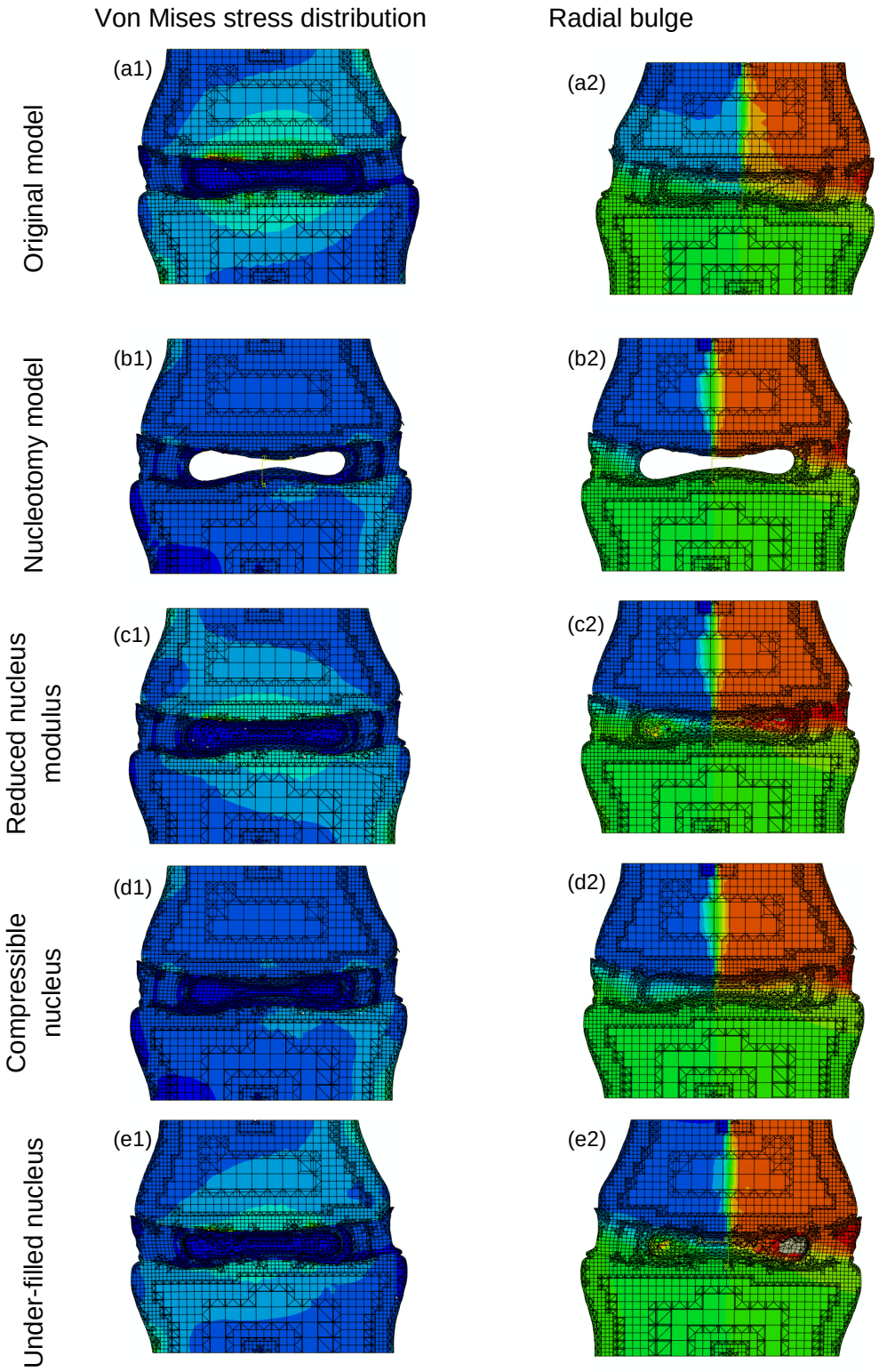

Figure 6.10 - Results plots showing (1) Von Mises stress distribution and (2) radial bulge for the variations of the specimen specific model, plotted here as displacement in the radial direction relative to the origin at the centre of the disc. Legends for the distribution plots are presented in Figure 6.11.

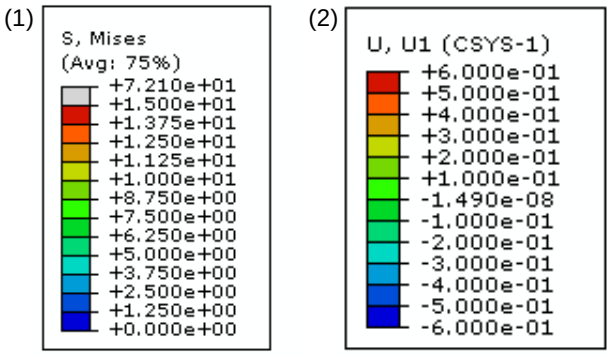

Figure 6.11 - Legends for the distribution plots presented in Figure 6.10 for (1) Von Mises stress and (2) radial bulge.

With the removal of the nucleus, stress was reduced in the vertebral bodies but was increased in the annulus. Similar results were observed for the compressible nucleus test.

For the test with the reduced nucleus modulus, a similar stress distribution across the vertebral bodies to the original model was recorded, although the magnitudes of the stress concentrations were reduced.

The under-filled nucleus test did not significantly change the performance of the specimen specific model.

6.4 DISCUSSION

This study has illustrated an application of FE models of the disc in the development of back pain treatments. The material property parameters of the nucleus were varied to investigate those that are relevant to the development of injectable hydrogels for nucleus replacement.

The results have shown that replicating the incompressibility of the healthy nucleus is important for restoring the natural mechanics of the disc tissues. This had a greater effect than variations to the modulus of the tissue. These observations were expected, as the incompressibility of the nucleus was the dominant parameter in the mechanics of the system. For a compressible nucleus, it is likely that the system would become sensitive to changes in the modulus of the nucleus, although this was not investigated in this study.

With a compressible nucleus, the inner annulus bulged inwards during disc compression. The annulus was not loaded in circumferential tension as it was during healthy disc function. Similar mechanics were recorded during the

nucleotomy tests. When the nucleus was incompressible, the mechanics of the disc were restored even with a 97% reduction in the modulus of the nucleus.

Restoration of the stress transferred from the disc into the adjacent vertebrae is an important consideration for the long term success of spinal implants. The high failure rate of total disc replacements has been attributed to the change in stress distribution through the FSU (Chapter 2). If material properties of nucleus replacements can better replicate those of the natural tissues, the risk of such failure mechanisms is reduced.

Similar changes to the gross disc mechanics were observed for the parametric tests in both the generalised and specimen specific models. The most noteworthy difference between the two was that inward bulging of the annulus was not observed in any variations of the specimen specific model. This was attributed to the convexly curved shape of the nucleus/annulus interface prior to loading.

Meakin *et al.* (2001) conducted an experimental study into the effect of nucleotomy on annulus mechanics by bisecting discs through the mid sagittal plane and observing the deformation of the tissues during compression by sealing the cut face against a transparent Perspex screen. Similar observations were made of the annulus straining in tension in the radial direction and bulging inwards when insufficient nucleus tissue was present to instigate outward bulging at the annulus/nucleus boundary. The computational approach presented here facilitated an investigation into the same phenomena but did not require dissection of the disc and allowed a far more comprehensive output of tissue deformation data.

However the study is limited in many aspects. As across all models presented in this thesis, an instantaneous loading condition was assumed in all tests and so fluid flow in the disc was not considered. Boundary conditions were maintained as described in previous chapters. These may not be representative of *in vivo* conditions, and may need revising to accurately model the mechanics of a degenerated spine.

As discussed in Chapter 5, the size of the nucleus was based on dissection data but the shape was not based on specimen specific information, thus this aspect of the model performance may not be representative of how the specimen would have responded to these changes *in vitro*.

Clinically, the shape of the nucleus/annulus interface would depend on the cavity created in the disc during nucleometry. Improved data for this geometry, or that of the nucleus shape in the natural disc would increase confidence in this model.

Injecting the optimum amount of gel into the disc is one of the challenges of conducting this procedure surgically. Previous FE studies of nucleus replacements have suggested that over-filling of the nucleus cavity is inappropriate and results in detrimental changes in the distribution of stress through the FSU (Di Martino *et al.* 2005). This study investigated the effect of under-filling the cavity and showed that the mechanics of the disc were restored to a satisfactory level with 95% of the nucleus volume replaced. Reducing the volume of the nucleus (and adding void elements) changed the mechanics of the system by increasing the nucleus compressibility. This would eventually result in mechanics similar to those reported for the compressible nucleus test. A useful extension to this analysis would be an investigation into the minimum acceptable level of filling. However, in a degenerated disc, the disc height may be compromised, therefore just filling the same space may not eliminate pain.

In this study, parametric changes were considered individually. In practice a combination of these changes would be experienced. The wide range in natural nucleus material properties means that replacement materials will never exactly replicate the individual's nucleus tissue as it was when healthy. In practice, it would be difficult to exactly fill the nucleus cavity. For relevance to clinical applications, findings from parametric tests should be considered in parallel.

The study has highlighted the importance of restoring an incompressible nucleus and the priority of this over the modulus of the replacement material. Without nucleus incompressibility, the loading on the annulus is significantly altered and increased and new loading mechanisms such as radial tension may arise.

A clinically relevant application of both the generalised and specimen specific modelling approaches was illustrated. Differences in the response of the generalised and specimen specific models were highlighted although similar trends were observed in both models at the gross disc scale.

7 MODELLING THE ANNULUS FIBROSIS FROM MICROSCOPY IMAGES

Microscopy techniques were investigated for their potential for use in conjunction with finite element models of annulus tissue. Two histological techniques were used. The first test strained single slices of annulus tissue in tension. The second technique analysed the structure of the tissue by reconstructing consecutive tissue slices into a three dimensional model. Finite element models were developed from the image data to investigate the mechanical behaviour of the tissue constituents. The study focused on the minor and major interlamellar bridging elements and their relationship with the surrounding tissues.

7.1 INTRODUCTION

The method of representing interlamellar interaction in FE models of the disc has been shown to affect the gross disc mechanics in both the generalised and specimen specific models (Chapters 3 and 5 respectively). However, the behaviour of annulus tissue at the lamellar level and the mechanics of interlamellar interactions are not well understood.

Histological studies of the annulus have produced detailed geometric models of the 3D structure of the tissue, indicating how the tissue constituents relate to each other (Schollum *et al.* 2008, 2009). To date, the mechanical performance of these proposed structures has not been analysed using computational simulations, yet these techniques have potential for investigating tissue mechanics at a scale that is not feasible experimentally.

The presence of interlamellar bridges within the discs of humans and animal species is well documented (Smith and Elliott 2011; Schollum *et al.* 2008, 2009, 2010) and reasons for their development have been investigated. It has been questioned whether they help maintain interlamellar cohesion or if their disruption to the otherwise regular structure of the annulus, creates stress concentrations that could lead to damage of the tissue (Chapter 2).

The radial orientation of these structures means that their mechanical role probably becomes more significant to disc mechanics following the initiation of disc degeneration. The nucleus can become compressible as hydration levels reduce with age. The simulations presented in Chapter 6 showed how this can dramatically

affect the mechanical environment of the annulus, and may cause radial tension across the tissue. When loaded in this way, the risk of delamination increases and the bridges are loaded in tension.

The aim of this investigation was to use microscopy image data to create specimen specific models of annulus tissue samples. The lamellae and interlamellar bridges were individually represented with the aim of investigating their interactions under load. A two-pronged approach was adopted:

1. Microtensile study. A two-dimensional model was created for comparison against micrographs of a single slice of tissue loaded in radial tension.
2. Serial microscopy study. A three-dimensional model was created from serial micrographs. Variations of the model were generated with and without a major bridging element. The mechanics of these two model variations when loaded in radial tension were compared.

7.2 METHODS

For both the techniques, histological data was first captured using microscopy techniques.

7.2.1 HISTOLOGICAL METHODS

Ovine tissue was used throughout this study as an appropriate model for the discs of the human lumbar spine as discussed previously in Chapter 4.

TENSILE MICROSCOPY METHOD

The T13-L1 disc was dissected from a skeletally mature (aged 3-5 years) ovine spine (ewe) post mortem, wrapped in plastic and stored at -20˚C until use. A block of annulus tissue was taken from the anterior portion of the disc and mounted in a freezing stage sledge microtome (MR2 Series, HACKER Instruments & Industries Inc., Winsboro, USA) with the radial face of the tissue block towards the microtome blade. Slices 60µm thick were cut at 30˚ to the axis in plane with one direction of the fibres and transecting the alternating direction of fibres; as previously described by Schollum *et al.* (2009) and Pezowicz *et al.* (2006), illustrated in Figure 7.1. The slices were floated in saline at 5˚C and tested within 2 hours of extraction from the disc.

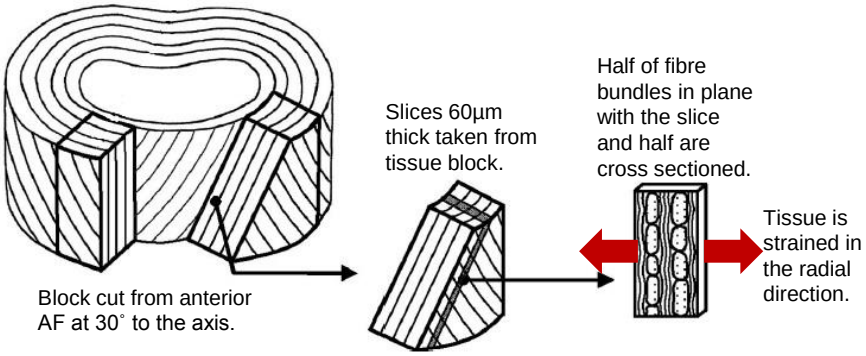

Figure 7.1 - Diagram to show the extraction, sectioning and loading of annulus tissue into "in-plane" slices. Adapted from Pezowicz et al 2006. The red arrows show the direction in which the specimens were strained.

The slices were individually placed into a bespoke tensile testing rig (Figure 7.2) previously described in detail by Broom (1984, 1986), with the radial ends of the slice securely clamped. The slices were sandwiched between two glass cover slips that allowed light to be transmitted through the specimen. The rig was mounted directly into the rotating stage of a conventional light microscope (Multizoom AZ100, Nikon Instruments, New Zealand).

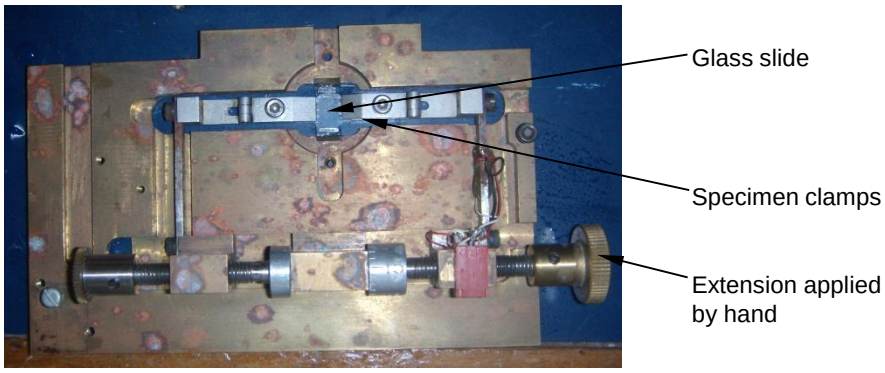

Figure 7.2 – Loading rig used to apply tension to tissue slices. Rig was positioned on microscope loading stage. Glass slide allowed light to pass through the sample.

The slices were incrementally strained in the radial direction, as illustrated in Figure 7.1. An image of the strained tissue was captured at 100 – 200 times magnification with every 0.5mm of extension until the specimen failed.

Initial failure was defined as the point of extension at which holes appeared in the tissue. Total failure was defined as the point at which the tissue had ripped over more than 90% of the specimen's height. Specimens that failed at the clamp edge were discarded from further analysis.

SERIAL MICROSCOPY METHOD

An intervertebral disc was dissected from the lumbar spine of a mature ewe that had previously been in storage at -20°C for less than three months. The disc was chemically fixed by soaking in a solution of 10% formalin for a week and then decalcified by soaking in a solution of 10% formic acid for three weeks. A portion of annulus tissue was dissected from the anterior region of the disc in preparation for cryo-sectioning as previously described for the tensile microscopy methods.

Slices of tissue 30µm thick were taken in plane with one of the fibre directions, as illustrated in Figure 7.1. Care was taken to ensure that each serial slice was intact so that a continual series of consecutive slices was achieved.

In total, 37 serial slices were obtained. Each slice was examined using a differential interference microscope (Eclipse 90i, Nikon, Instruments, New Zealand). Image settings were adjusted to optimize the contrast between the fibres with differing orientation and to highlight the interlamellar bridges.

7.2.2 COMPUTATIONAL METHODS

For both of the computational investigations, FE models were created from micrographs and meshed using imaging processing software, ScanIP (version 4, Simpleware Limited, Exeter, U.K.). The models were exported to a commercially available FEA software package (ABAQUS CAE, version 6.9-1, Dassault Systèmes Simulia Corp, Providence, RI, USA).

The experimental data did not include loading information, and with insufficient data available in the literature, the biomechanics of the tissue at this scale, *in vitro*, isolated from the surrounding tissues are unknown. It is not known whether the tissue has the same mechanical behaviour as it would *in vivo*. Thus the computational analyses did not include units. Instead, the relative material properties of the constituent tissues and their interacting structures were investigated.

TENSILE MICROSCOPY MODEL

From the preload and loaded images for specimen T3 as shown in Figure 7.13, a portion of the specimen was chosen that showed three lamellae: two in which the fibres were in-plane and one with cross sectioned fibres, as shown in Figure 7.3.

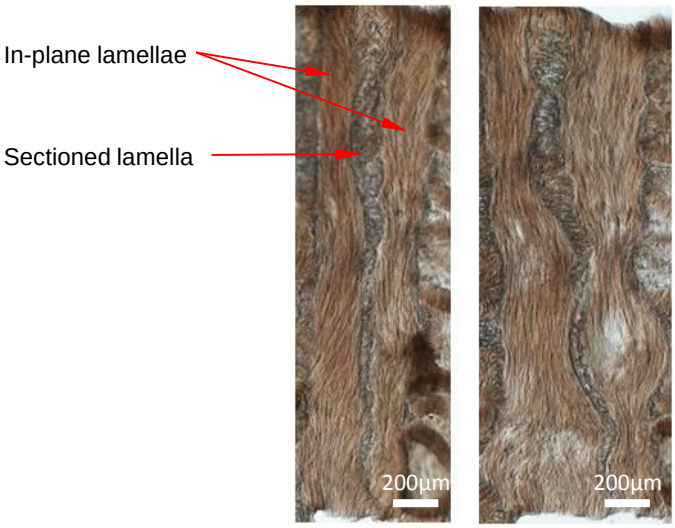

Figure 7.3 - Cropped micrographs of specimen T3 in its preload (left) and loaded (right) state, showing a region of interest containing the full height of the specimen for 3 lamellae.

A 2D model was developed from the preload image, specific to the experimental specimen's geometry. The in-plane and sectioned lamellae were segmented as separate components. Additional features, such as the interlamellar bridging elements were also segmented to be included in the models. The segmentation process was conducted manually, due to a lack of contrast between the tissue constituents.

The model was meshed and exported as a finite element model comprising a mix of quadrilateral and triangular 2D elements. This will henceforth be referred to as the "micro-tensile FE model".

Preliminary tests were conducted to verify the mesh density by analysing the sensitivity of the model to variations in element size (total number). The results of these tests are presented in Figure 7.4. The error incurred from mesh inaccuracies as a result of using 30,000 elements was deemed negligible relative to other anticipated sources of error in the model; there was 1.6% difference between the stiffness result for the mesh used in the study and the mesh with 72,000 elements. Thus the final mesh used in the investigation contained approximately 30,000 elements.

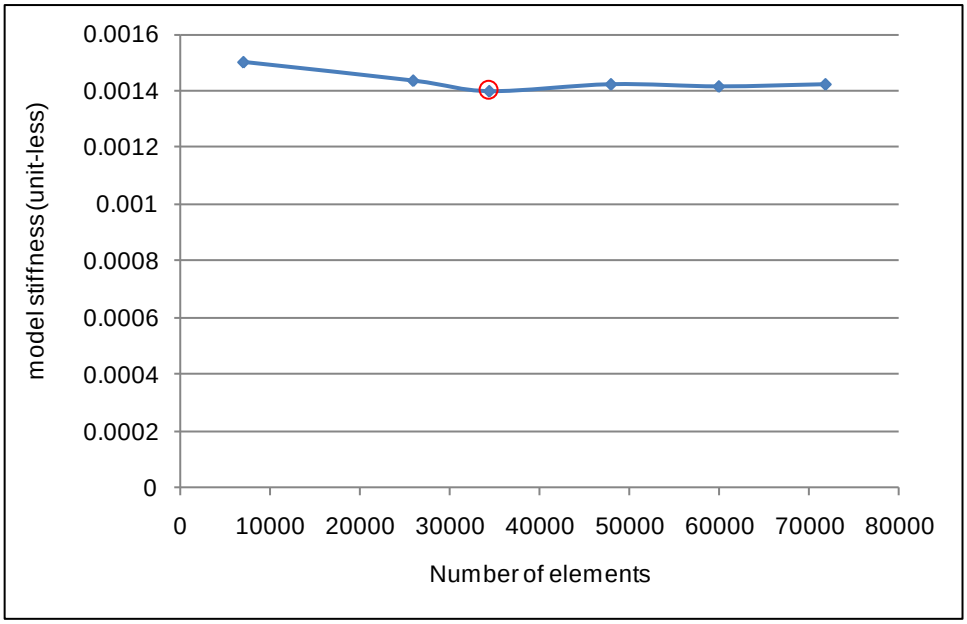

Figure 7.4 – Results from preliminary tests to verify the mesh density of the model. Result for the mesh used in the analysis is highlighted.

"Tied" connections were used between all components. Adjacent lamellae were assigned opposite material orientations to account for their differing fibre orientations. Previously derived orthotropic material properties for the annulus (Section 3.2.3) were used as a base to develop material properties for the lamellae. The ratios of the material properties in the x, y and z directions were maintained. The material properties were not assigned units, their relative magnitudes are presented in Table 7.1.

E_x	E_y	E_z	v_{xy}	v_{xz}	v_{yz}	G_{all}
0.0004	0.07	0.016	0.023	0.075	1.38	0.0001

Table 7.1 – Unit-less orthogonal material properties applied to the lamellar, based on previous material model development (Section 3.2.3). Shear modulus (G) is assumed to be the same in all directions. The values are arbitrary due to the unit-less assumption, but are maintained at the same values as used previously for reference.

The process of creating a model based on a single microscopy image was repeated using the loaded image. This allowed the experimental results to be represented in a form that was directly comparable with the computational results from the FE model built from the preload image. This will henceforth be referred to as the "strained experimental model".

An algorithm was written (Matlab, R2009a, MathWorks, Natick, USA) to extract the coordinates of the nodes along the outer edges of the FE and strained experimental

models. The origin of each model was defined at the centre of the specimen. Interpolation was used to find nodes in the two models with similar y values (height along the edge of the model). The coordinates of these similar nodes between models were compared and the difference was found between their x values. This difference was applied as a displacement boundary condition to the node in the FE model, as illustrated schematically in Figure 7.5.

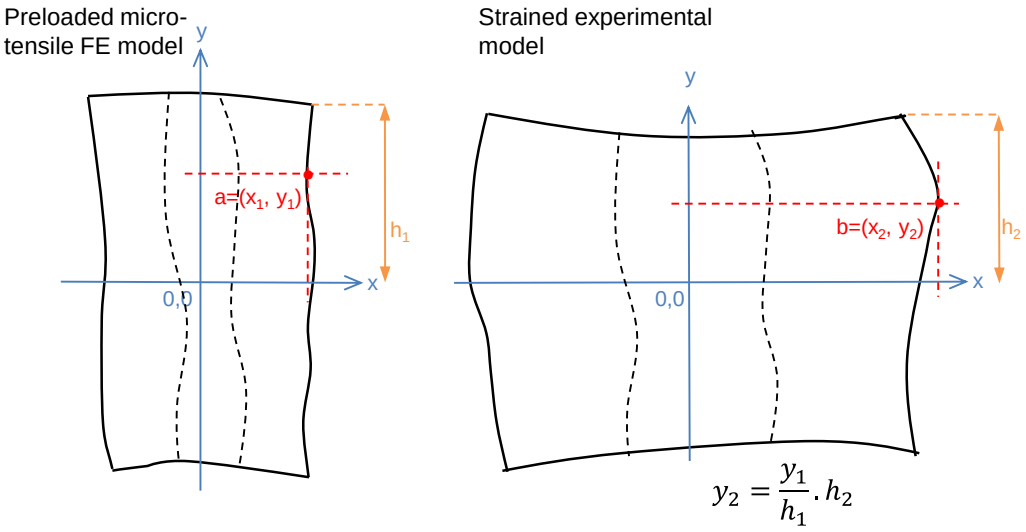

Figure 7.5 – For each node along the outer two edges of the model (e.g. point a at (x_1, y_1)), the y-value was used to find a point on the same edge with the same proportional y-value in the strained experimental model relative to the new height of the specimen (point b at (x_2, y_2)). The displacement applied to point a in the FE model was (x_2-x_1, y_2-y_1), i.e. node a was moved to be in the same position as point b to match the experimental model. This was repeated for all nodes along the outer two edges of the model.

This process was repeated for each node along the outer edges of the model in the radial direction. Thus in its deformed state, the FE model had the same geometry along its outer edges as the experimental model for the lamellae of interest. This method allowed a variable displacement to be applied to the outer edges of the model that ensured the deformation of the model was the same as that observed experimentally.

Two variations of the FE model were developed: the “bridges” model and the “sheath” model. This allowed a comparison of the two tissue models postulated in the literature, as previously described (Chapter 2). Details from these two model variations are shown in Figure 7.6. In the bridge model, bridges join the two in-plane lamellae. In the sheath model, the bridges are connected by an additional fine layer of sheath elements between the sectioned and in-plane lamellae.

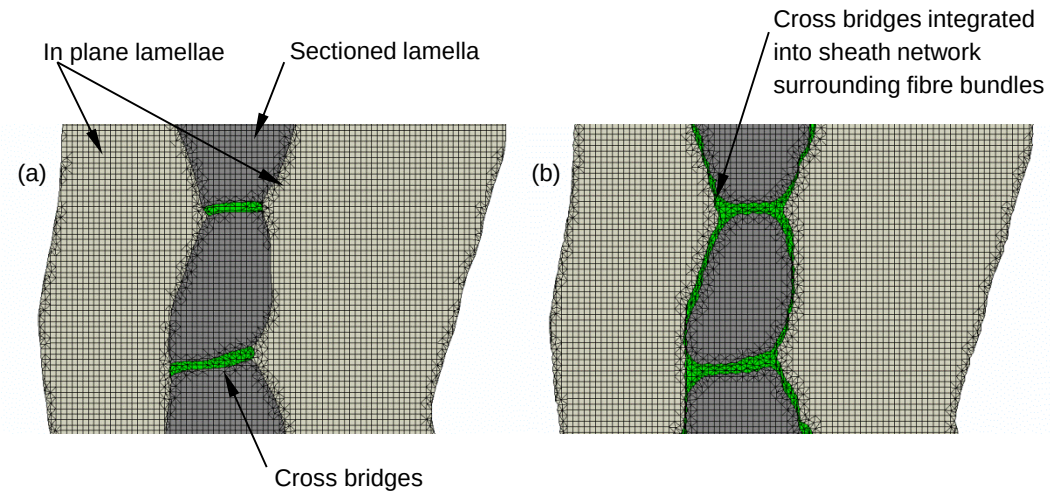

Figure 7.6 - Detail of FE models showing bridge variation (a) and sheath variation (b).

For both these models, the material properties of the bridges or the sheath network were varied. These material properties again were unit-less. The modulus was considered in the x direction (radial direction of the disc), because this is the direction in which the load is applied. The bridge/sheath elements were assigned isotropic linear elastic material properties. The modulus was varied by orders of ten, from one order of magnitude lower than the lamellae modulus in the x direction ($E_{lam, x}$:E_{bridge} = 1: 0.1) to five orders of magnitude higher ($E_{lam, x}$:E_{bridge} = 1: 100,000).

The mid-value for the range of bridge/sheath modulus was two orders of magnitude greater than the lamellae modulus in the x direction ($E_{lam, x}$:E_{bridge} = 1: 100). This was the ratio between the radial modulus of the orthotropic model developed for the annulus of the generic disc model (Chapter 3, as assigned to the lamellae) and the modulus of the isotropic model (as assigned to the bridges).

The tests in which the modulus of the bridges/sheaths was the same order of magnitude as that of the lamellae in the x-direction ($E_{lam, x}$:E_{bridge} = 1: 1) provide an equivalent scenario of there being no bridges or sheaths included in the model.

An algorithm was developed to extract correlated results between the deformed FE model and the experimental model. The coordinates of comparable nodes (based on their y values) along the internal lamellar boundaries were extracted and compared for agreement of their deformed location and displacement.

Landmark features were also compared in order to analyse how well specific characteristics of the deformed tissue were being predicted by the FE model. These included the length of the bridges, the depth of the puckers and the slope of the

internal boundary, as illustrated in Figure 7.2. The landmark features chosen for analysis were all in the upper portion of the model, as this was the region in which the interlamellar boundaries and features were clearest in the original micrographs.

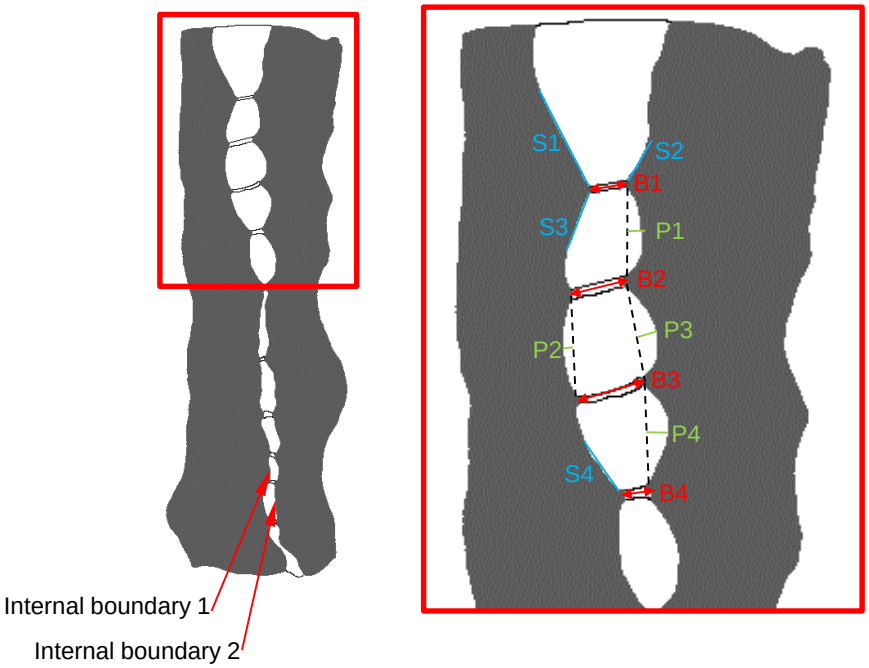

Figure 7.7 – Notation of internal boundaries (left) and landmark features (detail, right). In pane lamellae are shown in grey. B = bridge length, P = pucker depth, S = slope of boundary.

SERIAL MICROSCOPY MODEL

Schollum *et al.* (2008, 2009) published a method of using micrographs of serial slices of annulus tissue to reconstruct a generalised three dimensional representation of the tissue structure, in particular analysing the relationship of interlamellar bridges with their surrounding lamellar tissues.

In the current study, similar differential interference contrast (DIC) microscopy techniques were used to obtain micrographs of the annulus tissue. The serial slices were reconstructed using the same image processing software used for the tensile microscopy study. Whereas a single slice was used to create a 2D FE model in the tensile-microscopy study, here multiple slices were used to build a 3D model.

Slices were aligned visually in the stack using landmark features that were common to all the images. To reduce the error from slice misalignment, averaging filters were applied to the stack of images in the software, allowing some merging of image data between adjacent slices.

Voxels were identified and assigned as either in-plane lamellae, cross sectioned lamellae or interlamellar bridges. A combination of techniques, such as thresholding based on greyscale values and manual segmentation, was used to distinguish between the different constituents. The model geometry was then meshed and converted to a FE model, to which material properties and loading conditions were applied to analyse the potential mechanical behaviour of the tissue. The complete model is illustrated in Figure 7.8.

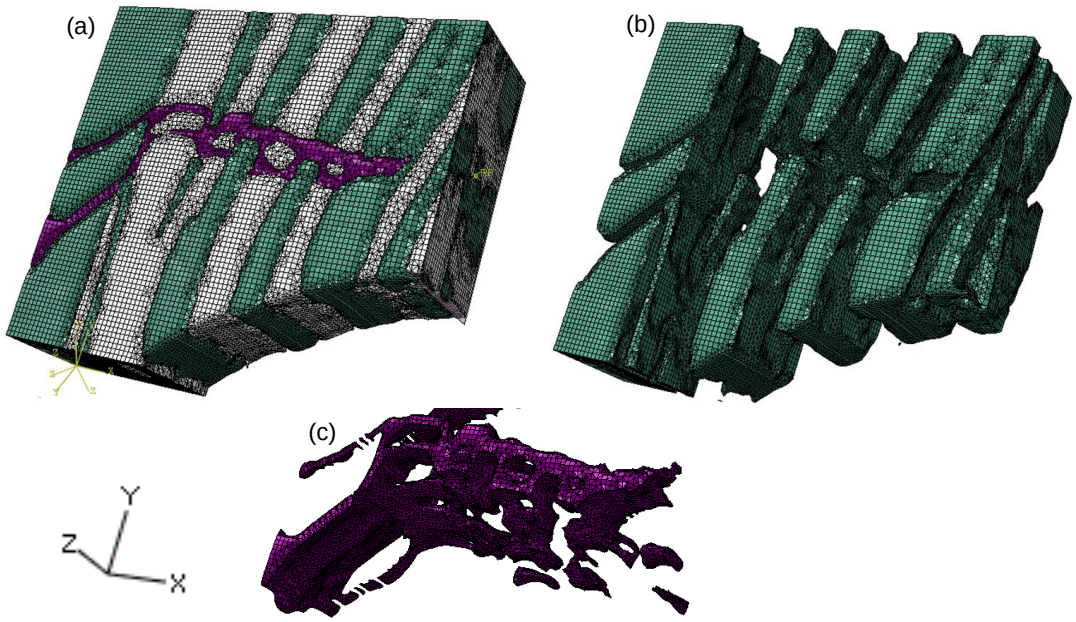

Figure 7.8 – Serial model with major interlamellar bridge: (a) complete model; (b) in-plane lamellae only; (c) interlamellar bridge.

A major interlamellar bridge was identified through the depth of the tissue sample. The bridge split and merged with minor bridging structures. Some minor bridging elements crossing three lamellae were also included (Figure 7.8, (c)).

An identical model was created that had the same lamellar structure but without the interlamellar bridges, as illustrated in Figure 7.9.

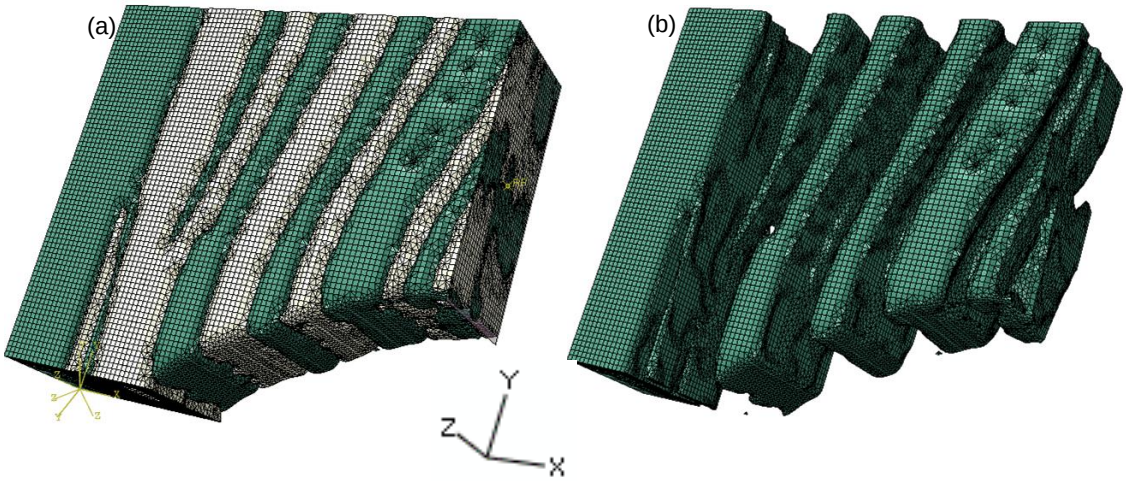

Figure 7.9 – Serial model without interlamellar bridge: (a) complete model; (b) in-plane lamellae only.

The models were meshed into approximately 550,000 3D, solid elements that were a mixture of hexahedral and tetrahedral.

The material properties assigned to the lamellar elements were the same as those used in the tensile microscopy model (presented in Table 7.1). The material coordination system was varied to account for the difference in fibre angle between the in-plane and sectioned lamellae.

The bridge elements were assigned the optimal isotropic material properties derived during the tensile microscopy study. These are presented in Table 7.3.

The face of the model on the outer annulus side was constrained in all directions. A rigid plate was attached to the opposite face of the model (Figure 7.10). A displacement was applied to the rigid plate to strain the model by approximately 30% in the radial direction, in line with the strain applied during the tensile microscopy study.

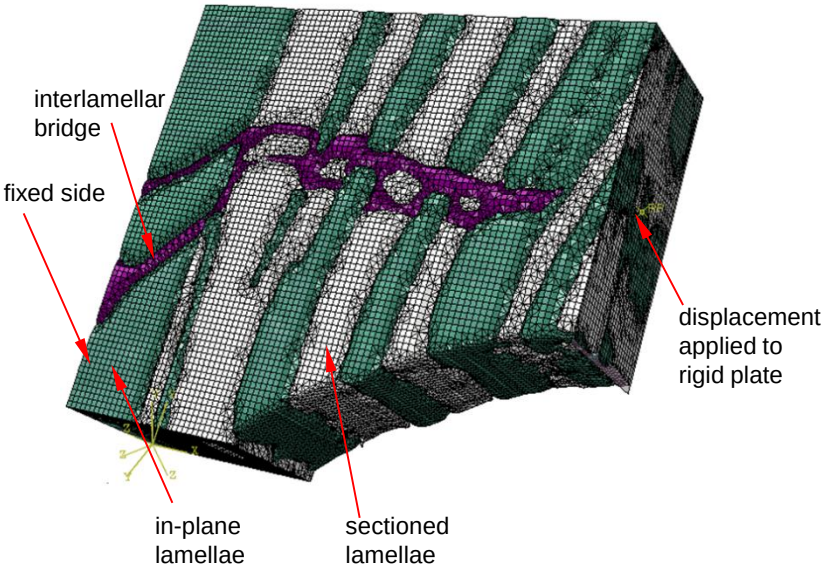

Figure 7.10 – Serial model showing applied boundary conditions.

7.3 RESULTS

Micrographs from the histological tests were examined for qualitative information about the structure and behaviour of the tissue. The deformation of models in the computational analysis were analysed to suggest the relative mechanics and properties of the constituent tissues.

7.3.1 HISTOLOGICAL RESULTS

The histological results were examined to assess the tissue structures recorded and their potential use in relation to generating computational models of the tissue samples.

TENSILE MICROSCOPY RESULTS

Of the 16 specimens tested, four were selected for further investigation, based on the quality of the images and the condition of the specimens (Table 7.2). Slices that had been damaged during the dissection or cryosectioning process were eliminated from the study. Example pre-load and strained tissue micrographs are presented in Figure 7.11.

	section	load direction	initial failure		total failure		number failure points
			extension (mm, strain)	location	extension (mm, strain)	location	
T1	in-plane	radial	3.5, 61%	clamp edge	6.5, 111%	at clamp edge	1
T2	in-plane	radial	4.5, 76%	sectioned lamella	6.0, 102%	sectioned, in-plane lamellae	3
T3	in-plane	radial	3.5, 61%	sectioned lamella	7.0, 119%	sectioned and in-plane lamellae	3
T4	in-plane	radial	4.0, 68%	sectioned lamella	7.0, 119%	sectioned and in-plane lamellae	3

Table 7.2 - Summary of results showing extension until initial and total failure of four microscopy tensile test specimens. Failure points were areas in the tissue where the tissue thinned significantly or holes appeared.

The strain at initial and total failure was relatively similar between specimens. Three of the specimens had similar failure patterns with initial failure located within sectioned lamellae and multiple failure points at the total failure strain. One specimen failed at the clamp edge, probably as a result of tissue damage caused by the clamp.

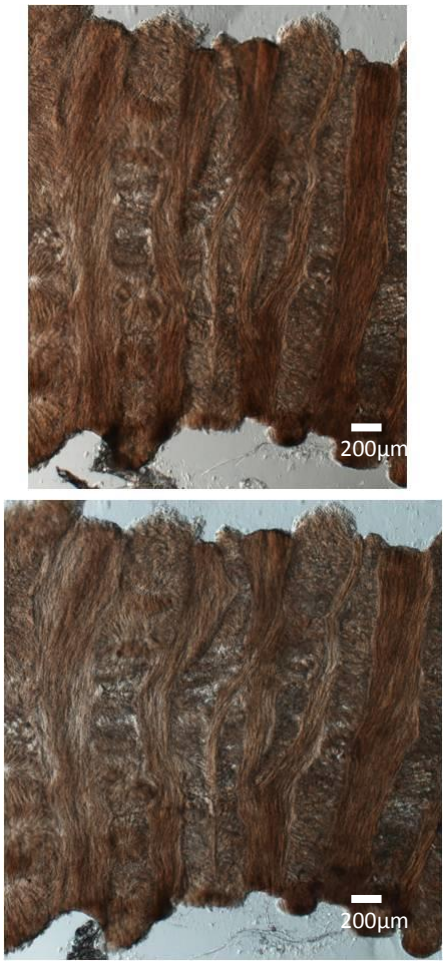

Figure 7.11 - Micrographs from tensile test sample T1 showing the unloaded specimen (top) and the specimen loaded (bottom) with an extension of 3mm.

During the testing of the five specimens, common characteristic features were observed, such as puckering of interlamellar boundaries and the thinning of tissue in localised areas, as highlighted in Figure 7.12.

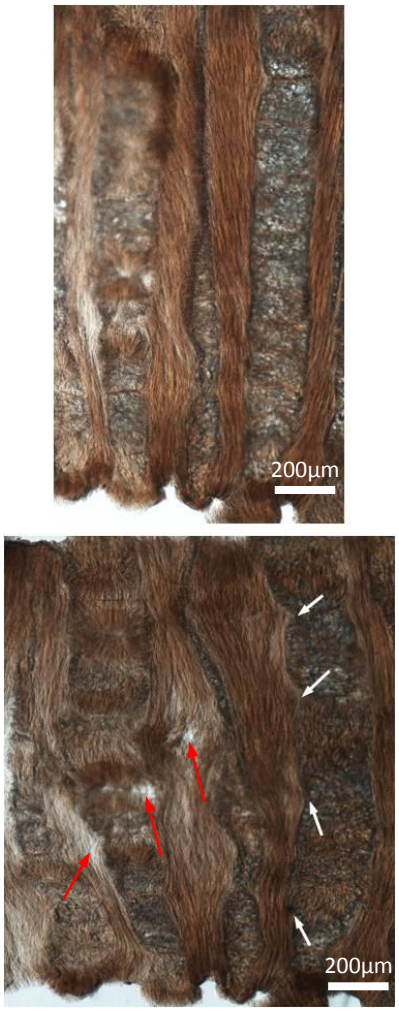

Figure 7.12 - Micrographs from tensile test sample T2 showing the specimen prior to loading (top) and the specimen loaded (bottom) with an extension of 4mm. The white arrows show an example of a lamellar boundary that has become puckered at the locations at which it intersects the interlamellar bridging elements. The red arrows indicate areas of lamellae that have thinned.

All specimens were tested to failure, as illustrated in Figure 7.13.

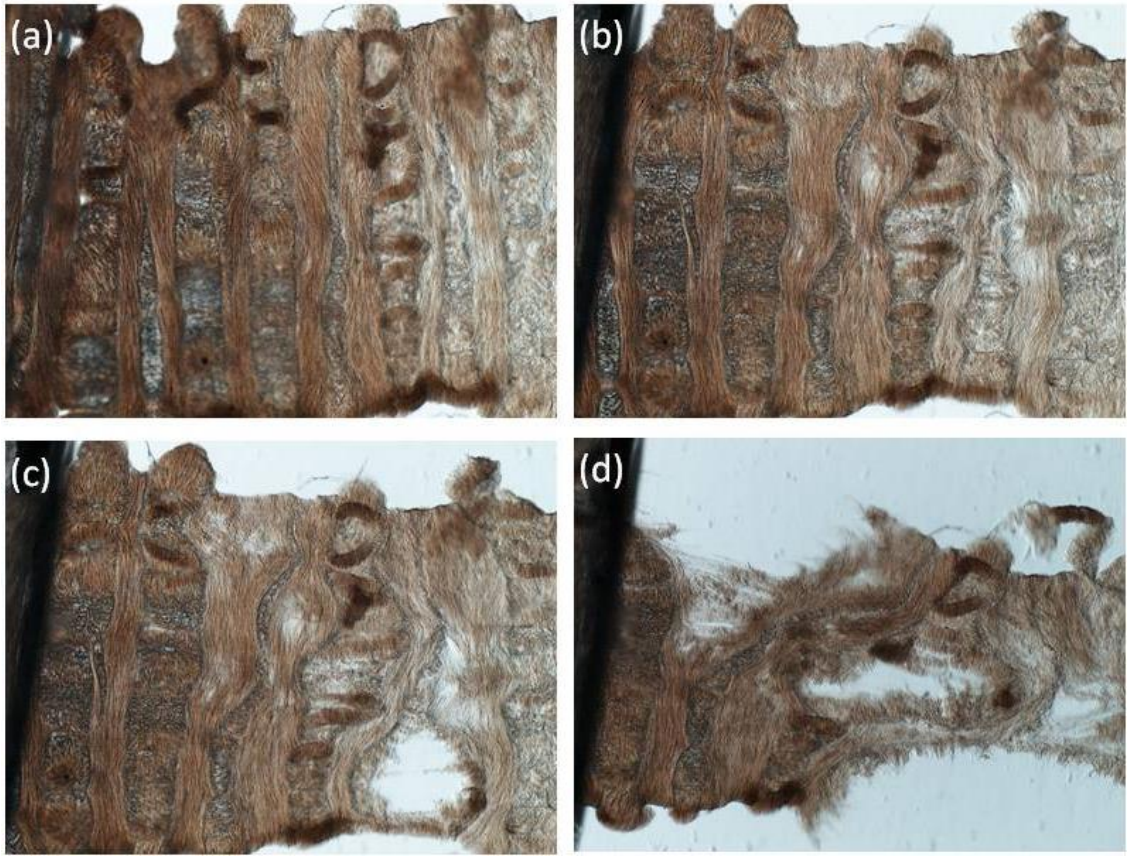

Figure 7.13 – Micrographs for tensile test specimen T3, showing the full field of view of the microscope. (a) specimen T3 unloaded; (b) specimen T3 loaded to extension of 3mm (51% strain); (c) specimen T3 at initial failure point (3.5mm extension); (d) specimen T3 at total failure point.

SERIAL MICROSCOPY RESULTS

The DIC microscopy images highlighted the variation in fibre orientation between lamellae and interlamellar bridges. An example image is presented in Figure 7.14. The full height of the disc is visible and the change in annulus structure between the outer and inner annulus is clearly illustrated.

A series of 16 consecutive micrographs that showed a major interlamellar bridge penetrating through several lamellae of the outer annulus was selected.

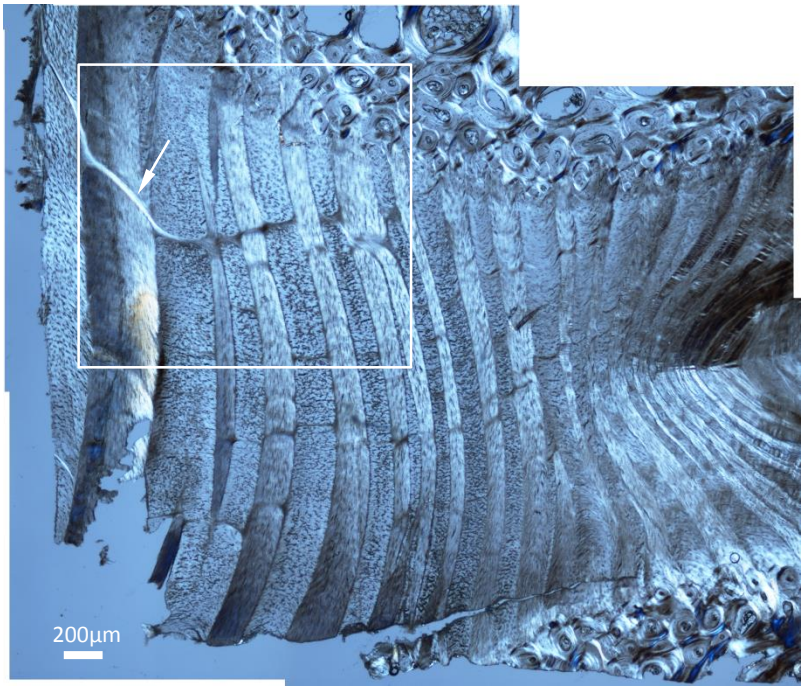

Figure 7.14 – An example micrograph of the series selected for model development. The box indicates the area that was cropped and used in the model. The arrow indicates the major interlamellar bridge that was visible in each of the selected 16 consecutive micrographs.

The change in the bridge geometry, structure and its relationship with the surrounding tissues is illustrated in Figure 7.15. Lamellae can be seen to split and merge with each other, a feature of annulus tissue that was also observed during the MRI and dissection study presented in Chapter 4.

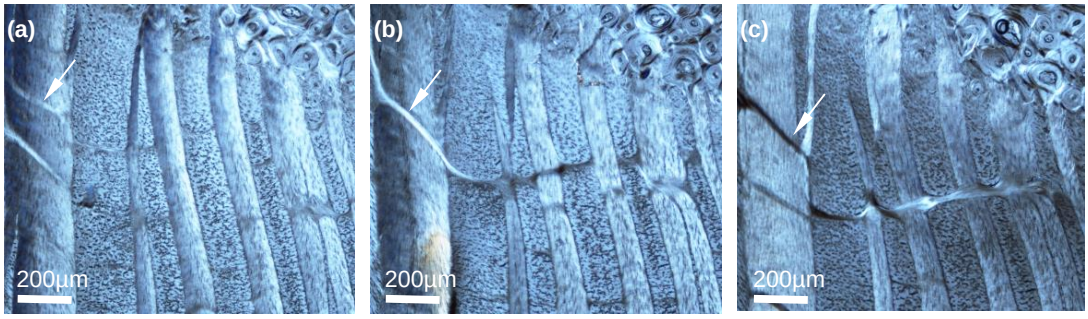

Figure 7.15 – Three of the cropped images used to create the 3D model. (a) The start of the series of images (slice #1, 0µm deep), in which the bridge (indicated by the white arrow) is originating, (b) the middle of the series of images (slice #9, 270µm deep) in which the bridge is fully established and integrated with the lamellae, (c) the last of the series of images (slice #16, 480µm deep) in which the bridge is reduced in thickness.

7.3.2 COMPUTATIONAL RESULTS

TENSILE MICROSCOPY MODEL RESULTS

The coordinates of the nodes along the internal boundaries for the FE model in its deformed state were recorded and compared to the equivalent nodes in the

experimental model. Typical results are presented in Figure 7.16 (bridge model) and Figure 7.17 (sheath model).

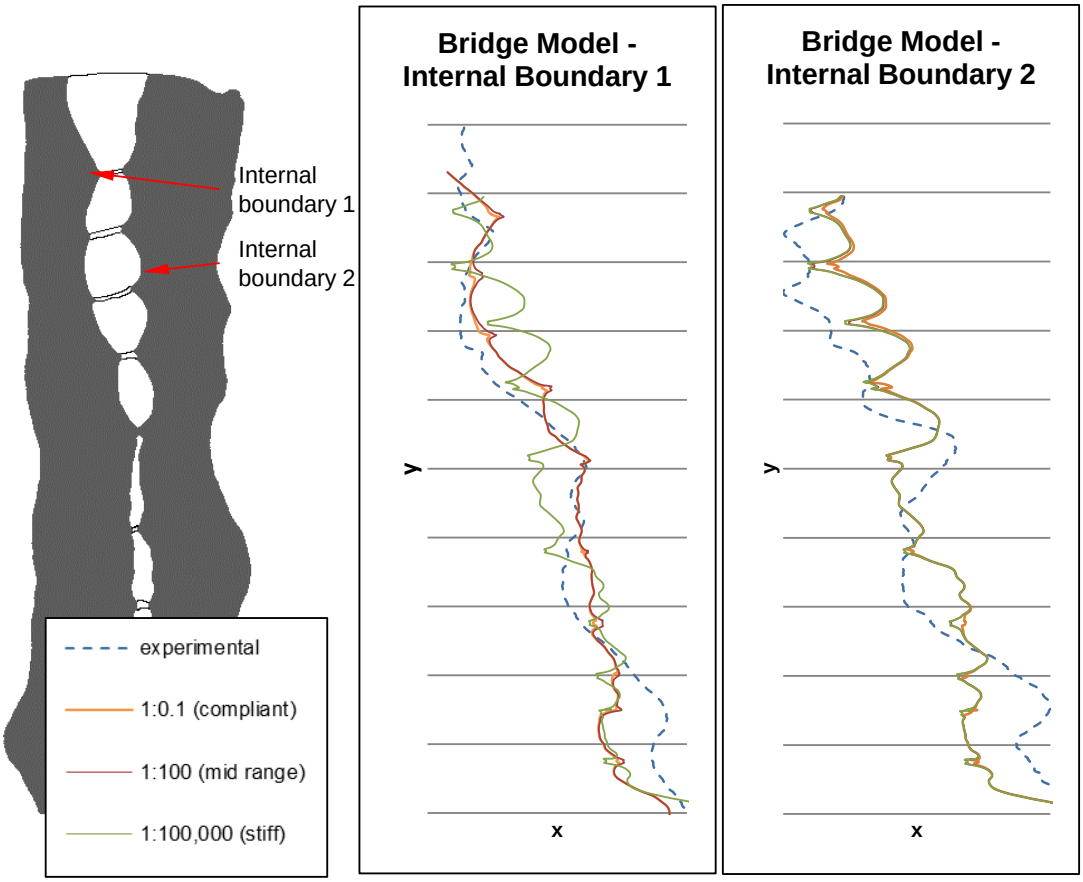

Figure 7.16 - Traces of internal boundaries for the bridge model for variation of bridge modulus relative to the experimental data. The shape of the boundaries changed as the material properties of the bridges were varied.

As the modulus of the bridges was increased, they deformed much less than their surrounding tissues, leading to more pronounced puckering along the internal boundary, as illustrated in Figure 7.16.

The characteristic profile of the internal lamellar boundaries was captured well in many instances, however these were often shifted in the y-direction so did not align with the profile of the experimental model.

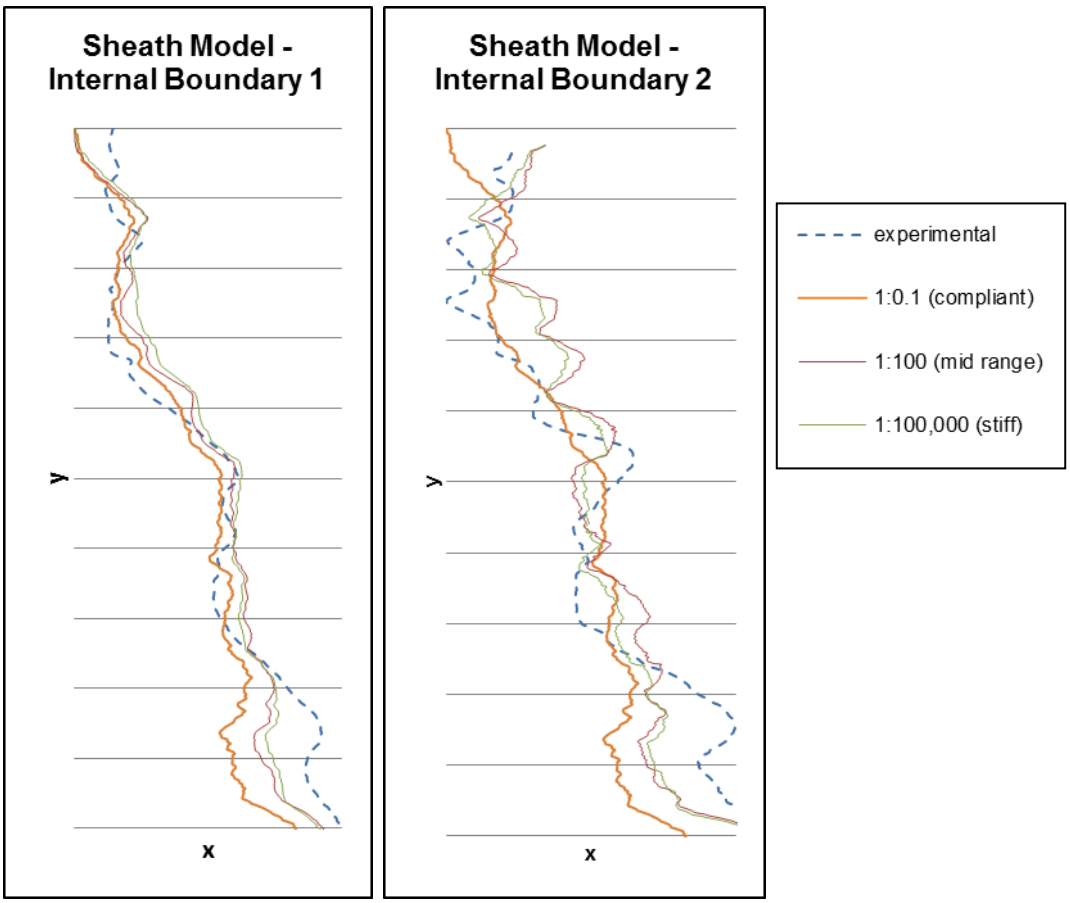

Figure 7.17 - Traces of internal boundaries for the sheath model for variation of sheath modulus relative to the experimental data. The shapes of the boundaries change as the material properties of the sheath are varied.

For the sheath model, the puckering of the internal boundaries was not as pronounced as for the bridge model. The presence of the sheath elements along the entire internal lamellae boundary resulted in a more even distribution of displacement.

The concordance correlation factor (Lawrence and Lin 1989) was calculated for each variant of the models to analyse how well the strained position of internal boundaries in the FE models agreed with those in the strained experimental model. This data is summarised in Figure 7.18.

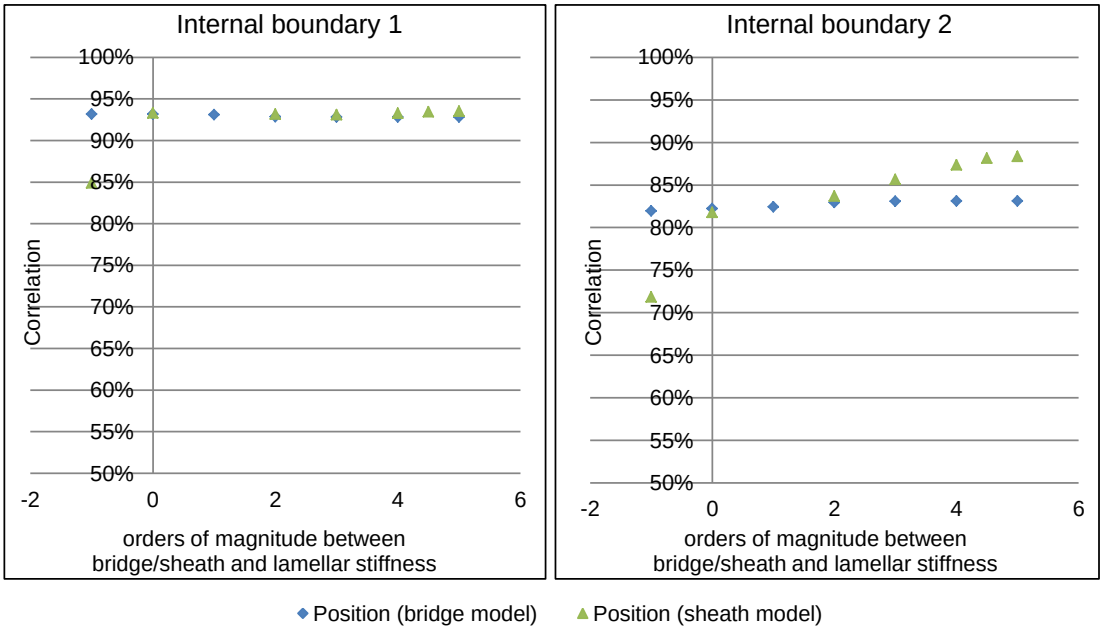

Figure 7.18 – Concordance correlation between FE and experimental results as bridge and sheath modulus varies relative to lamellar modulus. For reference to the data shown in Figure 7.16 and Figure 7.17, value "-1" on the horizontal axis refers to a lamellar/bridge modulus ratio of 1:0.1, value "2" refers to the ratio 1:100 and value "5" refers to ratio 1:100,000.

For the bridge model, there was very little change in the correlation of the FE results with the experimental data for both boundaries. Although a marked change in boundary shape was seen in Figure 7.16, as the bridges are only acting on the internal boundaries in concentrated areas, these become averaged out over the whole length of the boundary when the correlation was considered.

A slight improvement was seen in the correlation between the sheath model and the experimental data as the modulus of the sheath increased. This, however, does not necessarily indicate that the model accuracy increased. The sheath elements are acting along the entire length of the boundary. As their modulus increases, the model becomes stabilised and the boundary in its deformed position becomes smoother. Thus, when averaged, the agreement with the experimental data is improved because the overall shape is closer to the experimental data. This does not necessarily mean that the FE model is improved because it may not necessarily be an improved characterisation of the details observed in the experimental data.

A detail from Figure 7.16 is shown in Figure 7.19, in which a landmark feature – the puckered interlamellar boundary at the point of anchorage of a bridge – is shown for various bridge moduli. The variation in slope of the boundary either side of the bridge is illustrated.

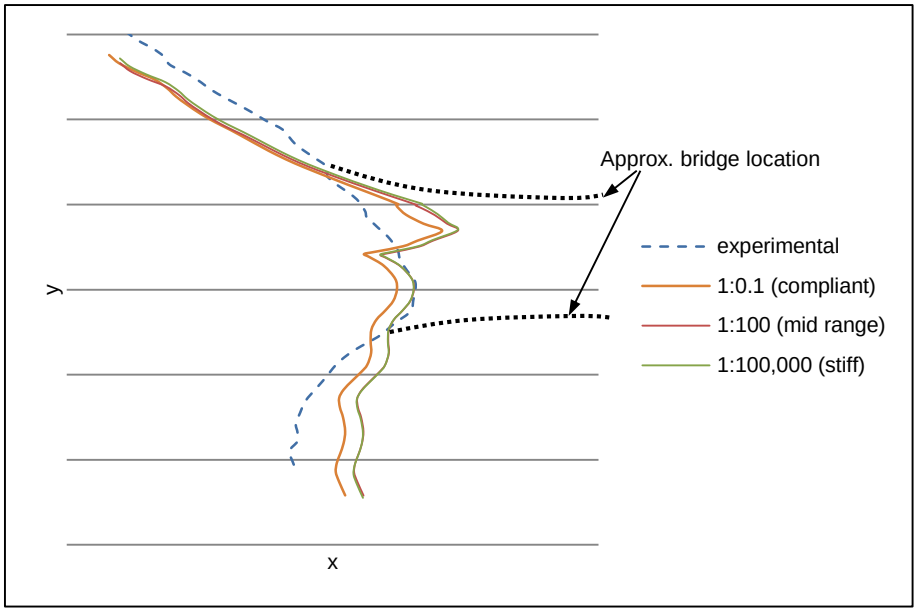

Figure 7.19 - Internal boundary traces for a region of interest with variation in bridge modulus.

Since the measurement of agreement along the whole length did not give a clear indication of which model most closely fitted to the experiment, the accuracy of specific landmarks were assessed based on their error with the equivalent features in the experimental model, as outlined in Section 7.2.2. These errors are summarised in Figure 7.20 to Figure 7.23 below.

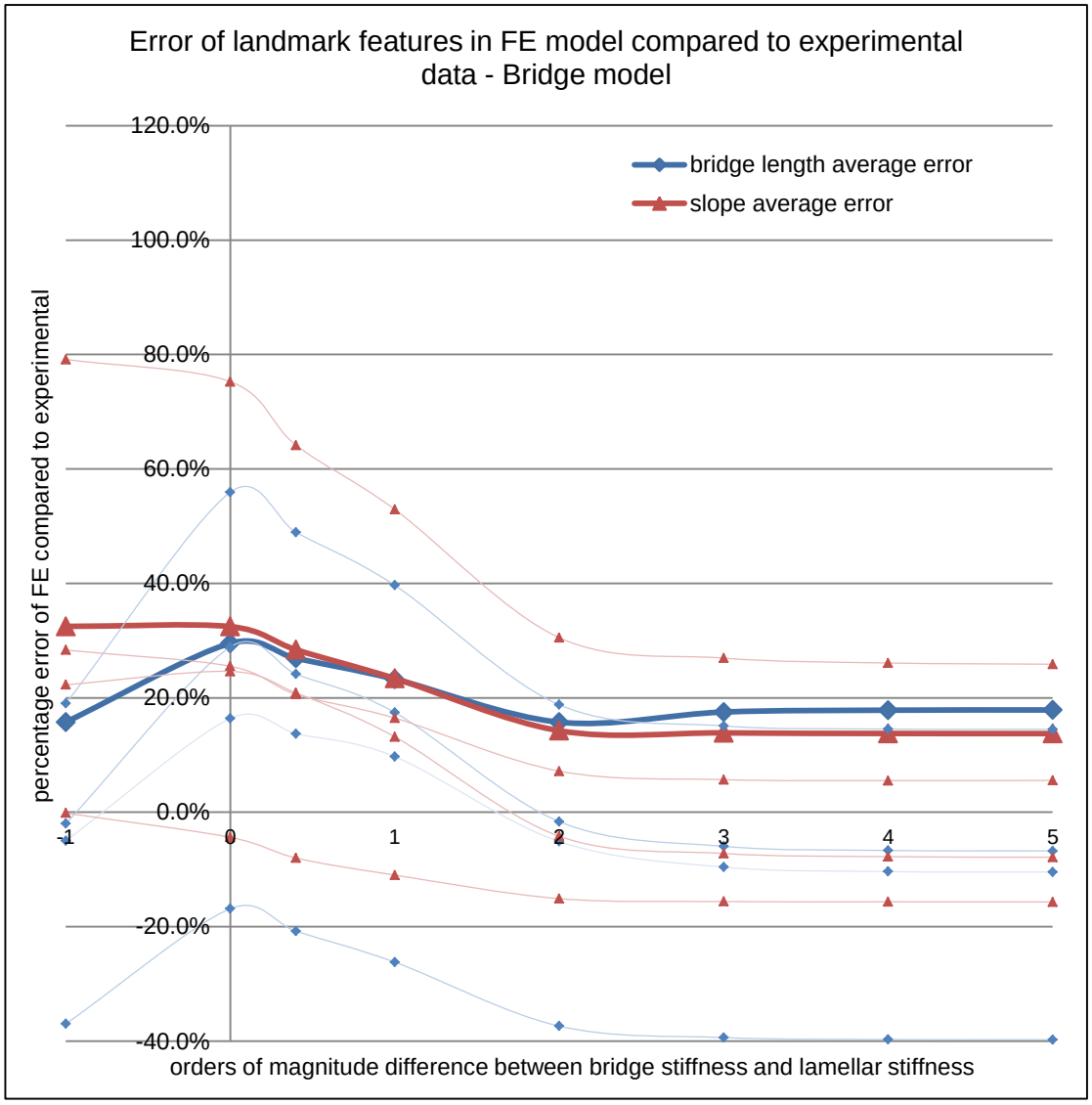

Figure 7.20 - Average errors of landmark features in the bridges model with respect to experimental data. The bold lines show the averages for the bridge length error and the slopes error. The pale lines show the data for the four landmarks for each of these categories. Value "-1" on the horizontal axis refers to a lamellar/bridge modulus ratio of 1:0.1, value "0" refers to the ratio 1:1, this is the equivalent to having no bridges in the model, value "2" refers to the ratio 1:100 and value "5" refers to ratio 1:100,000.

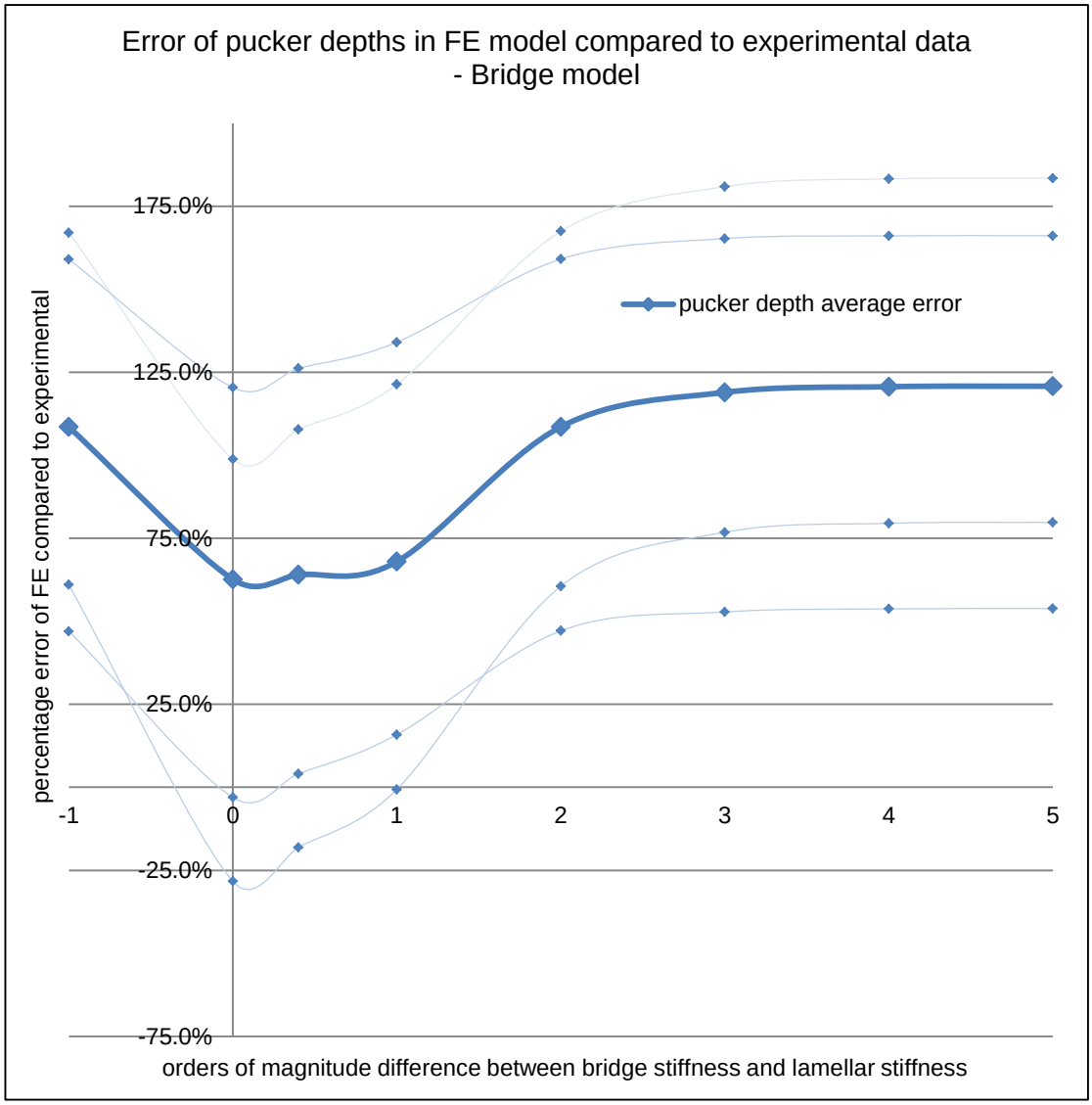

Figure 7.21 – Average error of pucker depths in the bridges model with respect to experimental data. The bold line shows the average error, the pale lines show the data for the four individual puckers. Value "-1" on the horizontal axis refers to a lamellar/bridge modulus ratio of 1:0.1, value "0" refers to the ratio 1:1, this is the equivalent to having no CBs in the model, value "2" refers to the ratio 1:100 and value "5" refers to ratio 1:100,000.

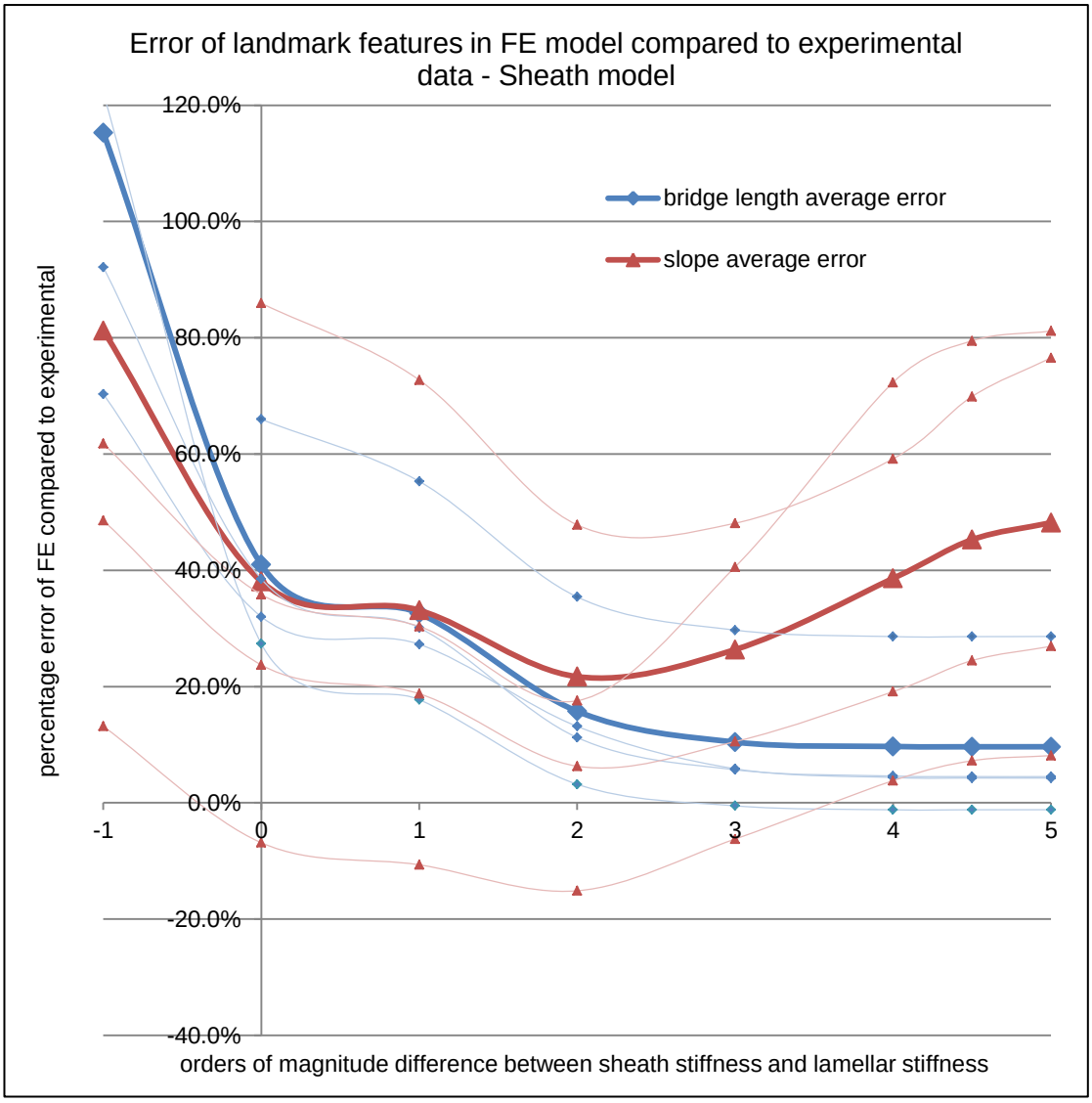

Figure 7.22 - Average errors of landmark features in the sheath model with respect to experimental data. The bold lines show the averages for the bridge length error and the slopes error. The pale lines show the data for the four landmarks for each of these categories. Value "-1" on the horizontal axis refers to a lamellar/bridge modulus ratio of 1:0.1, value "0" refers to the ratio 1:1, this is the equivalent to having no sheaths in the model, value "2" refers to the ratio 1:100 and value "5" refers to ratio 1:100,000.

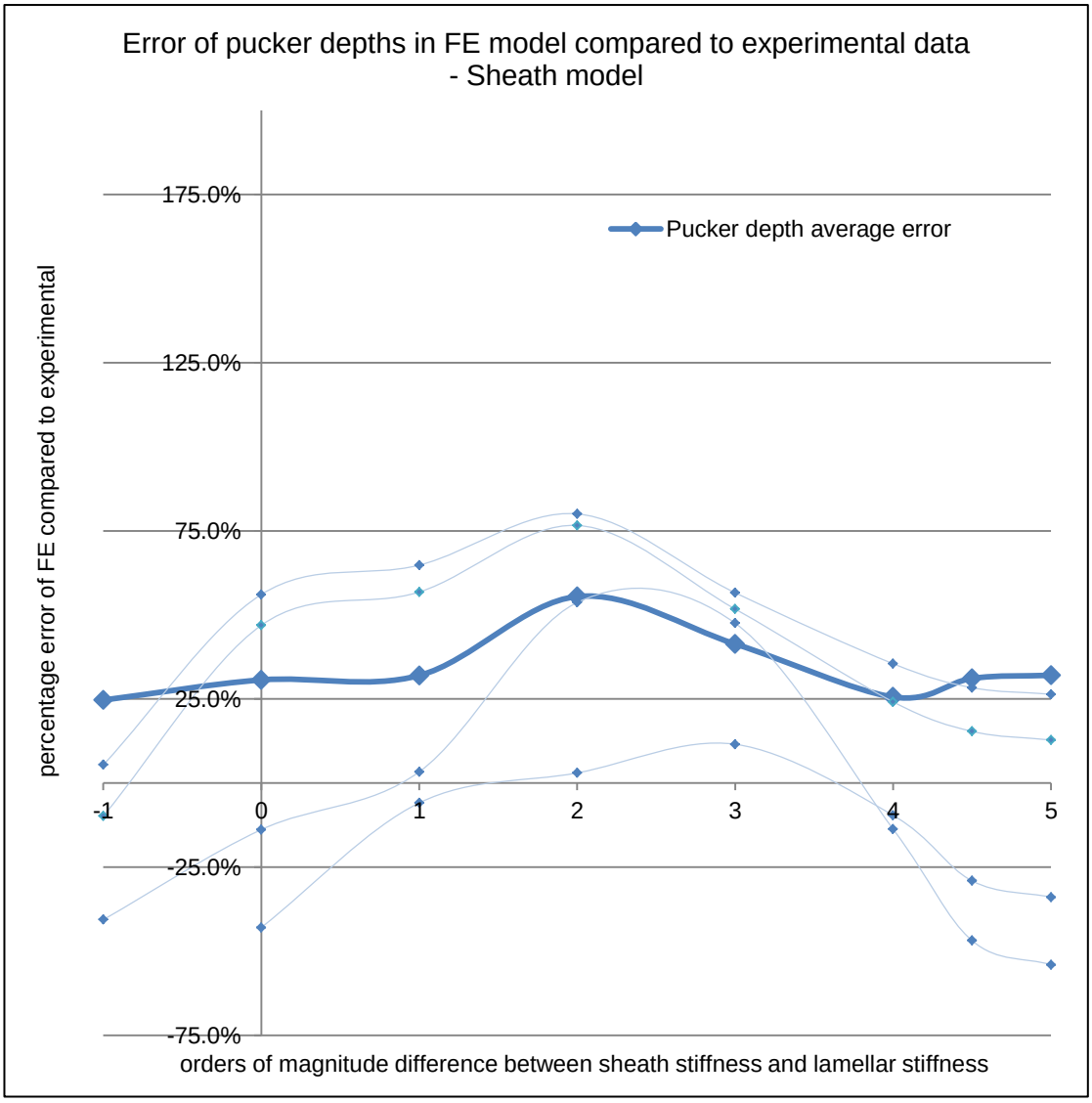

Figure 7.23 - Average error of pucker depths in the sheath model with respect to experimental data. The bold line shows the average error, the pale lines show the data for the four individual puckers. Value "-1" on the horizontal axis refers to a lamellar/bridge modulus ratio of 1:0.1, value "0" refers to the ratio 1:1, this is the equivalent to having no bridges in the model, value "2" refers to the ratio 1:100 and value "5" refers to ratio 1:100,000.

When the difference between the bridge/sheath and lamellar moduli was greater than three orders of magnitude, there was little change to the results, particularly for the bridge model. The bridge/sheath elements are effectively rigid (compared to the lamellar elements) so the strain in these elements is negligible.

Overall, it was determined that the model performance was improved with some representation of interlamellar constituent, be it the bridge model or the sheath model. The bridge model performed best with a bridge modulus two orders of magnitude greater than the modulus of the lamellae in the radial direction. Similarly, the sheath model performance was improved with a sheath (and bridge) modulus two orders of magnitude greater than the modulus of the lamellae in the radial

direction. The material properties that were derived for further use in the serial microscopy study are presented in Table 7.3.

$E_{bridges}$	0.04
$v_{bridges}$	0.4

Table 7.3 – Optimal material properties derived for the bridge elements. These were implemented in the serial microscopy model. Properties are relative and unit-less.

Compared to the model without interlamellar constituents, the average percentage error of the landmark features in the bridge model improved by 11.2% for bridge length and 14.2% for boundary slope. However, this compromised the error in pucker depth which increased.

For the same changes in the sheath model, the percentage error of the landmark features improved by 25.3% for bridge length and 16.4% for boundary slope. Again this compromised the error in pucker depth, however the overall boundary correlation was improved.

SERIAL MICROSCOPY MODEL RESULTS

As observed during the micro-tensile model study, the interlamellar boundaries puckered at the point of insertion of bridges when the model was loaded in radial tension. This is illustrated in the change to displacement plots between the bridge and no-bridge variants of Figure 7.24.

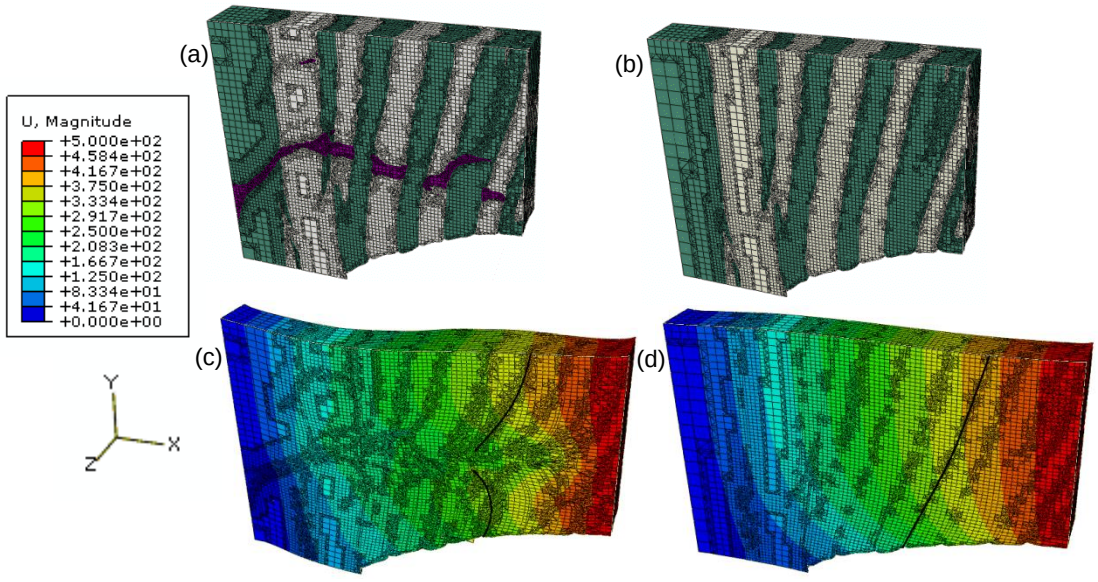

Figure 7.24 – Serial models sectioned through the mid x-y plane showing: (a) interlamellar bridge variation (undeformed); (b) no-bridge variation (undeformed); (c) interlamellar bridge variation,

deformed with displacement magnitude plotted; (d) no-bridge variation, deformed with displacement magnitude plotted. The same interlamellar boundary is highlighted in the two variations (c and d), illustrating the puckering caused by the bridge. Results are relative and unit-less.

The stress distribution also varied between the bridge and no-bridge variants, as illustrated in Figure 7.25 and Figure 7.26. Stress concentrations were observed in the lamellae surrounding the interlamellar bridges. For the no-bridge variation, the stress was evenly distributed throughout the model.

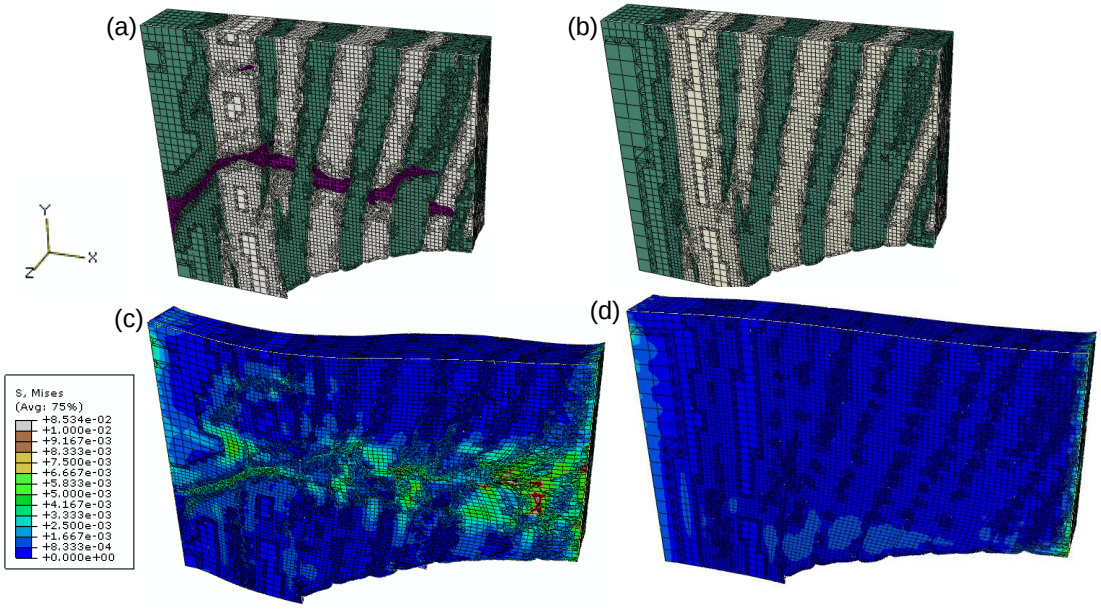

Figure 7.25 – Serial models sectioned through the mid x-y plane showing: (a) interlamellar bridge variation (undeformed); (b)no-bridge variation (undeformed); (c) interlamellar bridge variation, deformed with Von Mises stress distribution plotted; (d) no-bridge variation, deformed with Von Mises stress distribution plotted. Results are relative and unit-less.

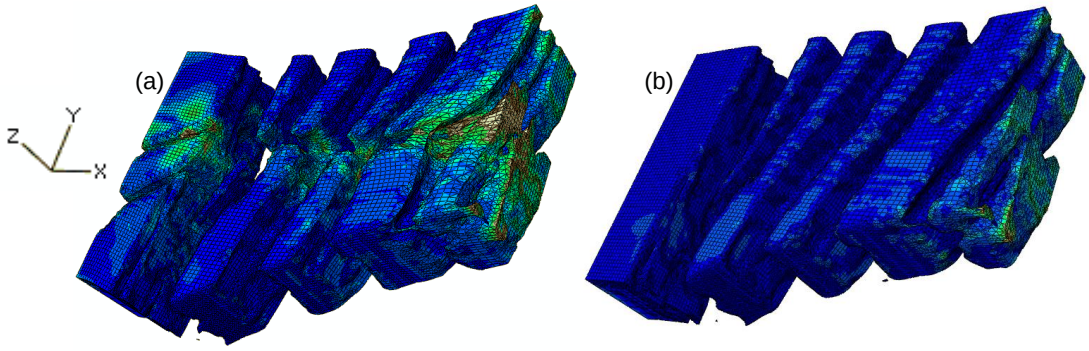

Figure 7.26 – In-plane lamellae isolated from the model for (a) the interlamellar bridge variation and (b) the no-bridge variation of the serial model, plotted for Von Mises stress distribution.

The tensile stiffness of the bridge model was 70% higher than that of the no-bridge model. Without experimental data, it is not possible to conclude which model more closely represents the *in vitro* tissue stiffness.

7.4 DISCUSSION

This study investigated the potential for creating FE models of the annulus structure based on qualitative image data. The development of the methodologies built upon existing histological and computational techniques with the aim of combining two previously isolated approaches of understanding the mechanical behaviour of the annulus.

Previous studies have used histological data to develop generalised FE simulations of annulus tissue deformation (Elliott and Setton 2001; Gregory *et al.* 2010). However this study was novel in its use of specimen specific geometric tissue data. This gives the technique more potential for calibration and validation with histological experimental data.

7.4.1 EXPERIMENTAL METHODS

The histological methods used during this study have been extensively applied during previous investigation of the microstructure of the annulus (Schollum *et al.* 2008, 2009; Pezowicz *et al.* 2005, 2006). The histological analyses conducted were here undertaken with the intention to use the data in computational simulations. Only the minimum number of experimental tests needed to satisfy the requirements of the computational studies were conducted because of the labour intensive methods.

The fragile nature of the tissue samples made them vulnerable to damage during experimental work. The slices may have suffered damage during their preparation that altered the structural integrity of the samples, ultimately resulting in misrepresentation of the specimen in the model. For example, fibres may have snagged during sectioning, which could lead to local weak spots that were not accounted for in the model. Such flaws may not have been evident during microscopy analysis until the tissue was strained. Testing a statistically significantly number of specimens would reduce this problem.

Future studies using this approach could modify the methods to make them more suitable for use in computational simulations. In particular it would be useful to obtain loading data for the micro-tensile test. This could facilitate more in depth validation of the simulations.

7.4.2 MICROSTRUCTURAL BEHAVIOUR

The micro-tensile histological study used similar methods to those employed by Pezowicz *et al.* (2006). Some similarity in the observations was also recorded. In both studies, micrographs showed the cross bridges pulled taut in comparison to the surrounding tissue constituents. This caused the interlamellar boundary to pucker, as illustrated in the detail from specimen T3 presented in Figure 7.27.

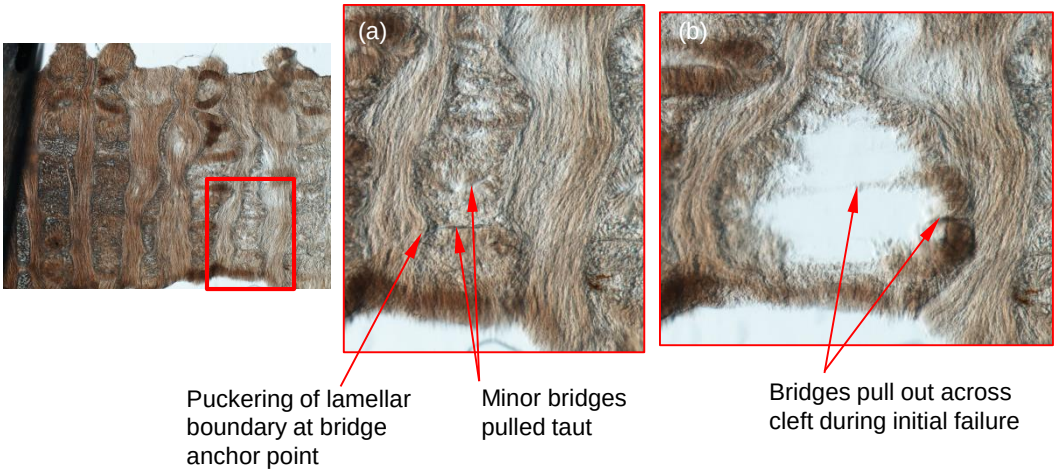

Figure 7.27 – Images from test T3. Detail (a) shows minor bridges pulled taut during applied tension causing the lamellar boundary to pucker. Detail (b) shows the same area of tissue at initial failure stage where the same minor bridges are shown pulled out from the tissue.

The greater resistance of the bridges to applied strain implies that the material properties of the bridges differ to those of the surrounding tissues, in the direction of the applied strain.

Also observed by Pezowicz *et al.* (2006) was the cleft formation in the in-plane lamella, adjacent to the anchor point of a cross bridge, illustrated in Figure 7.28. Pezowicz *et al.* suggested that this occurred because the bridge was strongly anchored towards the edge of the in-plane lamella. The centre of the lamella had weaker inter-fibre cohesion and therefore was more prone to cleft formation.

Figure 7.28 – Detail of test T3 in the loaded state. The lamellar tissue is seen thinning and fibres are pulled apart within the lamella's fibre bundle adjacent to the anchor point of the minor bridge. This is the initiation of cleft formation.

This hypothesis is supported by the mechanisms of failure seen in the micro-tensile experimental tests, in which the specimens were more likely to fail within lamellae rather than at the interlamellar boundaries. However, unlike Pezowicz *et al.*'s observations (2006b), cleft formation was more common in sectioned than in-plane lamellae for this study.

During the serial microscopy study, examination of consecutive annulus tissue slices revealed the integration of the major and minor interlamellar bridges with the surrounding tissue structure. The size and scale of the major bridge and its complex 3D structure that split and merged with other, smaller bridges agreed with the observations presented in Schollum *et al.*'s more thorough structural investigations (2008; 2009).

7.4.3 COMPUTATIONAL ANALYSIS

The micro-tensile computational study allowed the characteristic deformations of the tissue observed during the experimental study to be captured in a simulation that facilitated detailed analysis of the potential tissue mechanics.

The techniques for determining the displacement of the tissue observed in the experimental study and applying it to the FE model allowed inhomogeneous displacements to be accurately recreated in the computational simulation. This makes this method robust and versatile for application in further studies.

The level of error between the landmark features in the FE results and the experimental results was generally high. In particular the results for the puckers varied widely. However, a trend did emerge from the results for bridge lengths and boundary slopes. When combined with the observations of internal boundary shape correlation with experimental results, it was possible to make an estimate of the likely ratio of the bridge (or sheath) modulus to that of the lamellae.

The characteristic profile of the internal lamellar boundaries was captured well in many instances, however these were often shifted in the y-direction so did not align with the profile of the experimental model. This agreement may have improved from the inclusion of shear deformation in the models. It is likely that shear stressed would have occurred during the experimental deformation of the tissue.

Both the bridge and sheath variants of the micro-tensile model performed closest to the experimental data when the bridge or sheath modulus was two orders of

magnitude greater than the lamellar modulus (lamellar/bridge modulus ratio of 1:100). This large relative difference in properties of two adjacent tissue constituents agreed with the experimental observations of this study and those of Pezowicz *et al.* (2006).

This was also in agreement with results obtained in the previously presented computational study of a generic sample of annulus tissue strained in tension (Section 3.4.4). In the development of the "interface elements" (acting to maintain interlamellar cohesion, similar to the sheaths implemented in this study) in the generic annulus study, the model performance was closest to experimental data when the interlamellar material had a modulus two orders of magnitude greater than that of the lamellae in the radial direction.

From this study alone, it was difficult to quantify the difference in performance of the sheath and bridge variants of the micro-tensile model. Often for a single test of a model, some features would have good agreement with the experimental data, whilst other features had poor agreement. For example, the error of the bridge length was better for the bridge model than the sheath model, however the error of the pucker depth was better for the sheath model than the bridge model. These inconsistencies could have arisen as a result of errors and inaccuracies during the experimental and computational processes.

The methods presented in the serial microscopy computational study illustrate a novel approach to assessing the geometry and structure of the annulus tissue constituents. Using the image processing software, and a method similar to that used to create specimen specific models of the whole disc in Chapter 5, a specimen specific model of the tissue structure was generated. Extensive studies by Schollum *et al.* (2008, 2009) have developed three dimensional illustrative models of the tissue structure through histological studies, however this is the first study to use this approach to generate a computational simulation to evaluate the mechanics of the tissue.

The 3D specimen specific tissue model was useful for deducing the geometry and structure of the tissue. The model was used to assess potential mechanisms of deformation during loading, including possible roles played by the individual tissue constituents.

Analysis of the stress field through the model when loaded offers insight into potential roles played by the bridging structures in the tissue mechanics. The

bridges appeared to increase the resistance of the tissue to radial tension and experienced higher stresses than the lamellae, albeit under displacement control conditions.

High stresses were also observed in the lamellae surrounding the bridges which were not present in the no-bridge variation. The tied connections between the bridge and lamellar elements in the model caused increased deformation in the lamellar elements closest to the bridges. Had the interfaces between the bridges and lamellae been modelled as a moveable contact, the bridges would instead have acted to shield the lamellae from stress.

Tied connections were used because histological studies have suggested a high degree of integration of bridge fibres into those of the surrounding lamellae (Pezowicz *et al.* 2006). However tied connections represent an extreme case in which no relative movement between the two tissues is permitted. An interaction that permits some shear movement at the interface may be more realistic. An interesting extension to this study would be an investigation into the effects varying this surface interaction on the mechanics of the tissue.

Additionally, the material properties for the major bridging elements were based on those developed for interlamellar interfaces in previous computational analyses (Chapter 3). As discussed in the literature, the tissue composition of the major bridges differs from the surrounding tissues and interlamellar constituents, therefore a material model developed specifically for the major bridges would be more appropriate. Thus, from the outcomes of this study alone, it is not possible to conclude how bridging structures affect the stress in the tissue *in vivo*.

The serial microscopy method required the tissue to be chemically fixed and sliced to obtain micrographs. This limited the use of this method in mechanical analysis, as it was not possible to obtain specimen specific data of the same tissue sample under load and so validation of the model with experimental data was not possible.

However, it is useful to compare the deformation of the tissue with that observed in the micro-tensile study. The interlamellar boundary puckered and the bridges were pulled taut during applied tensile strain, as observed in the micro-tensile study and in Pezowicz *et al.*'s fixed-whilst-stretched tests (2006).

For both the micro-tensile and serial microscopy studies, isotropic material properties were assigned to the bridge and sheath materials. Although the exact

composition of these tissue components is still unknown, histological studies (Pezowicz *et al.* 2005, 2006; Schollum *et al.* 2009; Yu *et al.* 2007), have shown that they are fibrous in nature. Thus, directionally dependent material properties may be more appropriate and could facilitate the simulation of the constituent's varying strengths with and against the fibre direction.

The material properties developed were relative between the tissue constituents. They are only applicable to the environment and loading conditions of the experimental tests from which the micrographs were taken. The properties cannot be applied directly to simulations involving annulus tissue at a different scale or in a different loading scenario. The tests were a simulation of an experiment *in vitro,* and so the study's findings may not be representative of the tissue behaviour and performance *in vivo*, under physiological loading.

To fully validate the methods and draw general conclusions applicable to multiple specimens, it would be necessary to repeat these studies with a larger sample size. If this methodology were to be repeated using a wider range of loading regimes (e.g. straining the tissue in the tangential or axial direction), further information about the material properties of the constituents could be obtained.

User variability was probably a significant source of error in this study. The accuracy of the model construction techniques hinged upon the definition of tissue boundaries. These errors could be reduced if histological techniques could be tuned to achieve micrographs with greater contrast between tissue constituents. Thresholding techniques could then be used during segmentation of the tissue components.

7.4.4 CONCLUSIONS

The novel methodologies developed during this study have illustrated how histological and computational methods can be used in conjunction to improve our understanding of tissue level mechanics. The techniques developed have been successfully applied to the investigation of the relative material properties of tissue constituents. With supporting evidence from experimental and published data this study could provide the foundation for detailed characterisation of tissue constituent behaviour and properties in future work.

From the micro-tensile computational analysis, it was concluded that the performance of the sheath model better characterised deformation of the tissue.

This supports the hypothesis presented in several studies in the literature that the minor interlamellar bridges are part of a wider network of tissue constituents that penetrate between and around fibre bundles (Pezowicz *et al.* 2006, Yu *et al.* 2007).

The micro-tensile models performed with the best experimental data agreement when the modulus of the bridges/sheaths was two orders of magnitude greater than that of the lamellae, implying that they may provide reinforcement to the tissue during radial tension. An increase in tensile stiffness in the radial direction was recorded for the 3D bridge model compared to the no-bridge model.

Evidence has been presented from which the mechanical role of major interlamellar bridges can be postulated. The reinforcement and stiffening of the tissue in the radial direction by the interlamellar bridges could help prevent delamination; however this appears to be at the cost of areas of high stress. It is possible that the major bridges are a product of the vascularisation of the disc as suggested by Smith and Elliott (2011), either as a remainder of the vascular system, or by forming along the pathways left by blood vessels. Despite this, they could still assist in maintaining interlamellar cohesion and increasing the tensile stiffness of the tissue.

8 DISCUSSION

The intervertebral disc is a unique and complex joint. Relatively little is understood about the mechanics of the tissues at a sub-disc scale. To evaluate and develop new disc treatments, an improved understanding of disc biomechanics and the effects of intervention techniques on the function of the tissues is required.

FE techniques provide a tool for investigating the roles of internal soft tissue structures and understanding the mechanical environment of the disc.

The aim of this project was to investigate methods of deriving structural information about the tissues of the intervertebral disc for application in computational simulation, with particular focus on the mechanical function of the annulus fibrosis and how the behaviour of this tissue is governed by its substructures

8.1 OBJECTIVES REVIEW

8.1.1 SENSITIVITY ANALYSIS

Sensitivity analyses were used to establish an indication of the structural parameters that were most significant when developing models of the disc system. Although simplistic, with many assumptions made regarding geometry, loading and properties, the generalised models have proved to be a valuable tool in identifying trends in disc mechanics.

The disc system was most sensitive to changes in the size and position of the nucleus within the disc. The method of representing the interlamellar interactions was also shown to have an effect on the gross mechanics of the disc as well as the tissue level behaviour. As such, these features were investigated in further detail.

8.1.2 NON-DESTRUCTIVE IMAGING OF THE DISC

MR imaging techniques were examined for their potential use in the development of FE models. These techniques were identified as a method of capturing specimen specific geometries of discs in an intact and loaded condition and were analysed for

their capability to capture the soft tissue structures of interest: the nucleus geometry and the lamellar structure.

MR sequences were developed to produce high resolution images that captured the structure of the annulus soft tissues for the first time in three dimensions. Discs were imaged in their intact and loaded state, providing specimen specific data of the tissue mechanics *in vitro*. The image data was validated using a range of MR and dissection techniques with positive results.

Validation procedures confirmed that individual lamellae were visible in the images. Comparison of images of the disc in the prior-to-loading and loaded state illustrated the change in lamellar geometry experienced by the tissue during compression. However, due to the nature of MRI methods, it was not possible to identify the same lamellae between the loading states. This method was not suitable for tracking the relative interlamellar deformation and movement, illustrating the need to develop simulations to investigate these effects.

Defining the annulus/nucleus boundary based on the MRI data was not as successful. There was a lack of correlation between the nucleus geometry captured in the MR images and the observations made during dissection. With further development of MR sequences, it may be possible to improve this; however the difficulty of defining these geometries through imaging techniques is indicative of the natural lack of definition between the two tissues.

8.1.3 SPECIMEN SPECIFIC MODELS OF THE DISC

A novel method for converting the MR image data into specimen specific FE simulations was developed. The resultant models illustrated the wide variation in disc geometries and biomechanics between experimental specimens. Identical methods were used in the dissection, preparation and compression of all three of the specimens modelled, yet the deformations recorded varied widely.

The nucleus geometries were assigned based on dissection data because of the disappointing results from the MRI study for this feature. Thus the geometry of the nucleus was accurate to the experimental specimen in only the mid-axial plane.

The creation of specimen specific models facilitated a direct link between the computational and experimental models, previously lacking from computational studies of the disc and essential for the progression of simulation calibration and

validation. The levels of validation recorded between the models and the experimental data varied between specimens and throughout the sensitivity analyses. This illustrates the need for further development to these models before they are deemed reliable representations of the *in vitro* mechanics of the disc. In particular, the material models used for the tissues require further development.

8.1.4 MODELLING SURGICAL INTERVENTIONS

The nucleus replacement study provided a simple illustration of how computational simulations of the disc may be used as investigative tools for clinical applications. The results of this study illustrated the importance of an incompressible nucleus to the healthy function of the disc. The models were much more sensitive to changes to the Poisson's ratio than changes to the elastic modulus of the nucleus, suggesting that it is more important for nucleus replacement materials to replicate the incompressibility of the healthy nucleus than to replicate the elastic modulus.

8.1.5 MICROSCOPY BASED SIMULATIONS

The annulus tissue mechanics were investigated in further detail during the microscopy based simulation study. Interlamellar constituents, such as collagen bridges, have been identified in many histological studies, yet their mechanical role in the disc is still unknown. Modelling the annulus tissue on a smaller scale, isolated from the disc environment facilitated the investigation of constituent properties in increased detail.

To create specimen specific models of annulus tissue samples, methods similar to those employed to develop MRI based models were employed; segmentation techniques were used to define model components based on image data and stacks of images were used to construct three dimensional models. The resultant models served as useful investigative tools, but were of limited use because of the lack of loading data acquired during the experimental stage of the study.

The results of the study suggested that interlamellar interactions provide a strong bond between lamellae, in agreement with Michalek *et al.*'s (2009) "skewing" theory of annulus deformation and the results presented in the generalised model study. The major bridging elements were shown to assist in maintaining interlamellar cohesion but also created stress variations through the tissue that may ultimately be detrimental to the tissue health.

However, the derivation of these material properties was based on improving the mechanics of the disc models on a gross scale. Thus it is not appropriate to assume that the material properties derived are indicative of those of natural annulus tissue at the lamellar scale. Further experimental loading tests on tissue micro-mechanics would be recommended to improve characterisation of the tissue at this scale.

8.2 GENERALISED AND SPECIFIC MODELLING TECHNIQUES

Many of the sensitivity tests conducted using the generalised model were repeated for the specimen specific models. Similar trends were reported for the effects on gross disc mechanics for variation in the method of representing the interlamellar interaction.

This nucleus replacement study illustrated the application of both generalised and specimen specific models. The specimen specific model facilitated the effects of changes to the disc system for an individual to be analysed. If these techniques were developed further to create simulations of discs *in vivo*, there could be potential benefits for the development of patient specific medicine, using similar models to assess the most suitable treatment for an individual.

The generalised models did not account for population variation; however they were more suited to the identification of trends during the parametric analyses and were extremely useful for answering specific questions about disc system mechanics.

The wide range of parameters to consider in the natural disc system makes a truly complete specimen specific model extremely difficult to achieve. It is not possible to obtain experimental data for all of the parameters of a given specimen. However such models are useful for investigating the variation between specimens. Specimen specific models can also be useful for validating the performance of generalised simulations. Generalised models are valuable tools for identifying trends and for answering certain questions about the system mechanics. Both specimen-specific and generic models are likely to continue to have a role in the structural simulation of the disc.

8.3 MODELLING SCALES

Implementing the findings of a tissue sample model into a comprehensive model of the disc system presents the challenge of relating the mechanical behaviour of the tissue between the two scales. The boundary conditions and loading scenarios of the specimen and disc models were vastly different, thus the assumption that the tissue constituents would exhibit the same behaviour in both scenarios may not be valid.

To individually represent every lamella and all interlamellar interactions in a full scale disc model would require large amounts of computational power and time. As an alternative approach, these features were represented in bulk in the disc models. This approach still yielded useful results that were representative of the lamellar mechanics, however the additional assumptions required to implement this technique should be considered when interpreting results.

The microscopy models were loaded in radial tension during which, the major bridging structures were aligned with the direction of the tensile strain. Radial strain was shown to become significant when investigating the mechanics of the disc with a compressible nucleus, in Chapter 6. This suggests that the role of interlamellar interactions and bridging structures become more significant to the mechanics of the annulus following the onset of degeneration, during which the nucleus often dries and becomes more compressible.

8.4 SUMMARY

A generalised model of the disc was developed based on published *in vitro* data. This model was useful in the investigation of how sensitive the disc system was to changes in the structure of the soft tissues. The position and size of the nucleus and the method of representing the annulus lamellar structure were highlighted as significant influential factors to gross disc mechanics. The parametric sensitivity study of the specimen specific models again illustrated how the method of representing the annulus structure can affect the gross mechanical behaviour of the disc.

A novel method was developed for imaging the disc in an intact and loaded state using MRI techniques. The resultant images illustrated the structures of the disc in high resolution and three dimensions.

Novel methods were used to construct specimen specific models of the disc based on this image data. These models and the accompanying image data of the disc under load facilitated one to one validation of the models. These methods will form the foundations for future work on the development of specimen specific models.

The structure and mechanics of the annulus were investigated on a smaller scale and a novel method was developed for constructing specimen specific models based on microscopy data. These models were used to develop a mechanism for the soft tissue deformation in which lamellar cohesion was maintained by interlamellar interactions and structures.

In summary, the study has successfully contributed to the progression of computational simulations of the disc by utilising soft tissue image data. The previous understanding of the mechanical function of interlamellar constituents has been built upon and probed using computational analysis and the stage is now set for continued development in this field of study.

8.5 FUTURE WORK

The methods of model construction developed throughout this study could provide a foundation from which future studies may evolve. The study has highlighted the challenges that are faced and considerations that should be made when modelling the disc. This foundation of research is now primed for developments in this field.

The specimen specific method for modelling the disc would benefit greatly from the inclusion of loading data if this could be acquired during imaging of the specimens. O'Connell *et al.* (2007) presented a method for remotely loading disc specimens in an MR scanner. These methods could be combined with the MR sequences developed in this study to achieve three dimensional images of the discs in compression as well as loading data.

Further investigation and development of the MR sequences could yield improved representation of the nucleus geometry. This would be of particular benefit to the

improvement of specimen specific models, as the results of the generalised model tests showed the models were sensitive to nucleus size and position.

All the studies presented in this thesis did not include fluid flow or time-dependence of the tissues since the focus was on the instantaneous structural behaviour. Future studies could combine these findings with the biphasic models developed by Shirazi-Adl *et al.* (1989, 1992, 1996) and others. Such a modelling strategy could be especially fruitful if MR imaging could be used as a validation tool.

Further validation research may allow a relationship between MRI greyscale and disc hydration to be determined. This could be beneficial in the development of specimen specific material properties for the disc soft tissues and may assist in determining the relationship between disc hydration and mechanics.

Using the MR techniques presented in this study, there is potential to include an increased level of structural detail to the annulus tissue representation in the specimen specific models. This would facilitate analysis into the effects of representing the lamellar structure of the annulus in bulk as opposed to representing individual lamellae in the model. An automatic method of generating annulus tissue structures (e.g. lamellar shapes geometries) based on the MRI data would be useful for this.

The models presented in this study focused on developing structural details of the disc tissues, the material models used to represent the properties of the tissues were highly simplified. The methods of developing geometric and structural details could now be combined with more sophisticated material models that could capture more of the characteristics of disc mechanics, such as non-linearity and biphasic material properties.

The methods for constructing specimen specific models of tissue samples presented in Chapter 7 took a novel approach of utilising qualitative microscopy data. As such, there are many improvements that could be made to the methods to improve their robustness, validation and usefulness. Loading data acquired during the experimental tensile tests would improve the usefulness and validation of the two dimensional tissue model. Improving the imaging techniques to establish reliable markers between serial images would improve the accuracy of the three dimensional models. Both modelling techniques would benefit from increased contrast distinction between the in-plane and sectioned lamellae in the microscopy data so that manual segmentation could be reduced.

Further investigation is recommended in to the interaction between the bridging structures and surrounding lamellae. As with the MRI-based models, experimental loading data would be very useful in validating these models.

8.6 CONCLUSIONS

The importance of nucleus size, location and incompressibility in the replication of natural, healthy disc mechanics has been illustrated. These parameters should be carefully considered during simulation of the disc system and in the development of intervention techniques.

The interlamellar interactions have been shown to affect the gross mechanical function of the disc and have been shown to provide a strong bond between lamellae.

Bridging elements in the annulus have been shown to assist in maintaining interlamellar cohesion in the radial direction. However, it has been suggested that they may also cause areas of high stress in the tissue.

During this study, novel methods have been developed to utilise magnetic resonance and microscopy image data to construct specimen specific models of the whole disc at a macro scale and annulus tissue samples at a micro scale.

The parameters and variables involved in the mechanical system of the disc pose major challenges for experimental investigation. This study has successfully laid the ground work to negotiate these challenges using a computational approach.

9 REFERENCES

Adams, M., Bogduk, N., Burton, K., & Dolan, P. (2002). *The Biomechanics of Back Pain*: Churchill Livingstone.

Adams, M. A., & Dolan, P. (1995). Recent Advances in Lumbar Spinal Mechanics and Their Clinical-Significance. *Clinical Biomechanics, 10*(1), 3-19.

Adams, M. A., & Green, T. P. (1993). Tensile properties of the annulus fibrosus. I. The contribution of fibre-matrix interactions to tensile stiffness and strength. *Eur Spine J, 2*(4), 203-208.

Anderson, A. E., Ellis, B. J., & Weiss, J. A. (2007). Verification, validation and sensitivity studies in computational biomechanics. *Computer methods in biomechanics and biomedical engineering*, *10*(3), 171-184.

Argoubi, M., & ShiraziAdl, A. (1996). Poroelastic creep response analysis of a lumbar motion segment in compression. *Journal of Biomechanics, 29*(10), 1331-1339.

Ayotte, D. C., Ito, K., & Tepic, S. (2001). Direction-dependent resistance to flow in the endplate of the intervertebral disc: an ex vivo study. *Journal of Orthopaedic Research, 19*(6), 1073-1077.

Baker, B. M., Nerurkar, N. L., Burdick, J. A., Elliott, D. M., & Mauck, R. L. (2009). Fabrication and Modeling of Dynamic Multipolymer Nanofibrous Scaffolds. *Journal of Biomechanical Engineering-Transactions of the Asme, 131*(10), -.

Bass, E. C., Ashford, F. A., Segal, M. R., & Lotz, J. C. (2004). Biaxial testing of human annulus fibrosus and its implications for a constitutive formulation. *Annals of Biomedical Engineering, 32*(9), 1231-1242.

Belytschko, T., Kulak, R. F., Schultz, A. B., & Galante, J. O. (1974). Finite element stress analysis of an intervertebral disc. *Journal of Biomechanics, 7*(3), 277-285.

Beckstein, J. C., Sen, S., Schaer, T. P., Vresilovic, E. J., & Elliott, D. M. (2008). Comparison of animal discs used in disc research to human lumbar disc. *Spine, 33*(6), E166-E173.

Beekley Medical, *MRI OrthoSpots,* 2012, www.beekley.com, cited November 2012.

Brinckmann, P., Frobin, W., Hierholzer, E., & Horst, M. (1983). Deformation of the Vertebral Endplate under Axial Loading of the Spine. *Spine, 8*(8), 851-856.

Broberg, K. B. (1983). On the Mechanical-Behavior of Intervertebral Disks. *Spine, 8*(2), 151-165.

Broom, N. D. (1984). Further Insights into the Structural Principles Governing the Function of Articular-Cartilage. *Journal of Anatomy, 139*(Sep), 275-294.

Broom, N. D. (1986). The Collagenous Architecture of Articular-Cartilage - a Synthesis of Ultrastructure and Mechanical Function. *Journal of Rheumatology, 13*(1), 142-152.

Brown, T., Hansen, R. J., & Yorra, A. J. (1957). Some Mechanical Tests on the Lumbosacral Spine with Particular Reference to the Intervertebral Discs - a Preliminary Report. *Journal of Bone and Joint Surgery-American Volume, 39*(5), 1135-1164.

Bruehlmann, S. B., Hulme, P. A., & Duncan, N. A. (2004). In situ intercellular mechanics of the bovine outer annulus fibrosus subjected to biaxial strains. *Journal of Biomechanics, 37*(2), 223-231.

Caner, F. C., & Carol, I. (2006). Microplane constitutive model and computational framework for blood vessel tissue. *J Biomech Eng, 128*(3), 419-427.

Caner, F. C., Guo, Z., Moran, B., Bazant, Z. P., & Carol, I. (2007). Hyperelastic anisotropic microplane constitutive model for annulus fibrosus. *J Biomech Eng, 129*(5), 632-641.

Carragee, E. J., Don, A. S., Hurwitz, E. L., Cuellar, J. M., Carrino, J., & Herzog, R. (2009). 2009 ISSLS prize winner: does discography cause accelerated progression of degeneration changes in the lumbar disc: a ten-year matched cohort study. *Spine*, 34(21), 2338.

Cassidy, J. J., Hiltner, A., & Baer, E. (1989). Hierarchical Structure of the Intervertebral-Disk. *Connective Tissue Research, 23*(1), 75-88.

Cassidy, J. J., Hiltner, A., & Baer, E. (1990). The Response of the Hierarchical Structure of the Intervertebral-Disk to Uniaxial Compression. *Journal of Materials Science-Materials in Medicine, 1*(2), 69-80.

Cheung, J. T. M., Zhang, M., & Chow, D. H. K. (2003). Biomechanical responses of the intervertebral joints to static and vibrational loading: a finite element study. *Clinical Biomechanics, 18*(9), 790-799.

Cloyd, J. M., & Elliott, D. M. (2007). Elastin content correlates with human disc degeneration in the anulus fibrosus and nucleus pulposus. *Spine (Phila Pa 1976), 32*(17), 1826-1831.

Costi, J. J., Hearn, T. C., & Fazzalari, N. L. (2002). The effect of hydration on the stiffness of intervertebral discs in an ovine model. *Clinical Biomechanics, 17*(6), 446-455.

Crawford, R. P., Rosenberg, W. S., & Keaveny, T. M. (2003). Quantitative computed tomography-based finite element models of the human lumbar vertebral body: Effect of element size on stiffness, damage, and fracture strength predictions. *Journal of Biomechanical Engineering-Transactions of the Asme, 125*(4), 434-438.

Di Martino, A., Vaccaro, A. R., Lee, J. Y., Denaro, V., & Lim, M. R. (2005). Nucleus pulposus replacement - Basic science and indications for clinical use. *Spine, 30*(16), S16-S22.

Dunn, J. F., Foniok, T., & Matyas, J. R. (2006). *Magic angle MR microscopy and T2 quantification of intervertebral disc highlights the 3-dimensional collagen structure.* Paper presented at the International Society for Magnetic Resonance in Medicine, Sydney.

Eberlein, R., Holzapfel, G. A., & Schulze-Bauer, C. A. J. (2000). An Anisotropic Model for Annulus Tissue and Enhanced Finite Element Analyses of Intact Lumbar Disc Bodies. *Computer Methods in Biomechanics and Biomedical Engineering, 4*, 20.

Elliott, D. M., & Setton, L. A. (2000). A linear material model for fiber-induced anisotropy of the anulus fibrosus. *Journal of Biomechanical Engineering-Transactions of the Asme, 122*(2), 173-179.

Elliott, D. M., & Setton, L. A. (2001). Anisotropic and inhomogeneous tensile behavior of the human anulus fibrosus: Experimental measurement and

material model predictions. *Journal of Biomechanical Engineering-Transactions of the Asme, 123*(3), 256-263.

Espino, D. M., Meakin, J. R., Hukins, D. W. L., & Reid, J. E. (2003). Stochastic Finite Element Analysis of Biological Systems: Comparison of a Simple Intervertebral Disc Model with Experimental Results. *Computer Methods in Biomechanics and Biomedical Engineering, 6*(4), 7.

Fagan, M. J., Julian, S., Siddall, D. J., & Mohsen, A. M. (2002). Patient-specific spine models. Part 1: finite element analysis of the lumbar intervertebral disc - a material sensitivity study. *Proceedings of the Institution of Mechanical Engineers Part H-Journal of Engineering in Medicine, 216*(H5), 299-314.

Freeman, B. J. C., & Davenport, J. (2006). Total disc replacement in the lumbar spine: a systematic review of the literature. *European Spine Journal, 15*, S439-S447.

Galante, J. O. (1967). Tensile Properties of Human Lumbar Annulus Fibrosus. *Acta Orthopaedica Scandinavica, S*, 9-&.

Giles, L. F. G., & Singer, K. P. (1997). *Clinical Anatomy and Management of Low Back Pain* (Vol. 1): Butterworth-Heinemann.

Goel, V. K., & Gilbertson, L. G. (1995). Applications of the Finite-Element Method to Thoracolumbar Spinal Research - Past, Present, and Future. *Spine, 20*(15), 1719-1727.

Goel, V. K., Monroe, B. T., Gilbertson, L. G., Brinckmann, P., & Nat, R. (1995). Interlaminar Shear Stresses and Laminae Separation in a Disc - Finite-Element Analysis of the L3-L4 Motion Segment Subjected to Axial Compressive Loads. *Spine, 20*(6), 689-698.

Gregory, D. E., Veldhuis, J. H., Horst, C., Wayne Brodland, G., & Callaghan, J. P. (2010). Novel lap test determines the mechanics of delamination between annular lamellae of the intervertebral disc. *Journal of Biomechanics, 44*(1), 97-102.

Guerin, H. A. L., & Elliott, D. M. (2006). Degeneration affects the fiber reorientation of human annulus fibrosus under tensile load. *Journal of Biomechanics, 39*(8), 1410-1418.

Guerin, H. L., & Elliott, D. M. (2007). Ouantifying the contributions of structure to annulus fibrosus mechanical function using a nonlinear, anisotropic, hyperelastic model. *Journal of Orthopaedic Research, 25*(4), 508-516.

Guo, Z. Y., Peng, X. Q., & Moran, B. (2006). A composites-based hyperelastic constitutive model for soft tissue with application to the human annulus fibrosus. *Journal of the Mechanics and Physics of Solids, 54*(9), 1952-1971.

Harris, R. I., & Macnab, I. (1954). Structural Changes in the Lumbar Intervertebral Discs - Their Relationship to Low Back Pain and Sciatica. *Journal of Bone and Joint Surgery-British Volume, 36*(2), 304-322.

Haughton, V. (2004). Medical imaging of intervertebral disc degeneration: current status of imaging. *Spine (Phila Pa 1976), 29*(23), 2751-2756.

Heuer, F., Schmidt, H., & Wilke, H. J. (2008). The relation between intervertebral disc bulging and annular fiber associated strains for simple and complex loading. *Journal of Biomechanics, 41*(5), 1086-1094.

Heuer, F., Schmidt, H., & Wilke, H. J. (2008). Stepwise reduction of functional spinal structures increase disc bulge and surface strains. *Journal of Biomechanics, 41*(9), 1953-1960.

HSE. (2009). Self-reported work-related illness and workplace injuries in 2008/09: Results from the Labour Force Survey In H. a. S. Executive (Ed.). Caerphilly: National Statistics.

Iatridis, J. C., & ap Gwynn, I. (2004). Mechanisms for mechanical damage in the intervertebral disc annulus fibrosus. *J Biomech, 37*(8), 1165-1175.

Jones, A. C., & Wilcox, R. K. (2008). Finite element analysis of the spine: Towards a framework of verification, validation and sensitivity analysis. *Medical Engineering & Physics, 30*(10), 1287-1304.

Jovicich, J., Czanner, S., Greve, D., Haley, E., van der Kouwe, A., Gollub, R., et al. (2006). Reliability in multi-site structural MRI studies: effects of gradient non-linearity correction on phantom and human data. *Neuroimage, 30*(2), 436-443.

Katz, J. N. (2006). Lumbar disc disorders and low-back pain: Socioeconomic factors and consequences. *Journal of Bone and Joint Surgery-American Volume, 88A*, 21-24.

Kim, Y. E., Goel, V. K., Weinstein, J. N., & Lim, T. H. (1991). Effect of Disk Degeneration at One Level on the Adjacent Level in Axial Mode. *Spine, 16*(3), 331-335.

Klisch, S. M., & Lotz, J. C. (1999). Application of a fiber-reinforced continuum theory to multiple deformations of the annulus fibrosus. *Journal of Biomechanics, 32*(10), 1027-1036.

Kurowski, P., & Kubo, A. (1986). The Relationship of Degeneration of the Intervertebral-Disk to Mechanical Loading Conditions on Lumbar Vertebrae. *Spine, 11*(7), 726-731.

Kurtz, S. M., & Edidin, A. A. (2006). *Spine Technology Handbook*: Elsevier Academic Press.

Laible, J. P., Pflaster, D. S., Krag, M. H., Simon, B. R., & Haugh, L. D. (1993). A Poroelastic-Swelling Finite-Element Model with Application to the Intervertebral Disc. *Spine, 18*(5), 659-670.

Lappalainen, A. K., Kaapa, E., Lamminen, A., Laitinen, O. M., & Gronblad, M. (2002). The diagnostic value of contrast-enhanced magnetic resonance imaging in the detection of experimentally induced anular tears in sheep. *Spine, 27*(24), 2806-2810.

Lawrence, I., & Lin, K. (1989). A concordance correlation coefficient to evaluate reproducibility. Biometrics, 45, 255-268.

Lewis, N. T., Hussain, M. A., & Mao, J. J. (2008). Investigation of nano-mechanical properties of annulus fibrosus using atomic force microscopy. *Micron, 39*(7), 1008-1019.

Li, H., & Wang, Z. (2006). Intervertebral disc biomechanical analysis using the finite element modeling based on medical images. *Comput Med Imaging Graph, 30*(6-7), 363-370.

Liebschner, M. A. K., Kopperdahl, D. L., Rosenberg, W. S., & Keaveny, T. M. (2003). Finite element modeling of the human thoracolumbar spine. *Spine, 28*(6), 559-565.

Lin, H. S., King Lui, Y., Ray, G., & Nikravesh, P. (1978). Systems identification for material properties of the intervertebral joint. Journal of biomechanics, 11(1), 1-14

Lu, Y. M., Hutton, W. C., & Gharpuray, V. M. (1996). Can variations in intervertebral disc height affect the mechanical function of the disc? *Spine, 21*(19), 2208-2216.

Luoma, K., Riihimaki, H., Luukkonen, R., Raininko, R., Viikari-Juntura, E., & Lamminen, A. (2000). Low back pain in relation to lumbar disc degeneration. *Spine, 25*(4), 487-492.

MacLean, J. J., Owen, J. P., & Iatridis, J. C. (2007). Role of endplates in contributing to compression behaviors of motion segments and intervertebral discs. *Journal of Biomechanics, 40*(1), 55-63.

Maniadakis, N., & Gray, A. (2000). The economic burden of back pain in the UK. *Pain, 84*(1), 95-103.

Marchand, F., & Ahmed, A. M. (1990). Investigation of the Laminate Structure of Lumbar-Disk Anulus Fibrosus. *Spine, 15*(5), 402-410.

Markolf, K. L. (1972). Deformation of Thoracolumbar Intervertebral Joints in Response to External Loads - Biomechanical Study Using Autopsy Material. *Journal of Bone and Joint Surgery-American Volume, A 54*(3), 511-&.

Markolf, K. L., & Morris, J. M. (1974). Structural Components of Intervertebral-Disk - Study of Their Contributions to Ability of Disk to Withstand Compressive Forces. *Journal of Bone and Joint Surgery-American Volume, A 56*(4), 675-687.

Matthews, C. (2006). *Engineers' Data Book* (2006 ed.). London: Wiley-Blackwell.

Mcnally, D. S., & Arridge, R. G. C. (1995). An Analytical Model of Intervertebral Disc Mechanics. *Journal of Biomechanics, 28*(1), 53-&.

Meakin, J. R., & Hukins, D. W. L. (2001). Replacing the nucleus pulposus of the intervertebral disk: prediction of suitable properties of a replacement material using finite element analysis. *Journal of Materials Science-Materials in Medicine, 12*(3), 207-213.

Meakin, J. R., Redpath, T. W., & Hukins, D. W. L. (2001). The effect of partial removal of the nucleus pulposus from the intervertebral disc on the response of the human annulus fibrosus to compression. *Clinical Biomechanics, 16*(2), 121-128.

Michalek, A. J., Buckley, M. R., Bonassar, L. J., Cohen, I., & Iatridis, J. C. (2009). Measurement of local strains in intervertebral disc anulus fibrosus tissue under dynamic shear: Contributions of matrix fiber orientation and elastin content. *Journal of Biomechanics, 42*(14), 2279-2285.

Middleditch, A., & Oliver, J. (2005). *Functional Anatomy of the Spine*. Philadelphia, USA: Elsevier.

Nachemson, A. L. (1981). Disk Pressure Measurements. *Spine, 6*(1), 93-97.

Natarajan, R. N., Ke, J. H., & Andersson, G. B. J. (1994). A Model to Study the Disc Degeneration Process. *Spine, 19*(3), 259-265.

Natarajan, R. N., Williams, J. R., & Andersson, G. B. J. (2004). Recent advances in analytical modeling of lumbar disc degeneration. *Spine, 29*(23), 2733-2741.

Natarajan, R. N., Williams, J. R., & Andersson, G. B. J. (2006). Modeling changes in intervertebral disc mechanics with degeneration. *Journal of Bone and Joint Surgery-American Volume, 88A*, 36-40.

Nazari, J., Pope, M. H., & Graveling, R. A. (2011). Reality about migration of the nucleus pulposus within the intervertebral disc with changing postures. *Clin Biomech (Bristol, Avon)*.

Nerurkar, N. L., Baker, B. M., Sen, S., Wible, E. E., Elliott, D. M., & Mauck, R. L. (2009). Nanofibrous biologic laminates replicate the form and function of the annulus fibrosus. *Nature Materials, 8*(12), 986-992.

Nerurkar, N. L., Elliott, D. M., & Mauck, R. L. (2010). Mechanical design criteria for intervertebral disc tissue engineering. *Journal of Biomechanics*.

Nerurkar, N. L., Mauck, R. L., & Elliott, D. M. (2008). ISSLS Prize Winner: Integrating Theoretical and Experimental Methods for Functional Tissue Engineering of the Annulus Fibrosus. *Spine, 33*(25), 2691-2701.

O'Connell, G. D., Johannessen, W., Vresilovic, E. J., & Elliott, D. M. (2007). Human internal disc strains in axial compression measured noninvasively using magnetic resonance imaging. *Spine, 32*(25), 2860-2868.

O'Connell, G. D., Vresilovic, E. J., & Elliott, D. M. (2007). Comparison of animals used in disc research to human lumbar disc geometry. *Spine, 32*(3), 328-333.

O'Connell, G. D., Vresilovic, E. J., & Elliott, D. M. (2011). Human intervertebral disc internal strain in compression: The effect of disc region, loading position, and degeneration. Journal of Orthopaedic Research, 29(4), 547-555.

Palmer, K. T., Walsh, K., Bendall, H., Cooper, C., & Coggon, D. (2000). Back pain in Britain: comparison of two prevalence surveys at an interval of 10 years. *British Medical Journal, 320*(7249), 1577-1578.

Peng, X. Q., Guo, Z. Y., & Moran, B. (2006). An anisotropic hyperelastic constitutive model with fiber-matrix shear interaction for the human annulus fibrosus. *Journal of Applied Mechanics-Transactions of the Asme, 73*(5), 815-824.

Pezowicz, C. A., Robertson, P. A., & Broom, N. D. (2005). Intralamellar relationships within the collagenous architecture of the annulus fibrosus imaged in its fully hydrated state. *Journal of Anatomy, 207*(4), 299-312.

Pezowicz, C. A., Robertson, P. A., & Broom, N. D. (2006). The structural basis of interlamellar cohesion in the intervertebral disc wall. *Journal of Anatomy, 208*(3), 317-330.

Pfirrmann, C. W. A., Metzdorf, A., Zanetti, M., Hodler, J., & Boos, N. (2001). Magnetic resonance classification of lumbar intervertebral disc degeneration. *Spine, 26*(17), 1873-1878.

Prendergast, P. J. (1997). Finite element models in tissue mechanics and orthopaedic implant design. *Clinical Biomechanics, 12*(6), 343-366.

Rehman, S. (2007). *Fibre orientation in the annulus fibrosus.* University of Nottingham.

Rolander, S. D. (1966). Motion of Lumbar Spine with Special Reference to Stabilizing Effect of Posterior Fusion - an Experimental Study on Autopsy Specimens. *Acta Orthopaedica Scandinavica, S*, 1-&.

Rodrigues, S. A., Wade, K. R., Thambyah, A., & Broom, N. D. (2012). Micromechanics of annulus–end plate integration in the intervertebral disc. *The Spine Journal*.

Schmidt, H., Heuer, F., Drumm, J., Klezl, Z., Claes, L., & Wilke, H. J. (2007). Application of a calibration method provides more realistic results for a finite

element model of a lumbar spinal segment. *Clinical Biomechanics, 22*(4), 377-384.

Schmidt, H., Heuer, F., Simon, U., Kettler, A., Rohlmann, A., Claes, L., et al. (2006). Application of a new calibration method for a three-dimensional finite element model of a human lumbar annulus fibrosus. *Clinical Biomechanics, 21*(4), 337-344.

Schmidt, H., Kettler, A., Rohlmann, A., Claes, L., & Wilke, H. J. (2007). The risk of disc prolapses with complex loading in different degrees of disc degeneration - a finite element analysis. *Clin Biomech (Bristol, Avon), 22*(9), 988-998.

Schmidt, H., Shirazi-Adl, A., Galbusera, F., & Wilke, H. J. (2010). Response analysis of the lumbar spine during regular daily activities-A finite element analysis. *Journal of Biomechanics*.

Schollum, M. L., Appleyard, R. C., Little, C. B., & Melrose, J. (2010). A Detailed Microscopic Examination of Alterations in Normal Anular Structure Induced by Mechanical Destabilization in an Ovine Model of Disc Degeneration. *Spine, 35*(22), 1965-1973.

Schollum, M. L., Robertson, P. A., & Broom, N. D. (2008). ISSLS Prize Winner: Microstructure and Mechanical Disruption of the Lumbar Disc Annulus Part I: A Microscopic Investigation of the Translamellar Bridging Network. *Spine, 33*(25), 2702-2710.

Schollum, M. L., Robertson, P. A., & Broom, N. D. (2009). A microstructural investigation of intervertebral disc lamellar connectivity: detailed analysis of the translamellar bridges. *Journal of Anatomy, 214*(6), 805-816.

Sharma, A., Pilgram, T., & Wippold, F. J. (2009). Association between Annular Tears and Disk Degeneration: A Longitudinal Study. *American Journal of Neuroradiology, 30*(3), 500-506.

Shirazi-Adl, A. (1989). On the fibre composite material models of disc annulus--comparison of predicted stresses. *J Biomech, 22*(4), 357-365.

Shirazi-Adl, A. (1992). Finite-element simulation of changes in the fluid content of human lumbar discs. Mechanical and clinical implications. *Spine (Phila Pa 1976), 17*(2), 206-212.

Shirazi-Adl, A. (1994). Nonlinear stress analysis of the whole lumbar spine in torsion--mechanics of facet articulation. *J Biomech, 27*(3), 289-299.

Shirazi-Adl, S. A., Shrivastava, S. C., & Ahmed, A. M. (1984). Stress analysis of the lumbar disc-body unit in compression. A three-dimensional nonlinear finite element study. *Spine (Phila Pa 1976), 9*(2), 120-134.

Simon, B. R., Wu, J. S. S., Carlton, M. W., Kazarian, L. E., France, E. P., Evans, J. H., et al. (1985). Poroelastic Dynamic Structural Models of Rhesus Spinal Motion Segments. *Spine, 10*(6), 494-506.

Skrzypiec, D., Tarala, M., Pollintine, P., Dolan, P., & Adams, M. A. (2007). When are intervertebral discs stronger than their adjacent vertebrae? *Spine, 32*(22), 2455-2461.

Smith, L. J., & Elliott, D. M. (2011). Formation of lamellar cross bridges in the annulus fibrosus of the intervertebral disc is a consequence of vascular regression. *Matrix Biology, 30*(4), 267-274.

Smith, L. J., & Fazzalari, N. L. (2006). Regional variations in the density and arrangement of elastic fibres in the anulus fibrosus of the human lumbar disc. *Journal of Anatomy, 209*(3), 359-367.

Smith, L. J., & Fazzalari, N. L. (2009). The elastic fibre network of the human lumbar anulus fibrosus: architecture, mechanical function and potential role in the progression of intervertebral disc degeneration. *European Spine Journal, 18*(4), 439-448.

Spencer, A. J. M. (1984). *Continuum Theory of the Mechanics of Fibre-Reinforced Composites*. New York: CISM.

Strange, D. G. T., Fisher, S. T., Boughton, P. C., Kishen, T. J., & Diwan, A. D. (2010). Restoration of compressive loading properties of lumbar discs with a nucleus implant--a finite element analysis study. *The Spine Journal, 10*(7), 602-609.

Swider, P., Pedrono, A., Ambard, D., Accadbled, F., & Sales de Gauzy, J. (2010). Substructuring and poroelastic modelling of the intervertebral disc. *J Biomech*.

Tarsuslugil, S. (2011). *Computational modelling of spinal burst fractures for the development of calcium phosphate cement.* University of Leeds.

Thompson, J. P., Pearce, R. H., Schechter, M. T., Adams, M. E., Tsang, I. K. Y., & Bishop, P. B. (1990). Preliminary Evaluation of a Scheme for Grading the Gross Morphology of the Human Intervertebral-Disk. *Spine, 15*(5), 411-415.

Tsuji, H., Hirano, N., Ohshima, H., Ishihara, H., Terahata, N., & Motoe, T. (1993). Structural Variation of the Anterior and Posterior Anulus Fibrosus in the Development of Human Lumbar Intervertebral-Disk - a Risk Factor for Intervertebral-Disk Rupture. *Spine, 18*(2), 204-210.

Urban, J. P., & Winlove, C. P. (2007). Pathophysiology of the intervertebral disc and the challenges for MRI. *J Magn Reson Imaging, 25*(2), 419-432.

Urban, J. P. G., & Roberts, S. (2003). Degeneration of the intervertebral disc. *Arthritis Research & Therapy, 5*(3), 120-130.

Vernengo, J., Fussell, G. W., Smith, N. G., & Lowman, A. M. (2008). Evaluation of novel injectable hydrogels for nucleus pulposus replacement. *Journal of Biomedical Materials Research Part B-Applied Biomaterials, 84B*(1), 64-69.

Viceconti, M., Olsen, S., Nolte, L. P., & Burton, K. (2005). Extracting clinically relevant data from finite element simulations (vol 20, pg 451, 2005). *Clinical Biomechanics, 20*(9), 1010-1010.

Videman, T., Battie, M. C., Gibbons, L. E., Maravilla, K., Manninen, H., & Kaprio, J. (2003). Associations between back pain history and lumbar MRI findings. *Spine, 28*(6), 582-588.

Videman, T., Battie, M. C., Ripatti, S., Gill, K., Manninen, H., & Kaprio, J. (2006). Determinants of the progression in lumbar degeneration - A 5-year follow-up study of adult male monozygotic twins. *Spine, 31*(6), 671-678.

Virgin, W. J. (1951). Experimental Investigations into the Physical Properties of the Intervertebral Disc. *Journal of Bone and Joint Surgery-British Volume, 33*(4), 607-611.

Wade, K. R., Robertson, P. A., & Broom, N. D. (2010). A fresh look at the nucleus-endplate region: new evidence for significant structural integration. *European Spine Journal*.

Wade, K. R., Robertson, P. A., & Broom, N. D. (2012). On the Extent and Nature of Nucleus-Annulus Integration. *Spine, 37*(21), 1826-1833.

Wagner, D. R., & Lotz, J. C. (2004). Theoretical model and experimental results for the nonlinear elastic behavior of human annulus fibrosus. *Journal of Orthopaedic Research, 22*(4), 901-909.

Walter, J. D. (1971). Tire stress and deformation. In *Mechanics of Pneumatic Tires* (pp. 405-444): U.S. Department of Commerce, pp.

Wilcox, R.K. (2007). The influence of material property and morphological parameters on specimen-specific finite element models of porcine vertebral bodies. *J of Biomechanics*. 40, pp.669-673.

Wilke, H. J., Kettler, A., & Claes, L. E. (1997). Are sheep spines a valid biomechanical model for human spines? *Spine, 22*(20), 2365-2374.

Williams, J. R., Natarajan, R. N., & Andersson, G. B. J. (2007). Inclusion of regional poroelastic material properties better predicts biomechanical behavior of lumbar discs subjected to dynamic loading. *Journal of Biomechanics, 40*(9), 1981-1987.

Wu, H. C., & Yao, R. F. (1976). Mechanical-Behavior of Human Annulus Fibrosis. *Journal of Biomechanics, 9*(1), 1-&.

Yao, H., Justiz, M. A., Flagler, D., & Gu, W. Y. (2002). Effects of swelling pressure and hydraulic permeability on dynamic compressive behavior of lumbar annulus fibrosus. *Ann Biomed Eng, 30*(10), 1234-1241.

Yin, L., & Elliott, D. M. (2004). A biphasic and transversely isotropic mechanical model for tendon: application to mouse tail fascicles in uniaxial tension. *J Biomech, 37*(6), 907-916.

Yin, L. Z., & Elliott, D. M. (2005). A homogenization model of the annulus fibrosus. *Journal of Biomechanics, 38*(8), 1674-1684.

Yoganandan, N. P., Kumaresan, S. M. S., Voo, L. P., & Pintar, F. A. P. (1996). Finite Element Applications in Human Cervical Spine Modeling. *Spine*.

Yu, J., Fairbank, J. C., Roberts, S., & Urban, J. P. (2005). The elastic fiber network of the anulus fibrosus of the normal and scoliotic human intervertebral disc. *Spine (Phila Pa 1976), 30*(16), 1815-1820.

Yu, J., Tirlapur, U., Fairbank, J., Handford, P., Roberts, S., Winlove, C. P., et al. (2007). Microfibrils, elastin fibres and collagen fibres in the human intervertebral disc and bovine tail disc. *Journal of Anatomy, 210*(4), 460-471.

Yu, J., Winlove, P. C., Roberts, S., & Urban, J. P. (2002). Elastic fibre organization in the intervertebral discs of the bovine tail. *J Anat, 201*(6), 465-475.

9.1 LIST OF JOURNAL AND CONFERENCE PUBLICATIONS

"Specimen specific simulation of the intervertebral disc based on three dimensional magnetic resonance image data" Luxmoore, B.J., Wijayathunga, V.N., Rehman, S., Wilcox, R.K., in preparation for submission to *Spine*

"Finite element models of the intervertebral disc developed from MRI data to include lamellar mechanics", Luxmoore, B.J., Wijayathunga, V.N., Rehman, S., Wilcox,

R.K., podium presentation, *International Symposium of Computer Methods in Biomechanics and Biomedical Engineering*, April 2012 (Germany)

“Finite element analysis of microscopy tensile tests of annulus fibrosis tissue”, Luxmoore, B.J., Wijayathunga, V.N., Rehman, S., Wilcox, R.K., poster presentation, *International Symposium of Computer Methods in Biomechanics and Biomedical Engineering*, April 2012 (Germany)

“Investigating the mechanical role of cross-bridging in the annulus fibrosis using finite element analysis”, Luxmoore, B.J., Wijayathunga, V.N., Rehman, S., Wade, K., Rodrigues, S., Broom, N., Wilcox, R.K., poster presentation, *Orthopaedic Research Society Annual Meeting*, February 2012 (USA)

“Interlamellar interactions in finite element analysis of the intervertebral disc”, Luxmoore, B.J., Wijayathunga, V.N., Rehman, S., Wilcox, R.K., poster presentation, *British Orthopaedic Research Society Conference*, June 2011 (UK)

“A constituent sensitivity finite element analysis of the intervertebral disc”, Luxmoore, B.J., Wijayathunga, V.N., Rehman, S., Wilcox, R.K., podium presentation, *BioEng 2010*, September 2010 (UK)